Proteomics and Nanocrystallography

Proteomics and Nanocrystallography

Eugenia Pechkova and Claudio Nicolini

Fondazione ELBA
Rome, Italy, and
University of Genova
Genova, Italy

Springer-Science+Business Media, LLC

ISBN 978-1-4613-4896-2 ISBN 978-1-4615-0041-4 (eBook)
DOI 10.1007/978-1-4615-0041-4

© 2003 Springer Science+Business Media New York
Originally published by Kluwer Academic / Plenum Publishers, New York in 2003
Softcover reprint of the hardcover 1st edition 2003

10 9 8 7 6 5 4 3 2 1

A C.I.P. record for this book is available from the Library of Congress

All rights reserved

No part of this book may be reproduced, stored in a retrieval system, or transmitted in any form or by any means, electronic, mechanical, photocopying, microfilming, recording, or otherwise, without written permission from the Publisher, with the exception of any material supplied specifically for the purpose of being entered and executed on a computer system, for exclusive use by the purchaser of the work.

This book is dedicated to our parents

Alexey Pechkov and Marina Pechkova

Alfredo Nicolini and Camilla Piantoni

Preface

The book addresses the most recent developments in structural and functional proteomics underlying the recent contributions given in these areas by our laboratory to the instrumentations, the methods and the procedures as mutuated from the nanoscale sciences and technologies. These developments introduced in the last few years make now possible protein massive identification (mass spectrometry and biomolecular arrays down to nanoamounts) and protein structural characterization in solution and in crystals down to the atomic scale to an extent and to a degree so far unmatched. Emphasis is placed in the growth by nanobiofilm template of protein crystals of any type and size from millimeter to micron, leading in combination with microfocus synchrotron technology and atomic force microscopy to the definition of a new field called nanocrystallography.

The few useful examples being shown, concerning yet structurally unsolved proteins, point this very promising approach nanotechnology-based in structural proteomics using highly focused X-rays. This has not to be confused with the important study of nanocrystals, both organic and inorganic, and novel diamond like nanocomposite materials and devices having 3D protein crystals as matrices to be equilibrated with nanoparticles/gold/silver to be utilized in the most diversified electronic applications here also summarized.

Acknowledgments

We are particularly grateful to Giuseppe Zanotti at the University of Padova for his fundamental collaboration during all the crystallographic studies. We are very grateful to Christian Riekel and all beamline staff of ID13 at ESRF/EMBL, Grenoble, Manfred Burghammer and David Flot for excellent conditions and support during data collection. We would like to thank Roberto Battistutta, Paola Ghisellini and Walter Bavastrello for their cooperation. We like finally to acknowledge the editorial support of Fabrizio Nozza. The work described in this book is entirely supported by the Italian Ministry of Education, Research and Universities to the Fondazione EL.B.A. both with a grant provided yearly for its functioning and with a FIRB research contract entitled "Organic Nanosciences and Nanotechnologies".

Contents

1 THE NEW FRONTIER AT THE CROSSING OF LIFE AND PHYSICAL SCIENCES 1

2 STATE OF THE ART IN PROTEOMICS, CRYSTALLOGRAPHY AND NANOBIOTECHNOLOGY 9

2.1 METHODS OF PROTEIN PRODUCTION 10

2.1.1 Recombinant DNA Technology: expression, purification and mutagenesis. 11

2.2 METHODS FOR PROTEIN IDENTIFICATION 15

2.2.1 Two-dimensional electrophoresis 16

2.2.2 Mass spectrometry and its principles 17

2.3 METHODS OF PROTEIN CRYSTALLIZATION 20

2.3.1. Importance of protein sample preparation 21

2.3.2 Protein solubility and supersaturation. Nucleation and crystal growth 22

2.3.3 Classical methods 25

2.3.4 Less common techniques 27

2.3.5 Advanced methods 30

2.4 METHODS OF CRYSTAL STRUCTURE DETERMINATION 35

2.4.1 Protein X-ray crystallography 35

2.4.2 Crystal structure determination 38

2.4.3 Data collection and data processing 39

2.4.4 Traditional X-ray diffractometer 41

2.4.5 Electron microscopy 42

2.5 OTHER METHODS OF PROTEIN STRUCTURE INVESTIGATION 42

2.5.1 Circular Dichroism measurements 42
2.5.2 High Resolution Nuclear Magnetic Resonance 44
2.6 METHODS OF PROTEIN IMMOBILIZATION IN SOLID THIN FILMS 50
2.6.1 Pressure-area isotherms 53
2.6.2 Surface potential 56
2.6.3 Methods of thin film deposition 57
2.6.4 Methods of thin film characterization 61
3 NANOCRYSTALLOGRAPHY 63
3.1 NANOBIOFILMS TEMPLATE 63
3.1.1 Substrate preparation 65
3.1.2 Protein thin film formation 65
3.1.3 Protein thin film characterization 66
3.2 ATOMIC FORCE MICROSCOPY 67
3.2.1 Design of the chamber 69
3.2.2 The hardware and software apparatus 71
3.2.3 Performances of the system 73
3.3 SYNCHROTRON RADIATION 78
3.3.1 Principles of Synchrotron functioning 80
3.3.2 Microfocus beamline and ultramicrocrystal diffraction 87
3.3.3 Protein crystals synchrotron radiation analysis 95
3.3.4 Structure determination and refinement 97
3.4 FROM ART TO SCIENCE WITH PROTEIN NANOCRYSTALLOGRAPHY 97
4 FROM ART TO SCIENCE IN PROTEIN CRYSTALLOGRAPHY 99
4.1 NEW METHOD VALIDATION WITH LYSOZYME AS A MODEL PROTEIN 99
4.1.1 Effect of the thin film template: kinetics of the lysozyme crystal growth 101
4.1.2 Thin film surface pressure influence on the template-induced crystallization 105
4.1.3 X-ray diffraction of lysozyme crystals 107
4.1.4 Synchrotron radiation analysis of lysozyme crystals 109
4.2 YET UNRESOLVED PROTEINS: BOVINE CYTOCHROME P450SCC 111
4.2.1 Cytochrome P450scc (Side-Chain Cleavage) 111
4.2.2 Sample homogeneity 111
4.2.3 Pressure-area isotherm 112
4.2.4 Quartz crystal nanobalance 113

4.2.5 Cytochrome P450scc crystallization 114
4.2.6 Atomic Force Microscopy of cytochrome microcrystals 118
4.3 YET UNRESOLVED PROTEINS: HUMAN KINASE CK2α CATALYTIC SUBUNIT 119
4.3.1 Protein kinase CK2α catalytic subunit 119
4.3.2 Sample homogenity 120
4.3.3 Pressure-area isotherm 123
4.3.4 Quartz crystal nanobalance 124
4.3.5 Human protein kinase CK2α crystallization 125
4.3.6 Synchrotron radiation: analysis, data processing and structure determination 128
4.4 CONCLUSIONS 136
5 FROM SCIENCE TECHNOLOGY IN PROTEOMICS 137
5.1 AUTOMATED MASS SPECTROMETRY 138
5.2 BIOMOLECULAR ARRAYS 141
5.2.1 The surface patterning 142
5.2.2 The instrumental layout and data analysis 153
5.3 UNSOLVED PROTEIN STRUCTURES OF SCIENTIFIC AND INDUSTRIAL INTEREST 164
6 FUTURE TRENDS 167
6.1 NOVEL COMPOSITE BIOMATERIALS AND NANODEVICES 168
6.2 NANOCRYSTALS 172

REFERENCES 175
INDEX 189

Proteomics and Nanocrystallography

Chapter 1

THE NEW FRONTIER AT THE CROSSING OF LIFE AND PHYSICAL SCIENCES

The present work is dedicated to the new frontiers of proteomics and crystallography based on nanoscience and nanotechnology (Nicolini, 1989; Nicolini 1996b; Rossof 2001; Nicolini et al, 2001a) with emphasis on the combination of leading edge technologies useful to functionally identify and structurally characterize the large number of proteins present in the leaving organisms.

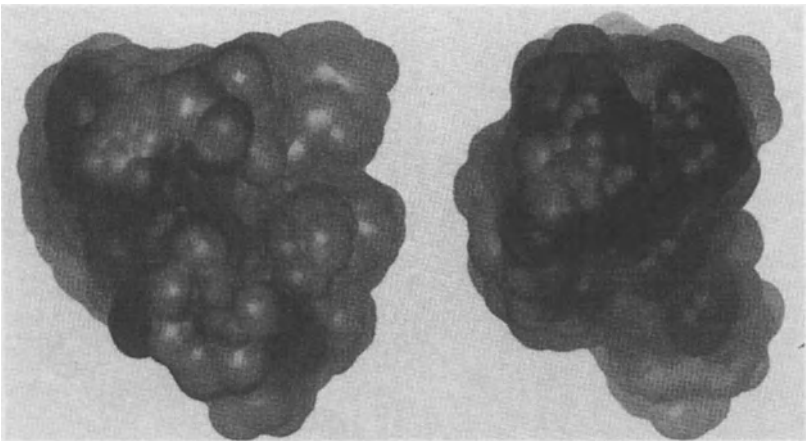

Figure 1-1. Three-dimensional structure of Penicillin G-aminase (PGA), with distribution of electrostatic potential over the surface at pH 7.5. left) front view; right) back view.

E. Pechkova et al., *Proteomics and Nanocrystallography*
© Springer Science+Business Media New York 2003

Both the massive identification of the numerous proteins and the knowledge of their protein 3D structure are needed to discover the molecular mechanisms and the atomic structures underlying molecular and cellular biology as well to find the proper technological transfer into human diagnosis and treatment. Figure 1.1 shows the example of an enzyme utilized in pharmaceutical industry to produce a drug by means of biocatalytic process.

This need is becoming always more actual for all research directions – molecular bioelectronics (Nicolini 1996; Nicolini 1998), biocatalysis (Nicolini 1996a, 1997), cancer research (Nicolini 1986, 1997a) and new drug design having profound implications for the pharmaceutical industry (Table 1.1).

Table 1-1. Example of proteins with yet unresolved 3D atomic structure and their roles in fundamental sciences and biotechnological applications.

PROTEIN	ROLES AND APPLICATIONS
Cytochrome P450scc	**Steroid synthesis** **Cholesterol monitoring** **Anti-inflammatory drugs** (Eldarov, et al 1998; Archakov et al 2003; Ivanov et al 1999, Usanov et al 2002, Shumyantseva et al., 2001; 2002, Bernhardt et al, 1998; Bernhardt 1998, 2000; Poulos et al., 1998, 1999; Li et al., 2002; Nicolini et al., 2001b)
Human protein kinase CK2α	**Cell cycle regulation** **Proliferation and tumorogenesis** **Fibroplast tranformation** **Antineoplastic drugs** (Orlandini et al 1998; Allende and Allende, 1995; Guerra and Issinger, 1999; Seldin and Leder, 1995)
Acute myelogenouse leukemia (AML1) protein	**Osteogenesis** **Bone tissue differentiation** **Control of acute leukemia** (Stein, 2000a,b; Stein et al., 1999, 2003; Tang et al, 1998;Choi, 2001)
Akt kinase	**Control of human mature T-cell leukemia** (Pekarsky et al, 2000, 2003; Croce 2001)

The main aim of this work is to outline the basic principles and the instrumentations of structural and functional proteomics as well as to define the new emerging field of nanocrystallography at the frontiers of nanotechnology and proteomics, leading to a transition from art to science and from science to technology in protein crystallography. Particular emphasis is given to the role of this new field resulting from the combination

of advanced nanotechnologies - namely atomic force microscopy, thin film nanotechnology and synchrotron radiation microfocusing - in the development of new methods in protein crystallization which represents a critical step in the protein three dimensional structure determination which in turn plays an important role in structural biology, pharmaceutical industry and medicine.

The present book consists of:

a) the description of the state of the art in proteomics, crystallography and nanobiotechnology, with emphasis on the different methods and procedures so far implemented;
b) the definition, principles and experimental layout of nanocrystallography, which is a new technology to produce and characterize crystals of any dimension by means of nanotechnology;
c) the route from art to science in protein crystallography by means of nanotechnology-based protein thin film template crystallization method in several protein system either known utilized as model system or yet unsolved. Figure 1.2 shows the most significant technological advancement in the field of thin protein film during the last several years.
d) the route from science to technology in life sciences, namely human diagnosis and treatments, with emphasis on the contributions from our laboratory;
e) the future trends leading to the integration of proteomics with protein nanocrystallography and inorganic nanocrystals for the development of 3D functional nanotechnology and molecular electronics.

First of all, it should not escape our notice that nanocrystallography as here described does not refer to the study of self-assembled nanocrystals (i.e., crystals of nanometer size) made of silver, cobalt, gold and/or nanoparticles as fabricated by means of reverse micelles or similar technologies (Pileni 1997, 2002).

The second chapter on the state of the art describes the existing methods and technologies concerning protein crystallization (see Figure 1.3. for an example of a typical crystal grown by classical procedures), protein identification as gel electrophoresis and mass spectrometry, protein immobilization and protein structure determination, outlining in detail the present situation in the relevant fields of thin film nanotechnology and the recent progress in protein crystallization.

Therefore from the state of the art, where big emphasis is placed to all developments in protein crystallography and nanobiotechnology regardless of our particular contributions, the promises of the post- genomic era appear kept considering that proteomics can be studied with both high speed and exceptional accuracy.

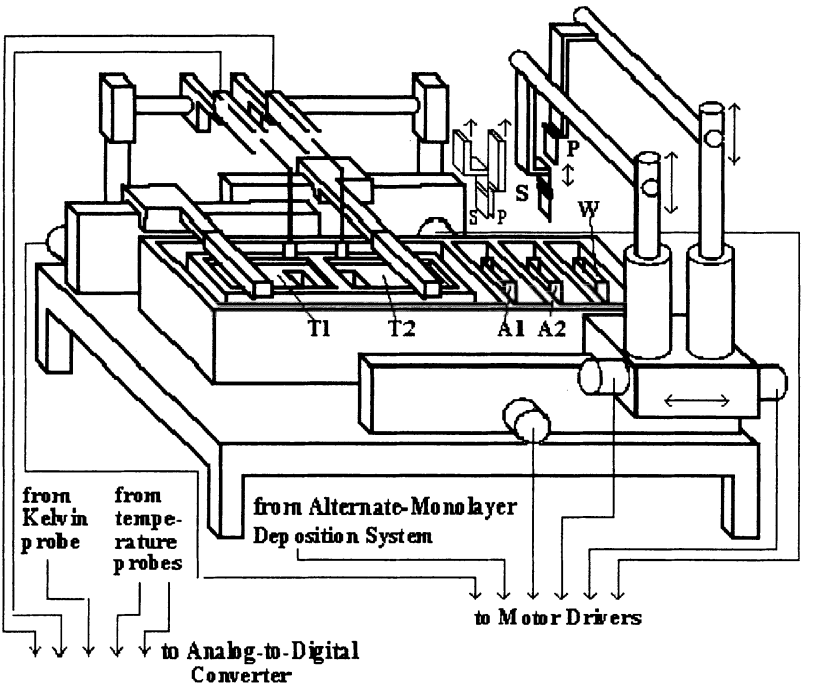

Figure 1-2. Schematic diagram of home-built LB instrument which allows the inclusion by means of a protective plate (P) adsorbed enzyme layers (S) into LB assemblies of alternating layers of different compounds without enzyme contact with air-water interface. (W)-compartment for washing; (T1), (T2)- sections of the trough, (A1), (A2) – compartments for adsorption (Troitsky et al., 1996a; Nicolini, 1997).

Proteomics projects usually start with the quick identification of large numbers of proteins from 2D-gel arrays via peptide mapping and may ends with the 3D structural characterization at atomic resolution of the chosen relevant protein.

In the third chapter the new method for protein crystallization based on protein thin film nanotechnology is described along with the new nanotechnologies. Namely neural network Atomic Force Microscopy with controlled environment and Microfocus Synchrotron Radiation are needed to structurally characterize the resulting microcrystals down to the nanometric and atomic resolution, respectively. While single protein molecules in solution or in monolayer can be readily studied by Scanning Probe Microscopy (Figure 1.4), characterization of entire crystal is more

complicated. In this third chapter the main problems still unsolved are stressed and the ways to solve them are proposed.

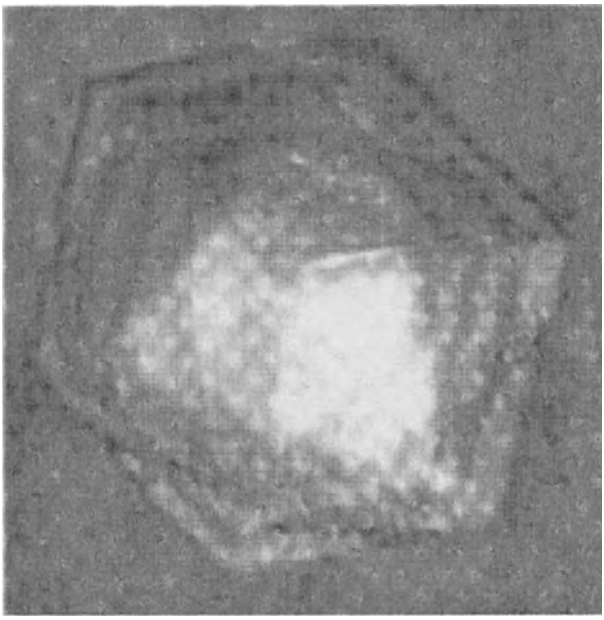

Figure 1-3. Large single concanavalin A crystal produced by common crystallization method (courtesy of A. Freemen)

In the fourth chapter, among the large number of proteins of potential scientific and industrial interest, few proteins of different classes are chosen to describe and exemplify the validation of nanocrystallography and the route from art to science in protein crystallography: chicken egg white lysozyme, bovine cytochrome P450 Side Chain Cleavage and human protein kinase CK2α subunit. Experimental part includes crystallization experiments, thin biofilm technology and structural characterization experiments such as X-ray diffraction, synchrotron radiation and atomic force microscopy.

A lot of discussion is dedicated to the interpretation of the experimental outcomes and validation of our new crystal manufacturing method. The novelty of the approach is proven in model system such as lysozyme, while the new technological implications in proteomics and pharmaceutics are underlined discussing the results obtained in a few of the wide class of yet structurally unresolved membrane proteins (cytochromes P450's) and human kinases.

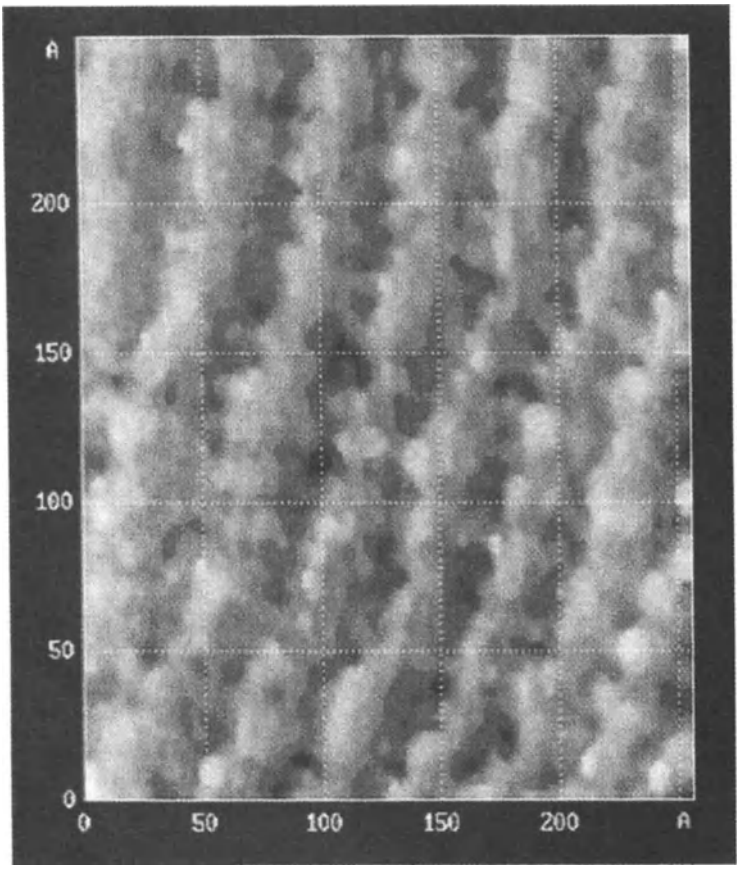

Figure 1-4. Scanning Tunneling Microscopy image of GST enzyme monolayer deposited on HOPG. The surface deposition pressure is 35 mN/m (Facci et al., 1996).

The future perspectives of the new method for protein crystallization based on protein thin film template are particularly stressed in terms of the apparent transition from art to science in protein crystallography. In the fifth chapter the transition from science to technology in Life Sciences is evidenced by the very recent advances made in key-areas of proteomics and post-genomics, underlying the recent contributions given in these areas by our laboratory to the instrumentations, the methods and the procedures as mutuated from the nanoscale sciences and technologies, namely:

- the identification and design of new drugs from the wide class of protein, particularly the membrane proteins, now crystallizable and thereby characterizable at atomic resolution.
- biomolecular array, as DNA chip and protein chip with functional assay in real time of thousand of genes and gene-products in all human cell system at very high speed and accuracy (Figure 1.5).

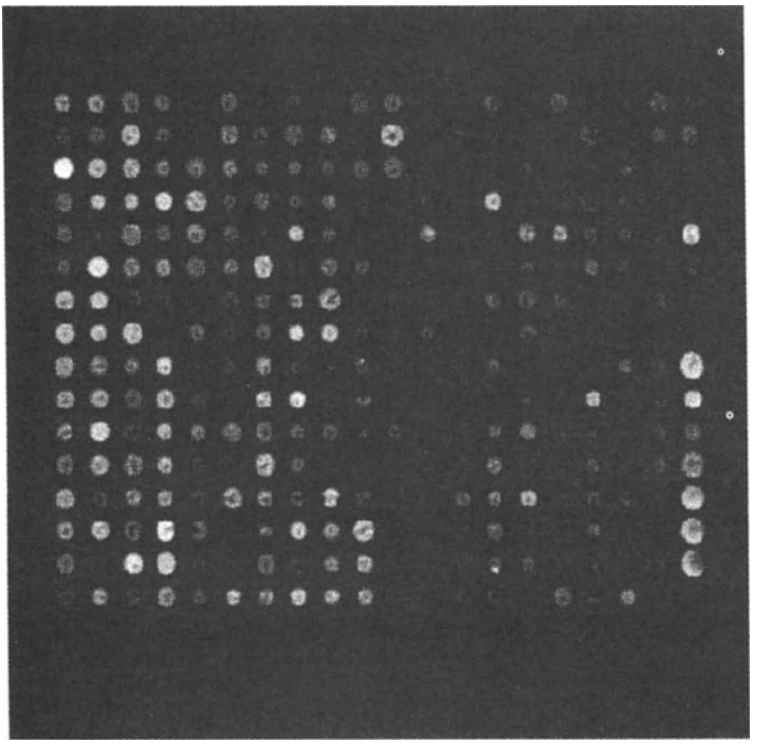

Figure 1-5. Microarrays of DNA molecules fluorescently label.

Particular mention should be made to the integrated mass spectrometry-based hardware and software suite which is making now feasible the automated protein identification and characterization from 2D gels, ranging from the peak picking in bidimensional gel until the interpretation of the spectrum with the support of proper database.

These tools are now designed for ultimate sensitivity, success rate, and throughput of protein identification. High performance of all system components, combined with a unique automated and flexible workflow

control, provide an unmatched overall productivity, enabling high success proteomics at a minimum of running costs and effort. This appears furthermore scalable and can be configured for use in small pilot phase studies up to full-blown industrial-scale proteomics initiatives with thousands of samples per day. Finally, in the sixth chapter an attempt is made to outline the future technological trends in integrating structural and functional proteomics and advanced protein crystal technology with the broad field of nanotechnology in terms of new nanomaterials and nanodevices of innovative physical and functional properties.

Chapter 2

STATE OF THE ART IN PROTEOMICS, CRYSTALLOGRAPHY AND NANOBIOTECHNOLOGY

With the development of genomics and proteomics, and their application in basic biological research and biotechnologies, there is an increasing need of functional and structural protein characterization. This need is becoming more and more severe with the rapid advances in biotechnology, molecular pharmacology and molecular medicine that require understanding of biological processes at the atomic level. Among the alternative methods of three-dimensional structural determination of proteins at atomic resolution X-ray crystallography has a central role, for its unique ability to solve the 3D structure of protein of any size once diffracting crystals at high resolution are obtained. This fulfills the aim to understand its structure–function relationship for the given protein of interest.

Only if the three-dimensional structures of proteins are known macromolecular processes can be described at a high level of accuracy as their interactions with ligands (including drugs) which modulate and regulate their biological action. Therefore, crystals are not the aim but the necessary requirements for protein structure determination by X-ray diffraction method (Rosenberger, 1996). It may be argued that structures can be solved by the NMR-spectroscopy shown later in this Chapter (Wutrich, 1986; Nicolini et al., 1995; Bartolucci et al., 1996). The NMR method however has an intrinsic limitation that the molecular weight of the molecules under investigation should not exceed 20.000-30.000 Da. X-ray crystallography does not have this limitation. (Giege et al., 1995). Furthermore, while until recently only X-ray diffracting crystals of rather big dimensions were needed, the establishment of Synchrotron Radiation

E. Pechkova et al., *Proteomics and Nanocrystallography*
© Springer Science+Business Media New York 2003

facilities world-wide overcame even this limitation making possible to structurally characterize even very small crystals (Cusack et al., 1998).

However, since synchrotrons constitute quite expensive centralized facilities not readily accessible to all scientists, most of the proteins nowadays are characterized by X-ray diffractometer, because this device is more available than synchrotron radiation facilities. Moreover, only focused X-ray beams from third generation synchrotron sources, such as the European Synchrotron Radiation Facility (ESRF), in Grenoble (France), allow the possibility of data collection for microcrystal analysis. For this reason crystal dimensions still remains the critical parameter for the protein 3-D structure characterization at the atomic level. In spite of recent advances in protein crystallization, such as surface response methods for optimizing crystal conditions (Carter, 1997) or the modification of charged residues (Rayment, 1997) and also crystallization at elevated temperature, which can increase the rate of crystal growth (Han and Lin, 2000), crystal growth remains the slowest step in protein structure determination. In spite of significant progress in protein crystallography, a large number of proteins playing a critical role in living mechanisms have so far not yet been crystallized. Indeed, protein crystal growth still remains the slowest critical step in protein structure determination. Protein crystallization techniques are often based on vapour diffusion methods, since they are easy to perform, require small amounts of samples and permit easy variation of physical parameters during crystallization (McPherson, 1989; Ducruix and Giege, 1999), but this approach can have random and unreproducible success, especially for proteins of fairly large size and/or high insolubility (Michel, 1991). Moreover, to be crystallized each protein requires its own specific conditions, which are often difficult to determine and that require empirical random searching. That is why protein crystallization is often called an art instead of a science. In this chapter we will summarize the state of the art in all related fields of proteomics, nanobiotechnology and crystallography. We will focus our attention on the various methods of protein production, identification, immobilization, functional and structural characterization. Particular attention is paid to both the traditional and the advanced methods of protein crystallization that have been implemented over the years with success in model systems and individual cases but with many problems still largely unsolved in most biological systems.

2.1 Methods of protein production

Large quantity of proteins are typically produced *in vitro* by recombinant DNA technologies (more effectively in most real cases) or in vivo by animal tissue or plasma isolation (in few model systems). A classical example of

plasma proteins frequently utilized as model system because of its ready accessibility is Lysozyme . Lysozyme is normally present in plasma (5.9 mg/l) but in trace amounts also in urine. It is widely distributed in animals and plants. Lysozyme from chicken egg white has been extensively studied as it will be shown later in Chapter 4.

2.1.1 Recombinant DNA Technology: expression, purification and mutagenesis.

Recombinant proteins (Figure 2.1a) represent a highly homologous population of proteins with controlled sequence, which can be ad hoc modified by site-specific mutagenesis. Furthermore, it can undergo cheap mass production and has the highest level of purity.

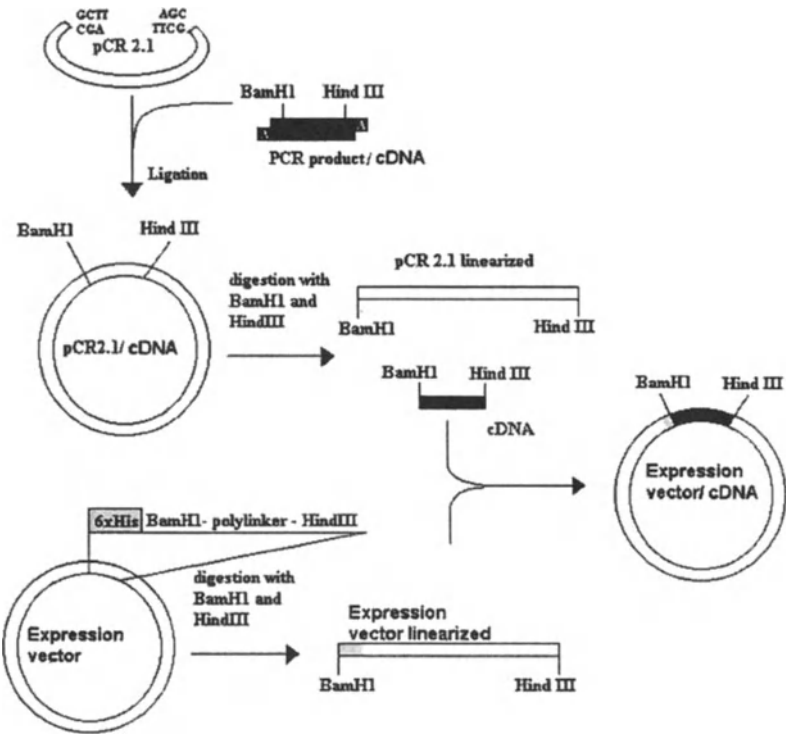

Figure 2-1a. Construction of expression vector containing the cDNA encoding recombinant protein. The cDNA was inserted into BamHI/HindIII site inside the polylinker region of expression vector.

Escherichia coli (*E. coli*) is a desirable organism for the heterologous expression of proteins owing to its ease of manipulation, the availability of a variety of cloning and expression vectors, well-understood genetics and the low cost of the culture (Porter and Larson, 1991). An example of recombinant protein expression and purification is shown in Figure 2.1b.

Two major classes of proteins of fundamental significance in both basic and applied biomedicine, but largely not yet solved, are the mammalian cytochromes and the human kinases, which are then here described to exemplify the methods of their production and separation (Figure 2.2a and Figure 2.2b) for sake of completeness.

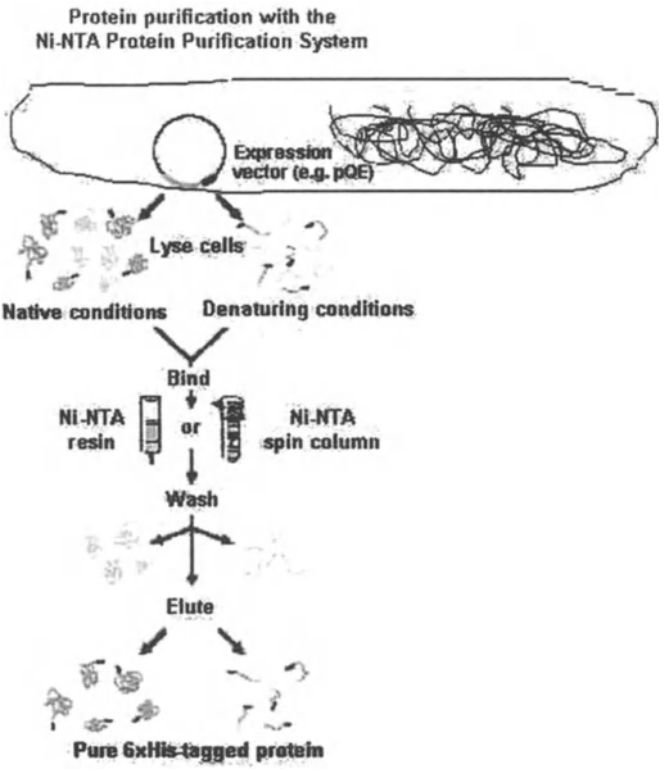

Figure 2-1b. Construction of expression vector containing the cDNA encoding recombinant protein. The cDNA was inserted into BamHI/HindIII site inside the polylinker region of expression vector.

2.1.1.1 Human kinases

Human Kinase as cDNA is usually cloned in *E. coli*. Purification of CK2α involves centrifugation, solubilization in apropriate buffer (for

example, 25mM Tris-HCl pH 8.5, containing PMSF 0.2mM, 2-Mercaptoethanol 7mM in the presence of a cocktail of protease inhibitors), ultracentrifugation and several steps of affinity chromatography with use of gradient elution of NaCl. For each step of the purification the presence of CK2 is monitored by SDS-PAGE (Laemmli, 1970) and the total protein content by Bradford assay. Finally, fractions containing alpha subunit of CK2α subunit are separated by gel filtration FPLC chromatography using a Sephacryl S-100 resin. The final preparation containing 1-3 mg of CK2 is checked by monodimensional SDS PAGE (Figure 2.2a) and also by Western blotting.

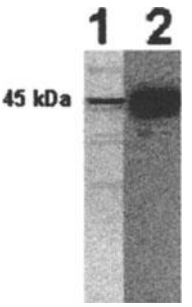

Figure 2-2a. Control of the purity of CK2α subunit kinase recovered at the last step of purification, the lane 1 show a SDS-PAGE of the sample after dialysis and the lane 2 show the same sample analyzed by Western Blotting technique (Pechkova and Nicolini; © 2002b, this material is used by permission of Wiley-Liss Inc. a subsidiary of John Wiley & Sons Inc.).

The purified protein was stored at –70 °C in 25mM Tris-HCl pH 8.5, NaCl 500 mM, 50% Glycerol, PMSF 0.2mM, 2-Mercaptoethanol 7mM, ATP 1 nM (Vergani et al., 2002). In the example later described in Chapter 4 three single point mutant (Lys10Ser, Glu27Ala, Lys76Asn) of the catalytic α subunit of *human* CK2 is expressed in *Escherichia coli* and purified according to a previously described method (Battistutta et al, 2001).

2.1.1.2 Mammalian Cytochromes

Mammalian cytochromes as the bovine P450scc recombinant here described as alternative example (Figure 2.3), is typically cloned in *E.coli* system expression: cDNA gene for mature form of P450scc was cloned in the pTrc99A vector (Amann et al., 1988) between the NcoI and KpnI sites to obtain bacterial expression of bovin P450scc (the product of CYPA11A gene). The cDNA gene of the mature protein was obtained deleting the N-

terminal mitochondrial targeting sequence coding the first 39 aminoacid residues (Du Bois et al, 1981; Perneckey and Coon, 1996). The correct orientation of the insert is confirmed by restriction mapping. The correct sequence of the insert was confirmed by the data of the sequence obtained with the automatic sequencer "Applied Biosystems" Model 373A 1.2.0 version. *Escherichia coli* JM109 is transformed with pTrc99-P450scc plasmid using standard protocol according to (Sambrook et al., 1989).

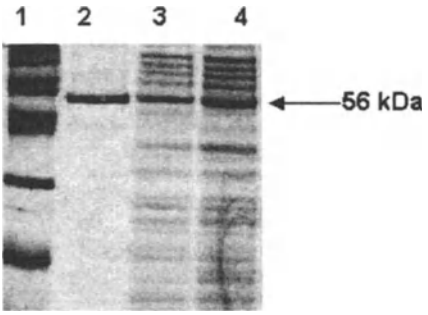

Figure 2-2b. Monodimensional electrophoresis of a recombinant bovine cytochrome P450scc (MW 56 kDa) on a SDS-polyacrilamide gel stained with Coomassie brilliant blue. Fraction from each purification step: line 1 molecular- weight marker, line 2 purified sample, line 3 fraction after DEAE column and line 4 before DEAE chromatography.

After centrifugation, expressed cytochrome P450scc can be purified by three different chromatographic steps: DEAE cellulose, hydroxyapatite and adrenodoxin-sepharose 4B columns.

The cytochrome sample was solubilized in 10 mM K phosphate buffer (pH 7.4) containing 0.1 mM EDTA, 0.2 sodium cholate and 20% glycerol. Protein concentration was determined using the BCA assay (Pierce), using bovine serum albumin as a standard. SDS-polyacrylamide gel electrophoresis (Figure 2.2b) is performed as described (Laemmli, 1970). Purified P450scc is stored at -20°C after adding cholesterol at final concentration of 20 μM (Vergani et al., 2001; Nicolini et al., 2001). Improvement in the purity level is achieved by using specific detergents or by applying the affinity resins (cholate-sefarose) to these proteins during the chromatography purification (Kastner and Neubert, 1991).

Mutant of protein can be designed *ab initio* by molecular modelling (Nicolini et al., 2001b), as the one designed to optimise thin film formation for optimal cholesterol sensing with P450scc cytochrome (Figure 2.3).

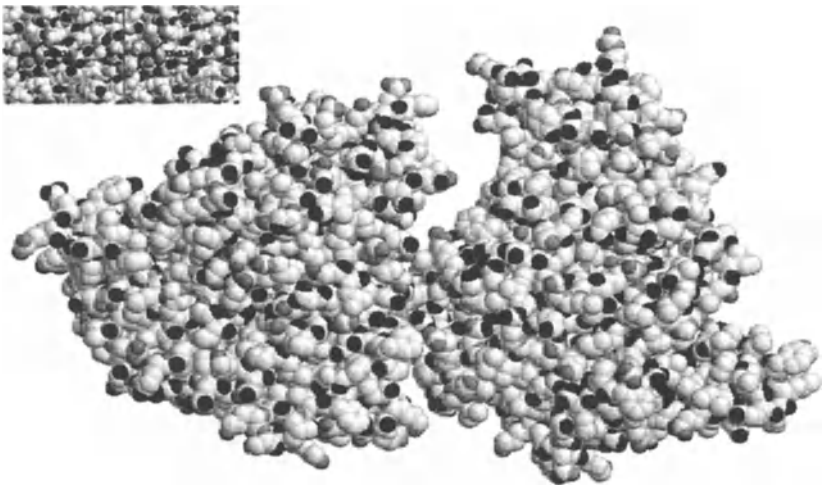

Figure 2-3. Prediction of mutation by molecular modeling. A hypothetical electrostatically-influenced complex between two molecules of cytochrome P450scc; in the inset, a fragment of the protein surface near the Glu124Ile mutation. Left, before mutation; right, after mutation.

2.2 Methods for protein identification

The identification of proteins in any given sample or biopsy has traditionally occurred by gel electrophoresis and subsequent spectrophotometry of the eluted fraction in the ultraviolet range. More recently massive identification is carried out by bidimensional gel electrophoresis followed by mass spectrometry, where the interpretation of the resulting complex spectrum is supported by the proper database. Today it is possible to find in the market an integrated mass spectrometry-based hardware and software appropriate for the automated protein identification and characterization from 2D gels. These tools are designed for the optimal sensitivity, success rate, and throughput of protein identification. The high performance of all system components, combined with a unique automated and flexible workflow control, provide an unmatched overall productivity, enabling protein identification with high success and at a minimum of running costs and efforts.

This protein identification is scalable and can be configured for use in small pilot phase studies up to full-blown industrial-scale with thousand samples per day. The high speed and the exceptional accuracy in protein

identification permit the keeping of the promises of the post-genomic era, where the quick identification of large numbers of proteins from 2D-gel arrays starts via peptide mapping. In successive steps the novel proteins of interest can be analysed in the greatest possible detail – including characterization of variations like splice variants, post-translational modifications and polymorphisms. Today these formidable challenges are met with a comprehensive proteomics platform capable of addressing all of the major analytical needs.

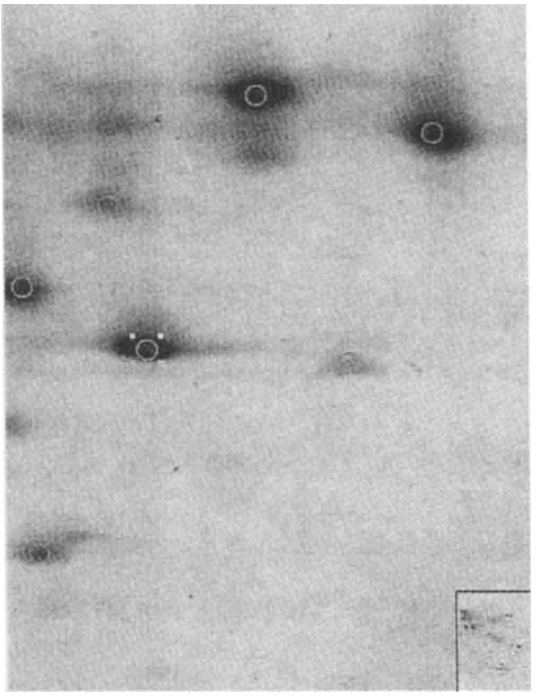

Figure 2-4. Imaging of two-dimension polyacrylamide protein gel, with the original data in the insert on the bottom corner (Bruker Daltonics Inc.).

2.2.1 Two-Dimensional Electrophoresis

While monodimensional electrophoresis is utilized to identify and purify a single protein, 2D polyacrylamide gels (Figure 2.4) is used in Proteomics for the preparation of samples containing large number of proteins for

subsequent Mass Spectrometry (MS), which is accomplished by a combination of robots performing the following sequence of events:

- gels are imaged and spots are picked to enable an automated processing capable to select the spots by m. ans of an appropriate gel matching software; alternatively this selection can also be performed manually;
- excised spots are transferred into hundreds-well plates for subsequent digestion; digestion is performed by tryptic digestion, utilizing also sample cleanup steps;
- sample preparation on MS targets utilizing about 30% of the sample and enabling at the same time on-target purification of the analyte. The remaining 70% is preserved for further analyses.

Many biological questions can be answered by analysing the qualitative and quantitative changes of specific proteins under study. These changes are visualized by comparing the protein patterns on different 2D gels, which represent the starting point for identifying the relevant proteins of interest.

2.2.2 Mass spectrometry and its principles

In mass spectrometry an organic molecule is commonly ionised by means of a beam of electrons with energy of about 75 eV.

In Figure 2.5 is represented the scheme of mass spectrometry process.

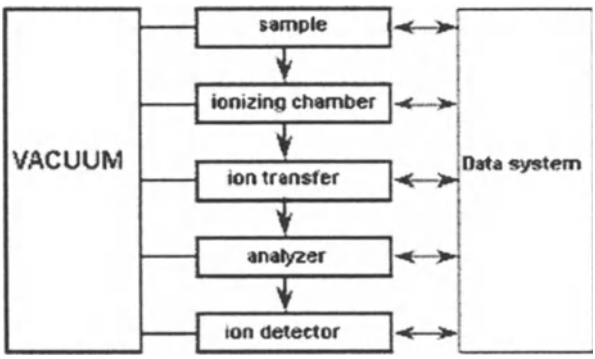

Figure 2-5. Scheme of mass spectrometry process.

The molecular ions, positively charged, partly split giving rise to molecules/neutral radicals and cations/radical cations, which are then separated and detected.

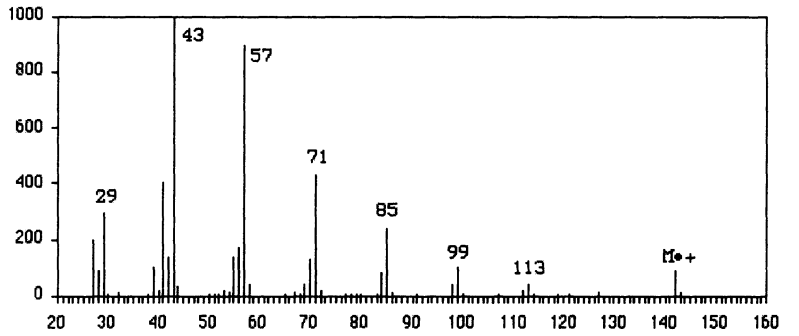

Figure 2-6. Mass spectrum of n-decane.

The signal obtained by the detector is thus transformed in a mass spectrum (as shown for n-decane in Figure 2.6). In the x axis is reported the mass/charge rate, while in the y axis is reported the relative abundance of the analysed ions. In order to obtain the spectrum of Figure 2.6 n-decane vapours have been introduced in the ionisation chamber, which is maintained at a pressure of 10^{-4} - 10^{-7} mmHg and where they interact with the electron beam.

The high vacuum is very important to avoid the collision of the formed ions with possible molecules of gases in the ionisation chamber. The molecular ion $C_{10}H_{22}(+)$ is partially decomposed according to the ionisation scheme of aliphatic hydrocarbons:

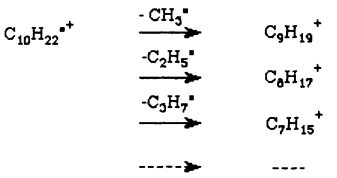

Neutral particles, like $CH_3(\ )$, $C_2H_5(\ )$, have been lost; charged particles, like $C_{10}H_{22}(+)$, $C_9H_{19}(+)$, $C_8H_{17}(+)$ and so on, are revealed in the spectrum according to their mass/charge rate.

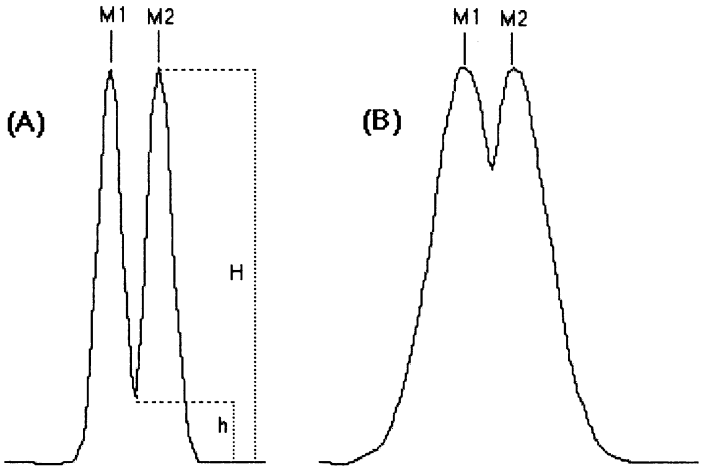

Figure 2-7. Signal resolution in mass spectrometry.

If the resolution of the mass spectrometer is good enough, it is possible to determine the exact mass of single ions from which it can be deduced the elementary composition of the ion itself. The nominal mass corresponds to the number of protons and neutrons of the isotope, while the exact relativistic mass takes into consideration also the nuclear binding energy. The measurements are calibrated assuming equal to 12 the mass of ^{12}C isotope. In summary, the mass spectrometer measures the mass/charge ratio of the ions, being thereby capable to distinguish the single isotopes of each element.

Figure 2.7 shows a simple scheme of signal resolution in two different cases. It is of immediate comprehension that in the case (A) we have a better example of signal resolution than case (B).

Nowadays, mass spectrometry techniques have an excellent resolution and represent a powerful method of analysis in proteomics.

The socalled "peptide map" is the basis for mass spectrometry-based protein identification and is obtained by the tryptic digestion of a protein which delivers peptides with masses of about 800 to 4,000 Daltons,. For the fast identification of large numbers of proteins from 2D gels, the intelligent use of available mass spectrometry (MS) technologies becomes thereby crucial and is dealt in the Chapter 5.

2.3 Methods of protein crystallization

It is well known that protein crystals play an important role in structural genomics and proteomics, but their growth appears the bottleneck for X-ray crystallography. Protein crystal growth is the most difficult and time-consuming step in the determination of a 3D protein's atomic structure. As X-ray diffraction becomes a commonly available tool in structural biology, the necessity for rational methodologies and protocols to produce single, high-quality protein crystals has come to the forefront.

The basics of protein crystallization conform to the classical understanding of crystallization of small molecules. A basic fondamental issue is how crystals are formed (Addadi et al., 2001). Furthemore, understanding the effect of solution variables such as pH, temperature, pressure, and ionicity on protein solubility allows the proper evaluation of the degree of supersaturation present in protein crystallization experiments. Physicochemical measurements such as laser light scattering, X-ray scattering, X-ray diffraction, and atomic force microscopy provide a clear picture of protein crystal nucleation and growth. This knowledge base is generating rational methods to produce protein crystals as well as means to improve the diffraction quality of such protein crystals.

In attempts to obtain protein crystals of a sufficient size and quality for structural studies, lack of knowledge of the physicochemical properties of protein solutions and of their crystal-growth behavior are the major problems for X-ray crystallographers. One of the reasons is that the physico-chemical aspects of protein crystallization process are not completely understood. Most theoretical investigations on crystal-growth phenomena have been focused on equilibrium studies, where the protein is soluble, and on the kinetics of crystal growth, which is related to both nucleation and crystal growth phenomena. Despite of progress in protein crystallography in the recent years, many proteins playing a key role in living mechanisms have not been crystallized so far. Fast development of the structural genomics and proteomics as well as drug design urgently requires a new and improved methodology to aid crystal growth. Until recently, the growth of large and well ordered crystals remained the single major obstacle in protein structural investigations by means of X-ray crystallography. While over the years the techniques for screening crystals have improved dramatically, the methods for obtaining large crystals have progressed more slowly. Although it is far easier to solve and refine structures when strong data is recorded from large crystals, many structures can today be solved from small crystals with synchrotron radiation. Extrasmall microcrystals of only a few micron in size, before unusable for the structural analysis, now can be indeed used for the

diffraction data collection by means of the third generation synchrotrons thanks to the introduction of microfocus beamline (see chapter 3).

In this chapter, we outline classical and advanced methods for protein crystallization. It is worth noticing that the division between these methods is sometimes hard to define. Many new methods which use the most advanced techniques and apparatus in terms of physical aspects are based on the same principles of classical methods (e.g. dialysis or vapour diffusion). For this reason, it may be opportune to call these methods principal methods. Moreover, many methods, like crystallization in gels and in lipid layers, or various seeding techniques being advanced time ago, now became commonly used by protein crystallographers.

We also pay attention to the physico-chemical aspects of protein crystallization. For the better understanding of the protein crystallization process general phase diagram is considered, and the importance of the solubility, supersaturation and supersaturation rate is underlined. It is also described how protein supersaturation, nucleation and growth, tightly connected in the protein phase diagram, can be now separated by the new decoupling methods.

Before beginning the discussion of crystallization methods, it is worth remembering the importance of sample preparation, since undesired heterogeneity can be an obstacle for high quality crystal nucleation and growth, and therefore, for successful structural data collection.

2.3.1. Importance of protein sample preparation

First of all, the chemicals as buffers, salts, polymers, precipitants and crystallizing agents used for the crystallization of biological macromolecules must be of purest chemical grade. All buffers and stock solutions should be prepared with distilled water and filtered with 0.22 μm minifilter. The buffers must be properly calibrated and stored at constant (4°C) temperature, because the pH of buffer is often temperature dependent. Polymers even if commercial should be purified before use.

Protein sample for crystallization have to possess the high degree of purity, homogeneity and proper concentration. Nowadays, crystallographers have a vast choice of the separation methods or their combinations, from fractionation with salt, organic solvent or specific precipitants, centrifugation or ultracentrifugation to different chromatography techniques. Ion-exchange, affinity gel permeation chromatography utrafiltration technique can be used for different steps of biological sample purification. The macromolecular impurities can be also removed by fast protein liquid chromatography (FPLC). If the protein sample contents a large amount of salts of unknown composition, dialysis of it against the large volume of well

characterized buffer of given pH can be used to remove unwanted salts and to adjust the pH. Finally, isoelectric focusing and gel electrophoresis remain favorite methods for protein separation and purification, since the fist one is extremely sensitive for the separation of closely related proteins while the last find its application as a high resolution tool for macromolecules as well as preparative technique in the final stage of protein purification.

Usually, all methods of protein crystallization requires rather high concentration of macromolecules. The choice of method for protein concentration depends on initial protein quantity. The common methods are centrifugation (e.g. by Centricon), liofilization, concentration under nitrogen pressure or dialysis, for example, against high molecular weight polyethylene glycol (PEG) solution (Ducruix and Giegé, 1999).

It is necessary to underline that protein concentration measurement can be very useful for the experiments reproducibility. For this aim absorbance measurements of diluted aliquots at 280 nm, colorimetric methods or activity tests (for enzymes). Bradford and Winterbourne assays or their modifications (Chayen, 1988; Micol and Giegé, 1989) can be also useful on this step.

2.3.2 Protein solubility and supersaturation. Nucleation and crystal growth

Protein solubility is defined as the amount of the protein (moles) in equilibrium with its crystal form at a given pH and temperature. It can be also defined as concentration of the protein in equilibrium with its crystals. This value is particularly important in protein phase diagram study.

The simple two-dimensional solubility diagram for protein crystallization is shown on the Figure 2.8. In this diagram, solubility curve (different for every protein) is plotted as function of protein solubility of precipitant (salt) concentration. However, in reality many chemical and physical parameters influence protein solubility. For example, as solubility depends on the temperature, it could increase or decrease depending of the protein. Nature and concentration of the salt or other solution components, pH, ionic strength – all these parameters influence protein solubility. Conditions corresponding to the solubility curve is saturated solution conditions.

Above the solubility curve lays the supersaturation area, where the concentration of the protein is higher than the concentration at equilibrium. Supersaturation is also defined as the ratio of the protein concentration over the solubility value. For protein nucleation, critical supersaturation of the protein solution must be achieved. Nucleation indeed present a free energy barrier which must be overcome in a specific way, which makes the crystal growth as an energetically favorable process (Feher and Kam, 1985) Nuclei

formation in protein solution is a stochastic process, including the protein interaction leading to formation of the aggregate of the critical size.

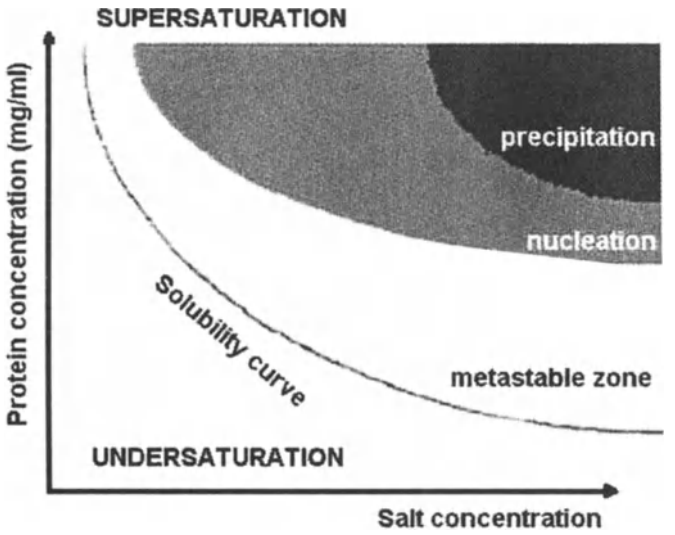

Figure 2-8. Schematic description of a two-dimensional solubility diagram showing the different zones of the super saturation domain.

At sufficient supersaturation, homogeneous nucleation can begins spontaneously when free energy barrier is overcome. On the opposite, heterogeneous nucleation occur even in lower supersaturation by inducing some surface, which can be microimpurities, dust or other particles. This fact is widely used in different protein crystallization methods, such as seeding techniques or epitaxial crystallization. Generally, any environment that favors a higher local concentration of macromolecules can induce a new nucleation point and therefore lower the nucleation energy barrier. The nucleation time of protein solution can be measured by recording the NMR spectra of crystallizing solutions as a function of time. For example, in the study of lysozyme nucleation, it is found that there is an appreciable induction time before the first nuclei appear in the solution and that this induction time depends strongly on the degree of supersaturation due to the protein concentration at a given ionic strength or due to the temperature. From the experimental data it is evident that (at least for lysozyme) crystallization under the prevailing experimental conditions is a transient process with an induction time and not a steady-state process (Drenth, 1998).

Although the phase diagrams can guide optimization of conditions for nucleation and subsequent crystal growth, our understanding of crystallization mechanisms is still incomplete. Protein-protein contacts in crystals are complex, involving a delicate balance of specific and nonspecific interactions. Depending on solution conditions, these interactions can lead to nucleation of crystals or to amorphous aggregation; this stage of crystallization can be successfully studied by light scattering. Post-nucleation crystal growth may proceed by mechanisms involving crystal defects or two-dimensional nucleation, as observed by atomic force and interference microscopy. By means of these methods it was also confirmed that impurities may play important roles during all stages of crystallization, often degrading the diffraction properties of protein crystals (Caylor et al., 1999; Durbin and Feher, 1996).

The role of contact interactions in crystallization process can be assessed by mutation of amino-acid residues on the surface, as it has been done for some membrane protein (Camara-Artigas, 2000; Nicolini et al., 2001b).

Between the solubility curve and nucleation area there is the metastable zone (Figure 2.8). Under these conditions, the protein solution is supersaturated, but the critical supersaturation for protein nucleation is not achieved. Numerical simulations of homogeneous crystal nucleation with a model for globular proteins with short-range attractive interactions showed that the presence of a metastable critical point drastically changes the pathway for the formation of a crystal nucleus. Close to this critical point, the free-energy barrier for crystal nucleation is strongly reduced and hence, the crystal nucleation rate increases by many orders of magnitude. Because the location of the metastable critical point can be controlled by changing the composition of the solvent, this study suggests a systematic approach to promote protein crystallization (Wolde, 1997).

Over the nucleation zone, precipitation area is shown (Figure 2.8). In these conditions supersaturation is very high and insoluble macromolecules undergo fast assembly in an amorphous state. However, such an experiment should not be discarded, but observed regurlarly, since the crystals may appear anyway, growing from remaining supersaturated solution.

In the attempt to understand the physical principles underlying protein crystallization, computational simulation of protein nucleation can be useful. (Pellegrini et al., 1997). Microscopic models that recognize the role of the shape of protein molecules in crystal formation can also be useful in efforts towards formulation of models that could become theoretical frameworks for the interpretation of voluminous experimental data collected on protein crystal growth (Kierzek, 2001).

2.3.3 Classical methods

There are many methods for biological macromolecules crystallization (McPherson, 1985; Giege, 1987; McPherson, 1990). The strategy used to induce crystallization of macromolecules is to bring the system very slowly toward a state of minimum solubility and thus achieve a limited degree of supersaturation. It was found a long time ago (Summer and Sommerse, 1943) that an excessive degree of supersaturation is unfavorable for crystallization. The solution that is saturated enough to yield amorphous precipitate is many times supersaturated with respect to crystals.

Among common used methods for protein crystallization dialysis methods and its variations, such as macro and microdialysis, evaporative dialysis (Bunick C, 2001) butch and microbutch methods as well as vapour diffusion methods are easy to perform and require quite small amounts of samples. (McPherson, 1989; Ducruix and Giege, 1999). Although unique in this respect, vapour diffusion methods permits easy variation of physical parameters during crystallization, and many successes were obtained by modifying supersaturation by temperature or pH changes (McPherson, 1995). Butch and vapor diffusion techniques are probably the most widely used throughout the world. Due to the simplicity of the procedure, these methods can be easily automated (Stevens, 2000). Moreover, these methods can be easily modified in different ways (see advanced methods) in order to improve crystallization or to study the influence of different factors on the crystallization. It must be reminded that these methods were first used for the crystallization of tRNA (Hampel et al., 1968).

The principle of vapour diffusion crystallization methods is indicated in Figure 2.9a. It is very well adapted for small drop volumes, down to 2µl or less. A droplet contains the protein to crystallize in buffer solution with crystallizing agent and additives is equilibrated against a reservoir, which contains a solution of crystallizing agent in a higher concentration than the droplets. Glass vessels in contact with macromolecular solutions should be treated in a way to obtain a hydrophobic surface.

Equilibration proceeds by diffusion of the volatile substances (water or organic solvent) until vapour pressure in the droplet equals the one of the reservoir. If equilibration occurs by water exchange from the drop to reservoir, it leads to the droplet volume decrease. Consequently, the concentration of all constituents in the drop will increase. For compounds with a vapour pressure higher than water, the exchange occurs from reservoir to the drop. In such a reverse system, the drop will increase as well as the concentration of the drop constituents. This last solution allowed crystallization of the $tRNA^{Asp}$ (Giegé et al, 1977) and several proteins (Richard et al., 1995; Jerusalmi and Steitz, 1997).

However, the other classical methods as batch (or microbatch) method, dialysis or crystallization by free interface diffusion (liquid-liquid diffusion) (Salemme, 1972) turned to be successful in crystallization of various proteins. In an effort to improve the size of a crystal, a strategy for a small-scale batch method in many cases yielded far larger crystal that attainable by vapour diffusion (Rayment, 2002). Variation of the chemical and physical parameters allow us to search for the optimal crystallization conditions for each protein. Temperature, pH, ionic strength, nature and concentration of the precipitant can influence on protein nucleation rate and kinetics of crystal growth by batch methods (Judge et al, 1999). The strategy of the combined precipitants turned to be also very promising (Huang, 1999).

Despite of the many proteins been crystallized by classical methods and their indispensability for initial screening procedures, classical methods in some cases can have random and irreproducible success, especially for proteins of fairly large size and/or high insolubility, like membrane proteins (Michel, 1991).

Crystallizing membrane proteins remains a challenging endeavor despite the increasing number of membrane protein structures solved by X-ray crystallography. The critical factors in determining the success of the crystallization experiments are the purification and preparation of membrane protein samples. Moreover, there is the added complication that the crystallization conditions must be optimized for use in the presence of detergents although the methods used to crystallize most membrane proteins are, in essence, straightforward applications of standard methodologies for soluble protein crystallization. The roles that detergents play in stability and aggregation of membrane proteins as well as the colloidal properties of the protein-detergent complexes need to be appreciated and controlled before and during the crystallization trials.

Usually X-ray quality crystals of membrane proteins grow from preparations of detergent-solubilized protein, where the heterogeneous natural lipids from the membrane have been replaced by a homogeneous detergent environment (Garavito, 1996).

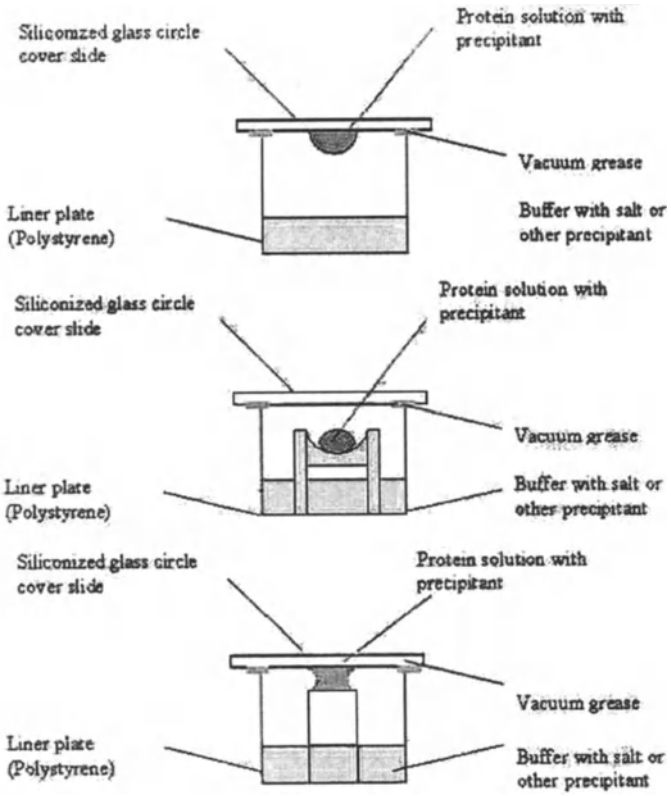
Siliconized glass circle cover slide
Protein solution with precipitant
Vacuum grease
Liner plate (Polystyrene)
Buffer with salt or other precipitant
Siliconized glass circle cover slide
Protein solution with precipitant
Vacuum grease
Liner plate (Polystyrene)
Buffer with salt or other precipitant
Siliconized glass circle cover slide
Protein solution with precipitant
Vacuum grease
Liner plate (Polystyrene)
Buffer with salt or other precipitant

Figure 2-9a. Protein vapour diffusion crystallization methods. (top) hanging drop method (Pechkova and Nicolini; © 2002b, this material is used by permission of Wiley-Liss Inc. a subsidiary of John Wiley & Sons Inc.), (middle) sitting drop method, (bottom) Protein sandwich drop vapour diffusion crystallization method (Pechkova and Nicolini 2002b).

2.3.4 Less common techniques

When classical procedures are not successful in protein crystallization, other less common techniques can be useful to prepare protein crystals for diffraction studies. For example, to make more systematic crystallization of proteins possible, ultracentrifugal crystallization, without the use of any precipitants, was used to produce data-quality crystals. This procedure can expand the range of conditions under which crystals can be grown successfully and can make new crystal forms available (Pjura 2000).

Then, various seeding techniques, (Stura, 1991) crystallization in gels as gel-acupuncture technique (Garcia-Ruiz et al., 1993; Garcia-Ruiz and Moreno 1994; Garcia-Ruiz and Moreno, 1997; Moreno and Soriano-Garcia, 1999), crystallization in lipidic cubic phase (Nollert, 2002; Gouaux, 1998) and related methods turned to be successful for a wide range of proteins.

One reason for introducing a gel in the crystallization medium of proteins is its ability to reduce convection in solution. This can lead to better nucleation and growth conditions, and to crystals having enhanced diffraction properties. Once obtained, crystals may be removed from the surrounding cubic phase mechanically, by enzymatic hydrolysis, or by detergent solubilization.

The crystalline quality of hen egg white lysozyme (HEWL) crystals grown in agarose gels and in silica gels has been characterized by measuring resolution and mosaic spread. These crystals have been compared to solution grown ones. A quasi-plane-wave X-ray topography study has also been done on some crystals. The study concerns triclinic, monoclinic, orthorhombic and tetragonal forms of HEWL. One observes that the resolution is not really changed by gelling the growth medium, even for rather high gel contents (agarose 0.5% wt/wt). On the contrary, mosaicity, characterized through reflection profile recordings allows to differentiate crystals grown by different techniques: agarose gel grown crystals are, on average, better than solution grown ones but the best crystals are obtained in silica gel. X-ray topography confirms this result (Vidal, 1999). Crystallization in gel might be used more generally to improve the quality of macromolecular crystals (Sauter, 2002).

It was experimentally proven, that metastable zone is much larger when protein solubility is very low. In such a system the nucleation rate can increase uncontrollably. In case low solubility system cannot be brought to higher solubility, seeding can be employed to grow large single crystals. Suitably pre-equilibrated metastable zone conditions are usually used for micro and macroseeding techniques. It is worth to notice that not only crystal fragment (microseeding) or single crystals (macroseeding) can be utilized, but also the precipitation material can be very useful for seeding as well as for the differentiation of amorphous precipitate from microcrystals: amorphous precipitate dissolves whereas microcrystals grow.

Such technique as crystallization in lipidic cubic phases can be very useful for the membrane protein crystallization. For example, all attempts to obtain good quality three-dimensional crystals of bacteriorhodopsin (bR) (Figure 2.9b) failed until recently when a new approach for crystallizing membrane proteins using a medium composed of lipidic cubic phases was employed (Landau, Rosenbursch, 1996). This protocol produced hexagonal plate bR microcrystals that were used for high resolution diffraction data

collection by Microfocus Synchrotron Radiation (ESRF) (see chapter 3). Crystals were fished with a small loop directly from the viscous lipidic cubic phase and frozen at 100K. Because of the small microcrystal size and the surrounding lipid phase, they were extrymely difficult to visualize and hence precisely aligned. Nevertheless, one crystal out of every 10-20 turned out to be well ordered enough to give isotopic high resolution diffraction patterns. Despite considerable radiation damage, sigle crystal of about $30x30x5\mu m^3$ produced a complete 2.5 Å data set, which led to the first high resolution model of bR obtained by X-ray crystallography Pebay-Peyroula et al., 1997).

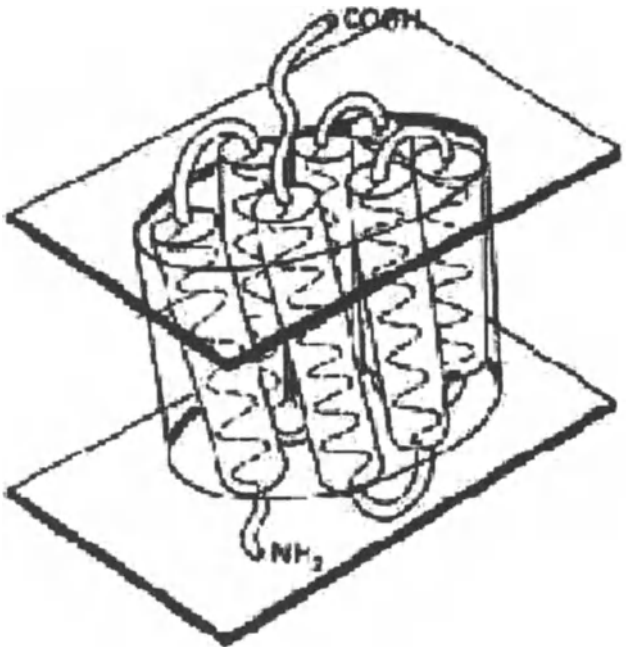

Figure 2-9b. Bacteriorhodopsin molecule.

To understand better the physical aspects of crystal nucleation and growth as well as to improve crystal quality, crystallization in different environments was also studied. Among them crystallization in magnetic (Han et al 2000) or electric or ultrasonic fields (Taleb et al., 1999, Nanev and Penkova, 2001), in centrifugation (Lenhoff et al., 1997) or under levitation. (Chung and Trinh, 1998).

Particularly, microgravity crystallization in space allows improvement in quality of the crystals. The microgravity environment of space is an ideal

place to study the complicated protein crystallization process and to grow good-quality protein crystals. Indeed, analyses of the crystallization in the space mission showed that the microgravity environment in space may be beneficial to improve size (Sygusch, 1996), external perfection, morphology, internal order, and nucleation of protein crystals. Some of these positive microgravity effects were also demonstrated by the growth of protein crystals in gelled solution. (Bi et al., 1994; Borgstahl, 2001). However, protein crystals, grown under reduced gravity conditions, can be either superior or inferior in their structural perfection than their Earth-grown counterparts (Vekilov, 1999; Chayen et al., 1999). Indeed, beside some improvement in terms of size and diffraction resolution limit for the microgravity crystals, the twinning observed in the Earth-grown crystals was also present for those grown in microgravity (Esposito, 1998). On the contrary, (or kilogravity) experimentation in centrifuges is rather unexplored method. However, also hypergravity can be regarded as variable in crystal growth. (Schlichta, 1992). After early success with tobacco mosaic virus (Wyckoff and Corey, 1939), it can be applied using a centrifuge available in any biochemistry laboratory (Pitts, 1992).

Finally, it is worth to be remembered, that nucleation and crystal growth of the macromolecules depend on supersaturation, but is also affected by the crystallization method used. Moreover, the rate of supersaturation is very important becuase it can influence the nucleation rate, which is defined as number of nuclei which appear in the unit of volume in the unit of time. The control of the nucleation rate is necessary for few large single crystals formation. Impossibility to restrain number of nuclei is the common problem to growth large single crystals instead of shower of microcrystals.

Although failure to obtain single crystal with the quality necessary to diffracrion analisys is often the consequence of problems at the growth phase, failure to obtain protein crystals at all or obtain single crystal is connected also with the difficulties during nucleation step.

Ideally, formation of a limited number of nuclei at the level of supersaturation low enough to support continued, ordered growth should occur. Moreover, the greater degree of reprodusibility in this process is preferred. For these reasons, many advanced method and techniques were recently developed.

2.3.5 Advanced methods

Advanced methods imply new techniques as well as classical method modifications for stimulation and control of the nucleation and growth or improvement of the crystal quality. It should be underlined that the physical principles of these methods remain mostly the same as in classical

crystallization methods. Many methods have been developed in the recent years, and this number is continuously increasing. We present here examples of these methods, successful for different proteins, in order to outline the variety of ideas in protein crystallization. Protein crystals are usually obtained by an empirical approach based on extensive screening to identify suitable crystallization conditions. In contrast, the aim of many of these advanced methods is not only to crystallize some individual protein, but to develop the systematic predictive procedure to obtain quality crystals.

In many studies, more then one model protein is used. Among them, the chicken egg white lysozyme is certainly leading. However, this choice also can be discussed. For example, Chayen and Saridakis noted that a series of potential heterogeneous nucleants, added to metastable solutions of lysozyme and of four other model proteins, as well as to a few target proteins, markedly affected the nucleation of lysozyme crystals, but did not influence the other proteins (Chayen and Saridakis, 2001).

2.3.5.1. Control of crystal nucleation and its decoupling from crystal growth

The ultimate way to control the crystallization process is to separate the phases of nucleation and growth. Methods to achieve this, other than seeding, involve changing the temperature (Rosenberger, 1993; Haire, 1996, Blow et al., 1994), e.g. incubating a sample at one temperature, where nucleation is occur, and than changing the temperature to conditions where there is growth but no nucleation. Other methods concern diluting of a nucleation sample, for example, microbatch drop after incubating them for a given time at spontaneous nucleation conditions (Saridakis et al., 1994). Dilution has also been adapted to vapour diffusion with similar results. This simple method for growing protein crystals in the metastable zone based on the vapor diffusion technique is described by Saridakis and Chayen. The coverslips holding the hanging drops are transferred, after being incubated for some time at conditions normally giving many small crystals, over reservoirs at concentrations that normally yield clear drops. Fewer, much larger and better diffracting crystals are obtained, compared with conventional crystallization at similar conditions (Saridakis and Chayen, 2000). These techniques have yielded improved crystals, but were very time-consuming, since many processes of trial and error were required to determine the right time at which to dilute (the time scale could only be guessed by reference to the time which it took to see the first crystals). Consequently these methods have not yet been adopted for routine use.

For both the dilution and temperature approaches, the most effective moment to intervene with a crystallization experiment (i.e. change the conditions) is soon after the formation of the first critical size nuclei which

will eventually form the crystals. However, by the time nuclei or crystals can be observed under the microscope they have already reached a size of approximately 2-5 microns and by then it is too late to act, since too many nuclei are likely to have formed. In this case Dynamic Light Scattering (DLS) can be applied in a very practical way to determine the time in which to intervene with a crystallization experiment and lead it from nucleation to growth conditions, since the time at which DLS showed a significant change in the size-distribution profile of compounds in solution, corresponded to the time at which the solution can be effectively transferred to metastable conditions, for optimal growth (Saridakis and Chayen, 2000).

Other methods for nucleation and growth decoupling can be also used, for example, double thermal pulse technique (Tsecova, 1999) or step gradient diffusion. This last experiments consist of first exposing protein solutions in diffusion wells for brief periods to initiating buffer solutions of high precipitant concentrations to induce nucleation followed by exposure of the same protein solutions to solutions of lower precipitant concentration to promote growth of induced nuclei into crystals. The two-step approach dissociates nucleation events from crystal growth allowing parameters affecting nucleation kinetics such as time, precipitant concentration and temperature of nucleation to be varied separately from conditions used for post-nucleation growth. This technique was successfully applied in the low gravity conditions, allowing to avoid convective disturbances that occur when solutions of discrepant densities are interfaced at normal gravity (Sygusch, 1996).

2.3.5.2 Stimulation of crystal nucleation

As nucleation is the necessary first step in the crystallization process, which also influences it decisively, many efforts have been done to stimulate protein nucleation by seeding, epitaxy, charged surface or mechanical means. Numerous studies attempt to find the substances (nucleants) which can induce efficient nucleation of protein crystals in the controlled manner. (Chayen, 1993; Blow, 1994). For example, heterogeneous and epitaxial nucleation of protein crystals on mineral surfaces (McPherson and Shlichta, 1988). Fifty different mineral samples were tested as potential heterogeneous or epitaxial nucleants for several commonly crystallized proteins. It was found that for each protein there was a set of substrates that promoted nucleation of crystals at lower critical levels of supersaturation than required for spontaneous growth. In all investigated proteins (canavalin and concanavalin from jack bean, beef liver catalase and hen egg white lysozyme) were observed modifications of crystals habit and, in some cases unit cell properties promoted by the presence of the mineral nucleants. Particularly, in the case the growth of lysozyme on the mineral apophyllite,

it was shown by lattice analysis and x-ray diffraction that the nucleation and growth of the protein crystals on the mineral was likely involved in a direct lattice match.

Epitaxial growth of three-dimensional protein crystals can be seeded by two-dimensional crystals formed on lipid layers. Crystals suitable for X-ray crystallography can be grown in this way more rapidly, and using substantially lower concentrations of protein and precipitants, than when using conventional methods (Darst, 1995). This approach may allow the crystallization of proteins that resist attempts at crystal growth by other means (Edwards, 1994). Although, two-dimensional (2D) crystals of proteins on lipid monolayers can initiate the formation of large three-dimensional (3D) crystals suitable for X-ray diffraction studies, the role of the 2D crystals in this process has not been firmly established. While it is likely that the 2D crystals serve as nuclei for epitaxial crystal growth, other mechanisms, such as non-specific nucleation induced by the high local concentration of the protein at the surface of the lipid layer, cannot be excluded. (Hemming, 1995). Various other attempts to induce nucleation on irregular or rough surfaces, or surfaces of special composition. For example, polylisine, plastic, chemically modified mica sheets – many materials have been tasted as heterogeneous nucleants surface (Chayen, 2001). It was also found that the number of nuclei, adhesion and preferred orientation of lysozyme crystals during heterogeneous nucleation, is influenced by changing the chemistry of the substrate (Tsekova et al., 1999). The following surface modifications were used: bare glass surface, negative charges being present on it in water, siliconized (rendered hydrophobic) surfaces, surfaces rendered hydrophobic by means of hexamethyl-disilazane (coverage by –CH3 groups), glass metallized by the evaporation of Cr or Ag, surfaces treated with poly-L-lysine (positive charges are present on the surface). The last one being especially important since lysine residues participate in two of the three strongest lysozyme intermolecular bonds, denoted as *X* and *Z* (Durbin and Feher, 1990).

Chemically modified mica sheets have been also tested as heterogeneous nucleants surfaces for lysozyme, concanavalin A and thaumatin, by hanging drop vapour diffusion technique modification Smooth mica surfaces with reduced hydrophilic properties and different density of ionisable groups have been prepared by a silanisation reaction using mixtures of n-propyltriethoxysilane and 3-aminopropyltriethoxysilane in different percentages starting from 0 to 100% of aminosilane. The results suggest that these mica surfaces act as heterogeneous nucleants agents, whose effectiveness is due to non-specific attractive and local interactions between charged residues of the protein and the ionisable groups on the mica surfaces (Fermani, 2002).

Then, polymeric films containing ionisable groups, such as sulfonated polystyrene, cross-linked gelatin films with adsorbed poly-l-lysine or entrapped poly-l-aspartate and silk broin with entrapped poly-l-lysine or poly-l-aspartate, have been tested as heterogeneous nucleant surfaces for proteins. In this study, concanavalin A from jack bean and chicken egg-white lysozyme were used as models. It was found that the crystallization of concanavalin A by the vapor diffusion technique is strongly influenced by the presence of ionisable groups on the film surface. Both the induction time and protein concentration necessary for the crystal nucleation decrease whereas the nucleation density increases on going from the reference siliconized cover slip to the uncharged polymeric surfaces and even more to the charged ones. Non-specific attractive and local interactions between the protein and the film surface might promote molecular collisions and the clustering with the due symmetry for the formation of the crystal nuclei. These results suggest that the studied polymeric film surfaces could be particularly useful for the crystallization of proteins from solutions at low starting concentration, thus using small quantities of protein, and for proteins with very long crystallization time (Fermani 2001).

A different approach, involving the use of mesoporous materials that is likely to constraint protein molecule and thereby encourage them to aggregate in the crystalline order, can be applied. For example, large crystals were obtained using porous silicon at conditions that are not sufficient for spontaneous nucleation. The size distribution of pores in the specially designed porous silicon plays a critical role in this process (Chayen et al., 2001).

2.3.5.3 Advances in crystal growth

The crystal growth stage is also continuously improving but, in spite of significant progress, still remains the slowest critical step in protein structure determination.

It have been proved that solubility and supersaturation of proteins is influenced by hydrostatic pressure. Advantage has been taken of this fact to crystallize proteins at high pressure (Visuri et al., 1990; Lorbet et al., 1996). Effects become significant for pressures higher than 50 Mpa (500-fold atmospheric pressure) as shown for lysozyme crystals that can be grown in the range 50-250 Mpa. Such crystals exhibit habits different from controls grown at atmospheric pressure and diffract at high resolution (Lorber et al., 1996). However, the method has only been occasionally used in the macromolecular field.

Undesired heterogeneous nucleation, which is often detrimental to the production of suitable crystals for X-ray diffraction, can be induced by the contact of a crystallization sample with the walls of its supporting vessel.

The floating drop method enables crystallization of biological macromolecules under conditions where the crystallizing solution has no contact with the containers wall (Lorber and Giegé, 1996; Chayen, 1996) Drops (5-100μl) are placed at the interface between two layers of Inert and non-miscible silicone fluids or oils contained in square glass or plastic cuvettes, thus realizing 'container less' environment for the growth of protein crystals (Chayen, 1999).

Microbatch crystallization under oil, a new technique allowing many small-volume crystallization trials has been introduced by Chayen and coworkers, describing the approach to rapid protein crystallization using very small samples. A computer controlled precise micro dispenser is used to make crystallization samples (1–2 μl) as microbatch droplets under oil. Thus, the samples are protected from evaporation, contamination and physical shock by the oil. When favorable conditions for crystallization have been found using one mode of the system, the size and quantity of crystals are optimized by a second program which generates a set of conditions throughout the area of interest. Crystals of diffraction size and quality have been grown in 1 μl drops. (Chayen, 1992). Several proteins and spherical plants virus were crystallized using this method. Its main advantage is to reduce the nucleation rate. Since the drop is not in contact with air, the method may be convenient for crystallizing proteins sensitive to oxidation.

In spite of recent advances in protein crystallization, such as surface response methods for optimizing crystal conditions (Carter, 1997) or the modification of charged residues (Rayment, 1997) and also crystallization at elevated temperature, which can increase the rate of crystal growth (Han and Lin, 2000), crystal growth remains the slowest step in protein structure determination.

2.4 Methods of crystal structure determination

The prime method of protein crystal structure determination is the X-ray crystallography based either on the traditional diffractometer or, more recently, on the Synchrotron Radiation being built in few avanced facilities world-wide (see Chapter 3). Electron microscopy still represents an alternative option in few selected cases as discussed later.

2.4.1 Protein X-ray crystallography

The scattering diffraction of X-rays is an interference phenomenon and the interference between the X-rays scattered from the atoms in the structure produces significant changes in the observed diffraction in different directions. This variation in intensity with direction arises because the path

differences taken by scattered X-ray beams are of the same magnitude as the separation of the atoms in the molecule; in other words, to 'see' the individual atoms in a structure it is necessary to have an incoming radiation of a wavelength similar to the interatomic distances, typically 0.15 nm or 1.5 Å. Radiation of this wavelength lies in the X-ray region of the electromagnetic spectrum. It is to be underlined that it is the electrons which scatter the X-rays and so what is in fact observed is the electron density of the sample. Because the electrons cluster round the atomic nuclei, regions of high electron density correspond to the atomic positions. (Ducruix and Giegé, 1999).

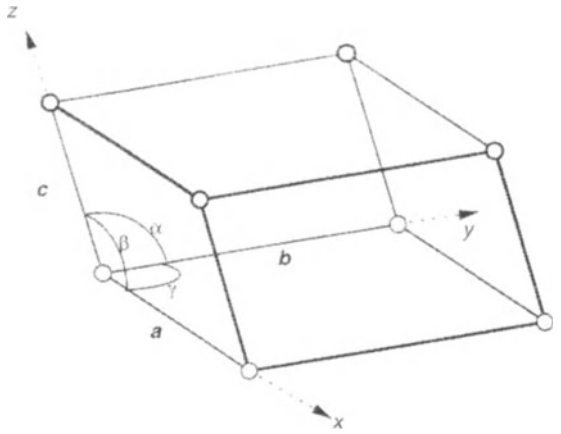

Figure 2-10. The unit cell specified by three lattice translations whose lengths are a, b and c. The angles between them are α, β, and γ.

Since crystal is a regular, repeating array of atoms or molecules in three dimensions, it is convenient to describe such an object with the aid of lattices, which is a geometric construction defined by three axes and the three angled between them. Along each axis direction; a point will repeat at a distance referred to as the unit translation or unit cell repeat and labelled, ***b***, and ***c***, respectively (Figure 2.10). The angles between ***b*** and ***c***, ***a*** and ***c***, and ***a*** and ***b***, are α, β and γ, respectively. The basic building block of a crystal, then, is a parallelepiped described by dimensions ***a, b, c*** and α, β, γ and called the unit cell. There are seven crystal systems which arise from the possible combination of these unit cell parameters. To simplify, crystallographers adopt the convention that the unit cell to be is chosen is one with angles nearest to 90°. Such a cell with only one copy of the molecular structure is called primitive one.

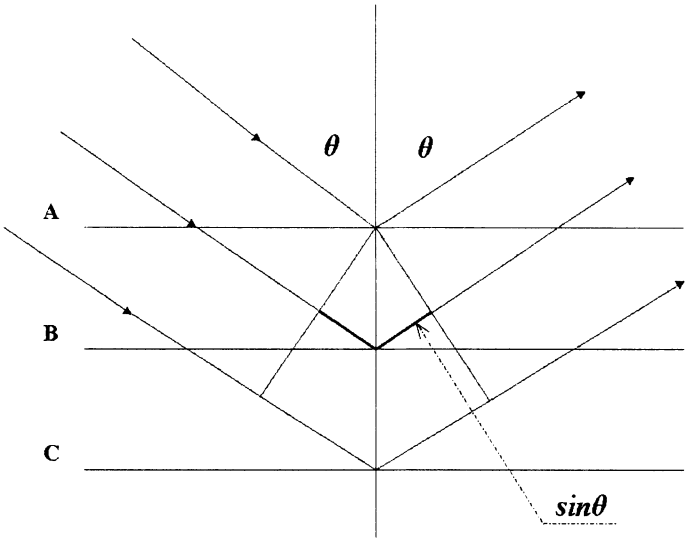

Figure 2-11. X-rays reflected from lattice planes A, B, C. To observe a scattered beam of X-rays in direction R, the thickened path must be equal a whole number of wavelength.

Although the basic building block of a crystal is the unit cell and the lattice produced by its repetitions a characteristic symmetry, within the unit cell there may be further symmetry. For example, the molecule itself may have symmetry about an axis, which is either a proper rotation of 360°, 180°, 120°, 90°, 60° only or an improper one, which involves 'inversion' through the point. Proteins are made up of L-amino acids and nucleic acids have a chiral ribose unit which preclude centers of mirrors.

The combination of this symmetries and the crystal systems leads to the 32 point groups or crystal classes, of which only 11 can accommodate protein molecules. Then, it can be shown mathematically that here are only 230 combinations of symmetry elements (threefold, twofold axis, etc.) possible in three dimensions.

Thus, any crystal must have a unit cell which conforms to one of this combination, its space group. Because all proteins and nucleic acids crystals comprise the optical isomer, there are only 65 space groups available for such chiral molecules.

The explanation of how X-rays are scattered by crystals is largely the result of the Bragg low (Bragg, 1968). Considering a crystal lattice,

represented in Figure 2.10 by rows of points A, B, C, for X-rays X2 scattered from row 2 to enhance those scattered from row 1, X1, there must be an integral number of wavelengths difference (Figure 2.11). The relationship between the spacing of the rows, ***d***, the wavelength λ, and the angle at which the emergent ray is observed relative to the direction of the rows, θ, is:

$$n\lambda = 2d \sin\theta$$

Thus, as Bragg pointed out, X-ray diffraction can be regarded as a reflection of the beam of X-rays from the planes of points in the crystal lattice. Provided there are the large number of plains contributing to the interference, the position in space in which are given reflection is observed is highly defined. These positions are defined by the crystal lattice and since very few, if any; atoms actually lie on the lattice points, the scattered intensity is modulated by the atomic arrangement within the unit cell. Therefore, the directions of a diffracted ray is defined by the crystal lattice, the intensity of the ray depends upon the atomic arrangement within the cell. One further point concerns ***n***, the order of diffraction, which is the number of wavelengths difference between the scattering from adjacent planes; the higher the order, the larger the angle of scattering. Alternatively, the scattering can be considered as arising from planes which are closer together: e.g. using the equation above, it can be seen that a reflection at θ can be considered either as ***n***th order from planes of spacing ***d***, or the first order from planes spacing ***d/n***. The latter approach is generally adopted by crystallographers.

2.4.2 Crystal structure determination

A diffraction pattern for a protein crystal contains many reflection which must be appropriately indexed and the most convenient system is to use the order of diffraction with respect to each if the unit cell axes. It is important to underline that each reflection contains the contribution from every atom in a crystal, and, conversely, each atom in the crystal contributes to every reflection. Thus, as the crystal is moved about in the X-ray beam, reflections can be recorded when the geometrical arrangement of X-ray beam, crystal orientation, and detector satisfied Bragg's low.

Crystal produces a diffraction pattern which needs to be recombined in the correct phase relationship, but in the case of X-rays, no lens exist which is able to perform this task and in recording the pattern the vital phase information is lost. Phase for each reflection must be calculated and this phase problem is central for crystallography. Whilst this problem may seem

insuperable, if the position of only few heavy atoms are known, whether these are added by soaking into crystals in the traditional way or introduced during protein biosynthesis with selenomethionine, their contribution can be calculated and this is generally sufficient to solve the phase problem for a protein: It should be pointed out that molecular replacement (Rossmann, 1990) is applicable where a similar structure already exist and this is increasingly found to be the case (AMORE programs, etc.).

A phase must be calculated for each reflection to be included in the calculation of the electron density map. The more reflection that are phased and included, the clearer the map will be and the better will be the resulting model of the protein. Thus the resolution of the data is usually reported and this refers to the minimum plane spacing included in the calculation. For example, for a 3.5 Å map, all reflection with plane spacing greater than or equal to 3.5 Å will be included. The higher the resolution, the greater the amount of X-ray data which be measured. Disregarding the symmetry of the reflection data, the total number of reflections is approximately $5V/d^3$, where V is the unit cell volume and d is the resolution.

The aim of the preliminary X-ray investigation should be to determine the unit cell dimensions and the space group. It is surely needed to solve the crystal structure, but is also dictated by the strategy for efficient data collection. The amount of data to be collected is determined by the diffraction symmetry of the crystal and it is often possible to reduce the number of exposures by ensuring that he crystal is mounted in particular way.

It is also normal practice to determine the volume occupied per unit molecular weight (V_m, often called the Matthews' coefficient) since this can be used to determine the number of molecules in the asymmetric unit. V_m has been found to be around 2.4 $Å^3$/dalton for globular protein crystals, although this value is subject to quite large fluctuations (Matthews, 1968).

It is obtained by dividing the unit cell volume by the product of the protein MW and the number of equivalent positions (asymmetric units). The approximate solvent content (V_{sc}) can be calculated from the formula:

$$V_{sc}(\%) = 100(1-1.23/V_m)$$

2.4.3 Data collection and data processing

Most data collection nowadays is done by the oscillation methods (Wonacott, 1977) with some sort of detectors, mostly imaging plate systems. Recently, the development of the charge coupled device (CCD) has provided the sensitivity and dynamic range of imaging plate but has eliminated the time consuming scanning step typical for phosphor-imaging plate

technology. Whatever device is used for data collection, however, the oscillation method remains the technique of choice. Unlike the precession methods, is not necessary and indeed is undesirable that the crystal be perfectly aligned before data collection start.

The crystal is rotated through a small angle (0.1-0.5) about an axis perpendicular to the X-ray beam. Several passes or oscillation trough the rotation range minimize the effects of fluctuation of X-ray intensity. Provided the rotation angle is not too large, adjacent levels will not overlap and data from many layers can be collected on each image.

The size of the oscillation range is chosen depending on the detector, crystal cell dimension, lattice type, properties of incident X-ray beam and crystal mosaic spread.

Maximum permissible rotation angle:

$$\Delta\phi < (dmax/q)180/\pi - \Delta$$

where:

dmax is the maximum resolution for which data are required;
q is the spacing of planes perpendicular to the X-ray beam;
Δ is the reflecting range of crystals, or mosaic spread.

After data collection, data processing package exist to measure intensities. A series of frames is read and a peak search procedure records the position of strong, well-defined spots to be used in autoindexing.

The unit cell dimensions, the crystal orientation and the crystal-to-detector distance are modified to obtain the best fit of predicted to observe pattern. The autoindexing routing employed by DENZO uses a different algorithm coined real space indexing whereby a complete search of all possible indices of reflection is carried out using Fast Fourier transform.

Ones the three best linearly independent vectors with minimal unit cell volume are found, the cell is reduced to describe a standard basis for description of the unit cell. When a basic set for each of 14 Bravais lattices is found and distortion index is calculated for the peaks, the decision about most likely cell dimensions and space group can be done.

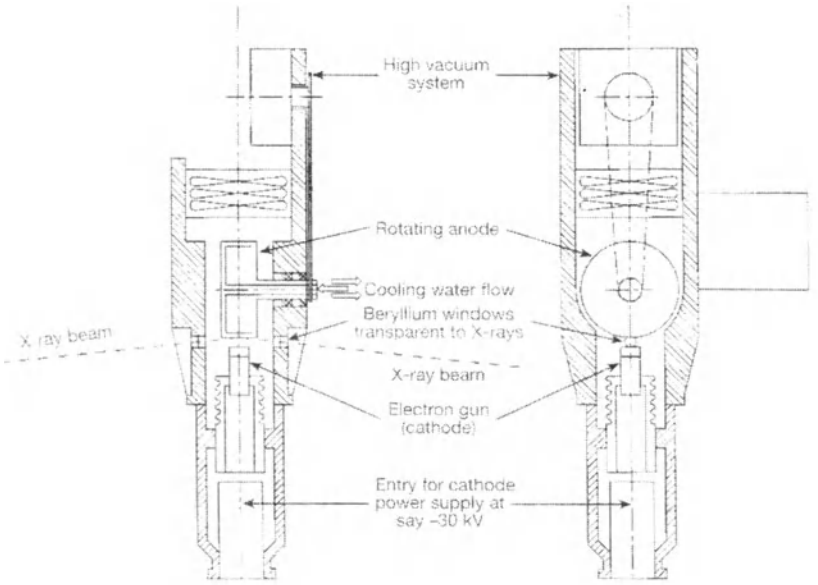

Figure 2-12. Schematic drawing of a rotating-anode X-ray generator (courtesy of Bruker Nonius B.V., Delft, The Netherlands).

2.4.4 Traditional X-ray diffractometer

The highest degree of resolution down to the angstrom level can be achieved by X-ray radiation of similarly small wavelength (Bacon, 1966; Nicolini, 1986). The way in which the regular three- dimensional structure of perfect protein crystals is determined at an atomic resolution with X-rays can be understood by the simple one-dimensional analogy previously described, namely the optical diffraction grating formed by a single row of atoms. The spectra from such a grating, illuminated by parallel monochromatic light, occur at given angular positions, which are dependent on the regular distance (period) between the centers of neighboring lines, and with given distribution of intensity among their different orders, which depends on the width and transmission function of the individual lines. The distribution of energy among the different orders (n) of spectra is the Fourier transform of the transmission factor of the grating line.

This led to the development of X-ray diffractometer, as the one constructed by Bruker (Figure 2.12) utilized in our experimentation with the lysozymes (described in Chapter 4) to find the size and shape of the unit of pattern and the details of the atomic arrangement of this unit. Diffraction pattern of a crystal of lysozyme grown from a solution of lysozymes in presence and absence of the thin film template of homologous proteins were subsequently taken at the diffractometer. A single frame, shown in the first subchapter of Chapter 4, corresponds to a rotation of 0.25 degrees, with a graphite crystal-to-film distance of 75 mm and an angle of -15 degrees.

2.4.5 Electron Microscopy

Whenever protein crystals have a size insufficient for X-ray diffraction analysis and are just visible in a light microscope at several hundredfold magnification, as it is very frequently the case, electron microscopy can be successfully employed to obtain low resolution image of 10 to 20 Å (McPherson 1989). The most common method for obtaining a good image of the protein in the crystal is to apply the classical negative staining procedure followed by photography under the electron microscope (Beeston et al., 1973). Occasionally by further applying digital or optical filtering techniques to crystal micrographs, some more information can be obtained about the size, shape and structure of the protein down to a level near 5 Å, also in terms of crystallographic parameters such as the space group and the hydrated unit cell dimension as well as the packing arrangement of the protein under study in the lattice. The atomic resolution can instead be readily reached at the 3D level by Scanning Probe Microscopy as it will be shown in the later chapter on the surface of cytochromes microcrystals (Pechkova and Nicolini, 2002a). In the past a three dimensional structural approach near atomic resolution (around 6 Å) has also been attempted by a sophisticated extension of electron microscopy of 2D crystals through Fourier analysis at different angles (Matricardi et al., 1972).

2.5 Other methods of protein structure investigation

2.5.1 Circular Dichroism measurements

Circular Dichroism (CD) spectra are recorded on a spectropolarimeter. The instrument must be first calibrated using (+)-10-camphorsulfonic acid. All spectra were recorded, in our laboratory, with a Jasco spectropolarimeter in nitrogen atmosphere at room temperature using 0.05 cm path-length quartz cell. Each spectrum represents an accumulation of ten scans over 260-

180 nm. The data were collected at a rate of 20 nm/min with a wavelength step of 0.2 nm and a time constant of 2 s. No filtering for noise reduction was applied. The spectra are corrected for the baseline and normalized for the aminoacidic concentration in order to obtain Molar Ellipticity values. The data are converted into ASCII format using JASCO software. The CD spectra are analyzed in terms of contribution of secondary structure elements using different methods based on comparison with CD spectra of proteins and peptides with known secondary structure (Carrara et al, 1992).

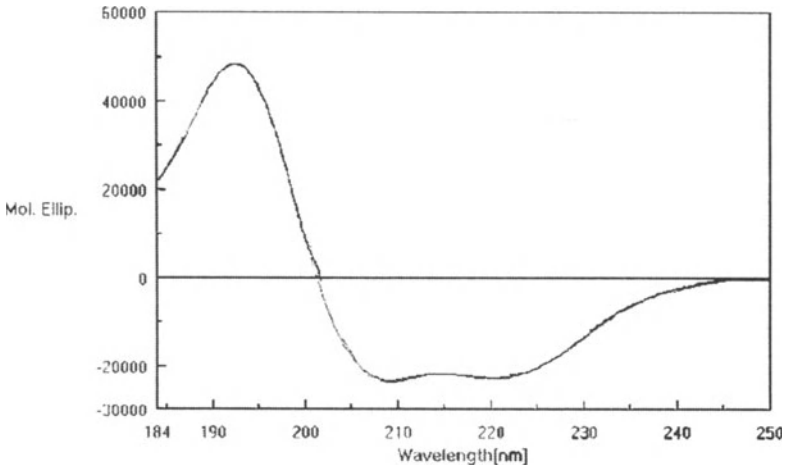

Figure 2-13. CD spectra of cytochrome P450scc.

For each protein the best results can be obtained by using a program where a CD spectrum is analyzed as a linear combination of 16 original proteins used by Provencher and Glockner (1981) as references plus poly-L-glutamate suggested by Sreerama and Woody (1994) as standards. The conformations are calculated according to the method of Kabsch and Sanders (1983). In this way contributions for alpha-helix, turn, bend and coil were obtained. Alternatively (Carrara et al., 1992), the CD spectra can be analyzed using VARSELEC program. In the variable selection method (VARSELEC), the spectra database contains 33 proteins but unimportant variables can be removed from an underdetermined system of equations so that it is possible to solve for the important ones.

Moreover, the CD data were compared to the predicted ones by using AGADIR, a prediction algorithm based on the helix/coil transition theory. AGADIR predicts the helical behavior of peptides; conditions such as pH, temperature and ionic strength are used in the calculation. The average

deviation of the prediction from experimental values (obtained from CD measurements) is 2 percent in helical content, with a standard deviation of 6 (percent in helical content).

Figure 2.13 and Figure 2.14 show the CD spectra respectively of cytochrome P450scc and of polypeptides with different percentage of secondary structure.

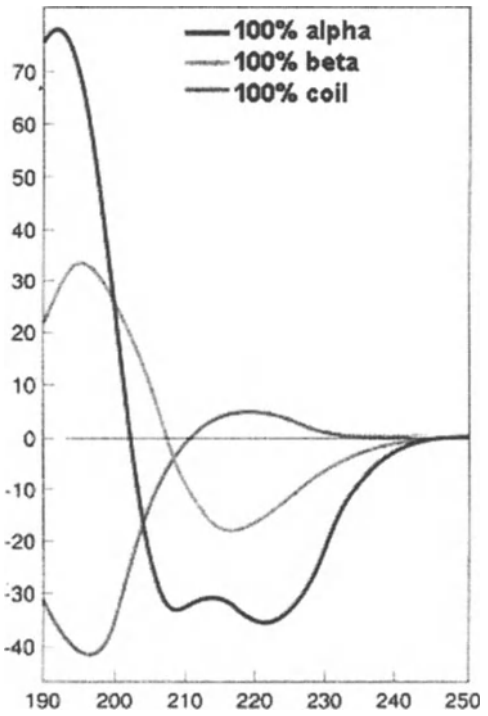

Figure 2-14. CD spectra of proteins of different secondary structure.

2.5.2 High Resolution Nuclear Magnetic Resonance

The higher order structure at atomic resolution can be determined in solution by high resolution NMR only for proteins with molecular weight smaller than 30.000 daltons, as for the case here exemplified (human histone H1 chromosomal protein, thioredoxin from Bacillus acidocaldarius). ^{1}H NMR experiments were in our laboratory recorded on Bruker AMX 500 MHz Advance on a Silicon Graphics SGI Mod. O2 (S.O. IRIX 6.3), with

time proportional phase incrementation (TPPI) for quadrature detection in the F1 dimension. The probe temperature is usually mantained at 300 K and the water suppression is carried out using the DPFGSE scheme.

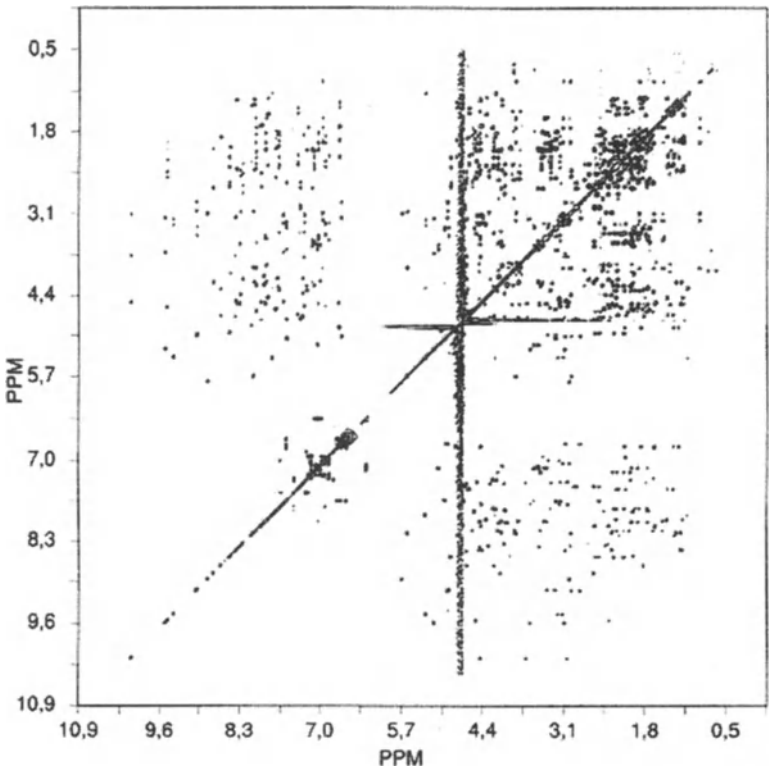

Figure 2-15. Contour plot of ^{1}H-TOCSY sensitive to the phase at 600MHz for basic protein trypsi inhibitor (BPTI) in H_2O.

Two-dimensional TOCSY and NOESY experiments are performed by the pulse sequences in the phase sensitive modality (Roberts, 1993).TOCSY (Figure 2.15) and NOESY (Figure 2.16) spectra were recorded with respective mixing time of 35 and 300 ms for spin system and sequential assignments (Wuthrich, 1986; Bartolucci et al., 1997; Nicolini et al., 1995).

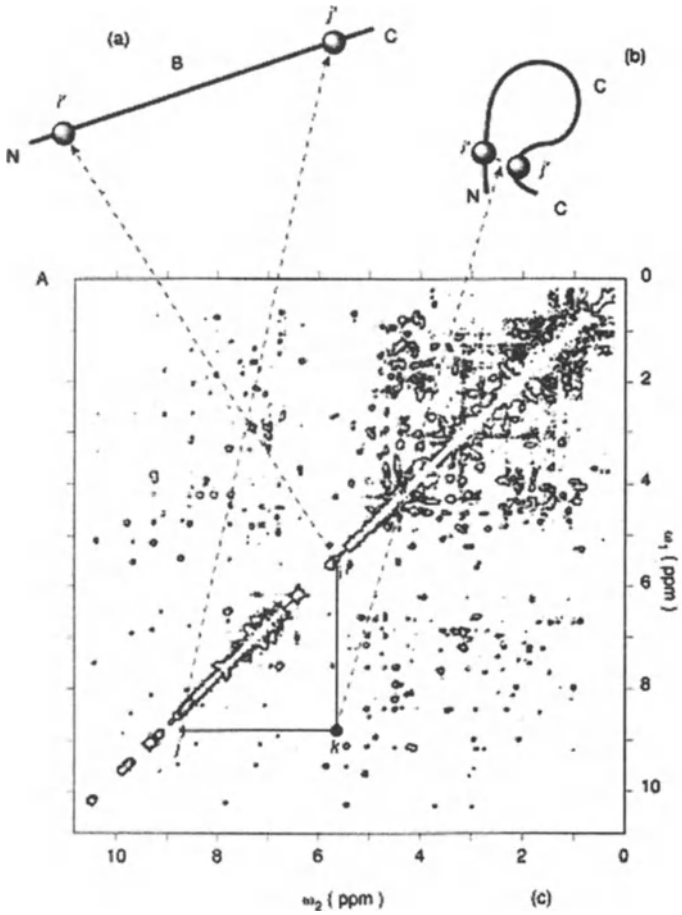

Figure 2-16. Example of NMR determination of protein structure solution. (A) Contour plot of NOESY spectrum t 500 MHz of BPTI. Crosspeak K is connected to diagonal i and j diagonal peaks; (B) In the peptide chain, the dotted lines connect protons i and j to the corresponding diagonal peaks. (C) Curves imposed to the polypeptide chain from the magnetization transfer (Nuclear Overhauser Effect, NOE) between i and j protons there separated by less then 5 Å.

In TOCSY experiments using a MLEVTPDG spinlock sequence a mixing time of 75 ms was applied to obtain remote scalar connectivities. The spectral width was about 12 ppm.

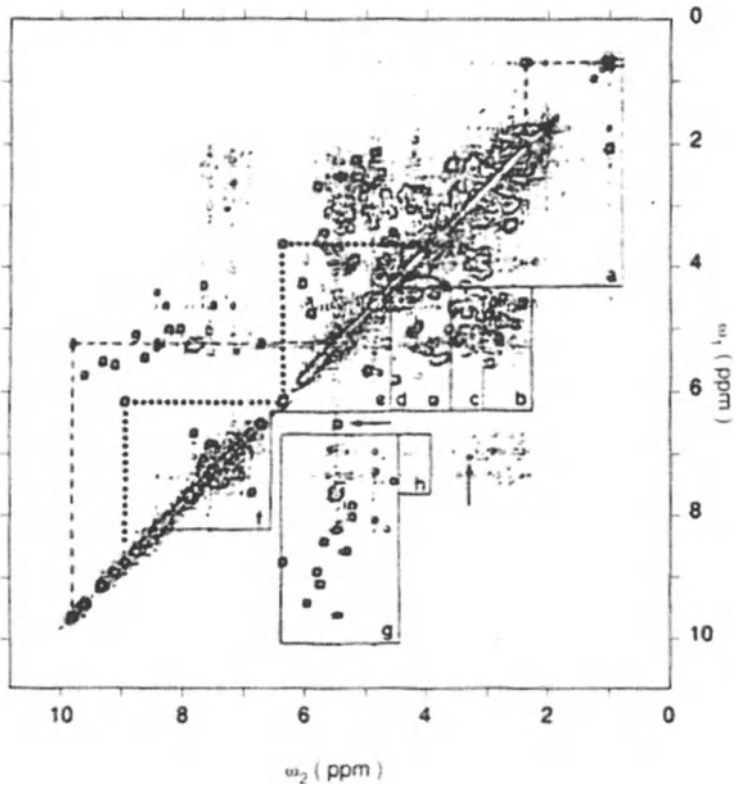

Figure 2.17. Contour plot of ^{1}H-COSY of a protease inhibitor solution. Above the diagonal, dotted lines isolate connectivity regions among diagonal cross peaks. Below the diagonal the dotted lines region containing cross peaks among distinct protons.

For two-dimensional experiments (Wuthrich, 1986), the F2 dimension was zero-filled to 2048 real data points, F1 dimension was zero-filled to 1024 data points.

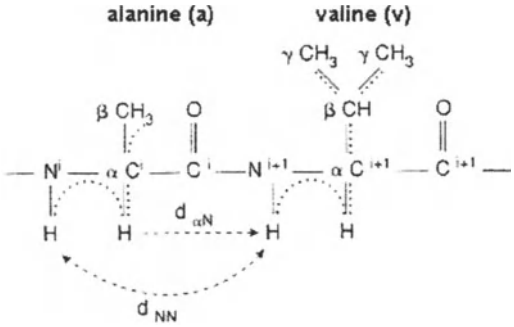

Figure 2-18. Sequential specific assignment. In the dipeptide Ala-Val, dotted lines represent ^{1}H-^{1}H connectivity established by spin-spin scalar coupling via COSY. The arrows point to protons in sequential residues obtained via NOESY, namely short sequential distance $d_{\alpha N}$ (between CαH and ammino protin of the following residues) and $d_{\alpha N}$ (among amminic protons of the adjacent residues).

For each protein, by combining data from COSY (Figure 2.17) and TOCSY experiments we defined the complete amino acid spin systems; from NOESY spectra, the sequential specific assignment is performed as shown in Figure 2.18.

The NOESY spectra were processed with a Lorentzian-Gaussian apodisation. Standard offset subtraction and baseline correction were applied in the time and frequency domains, respectively. All spectra were zero filled to either 512 or 1024 points in the t1-dimension prior to FT.

The structure determinations were performed for both the thioredoxin (Bartolucci et al., 1997) (Figure 2.19) and the histon protein using Discover_3 and InsightII softwares (Molecular Simulations Inc.) on a Silicon Graphics SGI Mod. O2 workstation. Structures were generated using a restrained dynamics simulated annealing protocol and refined by energy minimization (Karplus and Petsko, 1990; Koradi et al., 1996).

The energy of the system was calculated with the cvff forcefield with no cross-terms included into the energy expression. The energy of the system was minimized first with 500 step of "steepest descents", followed by 1000 steps of "conjugate gradients" to remove any strain in the starting conformation of the peptide. NOE cross-signal were analyzed in terms of peak volumes and classified into three categories: strong, medium and weak NOEs corresponding, respectively to internuclear distance of 2.0-2.5Å, 2.5-3.0Å, 3.0-4.0Å. A total of several hundreds distance constraints were derived from NMR experiments.

The following protocol was used for restrained molecular dynamics calculations and simulated annealing. The molecule was heated to a temperature of 1000 K and equilibrated at this temperature for 5 ps. The molecular dynamics trajectory was sampled every 100 fs to generate a total of 500 structures.

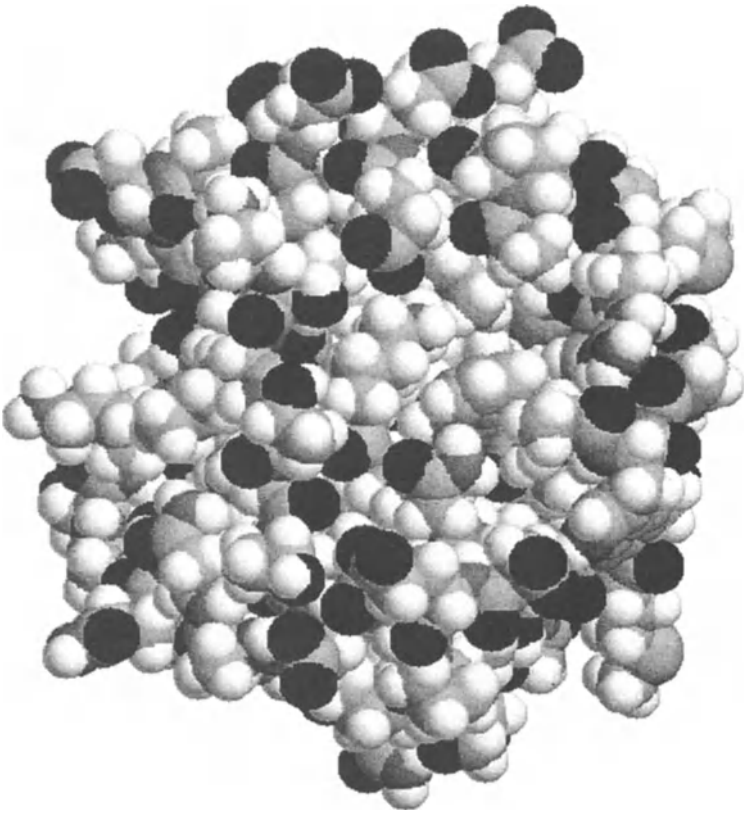

Figure 2-19. Three-dimensional graphic representation of solution structure of oxidized thioredoxin.

All of these structures were then cooled to 300 K in steps of 50 K; at each step the molecule was equilibrated for 1 ps and then cooling resumed for 5 ps. At the end of simulated annealing, all the structures were energy minimized for 500 steps of steepest descents followed by 1000 steps of conjugate gradients. Among all, several structures with low energy and least restraint violations were collected for further analysis. The quality of results

is evaluated with a molecular graphic program, MOLMOL (installed on a Silicon Graphics SGI CRIMSON, S.O. IRIX 5.3), that is able to superimpose, fit and calculate mean and secondary structure of a set of conformers. Finally, RMSD values with respect to the backbone were used for final structure analysis.

2.6 Methods of protein immobilization in solid thin films

The paradigm for molecular self-assembly at interfaces (Schief et al, 1999; Guryev et al., 1997) can be considered the streptavidin two-dimensional (2D) crystallization model. Indeed, quantitative Brewster angle microscopy (Figure 2.20) has resolved in situ the relative protein surface densities, allowing the detailed investigation of both the thermodynamics and morphologies of 2D crystal growth.

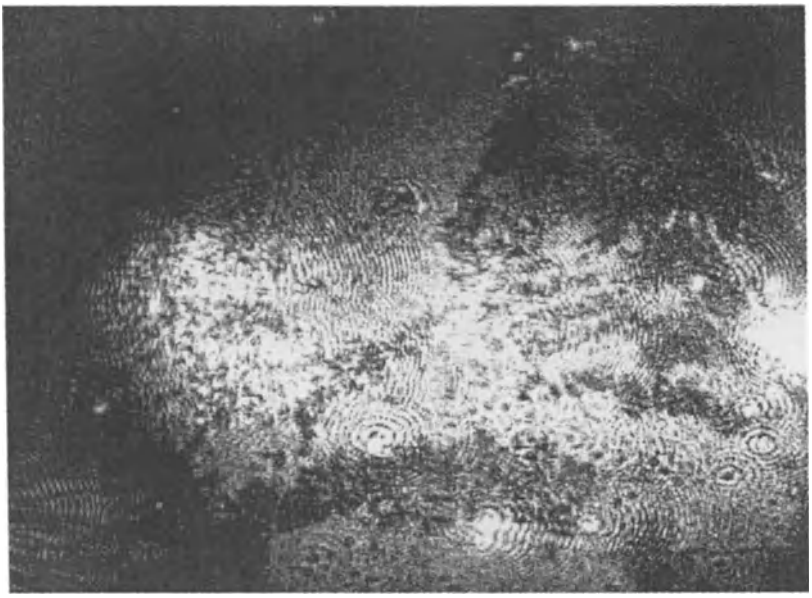

Figure 2-20. Brewster microscopy of protein LB films deposited onto a quartz support.

The resulting crystal structure analysis by means of Transmission Electron Microscopy on the growth of streptavidin 2D crystals transferred to solid substrates has provided new insight into the protein protein and

protein-lipid interactions that underline 2D crystallization (Schief et al, 1999).

Along this line, the controlled formation of "crystal-like" oriented protein array has been recently shown to occur at an unprecedented degree by protein monolayers engineering (Nicolini et al, 1993, 1995; Nicolini, 1996a,b; for an overview see Nicolini, 1997), namely by the modified thin Langmuir Blodgett protein film and the layer by layer shown in Figures 2.21 and 2.22) successfully used in different fields, such as biocatalysis (Nicolini, 1996a), biosensors and bioelectronics (Nicolini, 1996b).

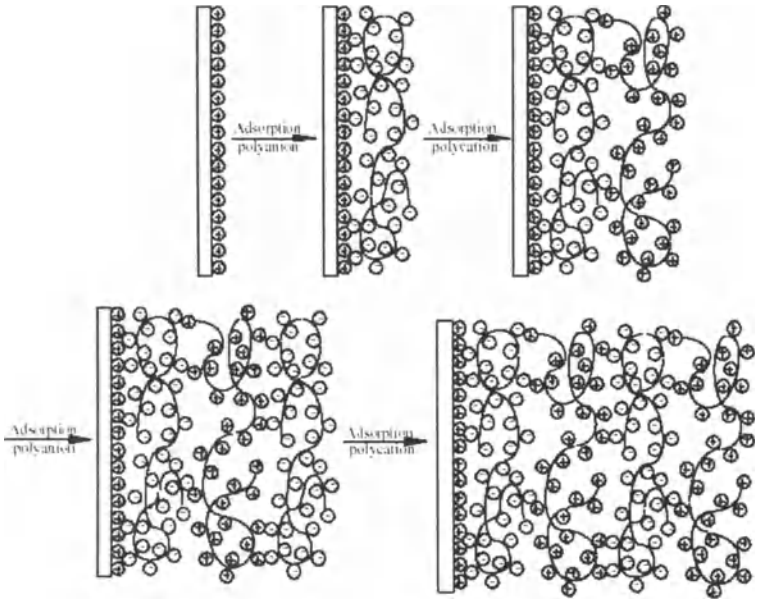

Figure 2-21. Layer-by-layer technique of deposition (Ram et al., 1999).

In fact, due to their order and exceptional thermal stability, thin protein film (namely the LB) appears to have a kind of implication interesting for a wide range of applications including those dealt in this book.

An absolute new application of this LB technique to the field of protein crystallization appears indeed the key element of the field of nanocrystallography introduced and defined later in this volume. For this reason in this subchapter we introduce the methods known worldwide of protein immobilization in thin solid film.

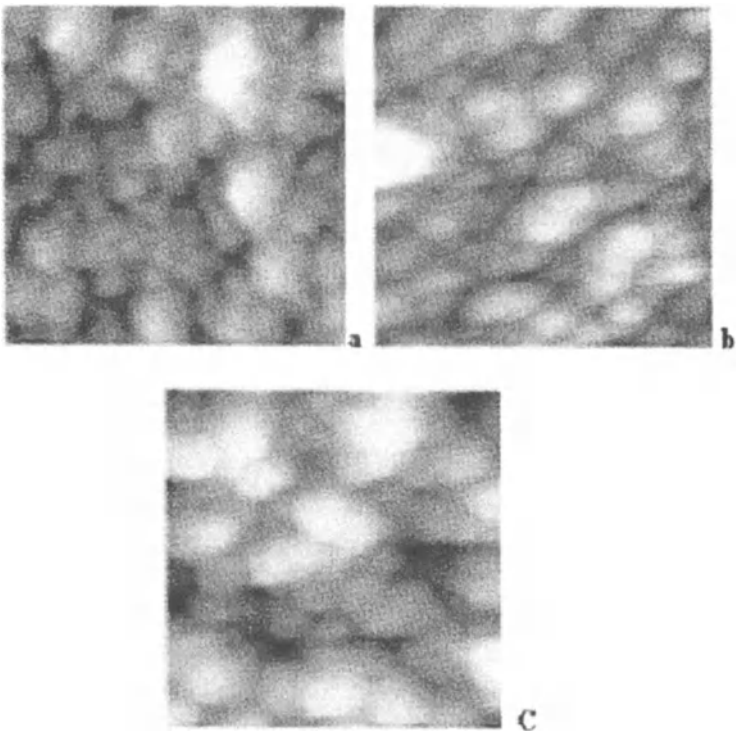

Figure 2-22. AFM images of 2 layers (a), 4 layers (b) and 20 bilayers (c) of PSS/PANI films of surface topography of 1x1 μm^2.

Firstly, we will consider the protein monolayer on the air-water interface, its surface pressure and potential, then give the determination of closely packed system and finally outline the basic methods of thin film deposition onto a solid surface. The most advanced method, namely the protein protective-plate (Troitsky et al., 1996) is shortly described in Figure 2.23.

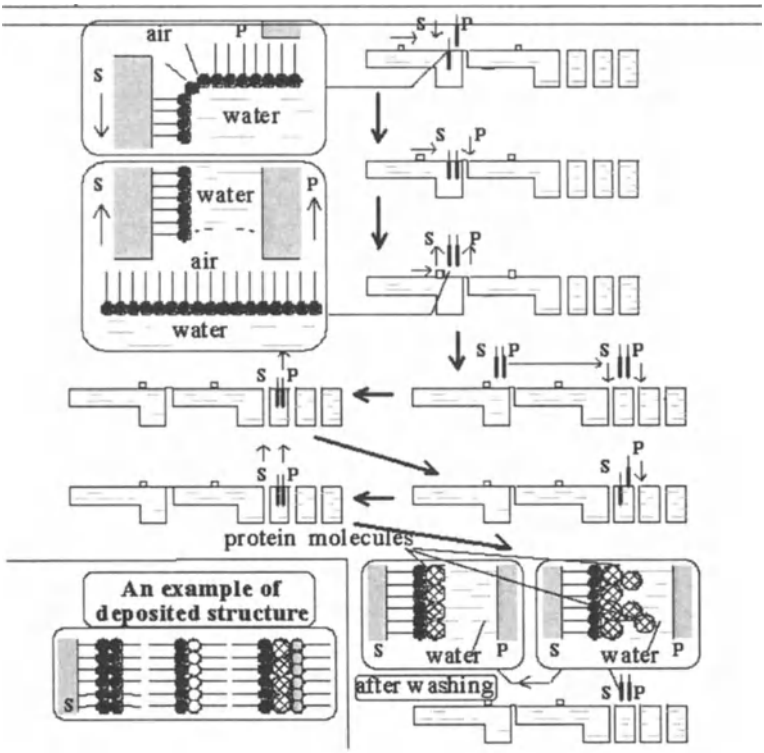

Figure 2-23. The protective plate method of film deposition includes the elements of LB, Self Assembly and layer-by-layer adsorbtion techniques and special protections of the deposited structures at the intermediate stages by thin layer of water kept near the film surface by capillary forces (Troitsky et al., 1996).

2.6.1 Pressure-area isotherms

For study of the protein monolayer behaviour at the air-water interface, it is necessary to consider what will happen when the protein monolayer layer is compressed with some kind of barrier. In this case the surface pressure π, which is the parameter describing the monolayer behaviour, is determined as:

$$\pi = \sigma_{H_2O} - \sigma_{ml}$$

where σ_{H2O} is the surface tension of free water and σ_{ml} is the surface tension in presence of the monolayer; it represents the decrease of the water surface tension due to the presence of the monolayer on its surface.

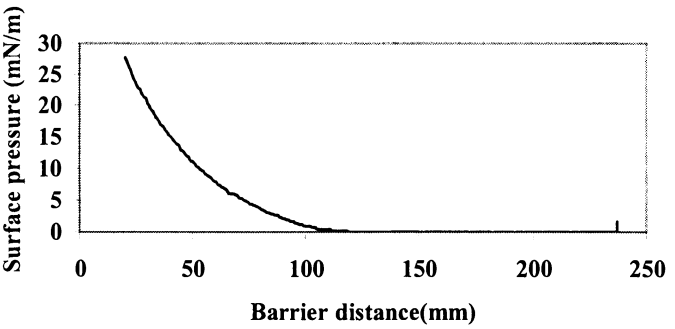

Figure 2-24. Pressure-air isotherm of protein (cytochrome P450scc) monolayer.

Typical compression isotherm is presented in Figure 2.24. This curve is the dependence of the surface pressure upon the area per one molecule, obtained at constant temperature. Usually, this dependence is called π-A isotherm. These measurements are practically always performed for studying the behaviour and namely the phase transitions occurring in the monolayers at the air/water interface. Initially, the compression does not result in any surface pressure variation since the molecules at the air/water interface are rather far from each other and do not interact.

This state is refereed as "two-dimension gas".

Further compression results in the increase of the surface pressure as molecules begin to interact. This state of the monolayer is referred as "two-dimensional liquid". For some compounds it is possible to distinguish also between liquid-expanded and liquid-condensed phases.

Continuation of the compression results in the appearance of "two-dimensional solid state" phase, characterized by the sharp increase in the surface pressure even for a small decrease in the area per molecule (Figure 2.25).

Dense packing of molecules in the monolayer is reached in correspondence to the called "close packing" system. The area per one molecule in this case corresponds to the geometrical parameters of the protein molecule, as determined from the experimentally measured protein structure or estimated from the 3D model of the protein. It is indeed

important to compare these two values in order to have an independent accurate estimate of the close packing of the system, namely the area per one molecule which can be compared to the value determined by nanogravimetric measurement of the protein thin film.

Further compression results in the collapse of the monolayer to the point that the regular 2D structure does not exist anymore and the multilayers themselves become highly disorganized (as shown by Brewster microscopy data).

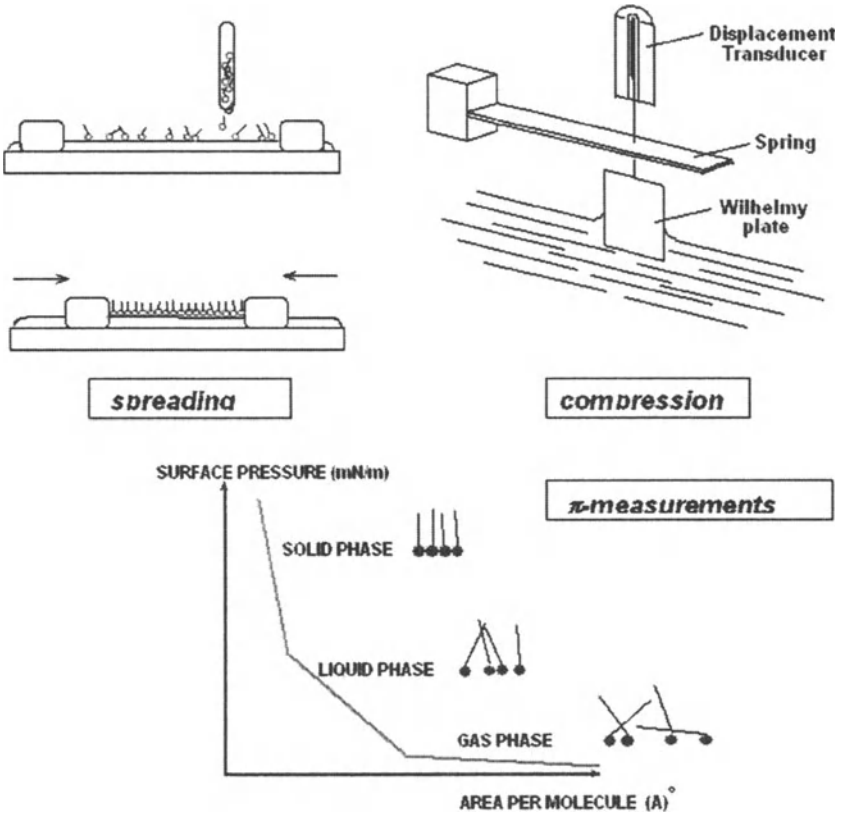

Figure 2-25. Scheme of thin film formation.

Two instruments are usually utilized for surface pressure measurements, namely the Langmuir balance and the Wilhelmy balance. Wilhelmy balance is more widely employed, even if it does not provide the direct measurement

of the surface pressure. The way the balance is made allows to perform measurements at the point, which corresponds, with respect to the barrier position, to the deposition point. It provides the deposition at the surface pressure value, which is maintained constant by a feedback system. The other advantage of Wilhelmy balance is the possibility of compressing the monolayer from both sides, obtaining a better homogeneity.

2.6.2 Surface potential

The other important parameter, which can be controlled, when working with monolayers at the air/water interface, is the surface potential. This parameter results from the orientation of charges and dipoles during the compression of the monolayer.

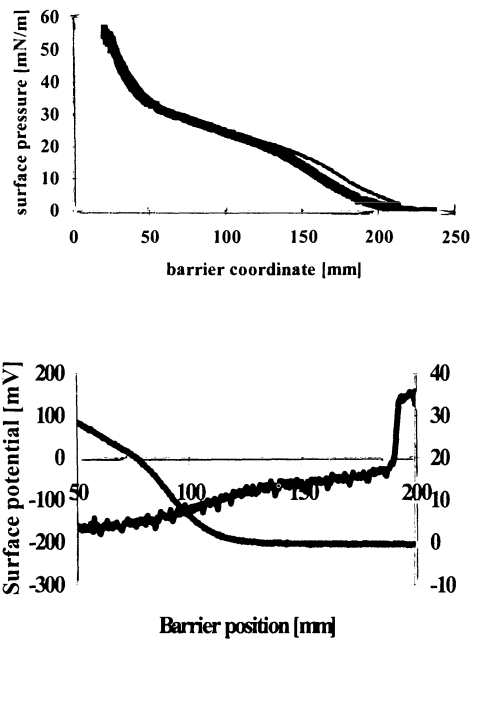

Figure 2-26. a) p-A isotherm of monolayer of wild type (bold line) and recombinant (thin line) of cytochrome P450scc at the water surface. b) Surface pressure and surface potential dependences on the area of the monolayer of cytochrome P450scc (Reprinted with the permission from Nicolini et al., 2001b, Copyright (2001) American Chemical Society).

Three different regions are usually considered for the surface potential interpretation.

The first one is the orientation of the C-H bonds in the hydrocarbon chains of the amphiphilic molecules during the monolayer formation. The second one is connected to the regular arrangement of the polar head-groups, and the third is due to the orientation of water dipole molecules in the area just under the monolayer. The input of each of these regions can be different and is due to the nature of the molecules forming the monolayer.

Typical dependence of the surface potential of the monolayer upon the area for one molecule is presented in Figure 2.26 (the π-A isotherm for the same monolayer is presented in the same figure for comparison). It is interesting to note that there are differences in the behavior of the surface potential with respect to that of the surface pressure. The variation of the surface potential begins much before than the surface pressure begins to increase. This behavior is due to the fact, that molecules begin to aggregate, forming dimers, trimers and small domains, at rather initial stage of the monolayer formation. Being aggregated, molecules tend to self-assemble orienting themselves in energetically adequate position, giving rise to the variation in the surface potential. It happens when there is practically no increase of the surface pressure. In the latter stage of the monolayer compression the variation of the surface potential is mainly due only to the increase of the monolayer density.

Kelvin probe is the tool, which is commonly used for the surface potential measurements. The instrument is equipped with a vibrating electrode, placed close to the water surface. The reference electrode is inserted into the water subphase. Vibration of the electrode provides the modulation of the capacity resulting, therefore, in the appearance of an alternating current proportional to the value of the surface potential.

The value of the surface potential of the monolayer can be both positive and negative, in comparison to the surface pressure, and the sign of the surface potential is determined by the nature of the molecules in the monolayer.

2.6.3 Methods of thin film deposition

The floating monolayer can be transferred onto the surface of solid supports (Figure 2.27).

Two main techniques are usually considered for the monolayer deposition, namely, Langmuir-Blodgett (or vertical lift) one and Langmuir-Schaefer (or horizontal lift) one.

The scheme of the Langmuir-Blodgett deposition is illustrated in Figure 2.28. A specially prepared substrate passes vertically through the monolayer.

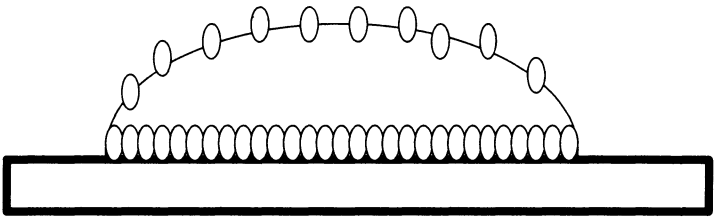

Figure 2-27. Monolayer at the solid surface after horizontal deposition.

The monolayer is transferred onto the substrate surface during this passage. The important point is to have the monolayer electrically neutral (Figure 2.25).

If some charges in the monolayer molecule head-groups are uncompensated, the deposition will not be performed, due to the electrostatic interaction of this charge with water molecules that would be higher with respect to the hydrophobic interactions of chains with the hydrophobized substrate surface. Let us consider the monolayer of fatty acids in order to demonstrate the necessity of the head group neutrality.

If the monolayer is formed at the surface of distilled water (pH is about 6.0), it cannot be transferred onto solid substrate. Its head group is dissociated and contains negative charge (COO^-).

There are two ways to provide the possibility of deposition. The first one is connected to the protonation of the head groups. It requires the decrease of the pH of the subphase. In fact, the deposition begins to take place, when the pH is less then 4.0. However, the monolayer of pure fatty acids is very rigid and its transfer results usually in defective LB films after the deposition.

Therefore, usually fatty acid salt monolayers are deposited instead of fatty acids. In this case, bivalent metal ions are added into the subphase.

Normally, their concentration is of the order of magnitude of 10^{-4} M. these ions attach themselves electrostatically to the dissociated fatty acid head groups, providing their electric neutrality.

The other method transfer a monolayer from the air/water interface onto solid substrates is illustrated in Figure 2.27. The method is called Langmuir-Schaefer (LS) technique or horizontal lift. It was developed in 1938 by I. Langmuir and V. Schaefer for the deposition of protein layers. A prepared

substrate touches horizontally the monolayer, and the layer transfers itself onto the substrate surface. The method is often used for the deposition of rigid monolayers and for protein monolayers; as a matter of fact, in both these cases the application of Langmuir-Blodgett method would result in defective films.

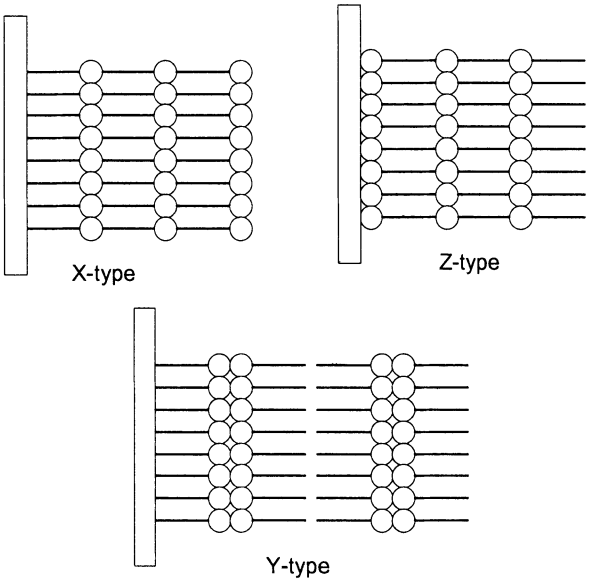

Figure 2-28. Types of Langmuir-Blodgett films.

In the case of the application of LS method to rigid monolayers, special care must be performed. The monolayer at the air/water interface must be divided into parts after reaching the desired surface pressure. This must be done with a special grid with windows, corresponding to the solid support sizes. The main reason of the utilization of the grid is the following one. If the monolayer is rigid, the removal of some of its part will result in the empty region in the monolayer; this empty zone will be maintained for a very long time.

Repeating of the deposition will result in the formation of many defects in the monolayer, and the resulting transferred layer will be absolutely not homogeneous. The use of the grid provides also the guaranty, that only one monolayer is transferred during one touch.

In the case of proteins the monolayer is soft. Therefore, the problems, mentioned above in this case do not exist, and the use of the grid can be avoided. In fact, the monolayer structure in the case of proteins is practically

amorphous; this is easily revealed by Brewster angle microscopy that will be considered in the following. Therefore, the removal of some monolayer regions can be rapidly compensated by the feedback system without the loss of the monolayer homogeneity.

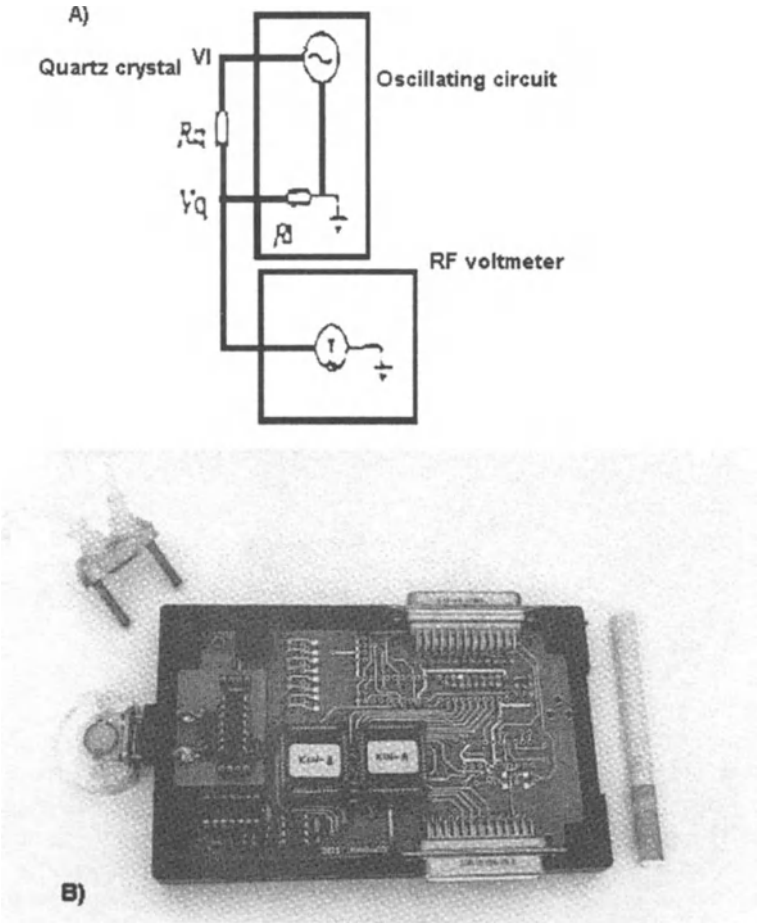

Figure 2-29. Nanogravimeter Instrument. a) a resonant oscillation is achieved by including the crystal into an oscillating circuit, where the electric and the mechanicl oscillations are near to the fundamental frequency of the crystal. b) hardware implementation of the oscillating circuit.

However, there is another problem in applying the LS technique for the protein monolayer transfer. The situation on the solid support after the touching the monolayer is schematically shown in Figure 2.27.

A regular closely packed monolayer is at the surface of the solid support. Some amount of water, transferred together with the monolayer, forms a drop at the substrate. Some protein molecules form not a regular layer at the top of this drop. If the sample is dried in a usual way, these molecules will not form a homogeneous layer. Therefore, they must be removed before the sample drying. The effective way to realize it is to use rather strong jet of inert gas, such as nitrogen, that removes the water drop together with randomly distributed protein molecules on its top, leaving only a regular layer, faced to the substrate surface. Deposited films are usually divided into 3 types, schematically shown in Figure 2.28, namely, X-, Y-, and Z-type. As it is clear from the figure, the Y-type is a centrosymmetric one, while X- and Z-types are polar ones and differ one from the other by only the orientation of the head-groups and of the hydrocarbon chains with respect to the substrate surface. Such division appears due to the fact that in some cases there is no monolayer transfer during an upward or downward motion of the substrate (in the case of LB deposition). In the case of LS deposition, moreover, the layers seem to be always transferred in a polar manner. However, the X- and Z-types are practically never realized in practice.

Even if some nonlinear properties, such as pyroelectricity, realizable only in polar structures, were observed, and the structures were considered as polar ones, detailed investigations revealed that the films are of Y-type with not equal filling of odd and even layers.

2.6.4 Methods of thin film characterization

Above methods for protein monolayer characterization, as π-A isotherms measurements, surface potential measurements, There are many methods for the thin protein film characterization.

The most important among them are circular Quartz Crystal Nanobalance (nanogravimetry as shown by Figure 2.29), Brewster Microscopy (Figure 2.20), Circular Dichroism (CD), Ellipsometry, Fourier Transform Infrared Spectroscopy (FTIR), Atomic Force Microscopy (Figure 3.3), X-ray small angle scattering (Figure 2.12). Synchrotron radiation (Figure 3.11) can be used also for precise protein thin film structure investigation. In the present work nanogravimetry was used to characterize the uniformity of protein thin film deposition and calculate the thin film surface density. From the other hand, AFM technique allowed to obtain the images of the protein thin films and make the idea of their order (Nicolini, 1996).

Chapter 3

NANOCRYSTALLOGRAPHY

This chapter concerns the definition, the principles and the experimental layout of nanocrystallography which represents a significant advacement in protein crystallography. Nanocrystallography is indeed a new technology introduced to produce and characterize crystal of any dimension by means of nanotechnology. By means of it several protein systems either known or yet unsolved can be crystallized and thereby their 3D structure solved at atomic resolution paving the route from art to science in proteomics and nanocrystallography. It should not escape our notice that nanocrystallography as here described does not refer thereby to the production and characterization of self-assembled nanocrystals (i.e., crystals of nanometer size) made of silver, cobalt, gold and/or nanoparticles as fabricated by using reverse micelles or similar technologies (Pileni 1997, 2002) which is going to be addressed in the last chapter.

3.1 Nanobiofilms template

The main idea of the innovative method here described is demonstrated on the Figure 3.1a. It should be underlined that the protein thin film template is created by means of Langmuir-Blodgett technology and its modifications (Nicolini 1996a, 1997) and subsequently is deposited on a solid glass support to be placed in the appropriate vapour diffusion apparatus. This LB protein thin film (not necessarily a monolayer) assumes the role of the template for protein stimulated nucleation and protein crystal growth acceleration. During the screening procedure the following parameters were varied: protein monolayer surface pressure, precipitant nature and concentration, number of the protein thin films monolayer. All experiments should be carried out at the controlled temperature. However, temperature variation can be also used in order to control protein crystal nucleation and

E. Pechkova et al., *Proteomics and Nanocrystallography*
© Springer Science+Business Media New York 2003

growth. To develop the above thin film-based method we have elected the traditional hanging drop vapour diffusion method, because this protein crystallization technique is, as described in the previous chapter, widely utilized among protein chemists and biochemists, easy to perform, requires small amounts of samples and permit easy variation of physical parameters during crystallization (McPherson 1989; Ducruix and Giege 1999).

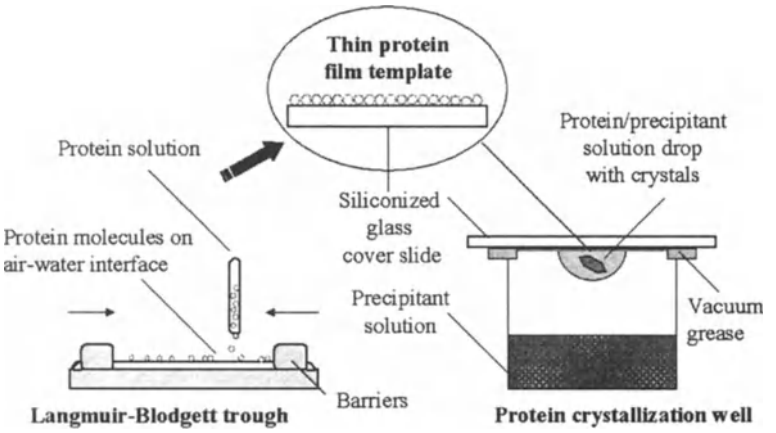

Figure 3-1a. Thin film template protein "hanging drop" crystallization method (Pechkova and Nicolini, 2003a).

However, the possibility to modify the other crystallization method cannot be excluded, although the sitting drop modification (Figure 3.1b) was less successful in our experience.

Protein thin films can be engineered onto solid substrates using LB trough (Troitsky et al., 1996; Facci et al., 1994) with distilled water or approptiate buffer solution used as a subphase. Protein solutions were uniformly spread over the water surface, e.g. with Hamilton syringe. The films were compressed immediately after spreading with a compression speed of 10-100 cm/min, depending of the trough size and the nature of the protein. The more soluble protein is, the fester the through barriers should be moved.

π-A Isotherms measurements can be performed for a preliminary characterization of protein monolayers at air-water interface (see chapter 2).

As a control, all experiments must be carried out in parallel without nanobiofilm template. In this manner, the influence of the thin film template on the individual protein crystallization becomes clear.

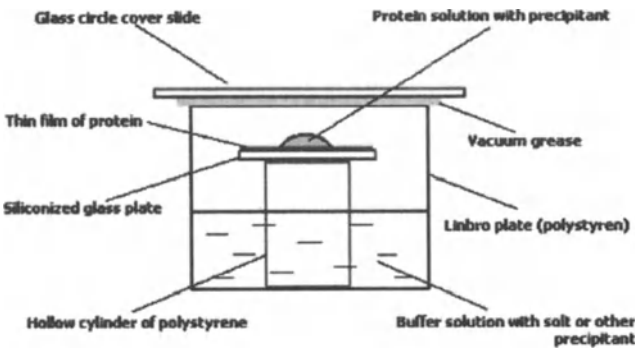

Figure 3-1b. Crystallization method using sitting drop modification.

3.1.1 Substrate preparation

Siliconized circle glass cover slide (e.g. commercially available from Hampton Research) can be easily used as a substrates, used for thin protein film deposition for modified hanging drop crystallization method. Glass substrate can be also siliconized in the laboratory, using one of the numerous existing protocols or special siliconization solutions. The following procedure can be recommended: carefully washed, glass substrates must be treated with heated concentrated sulphuric acid for 15 min. Then they have to be rinsed with water, dried and treated consequently with 5% demethyldichlorsilane solution hexane in for 30 min, with hexane for 15-20 min, with acetone for 15-20 min, and again with hexane for 15-20min. After that they can be dried in nitrogen flux and rinsed with distilled water and dried before use.

It can be recommended to deposite the series of protein monolayer in the same conditions on quartz resonators, which can be used later for nanogravimetric measurements.

3.1.2 Protein thin film formation

As it was described in the chapter 2, the transfer of protein monolayers from the subphase surface onto the previously siliconized solid (glass) substrate can be performed by Langmuir–Blodgett (vertical lift) or Langmuir-Schaefer technique (horizontal lift) (Langmuir and Schaefer,

1938). The last technique can be realized by touching the support in parallel to the subphase surface at desired protein surface pressure.

The protein surface pressure, chosen for the deposition, should corresponds to highly packed, ordered monolayer. Since protein geometric parameters are different this surface pressure also differ from one protein to another. From our experience, surface pressure corresponding to the closely packed system is 18 mN/m for chicken egg white lysozyme, 10mN/m for human protein kinase CK2α and 15 mN/m for bovine cytochrome P450scc. Generally, the protein dimensions, solubility and surface charge distribution influence on optimal surface pressure value. It should be born in mind that this surface pressure can be also influenced by subphase composition.

After deposition of every protein monolayer, the excess water transferred with monolayers can be removed by nitrogen flux. Repeating this procedure, substrate with desired number of protein monolayers can be prepared. After film deposition, supports must be dried in a nitrogen flux, incubated for a 8 h at +4°C, then rinsed carefully and dried again in nitrogen flux.

In the three key examples used to validate our method the film formation is carried out under different conditions, as it will be shown in Chapter 4.

3.1.3 Protein thin film characterization

Quartz crystal nanobalance measurements can be carried out (see a calibration of it in Figure 3.2) by means of a home-made gauge having a sensitivity of 0.57 ± 0.18 ng /Hz using quartz oscillators with frequency of 10 MHz.

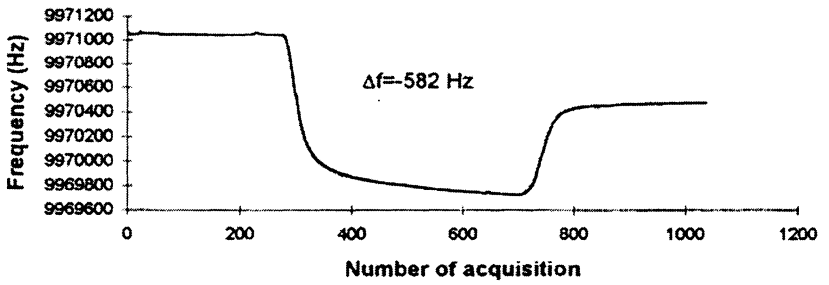

Figure 3-2. Frequency shift versus time by means of quartz nanogravimeter for a quartz covered with BSA (by silanization) and exposed to a flowing solution containing antibodies specific to BSA.

Nanogravimetric measurements were carried out by means of a homemade gauge (Figure 2.29) with a sensitivity of 0.57 ± 0.18 ng/Hz using quartz oscillators with frequency of 10 MHz. By the Sauerbrey equation (Sauerbrey, 1964) it is possible to correlate the frequency shift with the mass deposited onto the quartz oscillator. To obtain a direct connection between the frequency shift and the surface density, the Sauerbrey equation was changed as follows:

$$\Delta s = -K \Delta f$$

where Δs and Δf represent the surface density and the frequency shift, respectively, and K is a constant determined from the physical parameters of the utilized resonator. Calibration of the quartzes balance was performed according to Facci et al., 1993.

From the nanogravimetry curve, plotted as surface density as a function of the number of protein monolayers, the information on the uniformity an dreproducibility of deposition can be obtained.

Moreover, knowing molecular weight of the protein molecule, it is possible to calculate area per one molecule in the obtained film and to compare it with that for the closely packed system. The latter value can be easily estimate knowing the geometrical parameters of the protein from PDB bata bank. In case the structure of the protein is not resolved yet, homologous protein parameters or geometrical features from molecular modelling can be used for calculation.

3.2 Atomic force microscopy

Atomic force microscopy (AFM) has been frequently used to study protein, nucleic acid, and virus crystals in situ, in their mother liquors, as they grow (Malkin et al., 1995; McPherson et al., 2000). The growth of six protein and virus crystals was originally investigated in situ using atomic force microscopy (Malkin et al., 1995). Most of the crystals grew principally on steps generated by two-dimensional nucleation on surfaces though some grew by development of spiral dislocations. Furthermore while apoferritin grew by a rarely encountered mechanism, normal growth, usually associated only with melt or vapour phase crystallization. Cubic crystals of satellite tobacco mosaic virus (STMV) grew, at moderate to high levels of supersaturation, by the direct addition of three-dimensional nuclei followed by their rapid normal growth and lateral expansion, a mechanism not previously described to promote controlled and reproducible crystal growth from solutions. By means of these AFM studies biological macromolecules

apparently utilize a more diverse range of growth mechanisms in their crystallization than any previously studied materials.

More recently from the sequential AFM images taken at brief intervals over many hours, or even days, the mechanisms and kinetics of the growth process have been recently defined (McPherson et al., 2000). The appearance of both two- and three-dimensional nuclei on crystal surfaces have been visualized, defect structures of crystals were clearly evident, and defect densities of crystals were also determined. The incorporation of a wide range of impurities, ranging in size from molecules to microns or larger microcrystals, and even foreign particles were visually recorded. Thanks to these observations and measurements, a more complex understanding of the detailed character of macromolecular crystals has been emerging, one that reveals levels of complexity previously unsuspected. The unique features of these crystals, apparent only in AFM images, undoubtedly influence the diffraction properties of the crystals and the quality of the molecular images obtained by X-ray crystallography.

In order to acquire "on real time" images at the atomic resolution of the very small microcrystals obtained by nanocrystallography for a new class of never previously crystallized proteins, prior to their eventual characterization at the expensive and not readily accessible Synchrotron Radiation Beamline, a new Atomic Force Microscopy configuration has been developed in house for protein crystal characterization but also for all biological and organic films and materials produced in our laboratory.

Since the invention of the atomic force microscope, we have assisted to the strong commercial development of a large number of instruments capable of exploiting many measurements in ''air'' and in ''ultra-high-vacuum'' environments. Instruments produced by many companies (Binning et al., 1986; Decher 1996; Sartore et al., 2000) are great examples of such developments that the biotechnologist can find suitable for most of their experimental situations.

However, until recently improvements were still necessary in the field of high-vacuum or of controlled-atmosphere instruments like those needed for crystal characterization at atomic resolution in which the above-mentioned companies do not offer specific solutions. Precise control of operating conditions is a critical aspect, in which the strong dependency of measurements on environmental factors, such as acoustic and mechanical noises, temperature, and humidity play an important role. In particular, the last aspect often affects morphological investigations because a meniscus force, between a tip and a sample, introduces artefacts and changes in the resulting image.

This effect is particularly evident with organic samples: the water molecules on the sample surface add some disturbing effects on the real

morphological image. Keeping in mind these problems, a new specific system has been developed (Sartore et al., 2000) comprising a tool for surface investigation installed in a chamber, designed for high-vacuum or of controlled-atmosphere operations. After some operative steps during which the chamber goes down to 10^{-6} Torr, the user, by introducing nitrogen gas, can vary the environmental conditions in the chamber and perform the sample characterization. Our AFM microscope can operate with organic compound or materials that suffer from high pressure , exploiting all benefits from a controlled environment in absence of any water layer between the tip and the sample surface. It yields , as it will be shown later, better contrast than in air (common to most commercial AFM) and without the utilization of the ultrahigh vacuum conditions, common to other commercial AFM and impractical to organic samples for their nature, composition and structure.

Our in house implemented Neural Atomic Force Microscopy (ElbaAFM, PNB-PST Elba) consists of an appropriate chamber and of an hardware and software configuration reported in separate communications (Sartore et al., unpublished data; Nicolini et al., 1996c; Sartore et al., 2000; Salerno et al.,1999).

3.2.1 Design of the chamber

The block diagram of the chamber of our AFM (Sartore et al., 2000) is shown in Figure 3.3 and the realized prototype is presented in Figure 3.4. The chamber is made of stainless steel with a cylindrical body and two DN250 flanges. The three main parts are: the top flange onto which an atomic force microscope (AFM) optical stage is positioned; the cylindrical body, which presents the connections to the pumping apparatus and to the vacuum measuring heads and the bottom flange, mounting a three-dimensional (3D) rough mover; and electrical feedthroughs for piezotube polarization. The pumping system is composed by a first-stage rotative pump (Vacsound D12, Galileo, Italy) and by a turbo molecular pump (Elettrorava, Italy), serially connected and suitable for obtaining a pressure down to 10^{-6} Torr. The chamber is positioned onto an antivibrating system and a bellows between the chamber and the turbopump allows us to minimize the vibrations.

The chamber can be used either with a contact-mode AFM or a "tapping mode" AFM (in the case of microcrystals being placed in an appropriate chamber). We focused our attention on three aspects: the optical system, the X– Y – Z mover, and the piezoelectric tube.

Using piezoelectric cantilevers should be promising within hermetically closed chambers, because they do not need optical beams, lasers, photocells,

and related circuitry; unfortunately, those commercially available still suffer from noise problems.

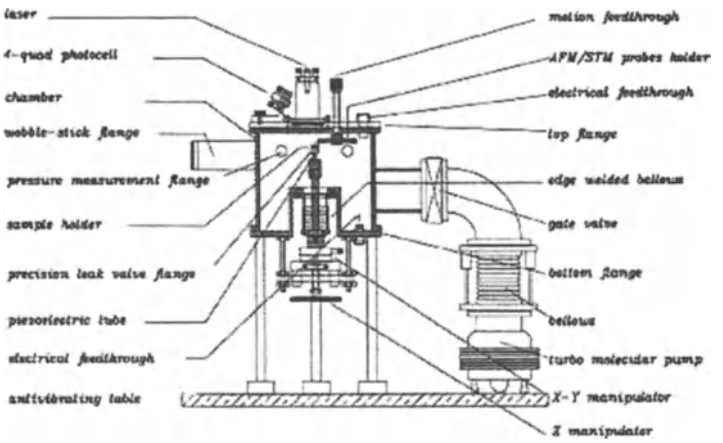

Figure 3-3. Schematic drawing of the controlled-atmosphere system. The various parts composing the instrument are evidenced directly inside the figure and the overall description is given in the text (Sartore et al., 2000, used with permission, Review of Scientific Instruments © American Institute of Physics 2000).

So, we decided to utilize the usual optical revealing system and gold-coated cantilevers purchased from Park Scientific Instruments. We have designed the AFM in order to minimize the number of components inside the chamber, therefore, locating the optical components, i.e., laser diode and four-quad photocell outside the chamber.

In order to minimize the optical pathway and to maximize the signal-to-noise ratio for the photodetector, we designed a very simple geometry: a laser diode (Futura Elettronica, Italy, emitting at 632 nm) impinges the backside of a metallized silicon nitride cantilever and reflects directly on a four-quad photocell, without any mirrors and lenses, and through a Pirex window located in the middle of the top flange.

The AFM, therefore, is based on a fixed sensing cantilever and on a movable sample, positioned onto the top of a piezoelectric mover. In order to better select the portion of the sample of interest to be measured, an X– *Y* – *Z* rough mover has been realized. An external stage is located at the bottom flange, consisting of a two-dimensional (2D) mover mounted onto a linear micrometer implementing the *Z* motion. The *X* and *Y* stages are commercial ones (Officine Magini, Italy), while the *Z* mover was designed *ad hoc* and is depicted in Figure 3.5.

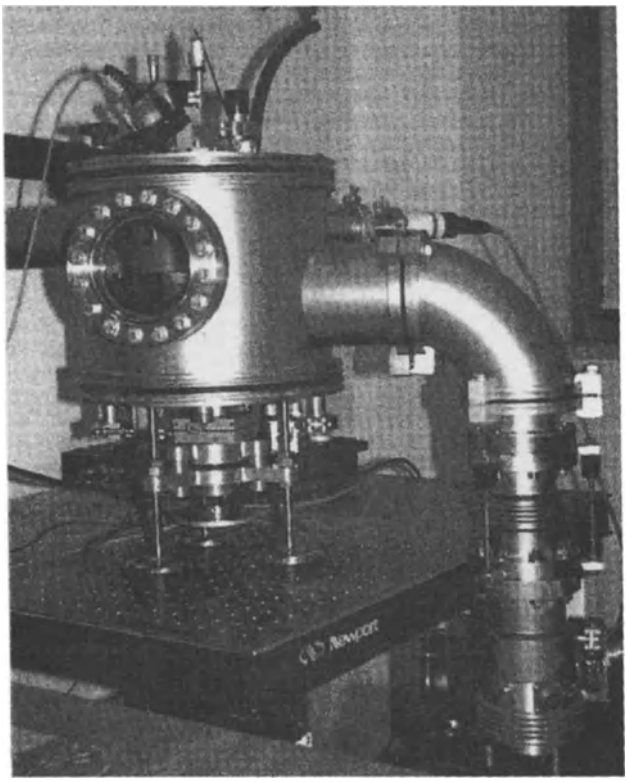

Figure 3-4. Picture of the complete system, where the chamber with the optical setup is mounted onto an antivibrating table. The turbomolecular pump is also visible on the right side of the chamber. The picture, in addition, shows some details such as a lateral inspection window, the Pirani measuring head, and the connection pipe for nitrogen input flow (Sartore et al., 2000, used with permission, Review of Scientific Instruments © American Institute of Physics 2000).

It was realized by means of a right-hand screw, connected from one side to a graduated disk and from the other to the standard X– *Y* movers. The precision of the Z-positioning stage is 10 μm. The X– *Y* – *Z* motion is transferred inside the chamber through a bellows, connected to the bottom flange through a DN40 flange.

3.2.2 The hardware and software apparatus

The instrument (called ElbaScan) is driven by a homemade controller based upon a commercial data acquisition board (National Instruments, AT-MIO-16X). This card is plugged into a personal computer, where the

acquisition software runs. The latter is written in C under LABWINDOWS CVI (National In-struments) and Microsoft VISUAL C++ environments (Sartore 1998).

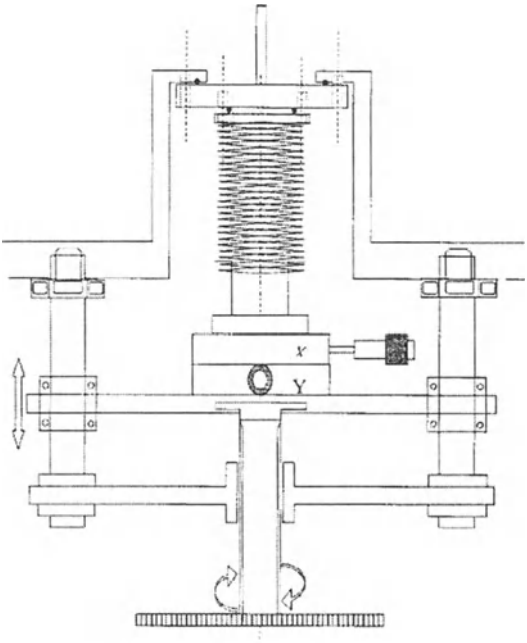

Figure 3-5. Schematic design of the X– Y – Z ''rough'' mover. The X– Y controls are positioned onto a Z-rotating screw, which transduces the motion to the interior of the chamber by means of a tube protected by a bellows selections, and directly program the card in order to fullfill the user's requirements. The instrument is being equipped with a neural network - based system for the automatic selection of feedback parameters (Sartore et al., 2000, used with permission, Review of Scientific Instruments © American Institute of Physics 2000).

The controller is configured in such a way that the analog-to-digital and digital-to-analog converters present on the data acquisition board are synchronized in order to get the data while the X– *Y* scan is in progress. Such synchronization is achieved by means of an internal counter-timer. The system comprises an analog feedback circuit implementing a proportional integral control. It continuously compares the deflection signal with a desired force value and produces a correction signal for the piezoelectric actuator. This signal, together with the X, *Y* DA outputs, is fed into a high-voltage amplifier for the proper driving of the piezo-mover. The amplifiers are also homemade and based on dedicated integrated circuits, the PA85

from Apex, which ensure an optimal frequency response and precision. The measuring head, above described from the mechanical point of view, is based on a four-quad photocell, whose outputs are preamplified and fed into the feedback and AD circuits. Therefore, the AFM can measure both deflection and torsion of the cantilever. The software is divided into two sections, the former being a low-level driver of the electronics, the latter being a graphical-user interface allowing the user to input the acquisition parameters and settings. The software operates under the Microsoft WINDOWS environments, because the real-time or fast data acquisition is achieved by means of the dedicated card and relative drivers. The researcher can, therefore, benefit from a friendly user interface without any limitation on the hardware performances. Basically, a window shows the available scan area, within which the user selects a portion of interest by the next acquisition step, after setting the desired image pixel dimen-sions, scan frequency, and measured signals. The data acquired are shown row by row on the same window, allowing a fast and simple monitoring of different portions of the sample. The low-level routines compute the necessary information to drive the AT-MIO-16X board, starting from the user selection, and directly program the card in order to fullfill the user's requirements. The instrument is being equipped with a neural-based system for the automatic selection of feedback parameters (Salerno et al., 1999).

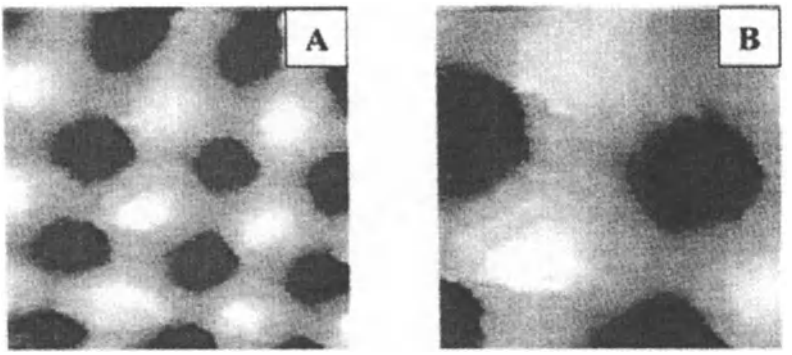

Figure 3-6. AFM images of a gold grid acquired in environmental conditions. The scan sizes are, respectively, 2 x 2 (A) and 1 x 1 μm (B) (Sartore et al., 2000 used with permission, Review of Scientific Instruments © American Institute of Physics 2000).

3.2.3 Performances of the system

The system can be best utilized in those cases where the samples under investigation, on one hand, would benefit from the absence of an

intermediate water layer between the tip and sample, and, on the other hand, cannot be tested under high-vacuum conditions for their own structure, nature, and composition.

Moreover, our device is much cheaper than an UHV system, and can be thought of as an add-on module for systems operating in HV, such as Joule-effect metal evaporators or others, exploiting all the benefits deriving from the possibility to have an *in situ* characterization of the sample deposited or modified with the instruments connected to the HV line.

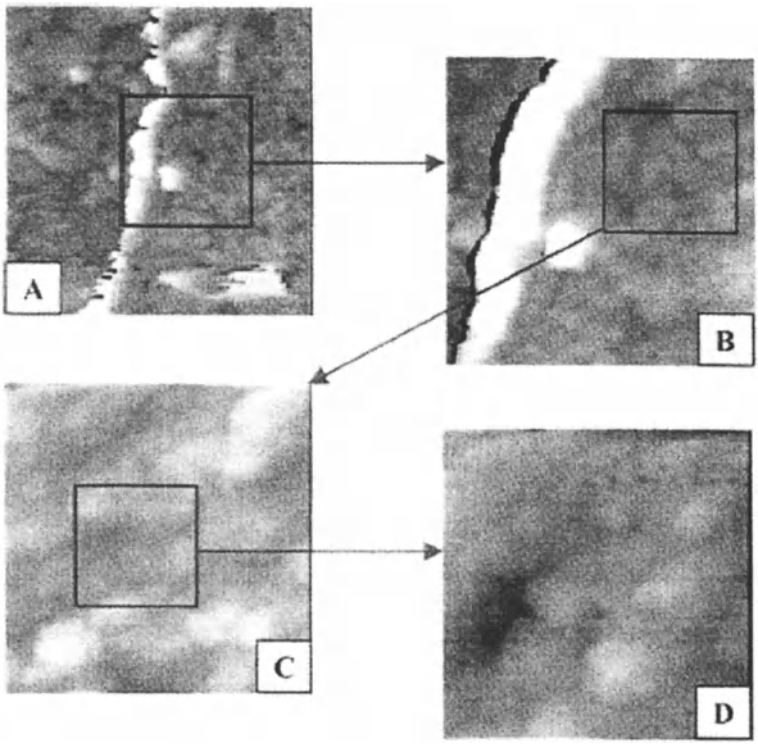

Figure 3-7. Acquisition results obtained in environmental conditions. The sample is polypirrole deposited onto glass by means of the layer-by-layer technique. The figure shows successive zooms at lateral dimensions of 2.2 x 2.2 μm for (A) 1.2 x 1.2 μm for (B), 0.45 x 0.45 μm for (C), and 0.25 x 0.25 μm for (D) (Sartore et al., 2000, used with permission, Review of Scientific Instruments © American Institute of Physics 2000).

In order to test the system, we initially focused our attention (Sartore et al., 2000) on the usual 1 μm step, gold calibration grids (first monitored in environment conditions).

In Figure 3.6 an example is shown: (A) represents a scan area of about 2 x 2 μm while (B) of about 1 x 1 μm. We can observe the spherical morphology of the objects, with a good image resolution on the micrometer scale. A test at higher lateral resolutions was performed investigating some organic samples, in particular, those composed by conducting polymers, obtained by depositing the poly-electrolites on a glass slide with the layer-by-layer technique (Decher 1996a,b, 1997).

In Figure 3.7 a sequence of images of such a sample is shown.

The image dimensions are 2.2 x 2.2 μm for (A), 1.2 x 1.2 μm for (B), 0.45 x 0.45 mm for (C), and 0.25 x 0.25 μm for (D), respectively.

Also, in this case, the microscope shows good resolution and reproducibility (Figure 3.7). In order to show the application capabilities of the pro-posed complete system, we performed experiments in controlled atmosphere comparing the results with the above images.

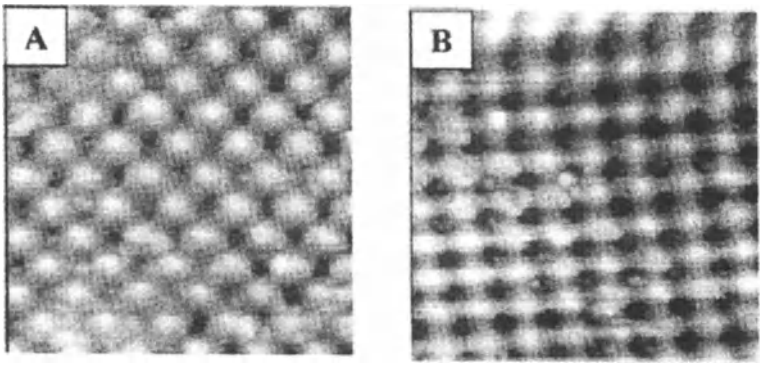

Figure 3-8. AFM images of a gold grid acquired in environmental conditions (A) and in nitrogen atmosphere (B). The image dimensions are 7 x 7 μm (Sartore et al., 2000, used with permission, Review of Scientific Instruments © American Institute of Physics 2000).

What we expected is a better resolution of the details, mainly due to the absence of the water layer between the tip and the sample surface. This was effectively achieved, as shown in Figure 3.8, where a calibration grid scan size of 7 x 7 μm has been imaged. (A) has been acquired in air conditions while (B), acquired in controlled atmosphere, presents a better contrast and allows us to focus even on the defects located within the grid array. The same results were also reproducibly repeated with organic samples and at higher resolutions, exploiting the real benefits of working under a controlled environment inside the chamber.

Figure 3.9 shows images of a polypirrole sample, again deposited by the layer-by-layer technique and, respectively, imaged at 2 x 2, 1 x 1, and 0.6 x

0.6 μm. The last two images represent a better detail of the previous one, indicating the good stability of the microscope, which was demonstrated to provide an improved quality of the morphological and structural investigation.

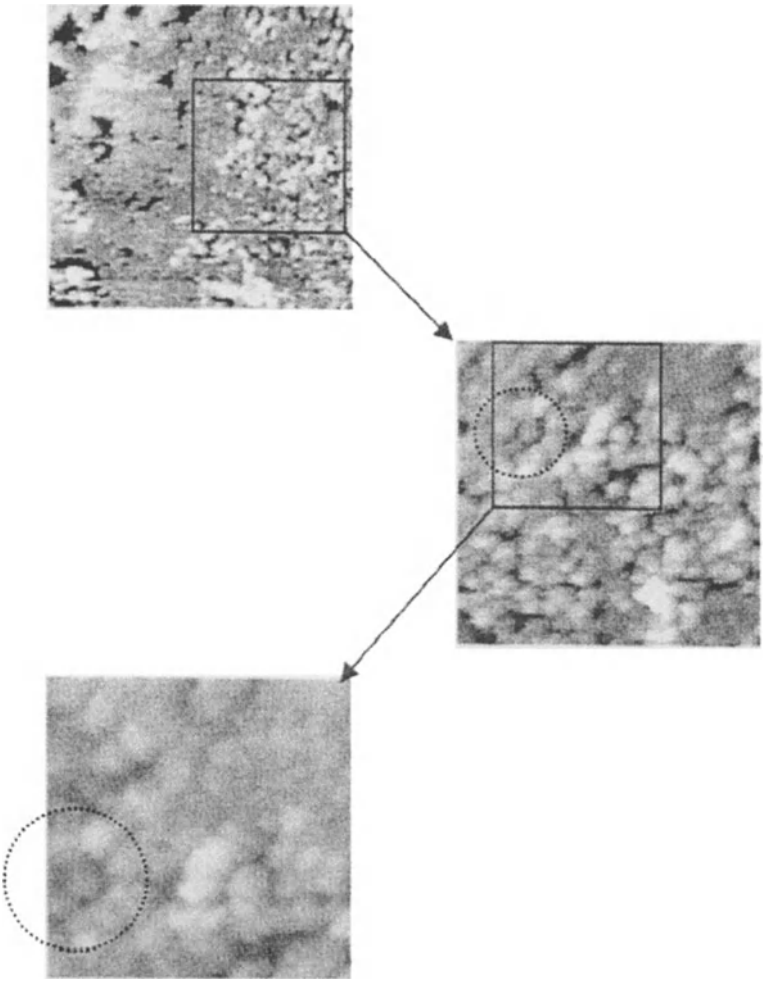

Figure 3-9. Example of the system operation in controlled-atmosphere conditions. The images show the surface of a polypirrole sample deposited as previously reported. The sequence focuses on details further and further defined, starting from a 2 x 2 μm image, through 1 x 1 μm, down to a 0.6 x 0.6 μm image. The circular selection is clear detail evidence of the zoom-ing procedure (Sartore et al., 2000, used with permission, Review of Scientific Instruments © American Institute of Physics 2000).

This conclusion is confirmed by the Atomic Force Microscopy (AFM) data on biological material, namely the P450scc cytochrome thin film shown in Figure 3.10. The periodic crystalline nature of the crystal materials being produced by means of our homologous protein template method as applied to cytochromes P450scc is confirmed by our neural AFM in "tapping mode" with the use of the above described chamber (see later in Chapter 4).

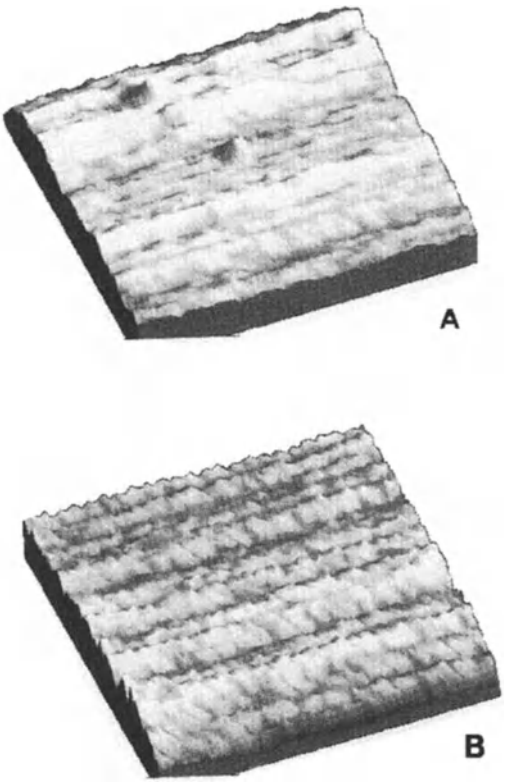

Figure 3-10. AFM of cytochrome P450scc monolayer. (a) Measurements in air (1 x 1 micron) (b) Measurements in water (0.1 x 0.1 micron).

The AFM microscope characteristics allow measurements in controlled environment with contact or tapping mode either in air or water. It was found that using the tapping mode for the protein experiments, the measurements in water gives resolution ten times higher (Figure 3.10b) than in air (Figure 3.10a). Moreover, with the measurements in water, the disturb

created by dust or other particles attached onto the surface by adhesion can be corrected.

AFM data obtained from cytochrome P450scc monolayer template (Figure 3.10) displays for each identifiable peak a cross section area of about 20 nm^2, which is smaller than the 30 nm^2 estimated area per the P450scc found in the Brookhaven Protein Data Bank It seems to be interesting to compare this value also with the experimental cross section area apparent in the AFM image of P450scc crystal as it will be shown in Chapter 4.

3.3 Synchrotron radiation

Generally, X-ray are produced in the laboratory diffractometer (Figure 3.10c) by accelerating a beam of electrons into an anode, the metal of which dictates what the wavelength of the resulting X-ray will be. Monochromatization is carried out either by using a thin metal foil which absorbs much of the unwanted radiation or, better, by using the intense low order diffraction from a graphite crystal.

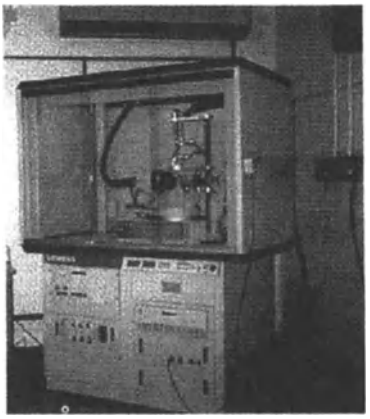

Figure 3-10c. The SMART Diffractometer - Bruker AXS.

To obtain a brighter source, an anode, which is water cooled to prevent its melting, can be made to revolve in what is known as a rotating anode generator. For most work with proteins, the target is copper and the characteristic wavelength of the radiation is 0.1542 nm (1.542 Å).

An alternative source of X-radiation is obtained when a beam of electrons is bent by magnet. This is the principle behind the synchrotron radiation sources which are capable of producing X-ray beams some thousand times more than a rotating anode generator (McGee 1993).

A consequence of this high intensity radiation source is that data collection times have been drastically reduced, making kinetic crystallography feasible (Johnson and Najdu, 1990). A further advantage is that the X-ray spectrum is continuous from around 0.05-0.3 nm, dependent upon the particular machine, and this has distinct advantage for crystallographers.

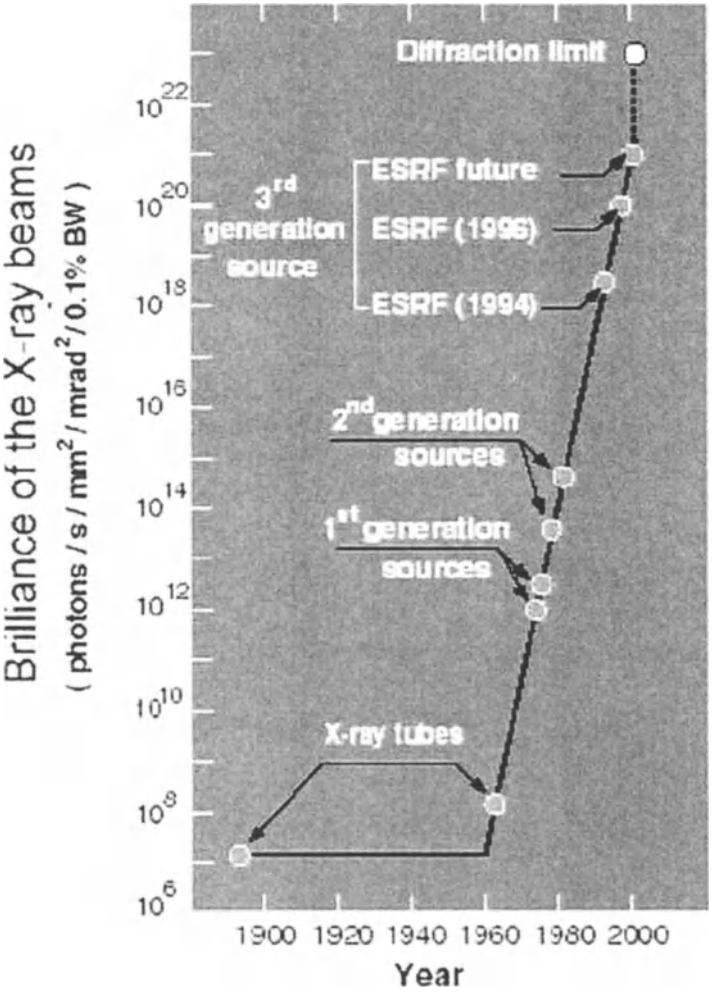

Figure 3-11. Brilliance of different X-ray beams with progress in physics in the last century (courtesy of ESRF).

The use of shorter wavelengths has usually been found to prolong the room temperature lifetime of a crystal in the X-ray beam. The main drawback is that synchrotrons are centralized facilities and consequently access is significantly less convenient, particularly for preliminary work. For proteins that are characterized by the X-ray diffraction method, crystal dimensions are the critical parameter for the protein 3D structure characterization at the atomic level. However synchrotron, contrary to the traditional X-ray radiation sources, require quite smaller crystals (Cusack et al 1998).

The brilliance of a light source is defined as the number of photons emitted per second, per unit source size, per unit space angle and for a bandwidth of 1/1000 of the photon energy The comparison between various sources of X-rays shows large differences in their brilliance.

Brilliance of different X-ray beams with progress in physics in the last century is shown on the Figure 3.11. Wilhelm Conrad Röntgen discovered X-rays in 1895 whilst working with cathode-ray tubes. Using the principle of fast electrons hitting a metallic target, a first substantial gain in brilliance was not obtained until the introduction of rotating anode sources (~1960).

The progress of high energy physics, with the construction of powerful particle accelerators gave birth to what we now call First generation synchrotron sources (~1970). Using the deflection of high energy electrons by a magnetic field for the production of X-rays proved so promising that a number of dedicated Second generation sources were built (~1980). Relying on the combination of needle thin electron beams and Insertion Devices, third generation synchrotron sources (~1995) are now emitting synchrotron X-ray beams that are a trillion (10^{12}) times more brilliant than those produced by X-ray tubes. Coupling electron and X-ray beams together, the Free Electron X-ray Lasers currently on the drawing boards could be the next generation of X-ray sources. While they promise to achieve an increase in peak brilliance by another factor of a trillion, the first prototypes may be operational around the year 2010.

One key experimental component of nanocrystallography is thereby an appropriate Synchrotron Radiation beamline like the Microfocus at ESRF in Grenoble, having appropriate beam intensity and width capable to obtain X-rays diffraction patterns from microcrystals ranging in size between 5 and 100 microns.

3.3.1 Principles of Synchrotron functioning

One of the most suitable annular experimental hall toward microfocussing is the one existing at the European Synchrotron Facility (ESRF) in Grenoble (France) which accommodates the Storage Ring

Tunnel, Beamlines and Preparation Laboratories (Figure 3.12). Other Synchrotron Radiation facilities are in USA, Russia (Kurchatov Synchrotron in Moscow) and even in Italy (Elettra Synchrotron in Trieste).

When high energy electrons are deflected by strong magnetic fields, they emit electro-magnetic waves called synchrotron radiation. Covering the whole spectral range from microwaves to hard X-rays, the light produced by a storage ring comes in the form of a fine and very intense beam, similar to that from a laser.

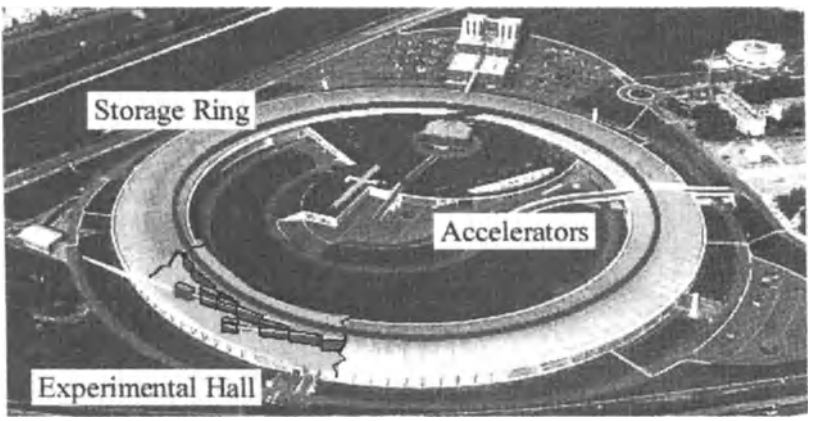

Figure 3-12. European Synchrotron Radiation Facility, Grenoble, France (courtesy of ESRF).

The European Synchrotron Radiation Facility, ESRF, operates a powerful source of light in the X-ray range. This 3rd generation synchrotron X-ray source is constantly pushing experimental possibilities to new limits and has been the first fully operational 3rd generation synchrotron radiation facility in the world operating in the hard X-ray range. Most strikingly, the X-ray beams at the ESRF are about a trillion times brighter (i.e. a factor of 10^{12}) than those of conventional X-ray sources used in laboratories and hospitals.

The scheme of synchrotron ring is presented on the Figure 3.13. In the storage ring, the needle thin electron beam is travelling with nearly the speed of light in ultra high vacuum. Prior to the storage ring we have:

-the Linac, a 16 m long linear accelerator, brings electrons to an energy of 200 MeV;

-the Booster Synchrotron, 300 m in circumference, repeatedly accelerates the electron bunches emitted from the Linac; once the electron beam reaches the operating energy of 6 GeV, it is injected in the storage ring.

In the Storage Ring, 844 m in circumference, the electron beam is maintained at the operating energy of 6 GeV. Here, electrons travelling with nearly the speed of light emit synchrotron radiation. In its normal mode of operation, the ESRF storage ring provides a current of 200 mA for a lifetime of about 50 h. Energy losses of the electron beam are compensated by 6 accelerating cavities, operating at a frequency of 352 MHz.

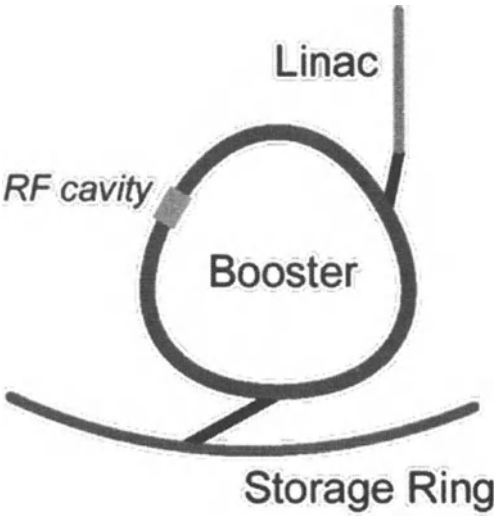

Figure 3-13. The scheme of synchrotron ring (courtesy of ESRF).

Generally, a storage ring is an assembly of stainless steel vacuum tubes in the form of a polygon with bending magnets at the corners. Their dipole magnetic field deflects the electron beam to maintain a closed orbit, whilst giving rise to the tangential emission of synchrotron radiation. The ESRF storage ring has 64 dipoles, each of which deflects the electron beam by 5.625. The basic layout allows for the operation of up to 32 bending magnet beamlines located upstream of insertion device straight sections. For storage ring operation at 6 GeV, the required magnetic field strength is ~0.8 Tesla, controlled within a tolerance of 0.05%, over a length of 2.45 m.

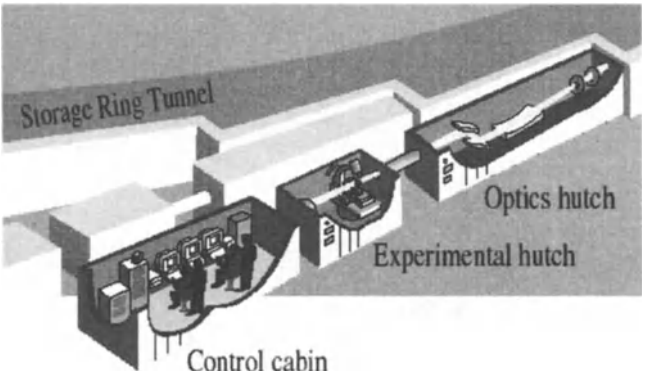

Figure 3-14. Organization of the synchrotron experiment (courtesy of ESRF).

The beamlines, are organised in functional compartments: the optics hutch, where the X-ray beam is conditioned, the experimental hutch, housing sample and detector, and finally the control cabin, allowing scientists to manage their experimental measurements (Figure 3.14).

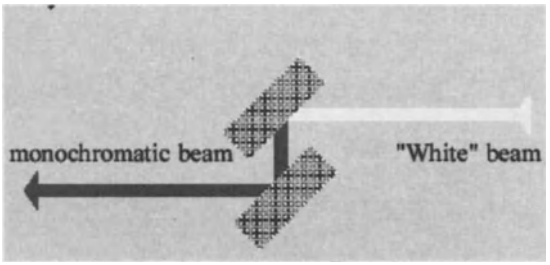

Figure 3-15. Synchrotron optics. crystal and multiplayer can be used to obtain a monochromatic beam.

In the optics hutch the X-ray beam coming from the synchrotron source is conditioned to yield a match with the requirements of the experiment. X-ray optical elements have to be able to withstand a heat load that can be up to 15 times larger than that on the surface of the sun. Tailored to the specific needs of ESRF beamlines, crystal and multilayer monochromators (Figure 3.15) determine spectral resolution, while, on bending, the same elements allow the x-ray beam to be focused. extreme focusing, down to micrometre (10^{-6} m) size can be obtained by either Bragg-Fresnel or refractive lenses (see later in Figure 3.16).

Generally, X-rays coming from a Synchrotron source are polychromatic ("White" beam), meaning that photon energies vary over a certain

bandwidth. Relying on the effect of Bragg diffraction, crystal monochromators single out a precise photon energy (i.e. wavelength) when required by experiment. The spectral resolution of an X-ray monochromator crystal is determined by its degree of crystalline perfection.

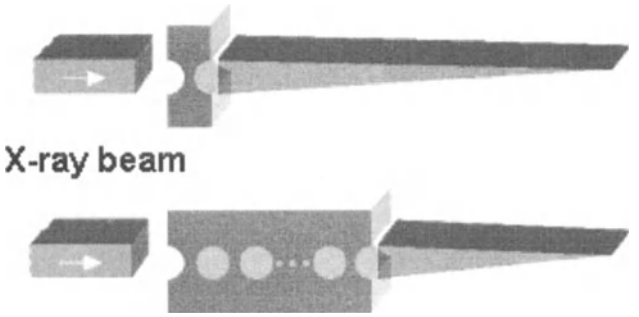

Figure 3-16. Refractive lenses (At the ESRF, a Compound Refractive Lens, in practice an Aluminum block with 30 holes of radius R=0.3 mm drilled on a straight line, succeeded in demagnifying the synchrotron source size by a factor of 20 for a focal length F of 1.8 m (courtesy of ESRF).

Multilayers used in X-ray optics are periodic structures made from alternating layers of light and heavy elements, like e.g. silicon and tungsten. Monochromators relying on multilayers rather than on crystals increase the photon flux at the expense of spectral resolution. Considering multilayers as artificial crystals, their "lattice constants" (or rather the length of a stacking period) can be chosen to fit the experimental needs. A large lattice spacing reduces the corresponding Bragg angles in the diffraction pattern, while the finite number of periods in the stack makes the Bragg peaks much wider in energy acceptance.

For a bending magnet source, the focal spot typically measures ~10 mm^2 for a focal length of ~0.5 m and photon energies of 10-30 keV. While refractive lenses (Figure 3.16) are commonly used to focus visible light, it has only recently been shown, that the same principle can be also used in the hard X-ray regime. Indeed, the small spot size and the low natural divergence of a synchrotron beam are required to efficiently focus hard X-rays with Refractive lenses.

The basic equipment in the experimental hutch comprises the sample holder and the X-ray detector, mounted on a frame allowing to adjust their mutual positions as well as their alignment with respect to the incoming synchrotron beam.

Scientist perform their experiment from the control cabin. Indeed, when the beam is on, the experimental and optics hutch are sealed, to eliminate any risk of radiation exposure. All functional elements of the beamline, from the insertion device to the detection of the signal are controlled by computers and can be adjusted on-line.

In summary, as shown in Figure 3.14,. the actual research instruments and the beamlines are organised in functional compartments: the Optics hutch, where the X-ray beam is conditioned, the Experimental hutch, housing sample and detector, and finally the Control cabin, allowing us to manage experimental measurements on small protein microcrystal at the Microfocus Beamline ID13 described later in great details.

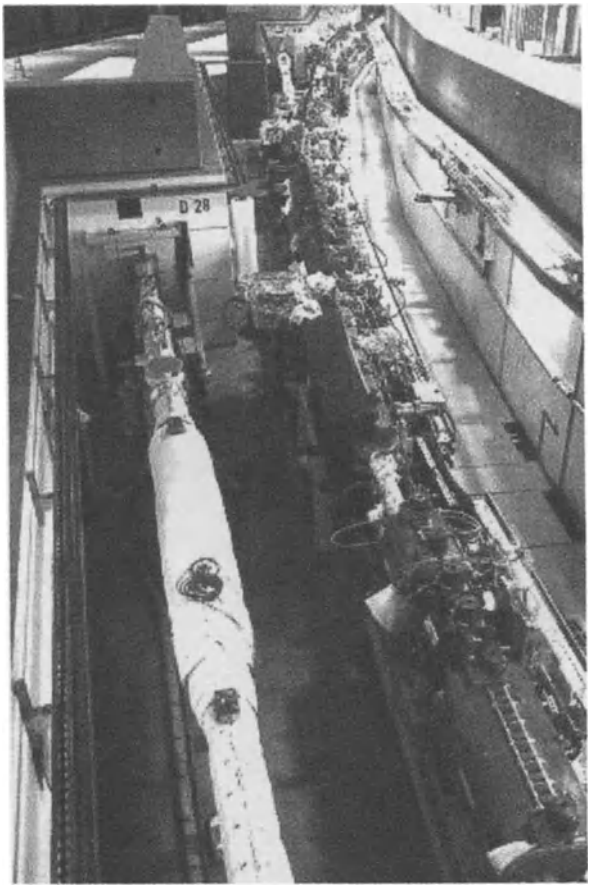

Figure 3-17 Synchrotron front-end image and tunnel (courtesy of ESRF).

When we look inside the tunnel (as apparent also in Figure 3.17), we can see the functional elements of the synchrotron X-ray source - bending magnets and insertion devices. Furthermore, focusing magnets collimate the electron beam, while front-ends carry the X-ray beam to the experimental hall.

Located within the storage ring tunnel, a front-end is not really part of the machine producing X-rays (Figure 3.17). Its main function is that of a shutter. When the shutter is open, the X-ray beam (Figure 3.18) is carried towards the experimental hall, while it is dumped safely, when the shutter is closed. The other components of the front-end are windows made from beryllium which isolate the ultra high vacuum in the storage ring from the experimental stations, and X-ray beam position monitors, which are used to align the optical elements in the optics hutch of the beamline.

The technical challenge for the front-end and its components is the high power density (1.5 kW/mm^2) in the X-ray beam. Faster than any welding machine, such a beam would take ~20 milliseconds to burn a hole in the stainless steel vacuum vessel of the storage ring.

Finally,taking the example of an undulator, the up-down oscillation of the magnetic field direction translates, via the Lorentz force, to a horizontal oscillation of the electron beam trajectory. The successive deflections of the electron beam result in the emission of synchrotron radiation of extremely high brilliance.

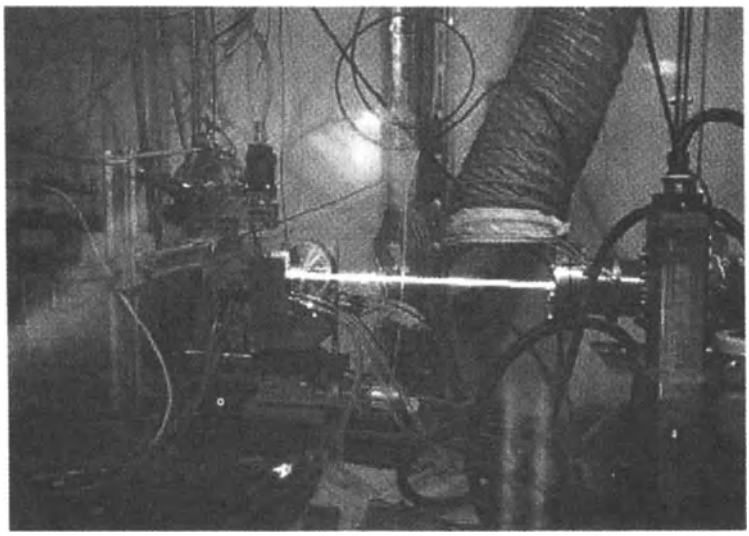

Figure 3-18. Synchrotron X-ray beam (courtesy of ESRF).

Insertion devices are the source of the high brilliance obtained from modern 3rd generation synchrotron sources. Placed in the straight sections of the storage ring (i.e. between two bending magnets), they comprise a succession of small magnets with well defined strength and polarity. At the ESRF, a large variety of insertion devices can be assembled from up to 3 segments per straight section. This modular approach enables the characteristics of the X-ray source to be matched to the various needs of individual experiments. Relying on pure and hybrid permanent magnets as well as superconducting magnet technology, about 50 insertion device segments, divided between undulators and wigglers, are currently installed in the ESRF storage ring.

The high brilliance of the X-ray source is also the result of a small spot size and a low angular divergence of the electron beam, i.e. the low emittance of the storage ring. The latter is due to focusing magnets, placed both up- and downstream of bending magnets and insertion devices. they define beam position and size by collimating the electron beam like funnels. The storage ring of ESRF has a total of 320 quadrupoles.

Worth of citation for its potential implication in nanotechnology (frequently addressed in this book) is also an interesting method which allows the characterization of ultra-thin layers, multi-layers systems and superlattices. This method (see Kovalchuk et al., 1994) ,named X-Ray Standing Waves (XSW), is based on the combination of high structural sensitivity of classical X-Ray diffraction method and spectroscopic selectivity under non-elastic secondary radiation (photoelectrons, fluorescence, etc.). Various modifications of XSW could allow indeed to manipulate ultra-thin layers for the construction of a new class of nanometer-scale materials (wave-guide structures and multilayers) and devices (Kovalchuk et al,1995).

3.3.2 Microfocus beamline and ultramicrocrystal diffraction

Microfocus ID13 Beamline was one of the three original ESRF test beamlines and saw its first beam at the end of 1992 (Figure 3.19 and Table 3.1).

User operation was started in September 94. The principal aim of the Microfocus Beamline is to provide small focal spots for diffraction and small-angle X-ray scattering (SAXS). Both single crystal and scanning diffraction (SXD) experiments are performed. Other applications, like scanning X-ray microfluorescence (SXRF), are feasible.

The main instrumental setup available for users is the microgoniometer (Figures 3.20 and 3.21) was developed in collaboration with EMBL for protein crystallography (PX) but can also be used for small- to medium cell

crystallography. Typical beam sizes available are 5/10/30 microns based on a condensing mirror and collimators.

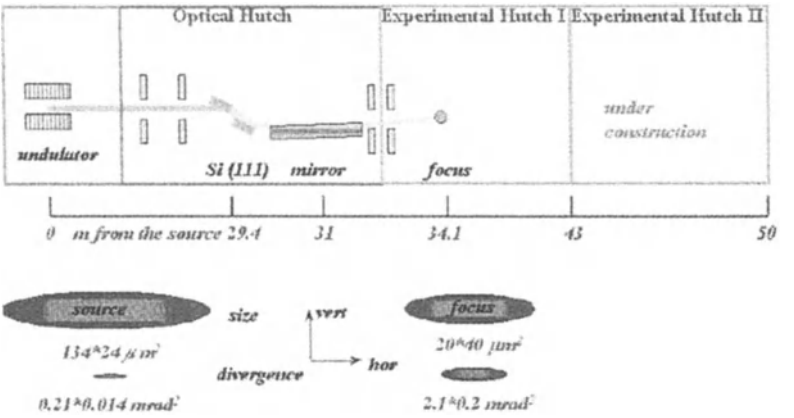

Figure 3-19. Microfocus Beamline Optics (courtesy of ESRF).

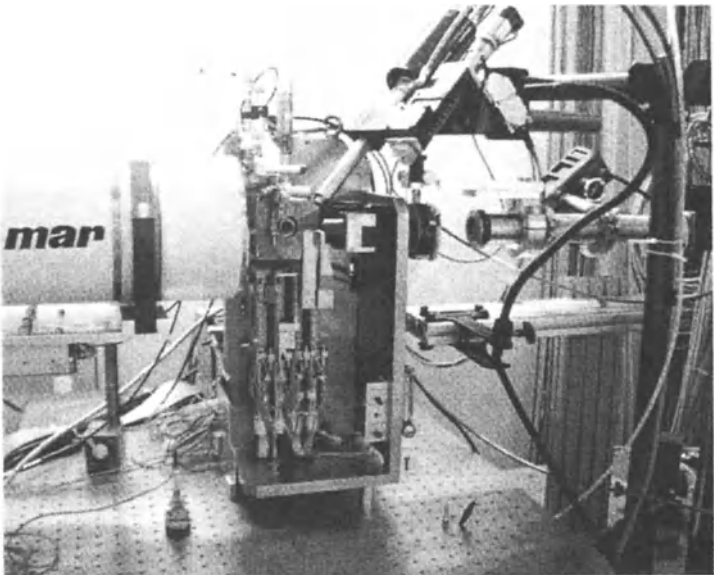

Figure 3-20. Far view of the Microfocus ID13 microgoniometer (courtesy of Christian Riekel at ESRF).

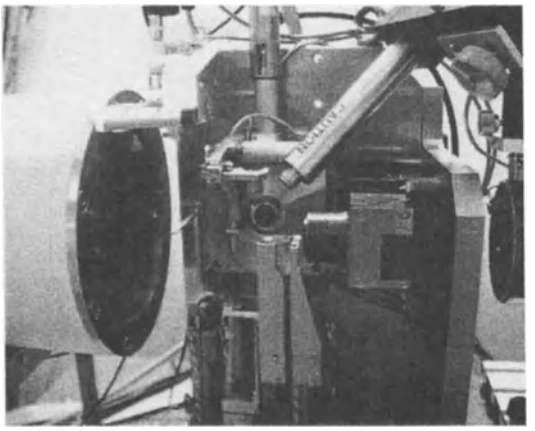

Figure 3-21. Close view of the Microfocus ID13 microgoniometer (courtesy of Christian Riekel at ESRF).

The scanning setup was developed for wide- and small-angle scattering. Typical beam sizes used are currently 2/5/10 microns based on a condensing mirror in combination with tapered glass capillaries or collimators. The scanning setup can also be used for SAXS-experiments. For a beam size of about 10 mm, the first order spacing of dry collagen can be resolved (65 nm).

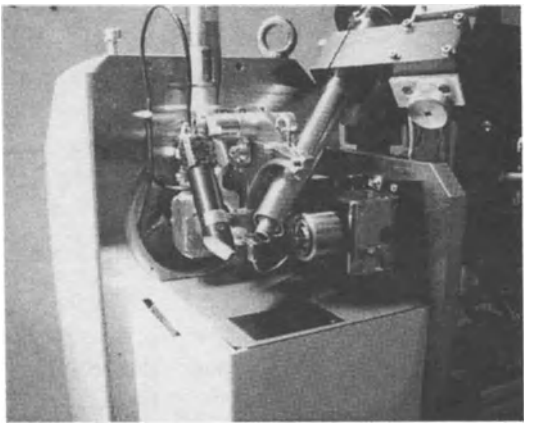

Figure 3-21b. Photography of the crowded sample position on the microfocus beamline with collimator (beam enters horizontally from the right), microscope (vertical), cryo-cooling system and beam stop (not present) all very close to the crystal which is moved by means of a Kappa-goniometer (courtesy of Christian Riekel at ESRF).

A 130 mm entrance window MAR CCD with 16 bit readout (~ 4 sec readout/frame) or a XIDIS detector with 12 bit readout (~ 0.1 sec readout/frame) are used for scanning.

Table 3-1. Microfocus ID13 X-ray source parameters.

source size (fwhm)	134(h) x 23(v) mm^2
source divergence (fwhm)	208(h) x 17(v) $mrad^2$
beam size at 30 m	6(h) x 0.5(v) mm^2

In particular it has been recently developed a waveguide set-up which combines both an alignment stage for a waveguide, a horizontally focusing mirror (about 3 mm at sample) and a sample stage.

Table 3-2. Microfocus ID13 undulator segments parameters

Period	gap	length
46 mm	>16.5 mm	1.6 m
35 mm	>16 mm	1.6 m

ID13 is installed at a low-b section. The X-ray source parameters are those indicated in Table 3.1. An overview on installed undulator segments is shown in the Table 3.2. Examples for the brilliance achieved at some ESRF beamlines as function of photon energy and for different types of Insertion Devices used at the ESRF is demonstrated on the Figure 3.22.

Microfocus Beamline at the Grenoble Synchrotron has been used to provide small focal spots for diffraction of our single protein crystal. The main instrumental setup being used by us during our experimentation has been the microgoniometer developed for protein crystallography (PX) with typical beam sizes of 5 to 10 μm based on a condensing mirror and collimators.

It is to remember that while for the traditional X-ray diffraction crystals of rather big dimensions have to be obtained, new synchrotron radiation sources require quite smaller crystals. Focused X-ray beam from third generation synchrotron sources can be used for characterization of protein crystals of less 30 μm in size, perhaps down to 5 – 10 microns. (Cusack et al., 1998).

Recently, as shown in a later chapter, diffraction data could be obtained for the first time on very small human CK2α microcrystals obtained by homologous protein thin film template. Due to the very small size of the crystals (of about 20μm in diameter), diffraction data could be collected only using a microfocus beamline of 20 x 20 μm^2 of the ID13 beamline of ESRF (Grenoble), which has utilized with great success in many other experimental circumstances (Cusack 1998; Henderson et al., 1995; Gonzalez et al., 1994; Engstrdm et al., 1995; Riekel et al., 1997; Bilderback et al., 1994; Jark et al., 1996; Landau et al., 1996; Pebay-Peyroula et al., 1997; Miller et al., 1998).

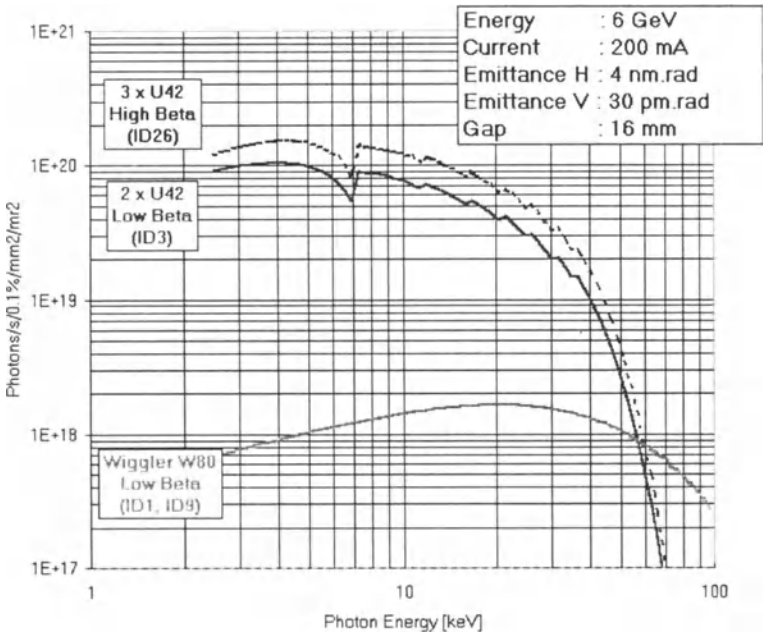

Figure 3-22. Examples for the brilliance achieved at some ESRF beamlines as function of photon energy and for different types of Insertion Devices used at the ESRF (as of January 1998) (courtesy of Christian Riekel at ESRF).

In our hands, pointing to good quality of our microcrystals, all diffraction patterns utilized to solve the structure of protein kinase CK2α catalytic subunit were obtained at ID13 Microfocus beamline from a single ultramicrocrystal (20 x 20 x 60 microns). The crystal structure of CK2α mutant could be determined at a good resolution (2.4Å) despite the very small size of the crystal used (Figure 3.23).

Three major innovations can then be drawn from this report on the human CK2α catalytic subunit which are bein generalized to a wide class of proteins yet unsolved and of significant pharmacological potential (such as cytochrome P450scc, P4502b4, and other membrane proteins now in progress):

- diffracting microcrystals are consistently obtained for the first time by a recently introduced thin film template method (Pechkova and Nicolini, 2001, 2002) for proteins so far never crystallized despite numerous efforts worldwide by standard methods;

- atomic resolution structure has been derived at the ESRF Microfocus Beamline for the first time from ultrasmall protein microcrystals with diameter less than 20 microns;
- the 2.4 Å resolution of the catalytic subunit of CK2α human kinase, a protein of central importance in life sciences.

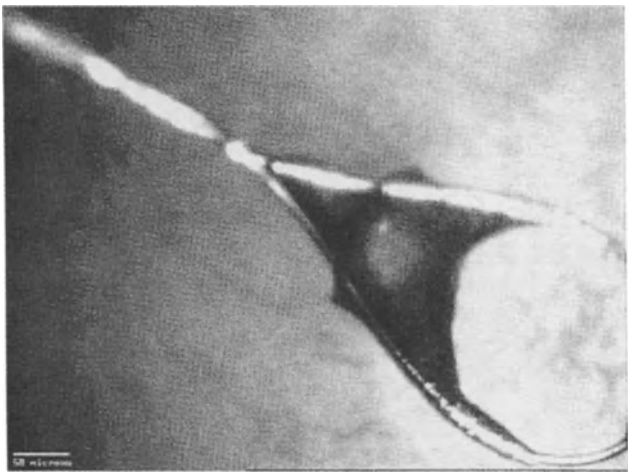

Figure 3-23. The needle human protein CK2α crystal in the mounted loop (Pechkova and Nicolini, 2003a).

In summary, every protein crystallographer has had the thrill of finding microcrystals of new protein with the subsequent frustration that they cannot get them to grow bigger. These recent advances in synchrotron radiation instrumentation has sown the possibility to routine data collect crystals of less than 30 pm in size, perhaps down to 5-10 microns. Microcrystals of macromolecules are generally unusable with conventional sources because they are weakly diffracting. We need that the same beam intensity going in a 200 micron be all focused into that 20 micron crystal, implying the need for microfocusing X-ray optics in addition to intense beams. However, one cannot indefinitely compensate for small crystal size with increased beam intensity since at some stage so much X-ray energy is being deposited in a small volume that the protein structure and crystalline order will be destroyed by primary radiation damage very quickly.

The limits imposed by radiation damage have been considered theoretically by Henderson and examined experimentally for protein crystals by Gonzalez and Nave Practical experience shows that cryocooling does not prevent severe radiation damage at 100 K if the X-ray dose is very high, for

instance from a focused undulator sòúrce on a third generation synchrotron. The implication is that with weakly scattering microcrystals where very high incident beam intensity is required to get statistically accurate Bragg intensity measurements, multiple crystals will generally be required for a full data collection, even when frozen. Neither use of ultra-short wavelengths nor cooling to liquid helium temperatures has yet been shown to circumvent in any significant way this fundamental physical limitation although efforts to ensure that there is no crystal heating may be important.

With microcrystal instrumentation focused X-ray beams from third generation synchrotron sources allow the possibility of data collection from previously unusable protein microcrystals of only a few microns in size. The following features are critical for a successful protein microcrystal station: (i) the matching of beam size to crystal size without loss of beam intensity, that is, microfocusing of synchrotron radiation, and (ii) a carefully designed crystal environment to visualize and accurately align extremely small frozen crystals and to minimize background, but at the same time allowing rapid throughput of crystals.

Microfocus optics used at the European Synchrotron Radiation Facility (ESRF) microfocus beamline (ID13) warrants all the above and is based on an ellipsoidal mirror as the unique focusing element in combination with a Si-111 double monochromator.

Given the present surface quality of mirrors one arrives at a focal spot size of -40 (horizontal) x 20 (vertical) $11m^2$ and a divergence of about 2 (horizontal) x 0.2 (vertical) mrad (ref. 4). For further beam definition and background reduction, micro-collimators of lOltm or 30 pm are placed in the focal spot. Typically a flux of $10'$ photons $s^{-'}$ $mA^{-'}$ is obtained for a 30 pm collimator although this could be increased with an optimized undulator source. The optical system of ID13 is sufficiently stable to allow operation over several days down to beam sizes of a few ltm by placing a glass capillary in the focal spot[3] although monochromatic beams of this size are used at present only for scanning diffraction applications. A reduction of the beam size in monochromatic single crystal diffractometry below the 10 pm barrier will require higher precision goniometers than are currentlv commercially available and in particular advances in sample observation. The limits in X-ray focusing are currently in the range of 50-100 nm.

Protein microcrystallography requires an order of magnitude higher precision (that is, microns compared to tens of microns) in alignment than on standard setups coupled with high mechanical stability. The requirement is to be sure that the microcrystal is in the microbeam and on the rotation axis. This calls for high power microscopes to visualize both crystal and beam position (for example, with a fluorescent crystal) and accurate motorized adjustments to bring everything into alignment. Visualization of time frozen

crystals in loops is not always easy and a crucial aspect of the optical visualization is correct illumination, possibly with an option of using polarized light. In order to record the weak diffraction, background must be minimized by having the collimator and a small beamstop verv close (a few mm) to the crystal. This,. together with the presence of a crvocooler and microscopes, means that the sample position is very crowded, making manual access for crystal mounting difficult (especially of pre-frozen crystals which require an arc or cryo-tongs) and greatly increasing the risk of mis-aligning something (such as the beamstop, collimator, microscope, crystal and so forth.

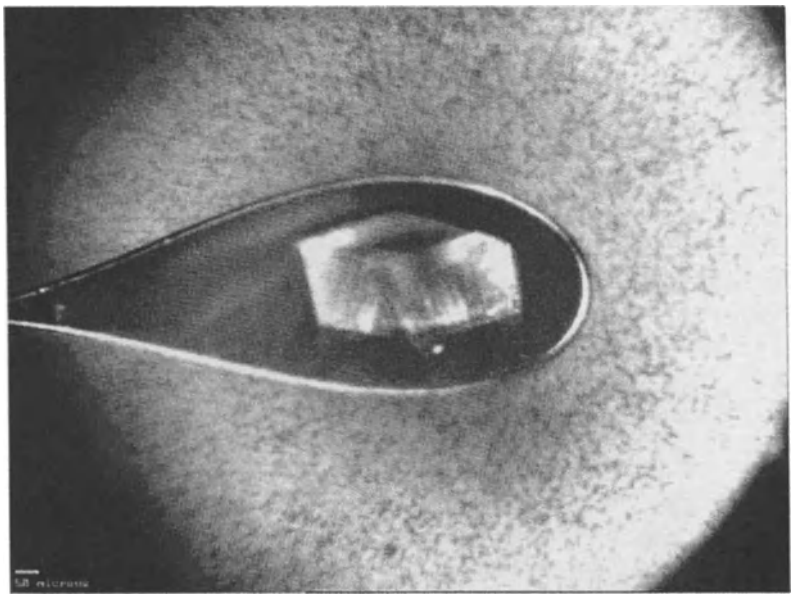

Figure 3-24. Mounted lysozyme crystal in the nylon cryoloop (Pechkova and Nicolini, 2003a).

In general, a better understanding of crystal morphology twinning and quality could be gained by more systematic microprobe diffraction experiments on protein crystals.

However, it is still early days in the exploitation of microbeam diffraction in protein crystallography although very promising results have already been obtained.

3.3.3 Protein crystals synchrotron radiation analysis

The typical image of the mounted protein crystal (in the case shown in Figure 3.24 - lysozyme crystal) in the special nylon cryoloop. The crystal dimensions is about 900 x 400 x 300 micron, the loop diameter is 0.1 mm.

The loop diameter chosen for the CK2α (Figure 3.23) frozen microcrystals analaysed at Grenoble were of the order of 0.02 mm, without the need to utilize any cryoprotectant.

The intensity of the beam line was 10 to the 12 photons per mm^2 per second, with a delta phi incremental rotation of one degree over 180 degrees for the acquisition time of 0.5 seconds per degree. The sample geometry for microgoniometer is presented on the Figure 3.25.

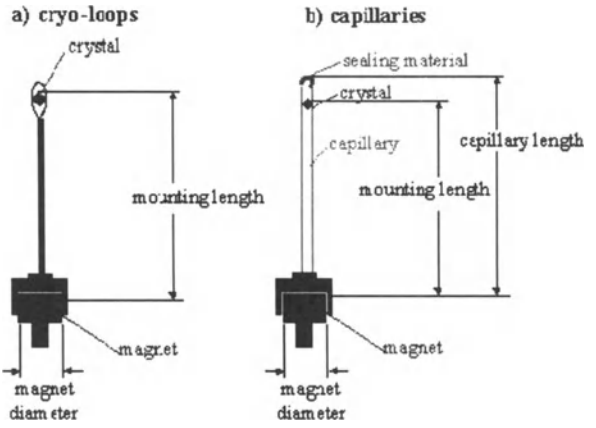

Figure 3-25. Sample geometry for microgoniometer (courtesy of ESRF).

The needle crystals of 120 x 10 microns (Figure 3.24) have been then exposed in different region Computer filing and data reduction was obtained by transferring the diffraction image from the NICE at Grenoble to the our computer in Italy and images were processed utilizing all the numerous reflections being accepted to a resolution of 2.4 Å.

Diffraction data were collected at a temperature of 100 K. Before mounting, the mother liquid solution was proved to be a sufficient cryo-protectant. The image of the CK2 mounted crystal before (a) and after (b) synchrotron radiation exposure is shown on the Figure 3.24.

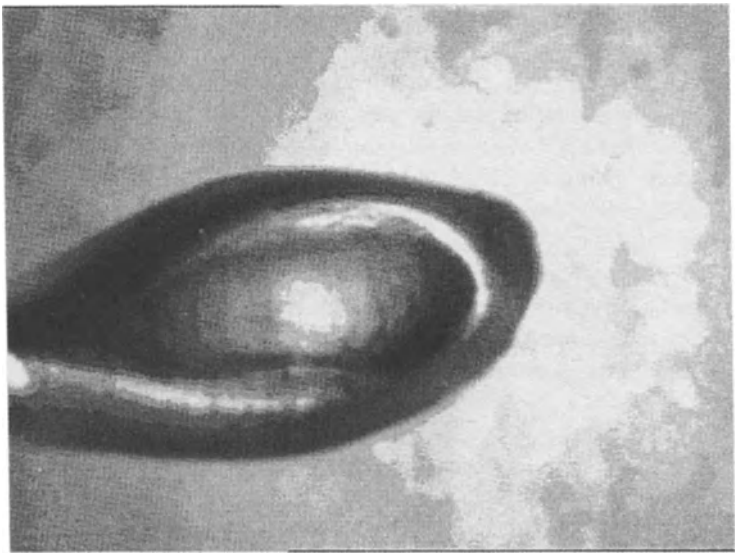

Figure 3-26a. The image of Ck2 mounted crystal of approximate size 0.06 x 0.02 x 0.02 μm^3 before synchrotron radition exposure (Pechkova and Nicolini, 2003a).

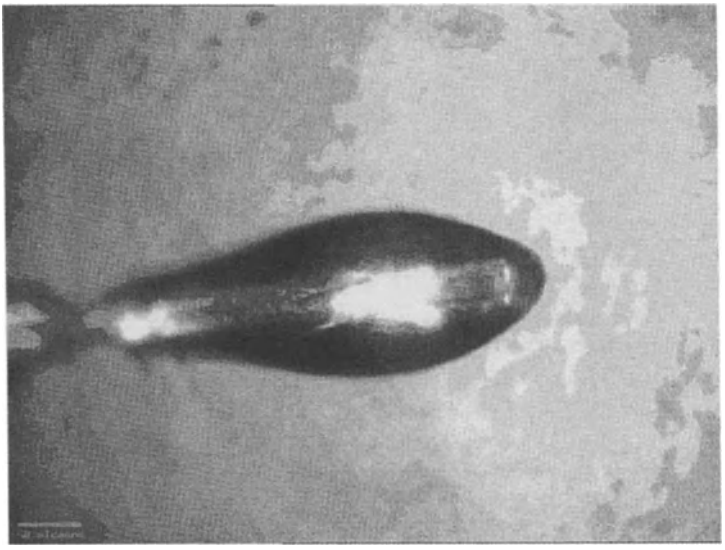

Figure 3-26b. The image of CK2 mounted crystal of approximate size 0.06 x 0.02 x 0.02 μm^3 after synchrotron radiation exposure (Pechkova and Nicolini, 2003a).

The wavelength used was of 0.955 Å and the crystal to detector distance 120 mm. Crystals diffract to a maximum resolution of 2.4 Å. The images of the Ck2α crystal being utilized to obtain the 3D structure at atomic resolution (obtained and discussed later in Chapter 4) before and after synchrotron radiation exposure are shown in Figures 3.26a and Figure 3.26b.

3.3.4 Structure determination and refinement

Data were indexed with MOSFLM (Leslie 1991) and then scaled with SCALA from the CCP4 software package (CCP4, 1994). The crystal structure was solved by the molecular replacement method with the program AMORE (Navaza 1994), using the structure of the CK2α subunit from Zea Mays as a template (PDB ID code 1NA7).

The crystallographic refinement of the structure was carried out with the CNS software package (Brunger et al., 1998) alternated with manual inspection of the electron density maps and rebuilding of the model using the graphic program QUANTA (QUANTA *98.1111 1986-191*). During the final steps of the refinement water molecules were added. The stereochemistry of the final model was checked with the program PROCHECK (Laskowski, 1993).

Statistics for data collection and final models are reported later in Chapter 4 for the human kinase protein being solved recently (Pechkova and Nicolini., 2003a).

3.4 From art to science with protein nanocrystallography

So far, by conventional protein crystallization techniques, some methods have been useful for individual proteins and/or in isolated cases but none have yet turned out to be of general use.

Its easy to see, that its quit impossible to find the key to every existing protein developing the general procedure for protein crystallization. The numerous trials to find the magic substance or environment to control the crystal growth proves that protein crystallization remains an art, like a philosophic stone search in the alchemists times. Indeed, to be crystallized each protein requires its own specific conditions, which are often difficult to determine and that require empirical random searching.

That is why protein crystallography is often called an art instead of a science. Thaw is why now it is really urgent the requirement of the real, scientifically based procedure which can permit to control both nucleation and growth of protein crystals. The complexity of the task is also increases by the completely different nature of proteins, hence no organic or inorganic

substance, surface or environment can fit to all the proteins. For this reason the new approach based on nanothechnology had been introduced (Pechkova, Nicolini, 2001).

Chapter 4

FROM ART TO SCIENCE IN PROTEIN CRYSTALLOGRAPHY

The encouraging results obtained with a model system, such as chicken egg white lysozyme that is summarized in the first part of this chapter, has opened new opportunities in the use of Langmuir-Blodgett protein thin film for the protein crystallization. Indeed, nanotechnology-based crystallization method appear to improve lysozyme crystals growth rate and crystal overall final size. Moreover, crystals obtained by means of this innovative method were proved to diffract perfectly. All these results turned to be quite explainable in terms of physical principles.

It seemed therefore to be interesting to apply this new method to the class of so far non-crystallized proteins of significant fundamental and pharmaceutical relevance, as mammalian cytochromes and human kinases.

Earlier findings have shown the effect of thin protein film template on the crystal growth of proteins, but still open questions remain on the role of thin protein film template in protein's crystal growth, namely the role of the orientation of proteins in the thin film. Furthermore questions remained on the detailed nature of the diffraction patterns of these crystals made by thin film nanotechnology.

4.1 New method validation with Lysozyme as a model protein

A classical example of proteins frequently utilized as model system because of its ready accessibility and easy crystallization is Lysozyme (Mucopeptide N-acetylmuramylhydrolase; E.C. 3.2.1.17). Lysozyme catalyzes the hydrolysis of 1,4 glucosidic linkages which occur in the cell

E. Pechkova et al., *Proteomics and Nanocrystallography*
© Springer Science+Business Media New York 2003

walls of microorganisms. It is a basic protein with a molecular weight of approximately 14 kDa.

Lysozyme is normally present in plasma (5.9 mg/l) but only in trace amounts in urine. In certain renal disorders, urinary excretion of lysozyme is significantly increased, which could be of diagnostic significance (Harrison et al, 1973). Analysis of serum lysozyme levels could also be used as a diagnostic tool in acute and chronic myelocytic leukemia and in acute lymphocytic leukemia (Grossowicz et al, 1979).

Being crystallized and characterized in 1945 (Alderton and Fevold, 1946) hen egg lysozyme has been the favorite model for the nucleation rates (Galkin and Vekilov, 2001) and crystallization mechanism studies under various conditions (Judge et al., 1999), for the mathematical microscopic modeling and theoretical interpretation of macromolecule nucleation and crystal growth (Jianwei and Nobuko, 2000; Kierzek et al., 1997, 1999, 2000; Bradley, 1999; Nadarajah et al., 1995a) as well as for the analysis of the crystallization kinetics (Bessho, 1994) and the X-ray topographic studies of protein crystal perfection and growth (Dobrianov et al., 1998).

In a great number of studies, chicken egg white lysozyme plays the role of the model protein for the new methodologies verification. Heterogeneous nucleation and adhesion of lysozyme crystals have been investigated using a double (thermal) pulse technique (Tsekova, 1999). Sanojoh and co-workers have reported the electrostatically driven heterogeneous nucleation of lysozyme on microfluidic silicon device. The inducement or avoidance of nucleation was dependent on the pH of the crystallization solution and the surface charge of protein molecules (Sanojoh and Tsukihara, 1999). Lysozyme is also known to be a model protein in researches dedicated to optimization of protein crystallization conditions or the growth rate modeling. Different methods were explored and discussed for the crystal growth rate control and stimulation, such as microgravity (Aibara, 1997) forced solution flow, hydrostatic pressure (Fermin et al., 1999; Vekilov and Rosenberger, 1998; Nadarajah et al., 1995b). High pressure and magnetic field influence on the rate control during lysozyme crystal growth has also been investigated (Forsythe et al., 1994; Sazaki et al., 1999; Suzuki et al., 2000; Yanagiya et al., 2000). Moreover, using lysozyme as an example, it was described, that sitting drop is well suited for attempting epitaxial growth of macromolecule crystals on appropriate mineral matrices (McPherson and Shlichta, 1988). It was also found that the number of nuclei, adhesion and preferred orientation of hen egg white lysozyme crystals were influenced by changing the chemistry of the substrate (Tsekova et al., 1999). However, it was also proved that number of nuclei can be influenced by a specific lysozyme nucleation (Chayen et al., 1993).

4.1.1 Effect of the thin film template: kinetics of the lysozyme crystal growth

After preliminary screening procedures by means of hanging or sitting drop vapour diffusion method, the different conditions (protein and precipitant concentration, pH, ionic strength, drop/well precipitant concentration ratio) for lysozyme crystallization can be compared. For example, kinetics of protein crystal growth at different ionic strength of buffer solution is plotted on the Figure 4.1.

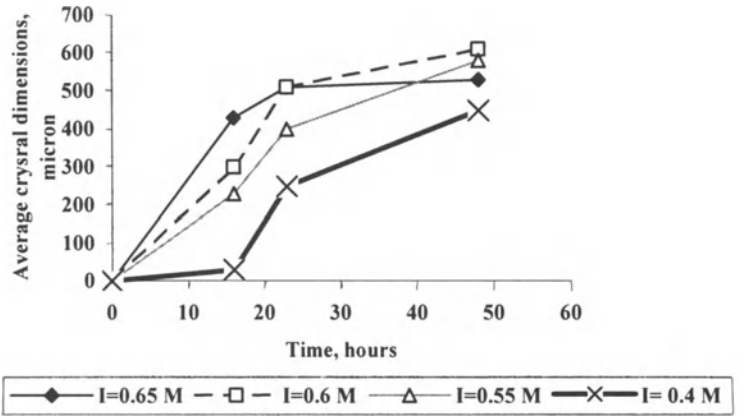

Figure 4-1. Lysozyme crystals growth by classical hanging drop method at different ionic strength of buffer solution.

On the base of these results, using the classical crystallization procedure the optimal condition for lysozyme crystallization can be chosen. From our protocols, the following conditions turned to be successful: lysozyme concentration in the drop was 20 mg/ml in 50 mM sodium acetate pH 4.5 while concentration of NaCl was 0.45 M in the drop and 0.9 M in the reservoir. Under these conditions few large lysozyme crystals were obtained. Crystallization experiments were carried out at controlled temperature of 20° C.

Some images of the "classical" lysozyme crystals are shown on the figure 4.2. The largest size of the crystals obtained was not above 600 micron along its longest axis.

To understand the influence of the lysozyme thin film template on its crystal nucleation and growth, the same experiment have to be repeated by means of nanotechnology based crystallization method.

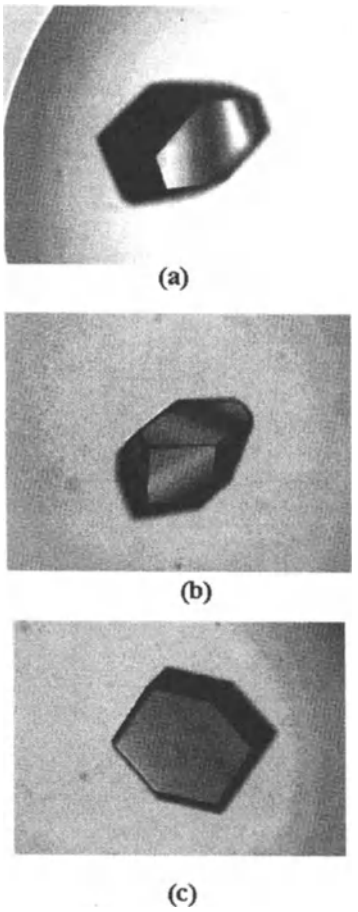

Figure 4-2. Single lysozyme crystals, obtained by classical hanging drop method. The average crystal dimensions (along the longest axis) are: (a) 600 micron, (b) 580 micron, (c) 570 micron.

For this aim, lysozyme thin film template can be prepared by means of Langmuir-Schaeffer deposition of protein monolayer on the siliconized glass cover slide of the crystallization well (see Figure 3.1 in the earlier chapter). Lysozyme monolayer of were formed in a proprietary Langmuir-Blodgett trough by spreading 500 mM phosphate buffer (10^{-3} M, pH 6.5) solution

with a lysozyme concentration 4 mg/ml with 10^{-3} M NaOH solution (pH 11) or distilled water solution was used as a subphase at controlled temperature 22° C. The formed protein monolayer was compressed with a barrier speed of about 0.1 mm/s up to surface pressure of 20 mN/m.

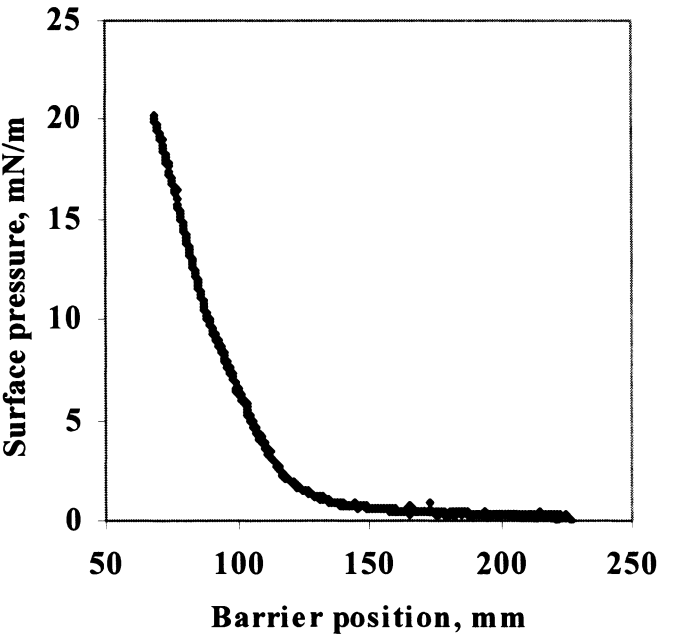

Figure 4-3. Surface pressure of lysozymemonolayer at the air-water interface.

Pressure-area (π-A) lysozyme isotherm is presented on the Figure 4.3. It is worth to notice, that X axis is expressed in barrier co-ordinate units, as it is impossible to calibrate the axis in area per molecule units due to impossibility of calculating the actual surface concentration of the protein. This problem is general for protein monolayers and it results from some partial solubility of proteins in the volume of the subphase (Lvov et al., 1991).

Several (from one to three) lysozyme monolayers were transferred on the glass slide (water rinsed or siliconized or pretreated with other chemicals) and then kept in the crystallization process as a template for the small drop of protein's solution under the same conditions as for classical hanging drop method. Average dimensions of lysozyme crystals, obtained

using thin film template after one week of equilibration were about 800 micron (Figure 4.4), while crystals, obtained by the classical hanging drop method in the same condition were about 600 micron (Figure. 4.2).

In the time frame being studied up to three months the difference in size remains the same. Indeed, using the new thin film template crystallization method, we managed to obtain good quality lysozyme crystals and their growth rate was increased in comparison with classical hanging drop case (Figure 4.5).

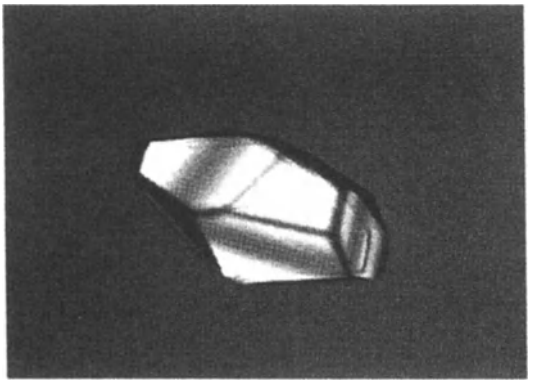

Figure 4-4. Large single lysozyme crystal, obtained by new protein crystallization method based on the thin film nanotechnology. Crystal dimension along the longest axis is 800 micron

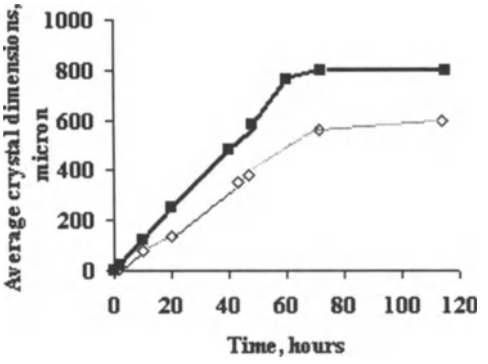

Figure 4-5. Acceleration of lysozyme crystal growth: grey line - classical hanging drop crystallization method; black line - nanostructured thin protein film crystallization method (Pechkova and Nicolini 2001, with permission from Elsevier).

Therefore, lysozyme thin film used as a template allowed acceleration of lysozyme crystal growth in the modified hanging drop crystallization method with respect to the classical hanging drop method.

4.1.2 Thin Film Surface Pressure influence on the template-induced crystallization

Taking into consideration the above results, it seems to be interesting to understand how the nature of the thin protein film influence on the crystal nucleation and growth.

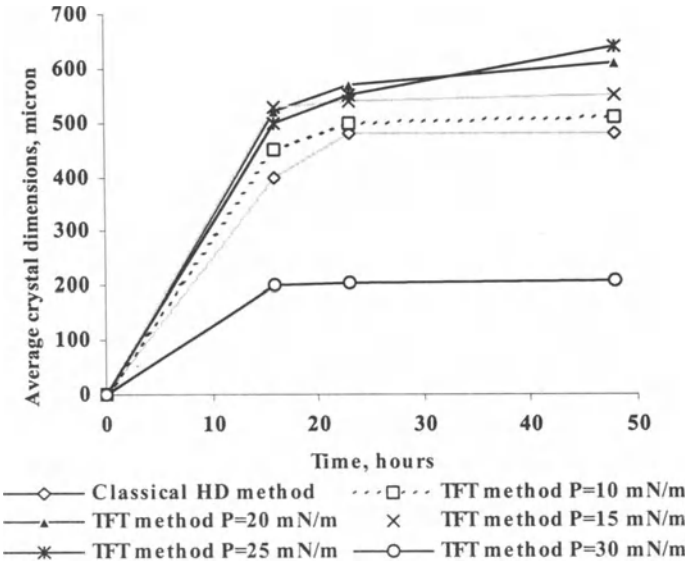

Figure 4-6a. Lysozyme crystals growth in the same crystallization conditions (ionic strength 0.6 M and the protein concentration 20 mg/ml in the crystallization drop) by classical hanging drop method versus homologous thin LB film template prepared with increasing surface pressure of protein mololayer at the air –water interface (Pechkova and Nicolini, 2003a).

To answer this question, further study has been carried out to investigate thin film surface pressure influence on the template-induced crystallization.

For this reason several templates of different protein monolayer with increasing surface pressure at th. air –water interface were prepared, and the crystal growth rate was compared for various cases at the same crystallization conditions (ionic strength 0.6 M and the protein concentration 20 mg/ml in the crystallization drop).

The results of this study are presented on the Figure 4.6a Analyzing this plot we can presume that the optimal protein template surface pressure is 20 mN/m. In fact, the largest crystal were grown on this template (Figure 4.6b (1)), while at 10mN/m is obviously not enough to accelerate protein crystal growth, because low protein monolayer orientation, as well as at 30mN/m, when protein monolayer is over compressed and disordered.

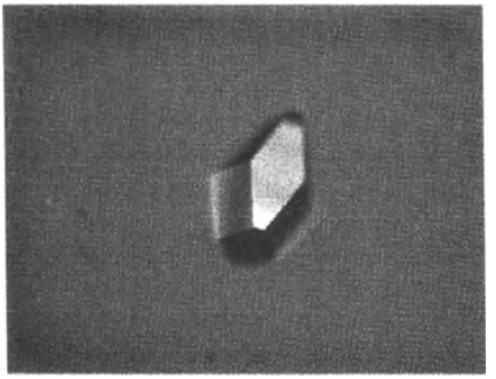

1

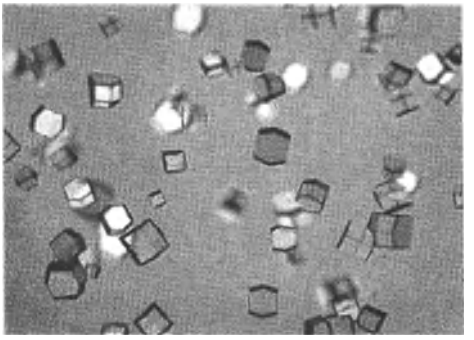

2

Figure 4-6b. Lysozyme crystals obtained by thin protein film template crystallizatyion method. (1) - suface pressure 25 mN/m crystal dimension along the longest axis is 680 micron; (2)- surface pressure of protein monolayer 30 mN/m, crystal dimension

It can be concluded that increased order associated with the increased surface pressure points to an increased acceleration and larger crystal growth. Indeed, protein's crystal growth in presence of thin protein film

template is shown indeed to be critically dependent on the orientation of proteins in the thin film until reaching a reproducible plateau value. The orientation appears properly controlled by changing the surface pressure at the air-water interface where the protein films are formed.

4.1.3 X-ray diffraction of lysozyme crystals

Diffraction pattern of a crystal of lysozyme grown from a solution of lysozyme in presence and absence of the thin film template of homologous proteins were subsequently taken at the Bruker diffractometer.

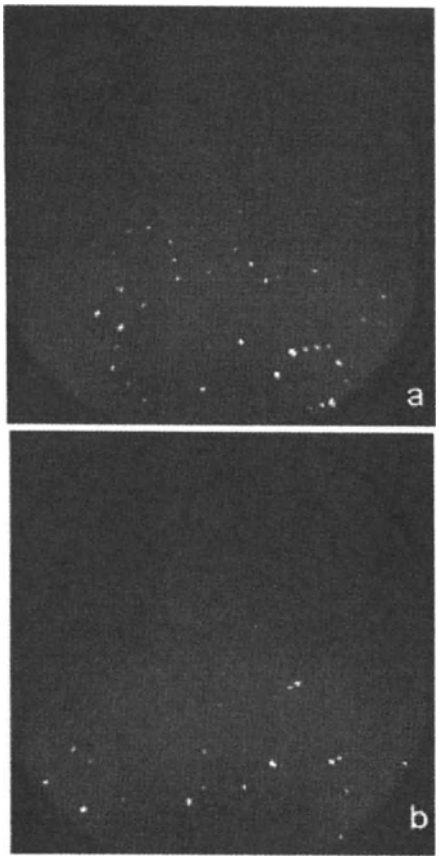

Figure 4-7. X-rays diffraction of lysozyme crystals obtained at -30° by hanging drop method (a) and protein thin film template method (b). Resolution: less then 1.7Å.

A single frame corresponds to a rotation of 0.25 degrees, with a graphite crystal-to-film distance of 75 mm at an angle of -15 degrees.

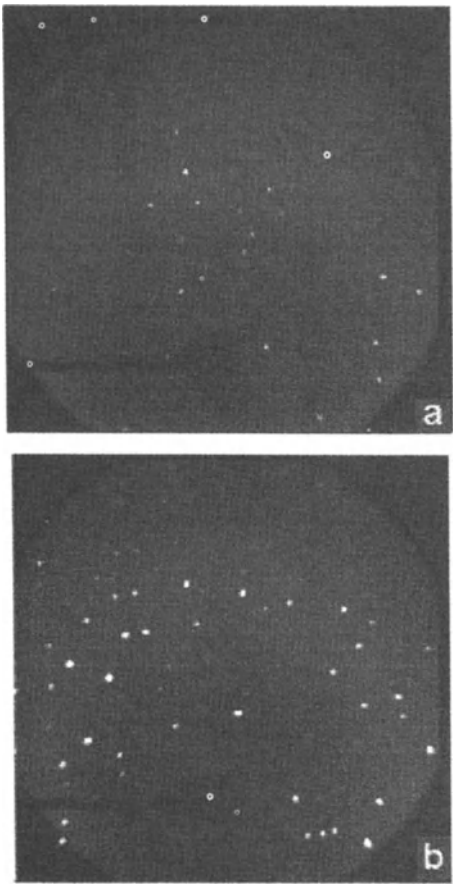

Figure 4-8. X-rays Diffraction of Lysozyme crystals obtained at -15° by Hanging Drop Method (a) and Protein Thin Film Template Method (b). Resolution: less then 1.7Å.

The radiation used was CuKα monochromatized. For the 3D reconstruction at atomic resolution we have utilized software web-accessible software packages to obtain the x,y,z coordinates of each protein atom from the observe h, k, l reflections. Diffraction pattern at -15 and -30 degree of a crystal of lysozyme grown from a solution of lysozyme in absence (a) and presence (b) of the thin film template of homologous proteins is shown on the Figures 4.7 and 4.8.

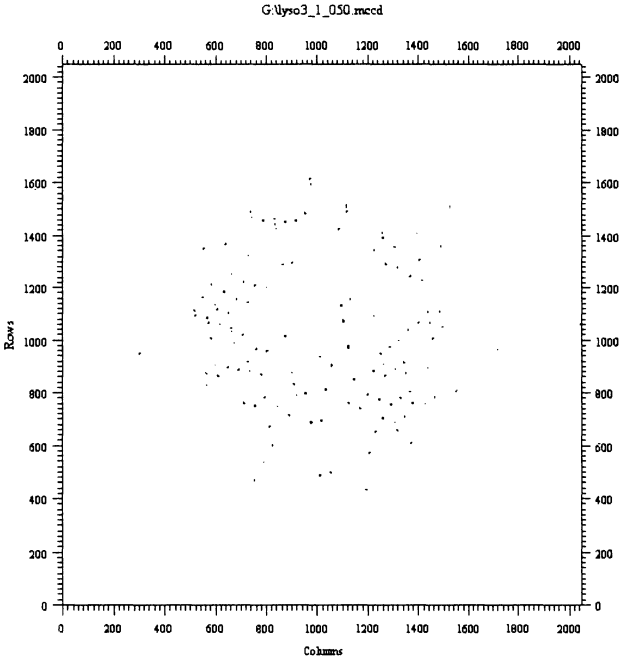

Figure 4-9. Diffraction pattern of lysozyme crystal grown by hanging drop method, at the Microfocus Beamline in Grenoble Synchrotron (Pechkova and Nicolini, 2003a).

These results have proved that both type of crystals have excellent diffraction patterns at both angles yielding a resolution at least of 1.7 Å, as it results from the X-ray diffraction data recorded at –15° (Bruker Diffractometer). The cell parameters founded corresponds to Protein Data Bank data (PDB code 1lys): for lysozyme crystal grown by classical hanging drop vapour diffusion method a = b = 79,124; c = 37,908; $\alpha = \beta = \gamma = 90°$, while for crystal obtained by thin film template crystallization method a = b = 78,580, c= 37,592, ; $\alpha = \beta = \gamma = 90°$.

4.1.4 Synchrotron Radiation analysis of lysozyme crystals

After comparison of the diffraction of crystals obtained by classical and thin film template method by X-ray diffractometer, the obtained results were confirmed by synchrotron radiation. In the first cases, the resolution that has been reached was about 1.7 Å, in the last case even better (Figure 4.9 and 4.10).

Several "classical" lysozyme crystals and crystals grown by thin film template method were investigated. Crystals obtained by thin film template

method demonstrated the same diffraction, and in some cases resulted in the higher resolution and more intensive spots.

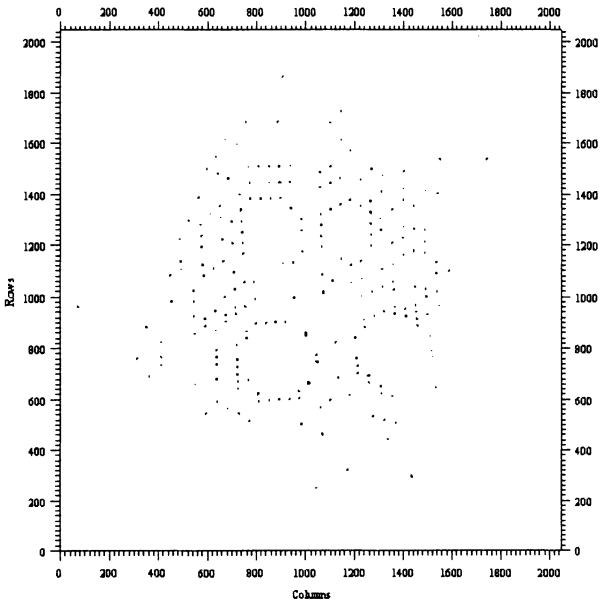

Figure 4-10. Diffraction pattern of lysozyme crystal grown by thin film technology, at the Microfocus Beamline in Grenoble Synchrotron (Pechkova and Nicolini, 2003a).

This fact may be explained by the crystal size and/or higher order of the crystals, obtained by thin film template method. Using the synchrotron radiation at the Grenoble ESRF Microfocus beamline ID13, this results have been confirmed. Indeed, the larger size and more order of lysozyme crystals obtained by thin film template method resulted in such intensive diffraction, that the special filter was needed to collect the data. The cell parameters were found the same, corresponding in all cases to Protein Data Bank values. Only one crystal was enough to collect all data set.

Several conclusions can be drawn from the data here presented about our new method based on a protein template obtained by thin film nanotechnology and on the modification of the classical vapour diffusion hanging drop method, namely:

- control of crystal nucleation (few large crystals were obtained by means of thin film template methods with optimal protein monolayer surface pressure)
- enhancement of crystal growth
- optimal resolution of the X-rays diffraction patterns better than 1.7 Å

- protein's crystals of equal sizes with significant lesser crystallization times with respect to the ones needed with the classical methods.
- crystals with larger sizes with respect to the ones from classical methods within the same crystallization time.

Finally, the increased anisotropy in thin film associated to the increased surface pressure points to the experimentally observed protein dipole moments (causing an increased surface potential from –0.2 mV in the self-assembly to –80 mV in the LB monolayer (Nicolini, 1997) as responsible for the increased acceleration and dimension in crystal growth.

4.2 Yet unresolved proteins: Bovine Cytochrome P450scc

4.2.1 Cytochrome P450scc (Side-Chain Cleavage)

Cytochromes P450 are an ubiquitous class of *b*-type hem protein that catalyze the hydroxylation of a vide variety of aliphatic and aromatic molecules. The cytochrome P450scc (Side-Chain Cleavage), EC 1.14.15.6 is the heme containing membrane protein, structurally similar to cytochromes, but functionally is the typical monooxygenase (Hanukoglu and Hanukoglu, 1986).

P450scc is a steroidogenic enzyme associated with the inner-mitochondrical membrane of steroid producing tissues. It catalyses three oxidative reactions resulting on the cleavage of the side chain of cholesterol to produce pregnenolone. This step is important in steroid biosynthesis, since it is the first and rate-limiting step, and occurs in all steroidogenic tissues. Most of our understanding of the reaction mechanism of cytochrome P450scc comes from the numerous studies on the recombinant bovine enzyme of molecular weight about 56kDa (Williams et al., 2000).

Cytochrome P450 are of particular interest also because, on the one hand, they display multiple pathways and, on the other hand, P450scc is unusual among members of this class of enzymes in showing a high degree of substrate specificity. Its complex with its electron transfer partner protein adrenodoxin can find their application in biophysical nanotechology, namely in artificial nanocomputers and nanosensors realization (Nicolini, 1996). For all above reasons P450 structure resolution at the atomic level is of high importance.

4.2.2 Sample homogeneity

The purity of cytochrome P450scc sample can be controlled by SDS-PAGE.

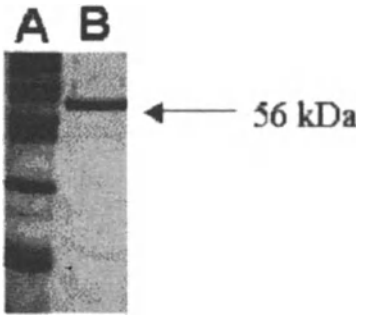

Figure 4-11. Electrophoresis of cytochrome P450scc on an SDS-polyacrilamide gel. Line A: molecular weight marker. Line B: purified sample, (Pechkova and Nicolini 2002b, © 2002, this material is used by permission of Wiley-Liss Inc., a subsidiary of John Wiley & Sons, Inc.).

For example, from the SDS PAGE of final fractions of cytochrome shown in the Figure 4.11, it becomes clear that cytochrome P450scc sample for crystallization was purified to the homogeneity. For the details in cytochrome expression and purification see paragraph 2.1.

4.2.3 Pressure-Area Isotherm

Monolayers of P450scc cytochromes were formed (Nicolini 1997) in a Langmuir Teflon trough by spreading 500 μl of protein solution with a concentration 0.17 mcg/ml (or 250μl with protein concentration 0.52 mg/ml) in 10 mM Potassium Phosphate buffer pH 7.4 which contains 0.1 mM EDTA and 0.2% Sodium Colate and 20% of glycerine. Distilled water was used as a subphase. The subphase temperature was a 22° C. The formed film was compressed with a barrier speed of about 100 mm/min up to pressure 15 mN/m. An example of typical π-A isotherms of cytochrome P450scc monolayers are presented in Figure 4.12.

From this isotherm on can conclude that protein monolayers exhibits well-defined surface pressure dependence. This is reflected by a change of the molecular orientation of the proteins at the surface.

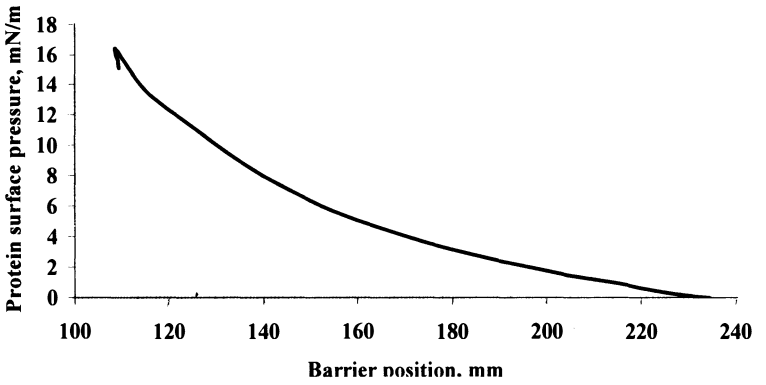

Figure 4-12. π-A Isotherms of cytochrome P450scc monolayers (Pechkova and Nicolini 2002b, © 2002, this material is used by permission of Wiley-Liss Inc., a subsidiary of John Wiley & Sons, Inc.).

4.2.4 Quartz crystal nanobalance

Nanogravimetric measurements can be performed in order to characterize the cytochrome thin-film deposition (Facci et al., 1993). We have transferred the films onto quartz oscillators and calculated the surface mass density as a function of the number of protein monolayers.

The linear dependence of the quartz oscillator frequency shift, and therefore the surface mass density, upon the number of deposited layers indicates the reproducibility and homogeneity of the deposition (Figure 4.13).

Knowing the molecular weight and theoretical dimensions of the homologous P450 scc protein, from Brookhaven Protein Data Bank (1scc code number) (Vijayakumar and Salerno, 1992), it is possible to compare the area per molecule in the film, calculated from nanogravimetric measurements (29.81 nm^2, which is of the same order of magnitude as that obtained in (Nicolini et al., 2001), with that for the closely packed system (about 30 nm^2) calculated from the theoretical geometric features of the protein from Protein Data Bank (Berman et al., 2000).

These values are very close for P450scc protein. Therefore the thin films used as template for the protein crystallization method are closely packed as a result of the rather high molecular ordering in the film.

Moreover, circular dichroism (Figure 2.13) spectra of thin P450scc films showed that the deposition procedure does not destroy the protein structure,

with the close packing of molecules being the reason for the high thermal stability of the protein secondary structure (Nicolini et al 1993).

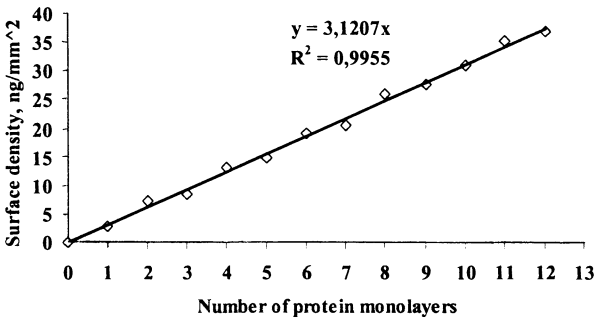

Figure 4-13. Nanogravimetric measurements of cytochrome P450scc multilayers (Pechkova and Nicolini 2002b, © 2002, this material is used by permission of Wiley-Liss Inc., a subsidiary of John Wiley & Sons, Inc.).

4.2.5 Cytochrome P450scc crystallization

Like in the case of lysozyme, cytochrome monolayer transferred from the air–water interface onto the siliconized glass circle cover slide was used as a template for modification of the classical vapour diffusion hanging drop method.

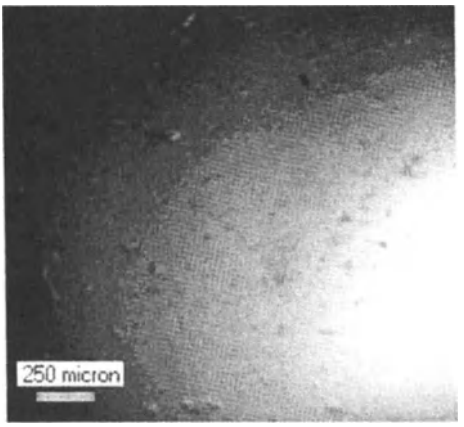

Figure 4-14. Light microscopy of cytochrome P 450scc microcrystals obtained onto the cytochrome thin film template (Pechkova and Nicolini 2002a).

During the cytochrome P450scc crystallization procedure, the following parameters were varied: precipitant nature and concentration; ionic strength, number of protein monolayers (from one to three). All experiments were carried out at the controlled temperature 20° C.

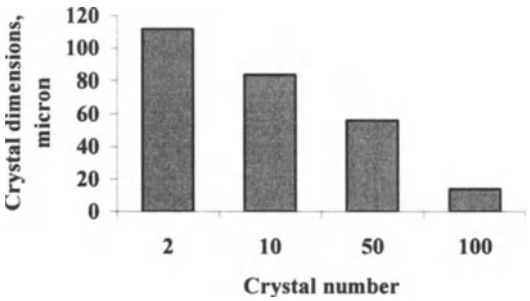

Figure 4-15. Cytochrome P450 SCC crystals dimension distribution (Pechkova and Nicolini 2002b, © 2002, this material is used by permission of Wiley-Liss Inc., a subsidiary of John Wiley & Sons, Inc.).

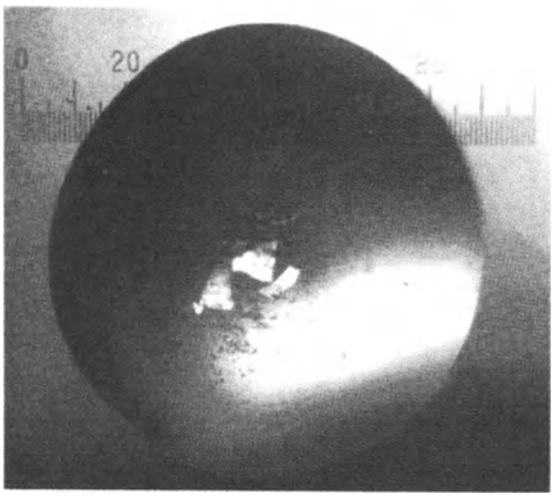

Figure 4-16. Light microscopy of cythochtrome P450scc crystals grown by classical hanging drop method in solution of 1M ammonium sul fate, 0.1M n-(2acetamido) iminodiacetic acid, pH 6.5. The 1mm graduation in the 100 mm ruler corresponds to 30 μm.

Using this new Langmuir-Schaeffer template crystallization method, cytochrome P450scc microcrystals of about 80–120 μm (Figure 4.14) were obtained in several drops under two different crystallization conditions, namely from the 1 M ammonium sulphate, 0.1 M n-(2-acetamido) iminodiacetic acid, pH 6.5, and also from 0.1 M ammonium sulphate, 18% polyethylene glycol (PEG) 400, pH 7.5.

Crystals dimension distribution is shown in Figure 4.15. In contrast, in solution, crystals are obtained only in one crystallization trial with the 1 M ionic strength of solution of among the numerous solutions tested. These crystals are rather large, but very thin (300 x 200 x 30 μm), having a leaf shape (Figure 4.16).

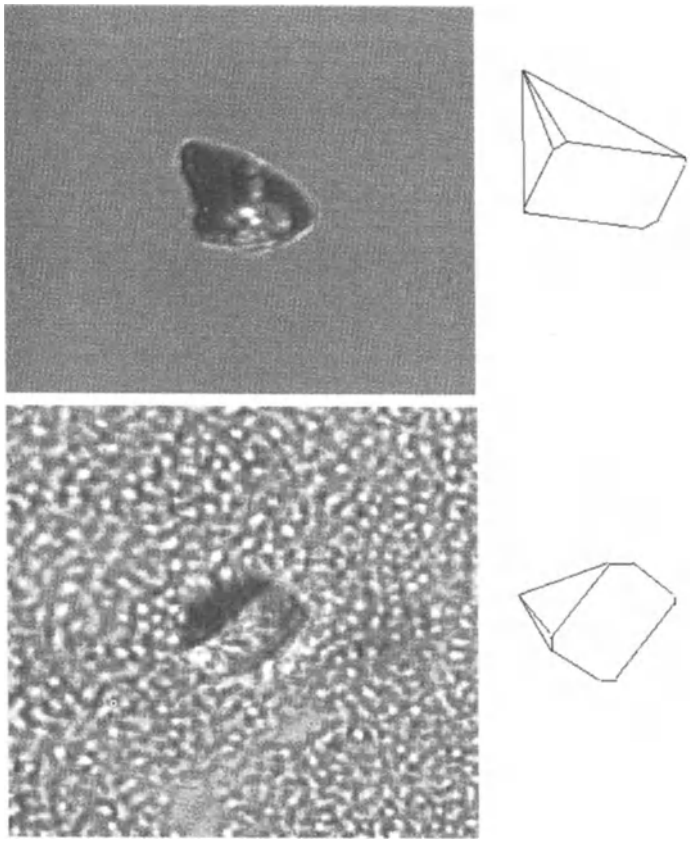

Figure 4-17. P450scc crystal geometry: a) pyramidal crystal 55 micron; b) pyramidal crystal 50 micron.

Unfortunately, we have obtained no reproducible result using classical vapour diffusion hanging or sitting drop crystallization method. On the contrary, different crystallization conditions were successful using thin protein film template method, resulting in reproducible cytochrome P450 SCC crystal growth. Moreover, almost all crystal have obtained the same pyramidal shape (Figure 4.17).

Using the new protein crystallization method based on the thin film nanotechnology, we managed to obtain single cytochrome P450scc crystals of dimensions up to 55 micron (Figure 4.18). These cytochrome P450scc crystals exhibit diffraction in polarized light.

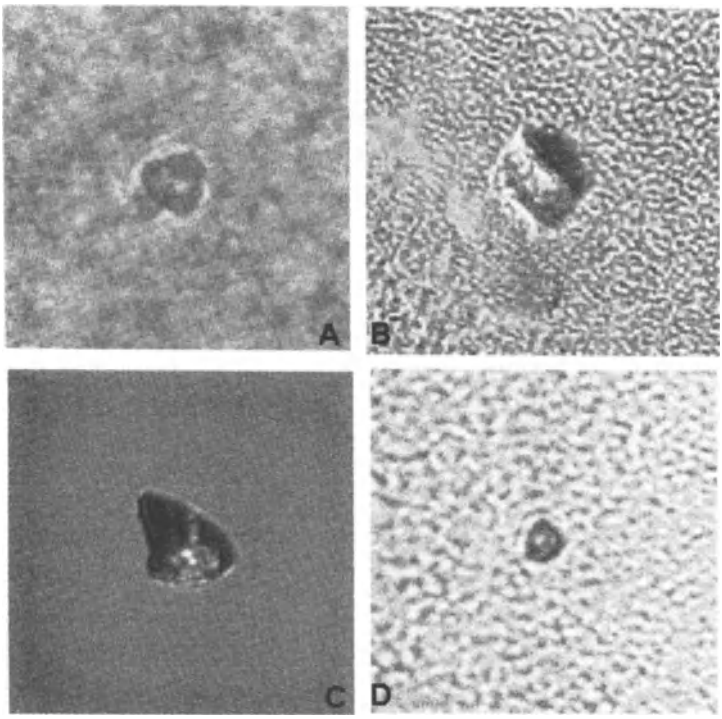

Figure 4.18. Cytochrome P450scc crystals, obtained by protein thin film template crystalszation method based onthe thin film nanothechnology. Average dimensions: (a)-30 micron, (b)-50 micron, (c)- 55micron, (d)-10 micron.

As it was poined by Cusack and coworkers, only microfocused X-ray beam from third generation synchrotron sources can be used for characterization of such a ultrasmall protein microcrystals (Cusack et al., 1998). Indeed, good quality microcrystal of P450scc (about 20x20x20

micron in size as can be seen by Atomic Force Microscopy in Figure 4.19) was analysed the Elettra Synchrotron in Trieste but unfortunately no diffraction pattern was apparent due to the wide X-ray beam size of about 300 micron diameter.

4.2.6 Atomic Force Microscopy of cytochrome microcrystals

In order to acquire crystal images at the nanometric resolution in the surface a new Atomic Force Microscopy (AFM) configuration has been developed and dedicated to protein crystal characterization at high resolution.

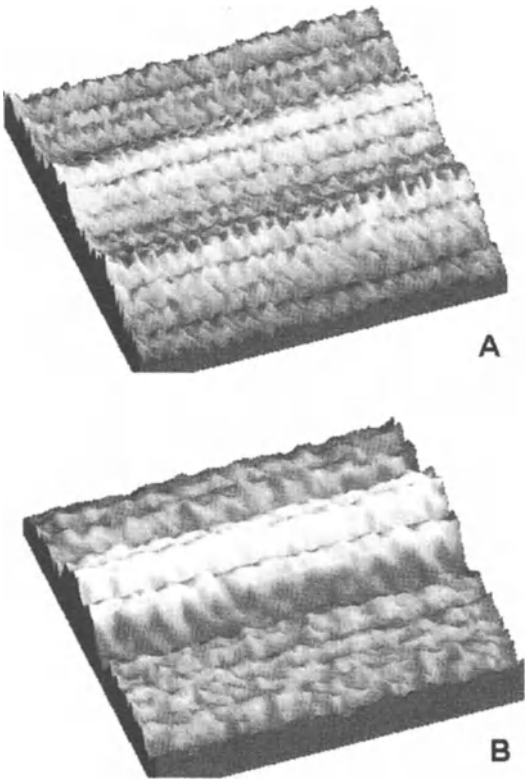

Figure 4-19. AFM images of cytochrome P450scc crystal: a) the full image dimension is 500x500 nm, b) the full image dimension is 50x50 nm (Pechkova and Nicolini 2002a).

AFM experiments were carried out in an in house modified AFM-Elbascan with appropriate chamber (PNB-PST Elba), which have been described before in the paragraph 3.2.1.

The periodic crystalline nature of the materials being produced by means of our homologous protein template method is apparent by the "tapping mode" AFM after placing the microcrystals in the appropriate and proprietary chamber.

At the beginning, AFM analysis was performed for the cytochrome P450scc monolayer, used as protein thin film template. (see Figure 3.11).

To our knowledge, nanometric scale images of the P450scc crystal have been acquired for the first time with an "in house" developed special AFM microscope (the original patent priority data) (Figure 4.19 and 4.20).

AFM data obtained from cytochrome P450scc monolayer template displays for each identifiable peak a cross section area of about 20 nm^2, which is smaller than the 30 nm^2 estimated area per the P450scc found in the Brookhaven Protein Data Bank; this being likely caused by the high compression of the protein being induced by the high surface pressure at the air-water interface.

Interestingly the experimental cross section area apparent in the AFM image of P450scc protein in the crystal (Figure 4.19) yielded instead the expected value of approximately 30 nm^2.

It can be explained by the fact that in the thin film template the protein molecules are compressed and well "packed", without the big amount of water around each, while in the crystal, containing as from 20% to more then 80% of solvent, the protein molecule configuration is close to that in the solution.

4.3 Yet unresolved proteins: Human kinase CK2α catalytic subunit

4.3.1 Protein kinase CK2α catalytic subunit

Protein kinases are a large family of enzymes, critically involved in almost every regulatable cellular process (Hanks et al., 1988). Protein Kinase CK2 – formerly called casein kinase II or casein kinase 2 – is ubiquitously distributed among eucariotic cell (Bossemeyer, 1995). The protein kinase CK2 is one of the most pleiotropic member of the protein kinase family, with more then 300 substrate known to date. Among these are key enzymes in different metabolic pathways and proteins playing important roles in a wide variety of cellular function, with special reference to transcription, translation, signal transduction, and cell cycle regulation (Allende and Allende 1995). Such an extraordinary pleiotropicity is likely

related to another unusual feature of CK2, namely its apparent lack of any mechanism of tight control.

Protein kinase CK2 is generally composed of two subunits, α and/or α' (the catalytic subunits) and β, which combine to form a native $\alpha_2\beta_2$ (or $\alpha_2'\beta_2$ or mixed, $\alpha\alpha'\beta_2$) tetramer. Despite that, it lacks a definite form of control: unlike most protein kinases, the catalytic α-subunits of CK2 are in fact constitutively active, either alone or when incorporated into the heterotetrameric holoenzyme. This is quite surprising, particularly if its pleiotropicity is considered (Allende and Allende, 1995) Moreover, its association with regulatory α-subunits may affect in opposite direction the catalytic activity, depending on the nature of substrate. Such a high intrinsic activity is invariably elevated in tumors (Pinna and Meggio, 1997).

Indeed, CK2 activity is always abnormally high in transformed cell lines as well as in solid tumors (Guerra and Issinger, 1999). In particular, the oncogenic potential of CK2α is highlighted by their ability to cooperate with Ha-ras in fibroblast transformation (Orlandini at al 1998) and to cause lymphomas developing in transgenic mice (Seldin, Leder P 1995; Kelliher, Seldin and Leder, 1996). On the other hand it is need to note the CK2 exploitation as phosphorilating agent by pathogens, such as viruses and parasites. These unique properties underlie the implication of CK2 in neoplasia and infectious diseases. For these reasons the 3D-structure resolution of human CK2α catalytic subunit at the atomic level has a crucial importance for its pharmaceutical application.

The crystal structure of the recombinant catalytic subunit (α) of CK2 from *Zea Mays* has been recently resolved, while human CK2α remains non crystallized because of its drastic instability. Recombinant maize CK2α consists of 332 aminoacids (its MW is about 45 kDa). The main difference between maize and human CK2α is found in the C-termins, which is ≅60 amino acids longer in recombinant human CK2α (Guerra et al., 1998).

Very recently, a low resolution (3.2 Å) crystal structure of the human holo enzyme has also been determined (Niefind, 2001). The human α subunit in the holoenzyme and the corresponding maize α subunit appear almost totally superimposable, but, due to this low resolution, fine details of the human CK2α structure are missed. This is a particularly relevant point, since, owing to the 70% homology between the two proteins, CK2α from Zea Mays is often used as a model for the human CK2 catalytic subunit studies.

4.3.2 Sample homogenity

The importance of sample homogenety and the ways of its purification were described earlier.

Protein purity both after purification and concentration is controlled by SDS C-terminal truncated form of α subunit can be obtained by enzymatic reaction with tripsin. 1.5 ml CK2α 0.27 mg/ml (in buffer 25mM Tris-HCl pH 8.5, 25mm NaCl, 7 mM β-mercaptoethanol, 0.2 mM PMSF, 1nM ATP), mixed with 0.25μg/ml tripsin (enzyme/substrate ratio ≅ 1000/1) and incubated at 27°C for 20 minutes. The CK2α, treated with tripsin (hereafter referred as tCK2α) is further purified in the absence of any detergent. Final purification of tCK2α requires anion exchange chromatography using a Mono Q HR 5/5 FPLC column. CK2α must be monitored by SDS-PAGE electrophoresis and the total protein content by Bradford assay.

The results show that alpha subunit was purified near to the homogeneity (Figure 4.20, line 1).

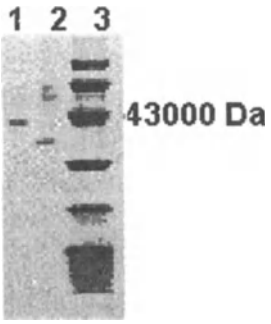

Figure 4-20. SDS PAGE of final fractions of CK2a entire (1) and truncated form (2). Alone with molecular weight marker(3).

The same result was obtained with CK2α truncated form (Figure 4.20). Moreover, preliminary structural characterization for the secondary structure of CK2α subunit that was performed by Circular Dichroism spectroscopy (Figure 4.21) has confirmed that Circular Dichroism spectrum of CK2α subunit purified as above described shows that denaturation of the protein during all purification steps cannot be considered as a serious effect.

CK2α can be also purified according to a protocol, described in the literature (Battistutta, 2001). In our experiments, three single-point mutant (Lys10Ser, Glu27Ala, Lys76Asn) was successfully purified by means of this methodology. Protein samples, purified by above methods was used for the nanostructured template preparation.

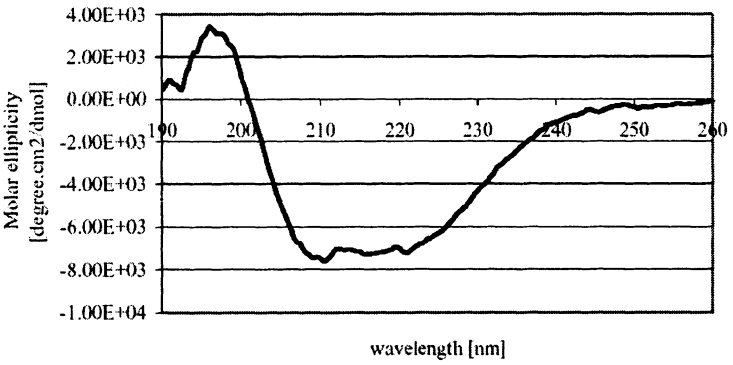

*Figure 4-21.*Circular Dichroism spectra of CK2α

For crystallization experiments kinase samples. were concentrated by centrifugation with Centricon Centrifugal Membrane filter (Cut-off 10 000 Da MW) which also allows to remove glycerol. The final protein concentration was about 8mg/ml in 25 mM NaCl, 0.05 % NaN3, 7mM β-mercaptoethanol, 25 mM Tris-HCl buffer, pH 8.5.

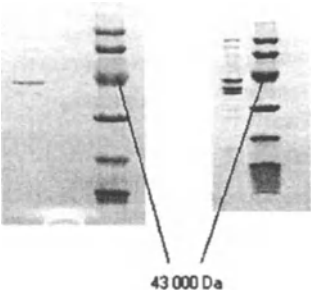

Figure 4-22. SDS Gel electrophoresis. On the left, corresponds CKα before the concentration 0.27 mg/ml. in following buffer 25 mM NaCl, 25 mM Tris-HCl, 7mM b-mercaptoethanol pH 8.5, 0.2mM PMSF, 0.2mM PMSF, 1nM ATP., 50% of glycerine; On the right - CKα after the concentration 8.5 mg/ml, 0.18% of glycerine (Pechkova and Nicolini 2002b, © 2002, this material is used by permission of Wiley-Liss Inc., a subsidiary of John Wiley & Sons, Inc.).

Protein purity after purification and concentration was controlled by SDS-PAGE. To monitor the effect of protein degradation, the sample was maintained at 20°C. Indeed, degradation bands appeared only after three-four days.

Gel electrophoresis results (Figure 4.22) have shown that this preliminary concentration of protein buffer solution as well as glycerine removing have not furthermore resulted in significant proteins denaturation.

4.3.3 Pressure-area isotherm

Human recombinant CK2α monolayers can be formed in a Langmuir Teflon trough by spreading 500 μl of protein solution with a concentration 0.22 mcg/ml in 25 mM NaCl, 25 mM Tris-HCl, 7mM β-mercaptoethanol pH 8.5 buffer and 50% of glycerine with distilled water was used as a subphase at the temperature of 22° C.

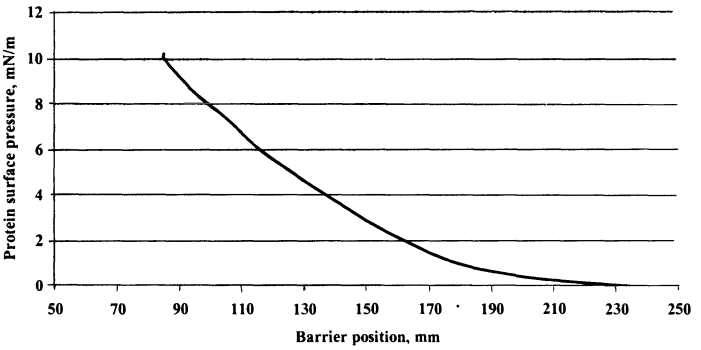

Figure 4-23. π-A Isotherms of human protein kinase CK2a monolayers (Pechkova and Nicolini 2002b, © 2002, this material is used by permission of Wiley-Liss Inc., a subsidiary of John Wiley & Sons, Inc.)

The formed film was compressed with a barrier speed of about 100 mm/min ut to monolayer surface pressure 20 mN/m. π-A isotherms of CK2α subunit are presented in Figure 4.25. As it results from the isotherms, kinase monolayers exhibits well-defined surface pressure dependence. Like in above cases (lysozyme, cytochrome) this fact can be explained by a change of the molecular orientation of the proteins at the surface.

4.3.4 Quartz crystal nanobalance

To further characterize thin film deposition, we have transferred the films on quartz oscillators and calculated the mass density as function of the number of layers.

The results of the gravimetric study of deposited monolayers are presented in Figure 3.21 for both type of proteins. Linear dependence of the frequency shift upon the number of deposited layers indicates the reproducibility and homogeneity of the deposition (Figure 4.24).

Knowing the molecular weight and dimensions of the protein it is possible to compare the area per molecule in the film, calculated from nanogravimetric measurements, with that for the closely packed system.

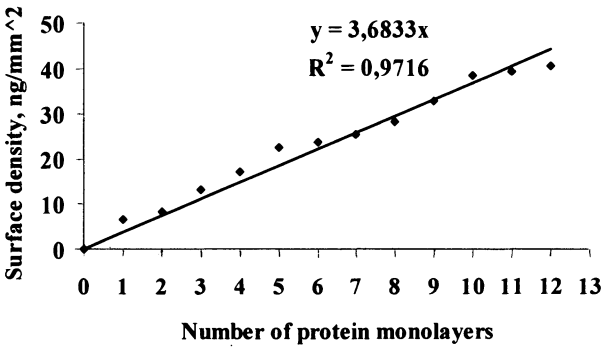

Figure 4.24. Nanogravimetric measurements of human protein kinase CK2α multilayers (Pechkova and Nicolini 2002b, © 2002, this material is used by permission of Wiley-Liss Inc., a subsidiary of John Wiley & Sons, Inc.).

For the human recombinant CK2α subunit mass density was about 3.68 ng/nm^2 which corresponds to the area of 20.36 nm^2 per one molecule of protein.

The CK2 molecule can be estimated as a shear which volume estimated knowing the molecular weight and average protein specific volume (Harpaz et al., 1994). Its radius is about 23,81 Å and one cross section area for the close film packing 17,81 nm^2.

Therefore the LB film used for the new protein crystallization method are closely packed, which could result from the rather high molecule ordering in the film.

4.3.5 Human protein kinase CK2α crystallization

Traditional crystallization of human recombinant CK2α was unsuccessful. It can be explained by high protein instability, in particular, the proteolitic degradation of its C-terminal.

Using our previously described template crystallization method we managed instead to obtain microcrystals of CK2α truncated form with dimensions about 85 micron (Figure 4.25).

Crystals was obtained in 0.2 M sodium acetate, 0.1M Tris-HCL, 25% PEG 4K, pH 8 only with the thin film template but not in solution. Crystals dimension distribution is presented in Figure 4.26.

The CK2 needle crystals (maximum size 60 x 20 x 20 μm^3) were obtained by crystallization with a new protein crystallization method, based on the homologous protein thin film template (Figure 4.27). Crystallization trials were made by mixing a 2 μl drop of stock solution with 2 μl of precipitant solution (25% PEG 3500, Sodium Acetate 0.2 M, Tris 0.1 M pH 8).

The drop was equilibrated against 700 μl reservoir of the same precipitant solution (25% PEG 3500). Crystals grew in few days at 293 °K. Diffraction data were collected at a temperature of 100 K. Before mounting, the mother liquid solution was proved to be a sufficient cryo-protectant.

Microcrystals of needle form with average dimensions 20 x 80 micron was observed under similar conditions with non-truncated form.

Crystals was obtained in 0.2 M sodium acetate, 0.1M Tris-HCL, 25% PEG 3500, pH 8.0 (Figure 4.27a).

Repeating the experiments with three single point mutant (Lys10Ser, Glu27Ala, Lys76Asn) crystal in order to verify crystallization results, many CK2 crystals (maximum size 80 x 20 x 20 μm^3) (Figure 4.29) nanotechnology. were obtained by crystallization with a new protein crystallization method, based on the protein thin film template.

Figure 4-25 Human Protein Kinase CK2α catalytic subunit (truncated form) microcrystals (80-20 micron) (Pechkova and Nicolini 2002b, © 2002, this material is used by permission of Wiley-Liss Inc., a subsidiary of John Wiley & Sons, Inc.).

Crystallization trials were made by mixing a 2 μl drop of stock solution with 2 μl of precipitant solution (25% PEG 3500, Sodium Acetate 0.2 M, Tris 0.1 M pH 8).

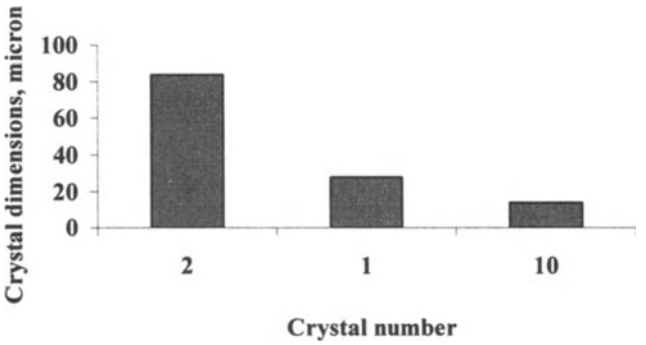

Figure 4-26. Human Protein Kinase CK2α catalytic subunit (truncated form) microcrystals size distribution (Pechkova and Nicolini 2002b, © 2002, this material is used by permission of Wiley-Liss Inc., a subsidiary of John Wiley & Sons, Inc.).

One can make the conclusion that when crystallized on the thin film template, protein stability do not takes such a critical role as during classical crystallization.

Nowadays, small dimensions of obtained crystal do not anymore seem to be a problem for the diffraction data collection.

Third generation synchrotron with microfocus beam allow to analyse the very small crystals before unusable for diffraction experiments, and therefore for protein atomic three-dimensional structure determination.

As it was underlined above, (Cusack et al., 1998) focused X-ray beam from sources can be used for characterization of protein crystals of less 30 μm in size, perhaps down to 5 – 10 μm. Therefore, human protein kinase microcrystals obtained by means of nanotechnology based crystallization method should be big enough for the X-ray diffraction data collection using the microfocus synchrotron beamline.

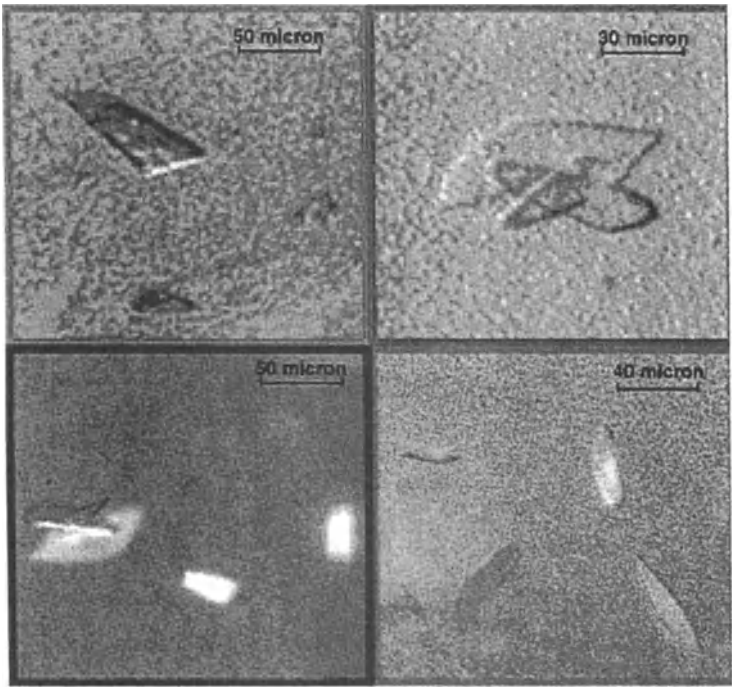

Figure 4-27a. Human protein kinase CK2α mutant microcrystals obtained by protein thin film themplate method (Pechkova and Nicolini, 2003a).

4.3.6 Synchrotron radiation: analysis, data processing and structure determination.

Three single point mutant (Lys10Ser, Glu27Ala, Lys76Asn) crystal of the catalytic α subunit of human CK2 was used for synchrotron radiation data collection and therefore for protein structure determination.

Diffraction data were collected at a temperature of 100 °K (Figure 4.28). Crystals were fished from the mother liquid and frozen in a nitrogen stream, without using any cryo-protectant solution.

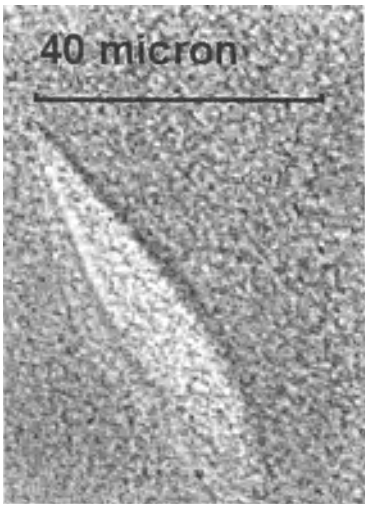

Figure 4-27b. Human CK2a microcrystal obtained by protein thin film template method (Pechkova et al., 2003).

As a prove of the quality of obtained microcrystals, only one needle crystal of approximate size 60 x 20 x 20 μm^3 (Figure 4.27b) was sufficient to collect a complete a date set at the Microfocus beam-line ID-13 of the ESRF (beam size 20 x 20 μm^2). The wavelength used was 0.955 Å and the crystal-to-detector distance 120 mm. Crystals diffract to a maximum resolution of 2.4 Å, which is quiat good, considering the very small size of the crystal used.CK2α crystals were found to belong to P21space group, with a = 58.68 Å, b = 45.95 Å, c = 63.96 Å and β = 111.8 Å. One molecule is present in the asymmetric unit. It is worth to notice that the space group and cell parameters of human CK2α crystals differ from those of the Zea mays protein.

Assuming a molecular mass of approximately 40000, the VM coefficient is 2.0 Å3Da^{-1}, whilst if the molecular mass of the protein is 45000 VM it becomes 1.78 Å3 Da^{-1}.

Table 4-1. Data collection and final model statistics. Numbers in parentheses refer to the highest resolution bin

Beamline	ID 13 Microfocus ESRF
Temperature	100 K
Detector	MAR CCD
Wavelength	0.9755 Å
Space group	$P2_1$
Cell dimensions	A=58.676 Å, b=45.954 Å, c=63.956 Å, β=111.8°
Resolution interval (Å)	29 – 2.40 (2.53 – 2.40)
Independent reflections	12457 (1817)
Multiplicity	2.3 (2.3)
$<I/\sigma(I)>$	4.3 (1.6)
Rmerge	0.13 (0.37)
Completeness (%)	99.0 (99.4)
Final model	
R	0.209 (0.245)
Rfree	0.273 (0.0300)
R.m.s. on distances (Å)	0.007
R.m.s. on angles (°)	1.4

Statistics on data collection is summarized in Table 4.1. Data were indexed and integrated with MOSFLM (Leslie, 1991) and then scaled with the program SCALA from the CCP4 software package (CCP4. 1994).

The crystal structure was solved by the molecular replacement method with the program AMORE (Navaza, 1994), using the structure of the CK2α subunit from Zea mays as a template (PDB ID code 1JAM). The crystallographic refinement of the structure was carried out with the CNS software package (Brunger et al, 1998) alternated with manual inspection of the electron density maps and rebuilding of the model using the graphic program QUANTA (QUANTA, 1986).

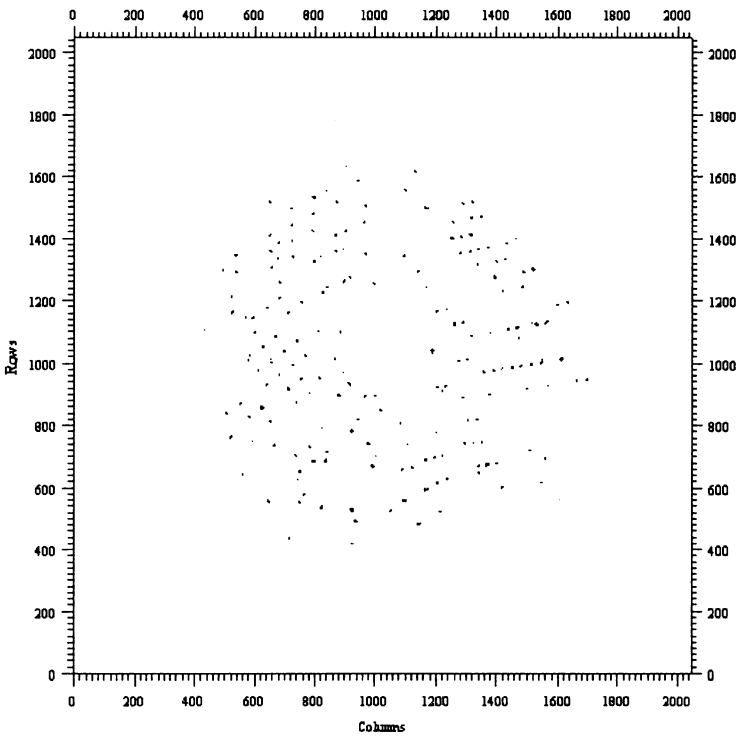

Figure 4-28. Diffraction pattern of human CK2 a microcrystal at the Microfocus Beamline (Pechkova and Nicolini, 2003a).

During the final steps of the refinement, 91 water molecules were added in correspondence of electron density peaks according to the possibility of forming H-bonds with protein atoms or other solvent molecules. The stereochemistry of the final model was checked with the program PROCHECK (Laskowski, 1993). Statistics on data collection, processing and refinement are summarized in Table 1. The final model presents an overall R factor of 0.209 (Rfree 0.273) with 91 water molecules and a good stereochemistry.

A portion of the electron density around residues from 152 to 156 (Figure 4.30) shows the quality of the map, which is generally quite well defined. Residues from 5 to 329 could be located in the map, whilst a short part of the N-terminus (residues from 1 to 4) and the entire C-terminal end (61 residues from 330 to 390) were not visible.

```
         10         20         30         40         50         60
Human SRARVYTDVNTHRPREYWDYESHVVEWGNQDDYQLVRKLGRGKYSEVFEAINITNNEKVV
      :.:::::.:::. ::.:::::::. .:.::.:::::..:::.:::::::::::.::..:::: .
Maize SKARVYADVNVLRPKEYWDYEALTVQWGEQDDYEVVRKVGRGKYSEVFEGINVNNNEKCI
                                                ** ** *            *

         70         80         90        100        110        120
Human VKILKPVKKKKIKREIKILENLRGGPNIITLADIVKDPVSRTPALVFEHVNNTDFKQLYQ
      .:::::::::::::::::::.:: ::::::. : :::.:  :.::.:.::.::::::: ::
Maize IKILKPVKKKKIKREIKILQNLCGGPNIVKLLDIVRDQHSKTPSLIFEYVNNTDFKVLYP
       *                                                * *

        130        140        150        160        170        180
Human TLTDYDIRFYMYEILKALDYCHSMGIMHRDVKPHNVMIDHEHRKLRLIDWGLAEFYHPGQ
      :::::::::.:.::.:::::::::.:::::::::::::::::: ::::::::::::::::::.
Maize TLTDYDIRYYIYELLKALDYCHSQGIMHRDVKPHNVMIDHELRKLRLIDWGLAEFYHPGK
                                      * * ** *          **

        190        200        210        220        230        240
Human EYNVRVASRYFKGPELLVDYQMYDYSLDMWSLGCMLASMIFRKEPFFHGHDNYDQLVRIA
      :::::::::::::::::::: : ::::::::::::::.:.:::::::::.::::.::::.::
Maize EYNVRVASRYFKGPELLVDLQDYDYSLDMWSLGCMFAGMIFRKEPFFYGHDNHDQLVKIA

        250        260        270        280        290        300
Human KVLGTEDLYDYIDKYNIELDPRFNDILGRHSRKRWERFVHSENQHLVSPEALDFLDKLLR
      ::::::. :  :..:: :::::::... ..::::::: : .:....:::::::::.::::::::
Maize KVLGTDGLNVYLNKYRIELDPQLEALVGRHSRKPWLKFMNADNQHLVSPEAIDFLDKLLR

        310        320
Human YDHQSRLTAREAMEHPYFYTV
      :::: :::: ::: ::::  :
Maize YDHQERLTALEAMTHPYFQQV
```

Figure 4-29. Alignment of the amino acid sequences of the catalytic subunit of human and maize protein kinase CK2α (Pechkova et al., 2003). The identity is 77.6% for 321 amino acid overlap. Stars indicate residues that possess at least one atom which is a distance shorter than 3.9 Å from the nucleotide analogue AMP-PNP, as calculated from coordinates take from Niefind et al., 1999. The numbering system used is that of the human protein. The alignment was obtained with the program LALIGN (Huang and Miller, 1991).

The presence of the space in the crystal cell in correspondence of the C-terminus seems to confirm the existence of a tail formed of these residues, highly disordered and thereby not visible.

Another possibility is that human CK2α has undergone proteolytic degradation at the C-terminal end during purification and/or crystallization, but this is not compatible with the existence of a very small degradation band which does not changed during purification steps and in entire time of crystal formation. From our gel electrophoresis results it would appear very unlikely that the protein crystallized is a truncated catalytic subunit. Indeed, it was our experience (Pechkova and Nicolini, 2002) that in both forms of

CK2α, truncated and untruncated, the same results were obtained with our thin film nanotechnology in terms of microcrystal nucleation and growth. The latter point is supported by the fraction of the solvent content of the crystal, which has the still acceptable value of about 31 % of the total crystal volume if the entire molecule is assumed present in the asymmetric unit, whilst it increases to about 39% if we consider a truncated protein.

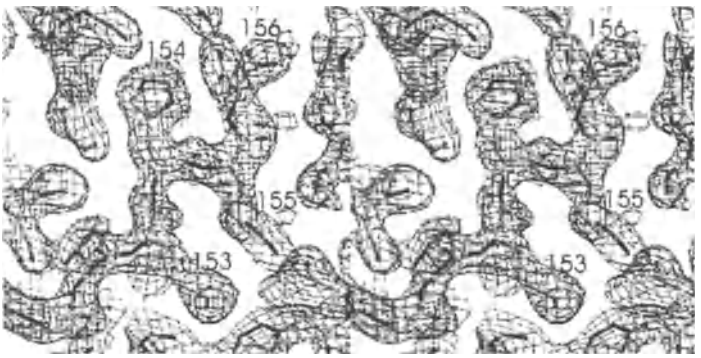

Figure 4-30. Representation of the portion of the electron density map, obtained with coefficients |2Fobs -Fcalc| and calculated phases. Contours are drawn at 1σ(I) level (Pechkova et al., 2003).

In summary, both possibilities strongly suggest that the long C-terminal tail is flexible, at least in the isolated catalytic subunit.

The overall structure of the human CK2α presents the classic fold of the catalytic subunit of protein kinases, formed by two domains: a N-terminal domain, mainly composed by β-strands, and a C-terminal domain, containing several α-helices (Figure 4.31). The nucleotide-binding site is locate in between the two domains.

The structure of the catalytic subunit of the enzyme is similar to that from Zea mais, as can be expected from the high sequence homology between the two proteins, at least in the portion we have crystallized (Figure 4.32). The overall root mean square deviation between equivalent α-carbons of the protein with the maize *apo* (PDB code 1JAM) is 0.8 $Å^2$. The electron density is generally well defined for main chain atoms. A break in the electron density is present only from residues 72 to 74 and from 122 to 123.

The first corresponds to the loop that connects strand β3 to helix αC, and the amino acid sequence of this region is identical to that of the maize protein. It must be observed that the beginning of helix αC is believed to be critical for substrate recognition in protein kinases (Pinna, 1996).

The second is the first turn of the short helix αD, where some significant differences are present in the amino acid sequence with respect to the *Z. mays*: residue 123 is a Gln instead of a Val, and Gln 126 substitutes a Pro, possibly inducing a perturbation of the structure.

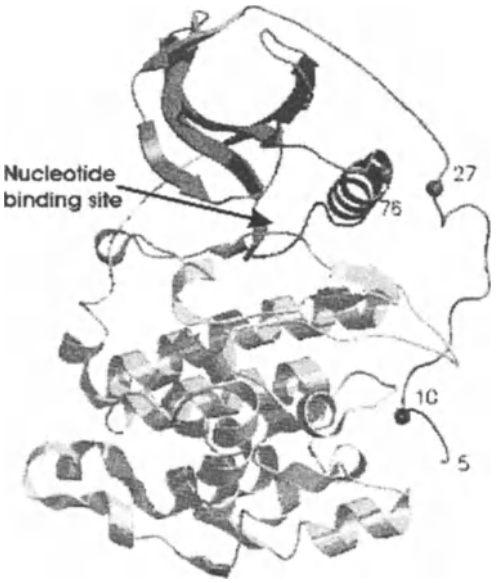

Figure 4-31. Cartoon representation of human CK2a protein kinase. The N-terminal domain is in grey, the C-terminal domain light grey. Small spheres indicate the positions of the three mutations with respect to the native protein (Pechkova et al., 2003).

The most significant conformational differences between the human and the maize protein are present mainly in the N-terminal domain. In particular, residues from 102 to 109, i.e. the loop connecting strands β4 to β5, and the area from 40 to 57. The latter is particularly relevant, since it contains the so-called Gly-rich loop (residues from 42 to 50) (Niefind et al., 1998) and, moreover, some of these residues directly interact with the nucleotide when it is bound to the protein. Conformational differences in this loop have been previously observed for the maize protein, either in the apo form or in some of its complexes with inhibitors (Battistutta et al., 2001).

On the overall, the structure of the C-terminal domain is more preserved, a fact that was observed in all the crystal structure of protein-inhibitor

complexes till now determined. The three point-mutations have no apparent structural effect, since the secondary structure around residues 10, 27 and 76 is totally conserved with respect to the maize protein. A comparison with the catalytic subunit of the human protein of the $\alpha_2\beta_2$ complex brings to similar conclusions. It must be considered that the latter structure is at relatively low resolution.

No ATP or analogues were added during the crystallization process. An examination of the nucleotide binding site cavity shows no density at all, indicating that the protein we have crystallized is in the apo form. The superposition of the co-substrate binding site cavities in the human and maize proteins is illustrated in Figure 4.33, where it is evident that they are very similar. Residues close to the nucleotide are indicated by a star in Figure 4.29

They are all conserved, with the exception of Ile 66, which is a Val in the human enzyme, but the latter substitution has apparently no effect on the co-substrate interaction with the protein. The only non-conservative substitution that takes place in the proximity of the nucleotide binding site is His 115, which is substituted by a Tyr in the maize protein. The OH group of Tyr 115 forms a H-bond with the side chain of Ans 117, but the latter in the human protein accommodates slightly in order to give the same kind if interaction with His 115. Minor differences in side chain positions in the human enzyme can more likely be attributed to the absence of any ligand in the co-substrate cavity, more than to real differences between the two proteins. Several water molecules are present in the active site pocket. In particular, two of them seem to be relevant for the active-site conformation, since they are invariably present in all the structures of the maize enzyme till now solved (Battistutta et al., 2001, with the exception of the CK2α-emodin complex (Battistutta et al., 2000).

They are also present in human CK2α, one of them being H-bonded to one of the oxygen atoms of the carboxyl group of Glu 81 (W 4 -OE2 Glu 81, 3.12 Å), the other interacting with the previous one (W 4 - W 59, 3.20 Å).

The crystal structure of the human catalytic subunit of CK2α at 2.4 Å resolution, confirms the idea that the molecular model of the human and maize proteins are very similar. This similarity, which is particularly pronounced as far as the active sites are concerned, yields some support to the validity of the previous use of the maize protein as a model for the human one. The similarity between two species evolutionary so distant could be possibly related to a conservation of physiological functions.

This is not reflected in the regulatory β subunit, that on the contrary appears to be significantly unrelated among different species. A distinctive feature of the catalytic α subunit of the human enzyme is that of having a C-terminal tail significantly longer and quite more flexible with respect to the

maize protein and to human α'. In this respect, one could speculate that the human α' and not the α is the homologous of the maize protein. Consequently, the structural similarity between the human α and that from Z. mays further support the hypothesis of a strong structural similarity between the two forms of the human enzyme.

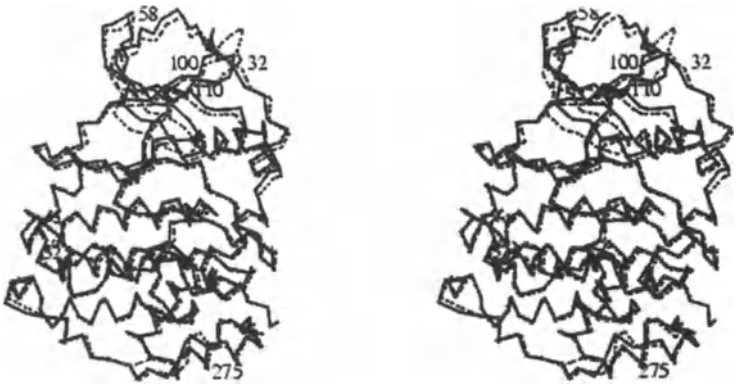

Figure 4-32. Superposition of Ca chain trace of the human protein (continuous line, PDB ID code 1NA7) to the apo form of Zea Mays CK2α (dashed line, PDB ID code 1JAM) (Pechkova et al., 2003).

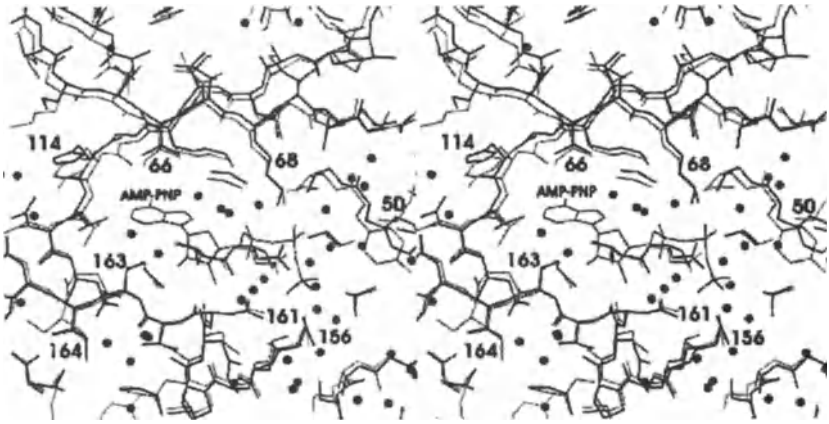

Figure 4-33. Superposition of the active sites of the human CK2 catalytic subunit to Z. mays CK2, holo form (Niefind, 1999) and ATP analogue (phosphoamino phosphonic acid-adenylate ester) as bound to the holo-CK2 crystal structure (Pechkova et al., 2003).

However, the crystal structure of human CK2α catalytic subunit, obtained for the first time by the combination of two frontier technologies, will allow to utilize the appropriate *Human* kinase CK2α to explore its potential pharmaceutical applications, rather than to rely on model system as done until now.

Towards this end it could be of interest to explore the complexes of CK2α human proteins with analogues of its natural co-substrates.

4.4 Conclusions

It can be concluded from the above results that, while other alternative protein crystallization approaches (see chapter 2) have proved effective only in isolated cases, our method appears innovative and reproducible in all protein systems so far tested. A possible physical explanation is the induction of dipole moments associated to the anisotropy in the protein monolayer acting as a substrate for the nucleation and growth of the protein crystal, which under this condition becomes then controllable and predictable. In all proteins systems being so far studied indeed the surface potential in the thin protein films increases significantly pointing to the increased anisotropy which in turns triggers the nucleation and crystal growth in all proteins, including those so far not cristallizable.

The new nanotechnology-based protein crystallization method seems capable to generalize the protein crystallization procedure by inducing both protein nucleation (cytochrome and kinase) and acceleration of protein crystal growth to an unprecedented large crystal (lysozyme).

The experimental results, summarized in this chapter, confirm that the emerging new field of nanocrystallography here defined might lead to the transformation of an hectic and unpredictable phenomenon, as protein crystal growth by traditional methods (typical of an art), into a controllable and predictable *ab initio* growth of diffracting crystals, as induced by the nanostructured protein template (typical of a science).

Chapter 5

FROM SCIENCE TO TECHNOLOGY IN PROTEOMICS

The recent advances in automated mass spectrometry, biomolecular arrays and industrial pharmaceutics constitute three clear examples of a transition from science to technology. In figure 5.1 are shown two examples of biomolecular arrays, where each site of the array surface is either a passive element, with only an attaching site for known oligo (or protein) strands, or an active element able to reveal the affinity between the known oligo (or protein) and the probe.

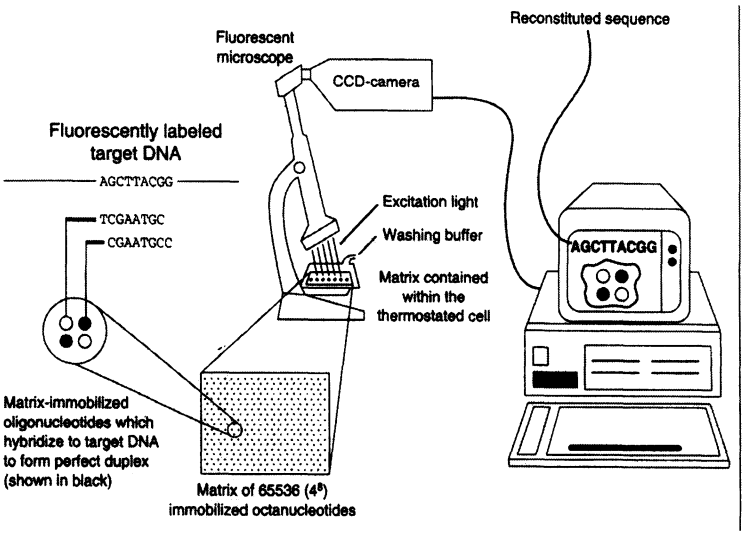

Figure 5-1. Examples of biomolecular arrays.

E. Pechkova et al., *Proteomics and Nanocrystallography*
© Springer Science+Business Media New York 2003

For this reason they are described in this chapter, along with the recent application of mass spectrometry automation to the massive identification of proteins and with the crystallization and structural characterization of yet unsolved protein structures of industrial and pharmàcological relevance. This chapter addresses also the most recent developments in structural and functional proteomics underlying the contributions from our own laboratory to these new instrumentations, methods and procedures resulting from frontier research in nanoscale science and technology.

5.1 Automated Mass Spectrometry

The MALDI-TOF analysis of the digest and subsequent database search leads to a list of proposed proteins. (Figure 5.2).

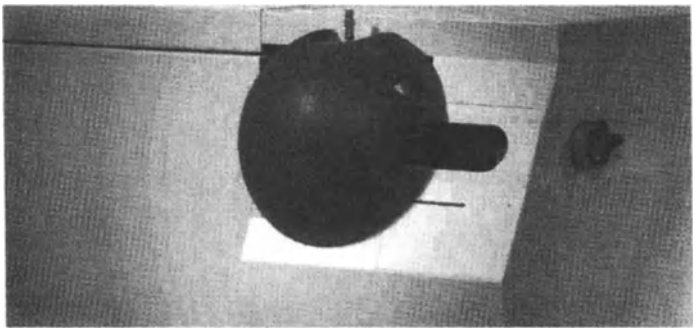

Figure 5-2. MALDI-TOF mass spectrometry (Bruker Daltonics Inc.).

The utilization of the fast MALDI-TOF (time of flight) and TOF/TOF technologies for the first rounds of screening reduces the samples numbers to a manageable size for in-depth LC-MS/MS analysis. The workflow can be adjusted to analyse a maximum of samples, or to analyse fewer samples with maximal depth.

This dynamic strategy provides outstanding success rates of protein identification at a minimum of analysis time. All hardware components (robots and mass spectrometers) allow sample identifications electronically, namely gel frames, MTPs and MALDI targets, and permit the exchange of the related processing parameters and of the results with the central control unit.

For fingerprint screening most analytical strategies use automated Mass Spectrometry for peptide mapping as an initial screening step of digested samples, aiming for the identification of large numbers of protein candidates.

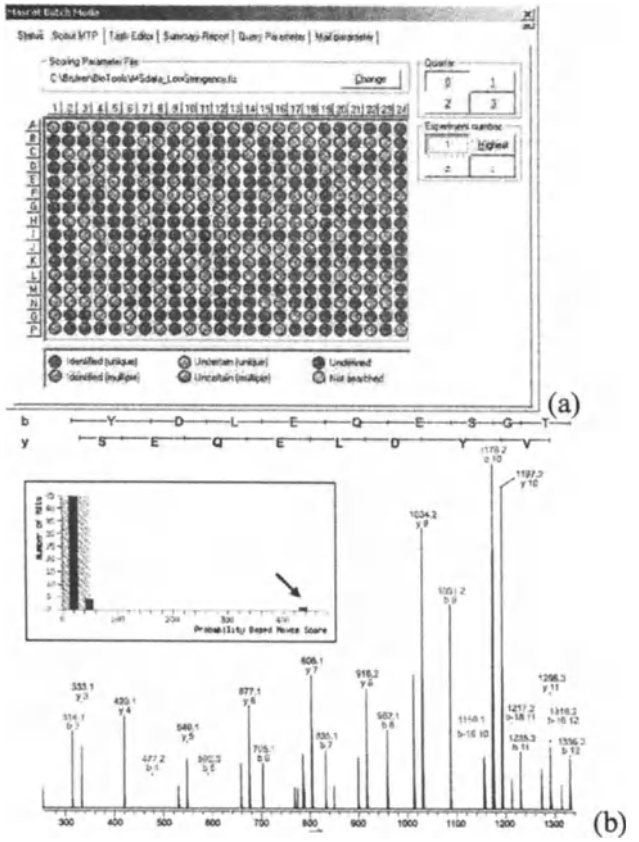

Figure 5-3. a) automatic protein identification; b) investigating protein primary sequence: MS/MS fragment analysis provides in-depth sequence information, including post-translational modifications (Bruker Daltonics Inc.).

This key first step provides the highest productivity by:

- high sample throughput, due to consistent automation of both the MS system and the data handling/database search routine;
- extremely high success rate of up to 90% of positively identified proteins, due to high quality data, namely the sensitivity and the mass accuracy (Figures 5.3 and 5.4). In case of ambiguous or failed identifications, MS/MS fragment analyses provide more detailed information for further protein database searches.

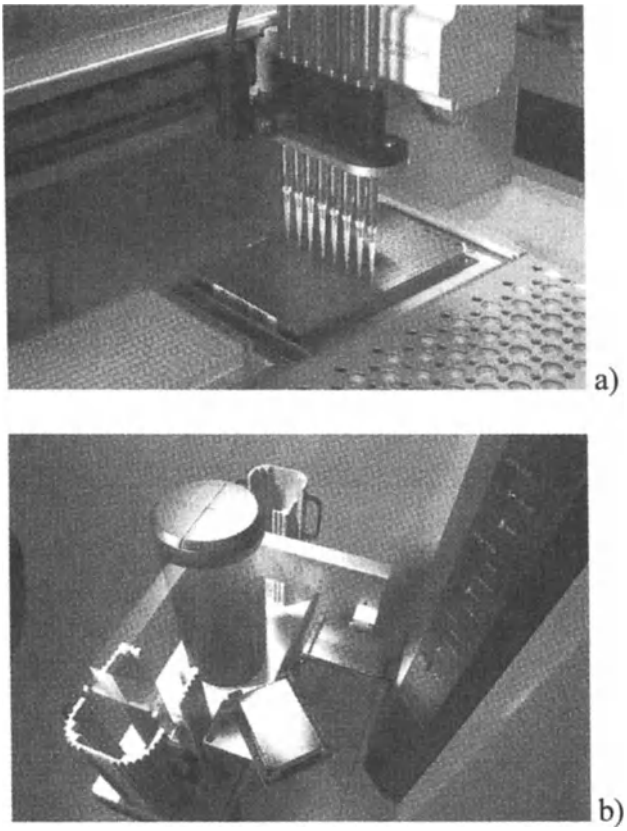

Figure 5-4. MALDI-preparation robots: a) gel spot picker, b) digest and prep station (Bruker Daltonics Inc.).

Both MALDI-TOF/TOF MS or nano LC-MS/MS can be used for this purpose. When using a TOF/TOF system, fragment analysis is performed within a few seconds and directly from the same MALDI sample increasing success rates to about 95%.

As an alternative or complementary method, nano LC-MS/MS, with its excellent information content (e.g. high sequence coverage and information on complementary peptides), confirms results and provides additional insight. Because of the high information content of these spectra, proteins can be identified even in complex mixtures. Once relevant candidates sequences result from the first screening phase, their primary structure may need to be characterized in the greatest possible detail.

Protein primary sequences can be investigated with MS/MS fragment analysis which provides in-depth sequence information, including post-translational modifications. Information on post-translational modifications (PTMs) can be gained by creating neutral loss traces during the dissociation of phosphates or glycosylation groups from the peptides in the MS/MS process.

Moreover, de novo sequencing using MALDI-TOF/TOF or SI-MS/MS data reveals new structural details, such as polymorphisms or modifications. Powerful mass spectrometers and robotics allow today to reach 100 fantomol protein-in-gel sensitivity, without any further sample purification needed. This coupled with efficient bioinformatics tools permits in-depth data interpretation of comprehensive database solution in even the most complicated project. Today robotics and database jointly developed with modular and scalable system can be readily customisable to the individual increasing demands (Figures 5.4a and 5.4b).

5.2 Biomolecular arrays

A novel biomolecular array recently introduced for real-time acquisition and elaboration of images from fluorescent DNA microarrays is the DNASER, acronym of DNA analyzer (Nicolini et al., 2002; Troitsky et al., 2002), which is being extended to protein array immobilizing proteins rather than DNA fragments. A white light beam illuminates the target sample allowing the images grabbing on a high sensibility and wide band CCD camera (ORCA II – Hamamatsu). This high-performance device permits to acquire images faster and of higher quality than the traditional systems. The DNA microarray images are processed to recognize the DNA chip spots, to analyze their superficial distribution on the glass slide and to evaluate their geometric and intensity properties.

Differently from conventional techniques, the spots analysis is fully automated and the DNASER does not require any additional information about the DNA microarray geometry. The new matrix integral part of the new DNA microarray instrumentation called DNASER is based on a novel DNA patterning on the solid support surface, as described in the following paragraph while the DNASER hardware and software architecture are illustrated later along with preliminary results from experiments performed on real DNA samples.

5.2.1 The surface patterning

Over the years a detailed process has been realized for the construction of DNA microarrays, their labeling, hybridization and data analysis (Figure 5.5).

The surface patterning introduced with the DNASER found the way of glass surface modifications for a precise positioning of small droplets of aqueous DNA solutions without special robots (arrayers) within the boundaries of the modified regions. The physically heterogeneous surface consists of highly hydrophilic spots surrounded by highly hydrophobic area leading to the surface patterning needed for a DNA microarray: a matrix of hydrophilic spots properly activated for immobilization of oligonucleotides has been fabricated on absolutely passive hydrophobic surface.

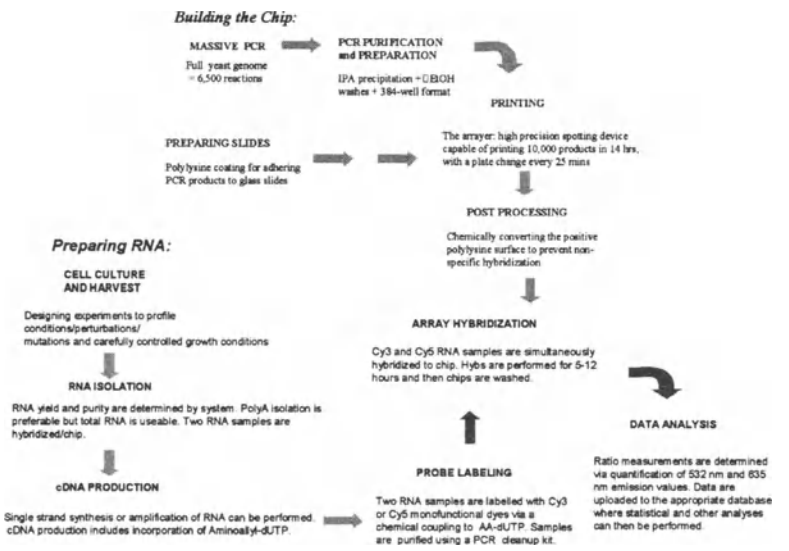
Building the Chip:
MASSIVE PCR
Full yeast genome
= 6,500 reactions
PCR PURIFICATION and PREPARATION
IPA precipitation +EtOH washes + 384-well format
PRINTING
PREPARING SLIDES
Polylysine coating for adhering PCR products to glass slides
The arrayer: high precision spotting device capable of printing 10,000 products in 14 hrs, with a plate change every 25 mins
POST PROCESSING
Chemically converting the positive polylysine surface to prevent non-specific hybridization
Preparing RNA:
CELL CULTURE AND HARVEST
Designing experiments to profile conditions/perturbations/ mutations and carefully controlled growth conditions
RNA ISOLATION
RNA yield and purity are determined by system. PolyA isolation is preferable but total RNA is useable. Two RNA samples are hybridized/chip.
cDNA PRODUCTION
Single strand synthesis or amplification of RNA can be performed. cDNA production includes incorporation of Aminoallyl-dUTP.
ARRAY HYBRIDIZATION
Cy3 and Cy5 RNA samples are simultaneously hybridized to chip. Hybs are performed for 5-12 hours and then chips are washed.
PROBE LABELING
Two RNA samples are labelled with Cy3 or Cy5 monofunctional dyes via a chemical coupling to AA-dUTP. Samples are purified using a PCR cleanup kit.
DATA ANALYSIS
Ratio measurements are determined via quantification of 532 nm and 635 nm emission values. Data are uploaded to the appropriate database where statistical and other analyses can then be performed.

Figure 5-5. Detailed process to realize microarray analysis.

The optimal efficiency of the above functionalization technology of glass-substrate in obtaining DNA microarray was confirmed by the Cy3-dCTP labeled DNA sample, as shown by CCD images of the DNASER previously describe. DNA microarrays consist of array of DNA sequences of varying length immobilized on a solid support (Graves et al., 1998). They

have emerged as a powerful new tool for genomic analysis and gene expression profiling, with application in DNA gene discovery, drug discovery and disease diagnosis (Schena et al., 1998). For analysis the test DNA to be analyzed is typically labeled with a fluorescent dye and then hybridized to the microarray.

The type of support and the imaging system used have a significant impact on the sensitivity, speed, and reliability of the assay.

The goal of this subchapter is to show the innovative, simple, and cheap approach of microarray fabrication for the immobilization of target molecules of either pre-synthesized oligonucleotides, polynucleotide or peptide sample.

A considerable part of commercial microarrays with the target oligonucleotide sets is manufactured using photolithographic methodology proposed by Affymetrix (Jacobs and Fodor 1994; Morgan et al., 1995).

In this case synthesis of the oligonucleotides with the required sequences is performed step by step directly on the derivatized glass surface. Chemical structure of the elementary blocks used to carry out every synthetic step ensures the surface protection after the reaction implementation. To activate the surface again the protection is removed at the selected sites by irradiating the sample with light through the photolithographic mask. The chemical reaction is then repeated with another nucleotide, and so on. Another approach of oligonucleotide synthesis on the substrate is based on successive ink-jet delivery of nucleotide precursors to the surface. In situ synthesis has some advantages over the deposition of pre-synthesized oligonucleotides. However, the amount of compound synthesized in this case on the surface is so small that high precision control of the sample composition at the selected spot of the array is impossible. Although special complicated analyses indicate that high quality structures can be thus produced, to carry out such a control routinely in ordinary laboratory conditions is a hard problem. Inevitable imperfections of both the oligonucleotide structure and the surface coating should arise. In addition, to produce microarrays with such techniques specific equipment is required and in the case of mass production simultaneous treatment of numerous glass slides is impossible.

On the contrary, pre-synthesized oligonucleotides can be carefully purified and controlled before the utilization. To produce a microarray from pre-synthesized oligonucleotides as well as from the DNA target samples, the activated surface of glass slide is spotted with the droplets of the required products using special robots (arrayers) (Walling et al., 2001). This apparatus should possess high precision characteristics because an amount of the supplied solution at the selected site of the glass surface and its spreading near the point of the droplet contact with the surface depend on many factors. In particular, high quality tips, which supply the solutions, should be

fabricated, the distances between the tips and the surface as well as the tip accelerations (forward and back) should be well controlled. Undoubtedly, the precise lateral positioning of the tips is also required. Nevertheless, such devices, although rather expensive, are commercially available, which contain the printing heads with up to 12 pen tips. This technique of immobilization of the microarrays is widely spread. The chemical reaction with the activated surface of the solid support is more efficient if the latter is in the contact with the solution during the incubation period. Usually, the incubation should be very long and the immobilization should be carried out in the presence of special chemical agents in the solution. However, in the case of microarray, water is quickly evaporated from the smallest deposited droplets in the conditions of normal humidity.

The research activity here reported has resulted on a patent pending and includes:

- fabrication of the master masks for evaporation of metal protective films;
- optimization of highly hydrolized glass surfaces;
- hydrophobic coating optimization;
- optimization of metal etching ;
- glass surface activation;
- immobilization of target molecules;
- production and characterization of DNA microarrays.

On the surface of glass slide a set of separated arrays of small dimension highly hydrophilic spots (about 80 μm) is constructed to develop a technique of DNA solution deposition which does not use robots (arrayers).

The surface of glass everywhere should be hydrophobic besides the sites of array location. To satisfy these requirements we used the masks 3 mm in diameter made of a copper foil 10 μm thick. Each mask contained a matrix of 240-250 holes with diameters of 80-100 μm (Figure 5.6).

An ordinary scheme of metal evaporation, i.e. the top position of sample and the bottom position of evaporator, is extremely difficult to use in this case. Any attempt to attach tightly such masks to the substrate surface fails.

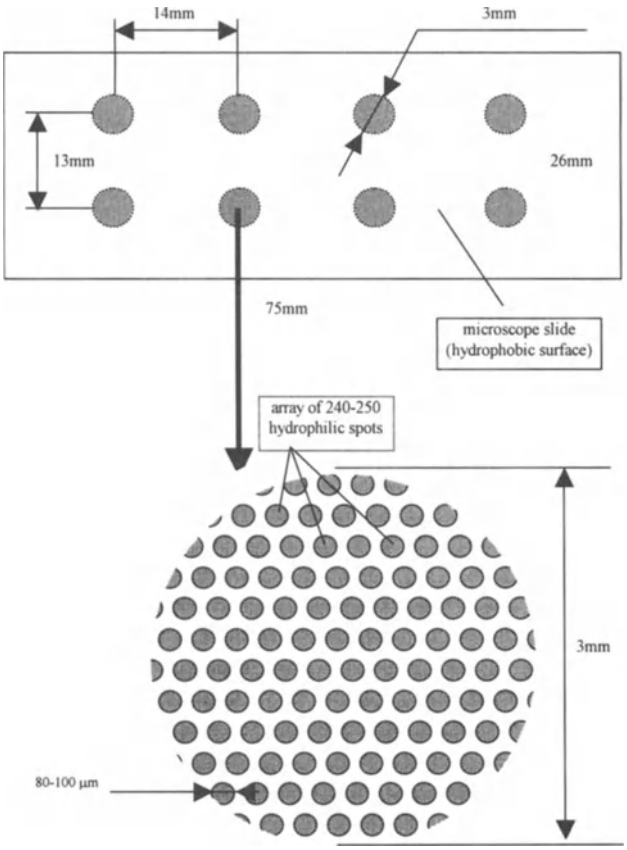

Figure 5-6. Samples with the arrays of hydrophilic spots prepared for the deposition of DNA solution (Troitsky et al., 2002) (© 2002 IEEE).

Thus, to carry out this work we were forced to make a new construction inside the vacuum chamber, which allows to evaporate metals from the evaporator located in the top position with respect to the sample. The resulting attachment is shown schematically in Figure 5.7.

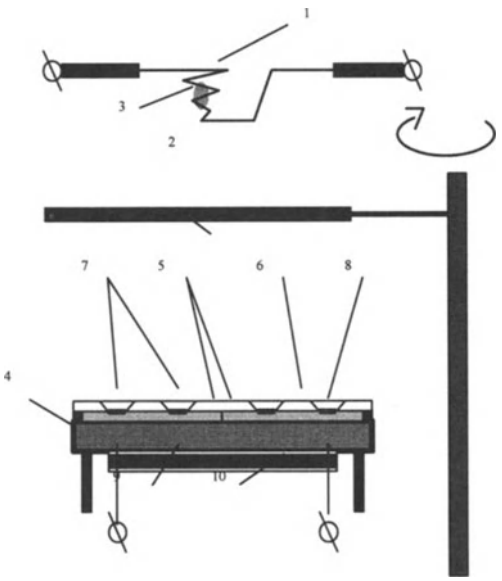

Figure 5-7. Scheme of chromium evaporation for the fabrication of a set of arrays of hydrophilic spots on the hydrophobic glass surface (1 – tungsten basket, 2 – shutter, 3 – chromium, 4 – support for the samples, 5 – microscope slides, 6 – stainless steel protective plate, 7 – holes in the protective plate (diameter of 3 mm), 8 – copper masks with the matrix of holes (diameter of 80-100 mm), 9 – tungsten heater, 10 – sapphire plates) (Troitsky et al., 2002) (© 2002 IEEE).

Chromium was evaporated from a tungsten basket (1), which can be considered as a point-like source providing a sufficiently uniform flow of metal atoms in any direction as well as in the direction down to the sample.

A shutter (2) under the basket is used to protect the sample from contamination during annealing of the basket filled with chromium (3) before the evaporation. The support (4) for the samples was made in such a way to fix precisely two standard microscope slides (5) with the dimensions of 26×75 mm. A flat stainless steel plate (6) containing 16 holes (7) (diameter of 3 mm) was placed over the microscope slides. This plate protects the surface of glass from evaporation of chromium everywhere besides the sites of array formation (i.e. 16 holes of 3 mm in diameter). The masks with the matrices for array preparation (8) were then put in these holes.

A powerful tungsten heater (9) isolated from the support with thermally conductive sapphire plates (10) was provided to heat the samples up to

temperature of about 200°C. This is necessary to achieve high adhesion of chromium to the glass surface. Glass surface was successively washed with organic solvents; soap and pure water; and heated in concentrated sulphuric acid. Defects occasionally arise because in the fabricated arrays the hydrophilic spots are located very near to each other, about 25-30 μm.

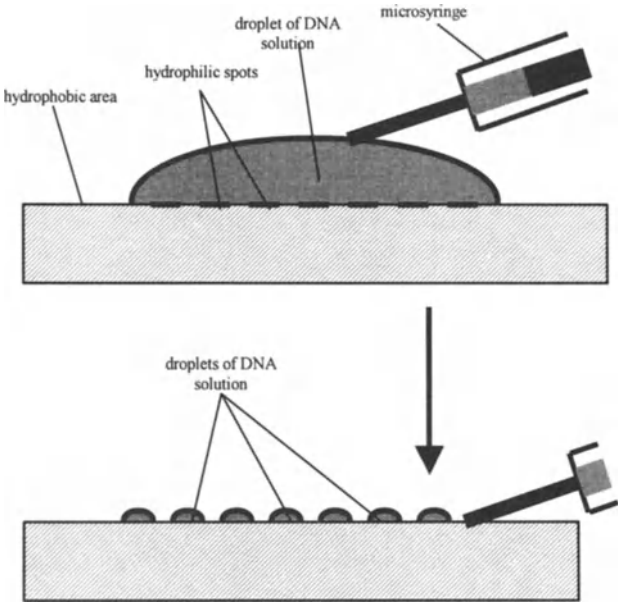

Figure 5-8. Deposition of DNA solution onto hydrophilic spots of the array (Troitsky et al., 2002) (© 2002 IEEE).

If the contact angles are not high enough after silanization, droplets of aqueous solution can appear to be non-separated between the adjacent hydrophilic spots. Moreover, defects can arise also at the sites of hydrophilic spots if the surface is not hydrophilic enough. A non-uniform coating of spots with several droplets of water (instead of one) was occasionally observed. To avoid all these drawbacks, we have introduced in the substrate preparation procedure an additional treatment of the glass surface in sodium hydrohide solution (1-2 g in 100 ml of water, 20 min at room temperature) with subsequent washing in pure water. Hyghly hydrolized glass surfaces were then obtained by utilizing chromium films about 100 nm thick thermally evaporated in vacuum of 10^{-6} torr after heating the samples up to 200°C for 20 min. Thus the arrays of chromium spots 80-100 μm in

diameter were formed on the hydrophilic glass surface. Then the glass surface was treated again for 10 min in sodium hydroxide solution, washed in pure water, dried with a stream of compressed air and the samples were silanized with dimethyldichlorosilane (5% solution in hexane, 15 min). Protective chromium films were removed in an aqueous solution of KOH and $K_3(Fe(CN)_6)$ (1 mole/ l and 0.6 mole/ l, respectively).

The DNA solution is placed onto the fabricated hydrophilic spots of the arrays without an arrayer (Figure 5.8).

Small droplet of the DNA solution was first placed with a microsyringe onto the whole area of the array.

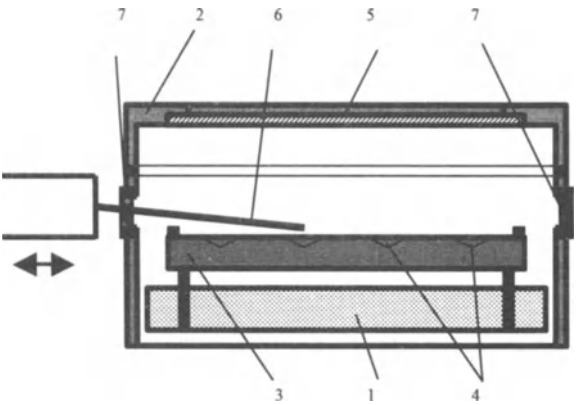

Figure 5-9. Chamber for the deposition of DNA solution (1 – wetted sponge, 2. – hermetic lid, 3 – support for the sample, 4 – marks of array positions, 5 – glass plate, 6 – needle of microsyringe, 7 – rubber valves (Troitsky et al., 2002) (© 2002 IEEE).

Then the tip of needle was shifted to the droplet border and the solution was drawn off with the microsyringe. As the result only the hydrophilic spots remain to be wetted, if an ad hoc made special chamber (Figure 5.9) is utilized, a configuration which enables to observe the sample surface with an optical microscope at magnifications up to 100. A very wetted sponge (1) placed at the bottom of the chamber allows to reach 100% humidity in approhimately 10 minutes after closing the lid (2).

The design of the support (3) for the sample allows to fix a microscope slide in an unique way so that the marks (4) on the support surface show the positions of the matrices on the slide. The surface of the sample can be observed with an optical microscope through the glass plate (5) sticked into the lid. The needle of syringe (6) can be inserted into the closed chamber

through the rubber valves (7) located from both sides of the chamber. The tip of needle can be easily shifted over the sample surface to reach any of eight arrays while the internal volume remains to be hermetically closed.

A large droplet of the solution of labeled DNA was initially deposited with the open lid, then the solution was concentrated by the evaporation of water excess from the deposited droplet (the lid was open), then the lid was closed, the rest of DNA solution was eliminated in 10 minutes with the microsyringe so that the droplets on the hydrophilic spots were separated from each other and water was evaporated at low rate.

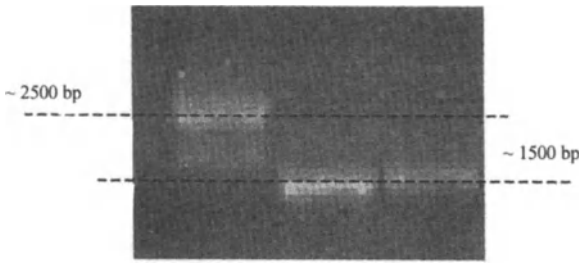

Figure 5-10. Electrophoresis gel (agarose 1%): 1 Hind III marker (line 1), DNA not labeled (lines 2, 3), DNA labeled (line 4) (Troitsky et al., 2002) (© 2002 IEEE).

With the lid not closed the droplets over the hydrophilic spots were separated spontaneously under water evaporation and then dried at a normal humidity in the room.

Fluorescence measurements were subsequently carried out.

To check the efficiency of our functionalitation technology of glass-substrate which is finalized to obtain DNA array for molecular genomics, Cy3-dCTP was used to label DNA sample (Yu et al., 2002, Bras et al., 2000).

As shown by the electrophoretic profile of Figure 5.10 and Figure 5.11 the DNA double strand utilized in our experiments (sequence of cDNA encoding human h4 histone) has a size of 1500 bp and is labeled by a PCR reaction (Table 5.1) using a dNTPmix containing Cy3-dCTP. The deposition of the solution onto the matrix surface is carried out in the conditions of saturated water vapour.

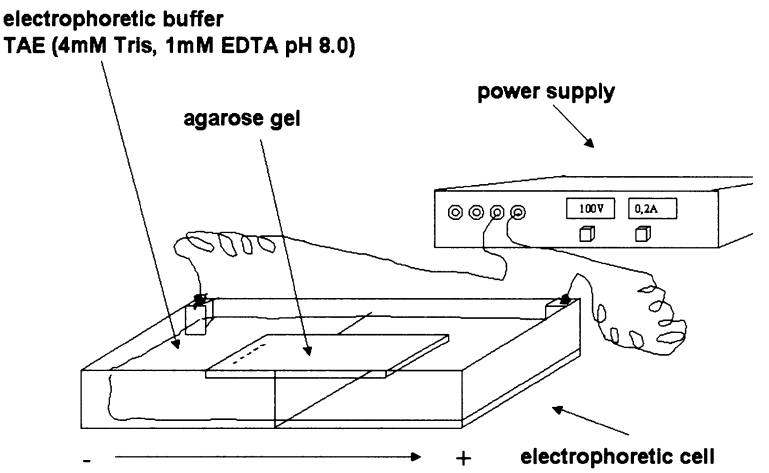

Figure 5-11. Gel electrophoresis apparatus for nucleic acid characterization.

The DNA solution used can be conserved for further experiments. The described procedure can be repeated eight times without opening the chamber with the DNA solutions prepared in different ways (for example, with the solutions of different concentrations).

Table 5.1. PCR reaction

Cycles	Temperature (°C)	Time
1	95	45 sec
30	95	45 sec
	65	42 min
	72	45 min
1	72	10 min

After that the deposited droplets can be observed with optical microscope to evaluate the quality of deposition. The concentration of the labeled DNA and purified was 170 ng/μl.

The primers used are the following:

5' AGT TGT AAG CTT CTA GCC TCC GAA GCC GTA GA 3'

5' TTG TAA TGT GGA TCC GGC AGA GGA AAG GGC 3'

In Figure 5.12 are shown the CCD camera images of the DNA labeled microarray as acquired with the DNASER apparatus (Nicolini et al, 2002).

DNA-labeled was synthetized by PCR reaction as described in the Materials and Methods. Tests were realized using aliquots of DNA labeled with Cy3-dCTP, purified and resuspended in H_2O MilliQ. In Figure 5.7 the fluorescence observed with the CCD camera was determined by DNA deposited in functionalized wells.

The removed DNA solution can be used in other experiments. Thus the loss of the compound is very small. Although some defects inevitably arise when using such a simple approach and non-uniformity of the solution distribution can take place, it seems the method can be successfully used for DNA immobilization.

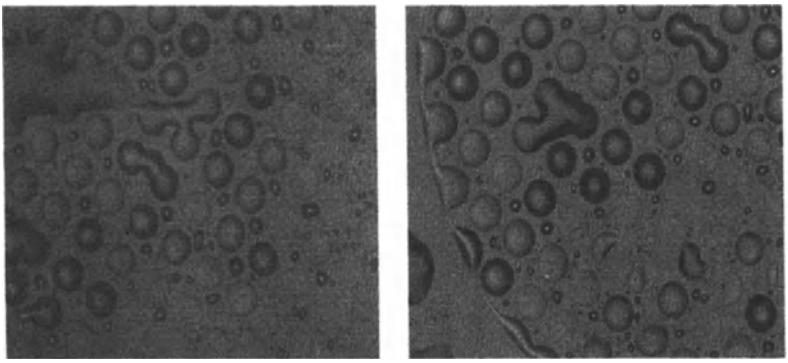

Figure 5-12. Migration of solution DNA versus hydrophilic spots. In a) a solution of DNA was spread on a glass plate and it was removed using an Hamilton (b). The diameter of hydrophilic spots is about 100 mm (Troitsky et al., 2002) (© 2002 IEEE).

More precise quantitative data should be then obtained with the application of an arrayer to put the DNA solution onto the hydrophilic spots of the matrix. If the procedure described above is carried out in ordinary conditions, at a normal humidity value, the process of water evaporation from the wetted spots can not be controlled because the amounts of the solution attached to the spots are very small.

Water is evaporated quickly during 1-2 seconds and to transfer the sample in some closed volume to prevent the evaporation is impossible. However, a final distribution of the compound over the spot surface depends on the rate of increase of DNA concentration in a droplet during water evaporation and to have a possibility to vary this rate is important. Figure 5.13 shows indeed three different fluorescent images of DNA solution spots taken under three different drying procedures of the sample, where the drying speed decrease from A) to C) with C) being the optimal.

The results of these studies (Figure 5.13) show that at high speed of water evaporation the fluorescent labeled DNA compound is concentrated at the boundaries of the spots (Figure 5.13a). At low speeds of water evaporation the fluorescent labeled DNA is concentrated in one big aggregate somewhere near the center of the spot (Figure 5.13b).

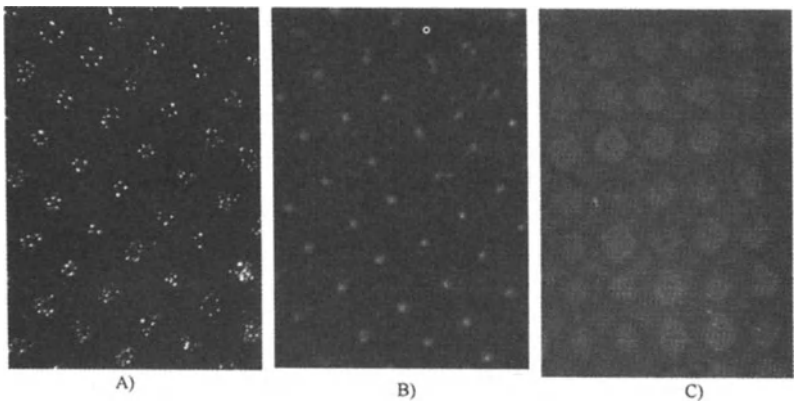

Figure 5-13. Three different fluorescent images of DNA solution spots taken under three different drying procedures of the sample. The drying speed decrease from A) to C) (Troitsky et al., 2002) (© 2002 IEEE).

Anyway, the fluorescent labeled DNA is all concentrated within the spot so that the integral intensities can be quantitatively compared with each other, and the intensity of fluorescence is high enough to carry out reliable measurements. However, if the solution was not previously concentrated by water evaporation, the intensity of fluorescence was low. Reliable signals were obtained only when the thickness is about one monolayer of DNA or more. Thus, the concentration of fluorescent labels along the DNA chain should be properly increased to carry out quantitative fluorescence measurements with immobilized DNA using the applied technique.

To continue experiments with the immobilized DNA it is necessary also to develop methods of surface activation for specific binding the DNA molecules to the substrate surface.

The glass slide is washed and the surface is treated to make it highly hydrophilic (hydrolyzed). In conclusion the results obtained from these first experiments suggest that the fictionalization technology here introduced constitute a good innovative approach to realize DNA microarrays which does not require robots. Extension of this technology to protein microarrays has also been planned and is in progress.

Several medical applications of DNA microarrays have been developed recently (Figure 5.14), and similarly is taking place for protein microarrays useful also in the identification of new drugs.

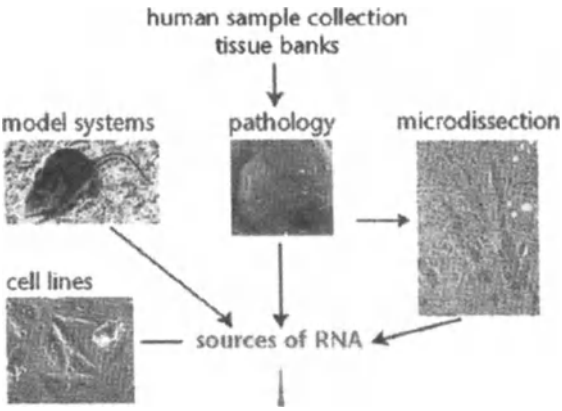

Figure5-14. Microarray medical applications.

5.2.2 The instrumental layout and data analysis

In biomedicine, the in vivo and in vitro studies of DNA are typically performed analysing images from fluorescence microscopy (Mascetti et al., 1996; Hiroshi, 1999). Nowadays, improvements in fluorescence microscopy (based on sophisticated laser systems), new oligomers deposition methods and ad hoc pattern recognition algorithms, allow automatic massive analysis of DNA samples processing images of microarrays of DNA fragments. Microarrays are matrix-shaped collections of DNA spots deposited on the surface of a glass or nylon slide. Each spot contains many copies of a single DNA sequence such as gene. Generally, DNA spots are left on the slide using a robotic arm as their dimension (less than 200 microns) does not allow a hand-made positioning. DNA microarrays (Schena et al., 1995; Nguyen et al., 1995) allow to interrogate expression of hundreds or thousands of genes simultaneously, both in yeast (Chu et al., 1998) and in human cells (Perou et al., 1999). Gene expression data derived from arrays may be used for gene clustering (Eisen et al., 1998), tissue differentiation (Alon et al., 1999), and other analysis. Then, DNA microarrays provide a medium for matching known and unknown DNA samples based on base-pairing rules and automating the process of identifying the unknowns.

In the last years, the design of DNA microarrays analysis devices has driven the development of specific techniques and instrumentation.

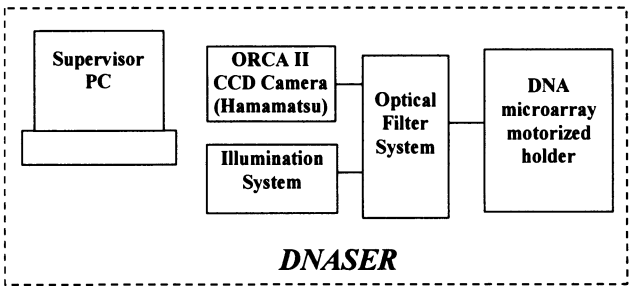

Figure5-15. Block diagram of the DNASER. The illumination system provides a collimated, a wide band and a high brilliant white light beam. The optical filter system allows maximizing the information coming out from the sample and strongly reducing noise that does not represent useful information. The DNA microarray motorized holder lets to position the sample on the focal plane of the CCD. The ORCA II CCD camera is able to acquire images fast and of high quality. On the supervisor PC runs the routines devolved to sample fine positioning, image acquiring and spot analysis (Nicolini et al., 2002) (© 2002 IEEE).

Complex co-focal microscope (Hiroshi 1999) (to focus the laser beam on the sample), samples preparation methods (Stewart et al., 2000) (to deposit spots on the slide), multicolor analysis systems (Harris et al., 2000) (to compare samples with reference data), image processing routines (to extract samples characteristics), statistic analysis routines (Ye et al., 2001) (to extract the gene characteristic) and data-bases (Davies et al., 2001) (to store the categories of genic expression).

Recently, CCD camera technology (Vysis) (Che 1998) has replaced the co-focal microscopy. These new systems are faster (there is no glass slide scanning), cheaper (CCD camera are cheaper than laser scan systems) and simpler to realize (it is no required laser beam motion control).

In what follow we present the DNASER (equipped with the ORCA II Hamamatsu CCD camera) introduced by us for the analysis of traditional and innovative DNA microarrays (Nicolini et al., 2002; Troitsky et al., 2002). The system hardware architecture and the image processing algorithms for the spots analysis are illustrated along with the preliminary results from experiments performed on a real DNA sample are shown.

This section describes how the DNASER works and its main hardware components. The prototype, thanks to the particular optomecanical structure joined to the high sensitivity CCD camera, generates wide area images in a single shot using samples with very low fluorescence intensity. That is possible because the sample is illuminated with a beam produced by a white light source. The beam, through a specific optical path, is accurately filtered and focused on the sample and then on the CCD camera sensitive area. A

Supervisor PC controls DNA microarray images acquisition and elaboration. Figure 5.15 shows the main hardware blocks of the bioinstrumentation.

The illumination system, the optical filter system and the motorized holder blocks constitute the opto-mechanical components. This part is shown in more detail in Figure 5.16.

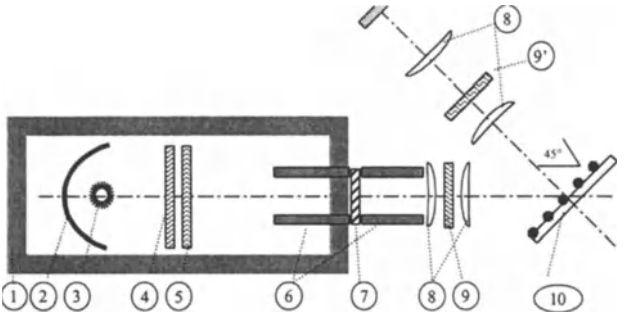

Figure 5-16. Opto-mechanical components of DNASER. 1, 6 light shields; 2 elliptical reflector; 3, High pressure Xe lamp; 4 UV blocking filter; 5, IR blocking filter; 7, iris; 8, achromatic doublets, 9,9', interference filters; 10, sample holder on a x-y-z-remotely controlled translation stages, 11, CCD sensitive area (Nicolini et al., 2002) (© 2002 IEEE).

The light source (3), a 150W Xenon lamp, generates a collimated beam through an elliptical reflector (2). Filters (4) and (5) eliminate IR and UV components. In this way one avoids excessive heating and ultimately damage, of the sample. Two interchangeable interference filters (9) and (9') are placed between two achromatic doublets (8) so as to work in parallel illumination conditions.

Filters (9) and (9') are different because are tuned respectively on the excitation and emission frequency of the DNA microarray fluorescent spots. This geometry is used both for illumination of the sample and collection of the fluorescence signal. The spectrally selected light is then focused onto the sample (10) at 45 degrees of incidence. The illuminated spot dimension is about 1.2x1.2mm. Three motorized linear translation stages, which are controlled by the computer, are used to fine position the sample on the focal plane (Z axis) of the CCD camera and to select the appropriate portion of area to be imaged (X, Y axis). An ad hoc software has been developed in order to position the sample with micron precision.

The ORCA II Dual Scan Cooled 12-14 bit B/W CCD Camera combines high resolution, low noise, and high sensitivity, high quantum efficiency, a wide spectral response (300-700 nm) and a high dynamic range (full well capacity of 16.000 electrons and of 40.000 with binning). The camera has two independent clock rates: 1.25MHz for high precision imaging, achieving 3 to 5 electrons read-out noise and 10 MHz for high frame rate imaging. The ORCA II incorporates a CCD with an effective 1280 x 1024 (1.3 Mpixel) pixel array and progressive scan interline design to eliminate the need for a mechanical shutter. The combination of Hamamatu's hermetic vacuum (10^{-5} Torr) sealing, and Peltier cooling, with air as a heat exchanger, enables the CCD chip to operate at -50 °C. This drastically reduces the dark current (0.001 electron/pixel x sec) of the CCD chip. Special analog contrast enhancement circuits increase versatility for even the most difficult imaging conditions.

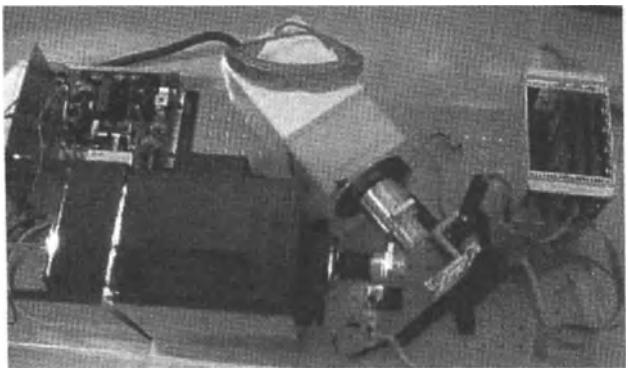

Figure 5-17. Picture of the DNASER prototype (Nicolini et al., 2002) (© 2002 IEEE).

The Supervisor PC is Pentium II 233Mhz, 128MB ram and 2GB hard disk. Figure 5.17 is a picture of the actual prototype layout (the PC is not shown).

On the supervisor PC runs the software routines (C language) that implement the image processing algorithms for the spot analysis.

Microarrays are built lying spots equidistantly in a grid. While the orientation error of the grid is negligible, its spatial position can significantly vary. Furthermore, depending on the arrayer used, the distance between spots is different. In order to develop a robust system, the image processing algorithm developed to perform the spot analysis estimates these data instead of supposing them given.

The input data to the spot analysis are the raw DNA microarray images. The output data of this processing are all the spot features:

- brightness features (spot foreground and background intensity)
- geometric features (spot foreground and background area, circularity).

The microarray geometry suggests to organize the output data using 3D matrices (Figure 5.18). The width and height of the matrix are given, respectively, by the number of columns and rows of the spots in the microarray. While, the depth is given by the number of features associated to each spot.

These data structures permit to store the spot features according to the relative positions that they have in the original image. This property allows to perform further microarrays data processing directly using the associated matricies, reducing the computational burden.

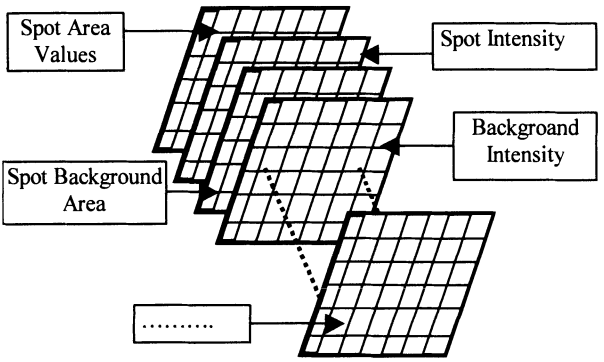

Figure 5-18. Spot features organization on 3D matrix (Nicolini et al., 2002) (© 2002 IEEE).

Also, this data representation is appealing to build an efficient data-base of microarrays features as it permits an intuitive and fast comparing of properties among correspondent spots.

The spot analysis can be logically divided in three main sequential steps:

- image segmentation;
- spot recognition;
- spot features extraction.

In the rest of the paragraph these algorithms will be illustrated separately.

The image segmentation processing is aimed to partition the pixels of the microarrays images in two classes: foreground pixels, that are the pixels belonging the microarray spots and background pixels, that are the pixels out of the microarray spots.

The microarrays images are typically very noisy (Figure 5.19). The not homogenous scene illumination, the light-scattering and not perfectly

cleaned glass slides generate unpredictable variations in the image background intensity and also introduce in the image false foreground entities.

The simplest solution to realize the image segmentation is the definition of a single intensity threshold and the partition of the image in background and foreground pixels according to its value. Indeed, due to the problems mentioned above, to use this approach is required a pre-elaboration to smooth the intensity variations in the image (rolling-ball algorithm) (Sternberg 1983). Alternatively, this pre-elaboration can be avoided considering more thresholds values evaluated, time from time, according the local intensity distribution in the image.

Microarrays images are typically characterized by intensity distribution that result in unimodal histograms. This property complicates the threshold estimation problem, involving the use of sophisticated techniques. We considered two algorithms to estimate the background/foreground threshold for images (or sub-images), both based on the image histogram analysis:

- isodata algorithm (Ridler and Calvard, 1978);
- triangle algorithm (Zack et al., 1977).

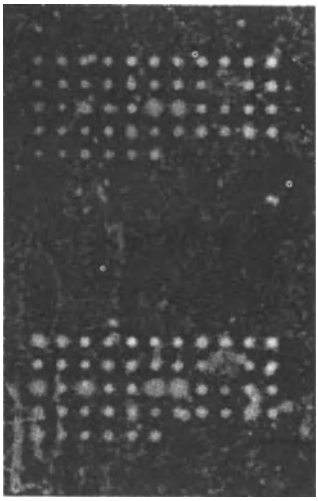

Figure 5-19. DNA microarray image acquired with the DNASER instrumentation. The image is been equalized to emphasize the noisy (Nicolini et al., 2002) (© 2002 IEEE).

The isodata algorithm addresses the search of the best threshold performing an iterative process on the intensity histogram of the image. In particular, it works considering two main steps:

At start, the image histogram is divided in two regions (foreground and background) using the initial threshold value θ evaluated as the mean of the whole histogram.

At each iteration, for both the background and foreground regions defined as in the previous step, are evaluated the mean intensity values, respectively m_b, m_f. The mean of m_b and m_f is assumed as the new threshold θ and according this value the background and foreground regions are redefined. If the threshold value evaluate in this step is the same than the one from the previous step the process stops. Otherwise, this step is iterated.

The final value of θ is then assumed as the best threshold value for the considered image.

The Triangle algorithm works directly estimating the threshold value, without generating any iteration. Given the histogram function of the image *h(b)* (*h(b)* is the number of pixels characterized by brightness b), a segment is constructed between the maximum of *h(b)* (at $b=b_1$) and the highest value of *b* in the image ($b=b_2$). The distance d between the segment and the histogram *h(b)* is evaluated for all values $b \in [b_1, b_2]$. The value of *b* where the distance *d* is maximal is taken as threshold value.

It is of worth to note that, while the Isodata algorithm is a general approach to the threshold estimation problem, the Triangle algorithm has been developed particularly to deal with unimodal histograms.

The spot recognition algorithm, working on the segmented image, identifies the spots present in the microarray image. In particular, this process can be divided in two main steps:

Spots preliminary identification: the pixels in the foreground set are partitioned, including in the same subset all the pixels that belong to the same spot. This phase builds the candidate spot set.

Spots identification refining: the features and position of the spots are used to check their consistency. Also, if the case, lost spots are recovered from the background set.

The spots preliminary identification is performed using a blob analysis technique (Horn, 1986). This algorithm using neighborhood connectivity rules extracts image blobs (spots), that are isolated groups of pixels in the image. Two main pixels properties drive this processing:

Neighboring pixels: two pixels such that their Euclidean distance in the image is less than two pixels.

Boundary pixel: a foreground pixel that has at least one background pixel as neighbor.

Said S_f and S_b, respectively, the foreground and background sets and S_{bl} the generic blob pixel set, the algorithm works iterating the following steps until S_f is empty:

- take a boundary pixel p_0 form S_f, add it to S_{bl} and fix a versus v along that boundary;
- starting with $k=1$, extract and add to S_{bl} all the pixels p_k evaluate ricorsively as the neighbor boundary pixel of p_{k-1} in the direction v until $p_k \neq p_0$;
- take all the pixels in S_f that lay inside the contour drawn by S_{bl} and add them to S_{bl};
- update S_f erasing all the pixels in S_{bf}.

At each iteration the algorithm extracts one blob, which pixels are stored in the correspondent S_{bl} set. When S_f is empty the collection of blob sets extracted S_{bf}^1, S_{bf}^2,..., S_{bf}^n gives the set of the candidate spots. Blobs made of too little number of pixels are not considered.

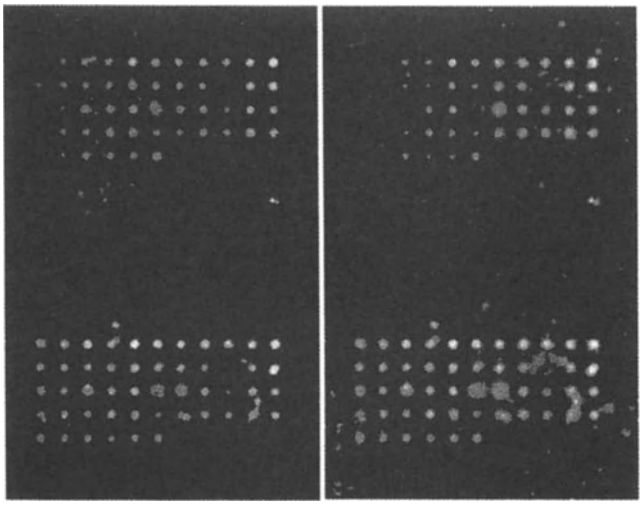

Figure 5-20. (a) isodata algorithm segmentation; (b) triangle algorithm segmentation (Nicolini et al., 2002) (© 2002 IEEE).

The spot identification refining algorithm works on the set of candidate spots performing two sequential elaborations. Firstly, the position of the candidate spots (center of mass of the relative blobs) are evaluated and used to reconstruct the microarray grid, that is, it is evaluated the best set of vertical and horizontal lines, equidistant from the spots and such that just one blob is inside one square (box) of the chess (Figure 5.13a). This grid allows to check the consistency of the candidate spots: if they are correctly positioned, they are real spots, otherwise they are noise.

Furthermore, if there are no candidate spots in a chess box it means that or the spot is occluded in the image or the pixels of this spot have been classified as background. If it is the last case, a new segmentation and blob analysis process can be performed, locally, on the image pixels that lay in chess box to try to recover the lost spot.

It is of worth to deepen the grid building task. From our hypothesis, we know that the spots in the microarray image are positioned along horizontal lines and are each other equidistant both, horizontally and vertically. The absolute position of the grid is unknown so as the spot distance, furthermore some spots can miss and others can be due to noise. We approached the problem clustering the spots (in the candidate set) that are supposed to belong to the same microarray row (it is tolerated a vertical positioning error less than the medium radius of the estimated spots). For each row set, the medium and the variance of the elements distances are evaluated and, among the sets with higher cardinality, the grid distance is taken as the medium distance of the set with the smallest variance.

The second step of the identification spot refining algorithm concerns the compatibility of each estimated spot features with both, the expected spot properties and the medium characteristics of the estimated spots. The medium value of the spot surface, spot circularity and positioning error in the grid are evaluated over the set of the estimated spot. These criterion are used to perform a quality check on the estimated spots and, if it is the case, to eliminate not reliable estimation.

Identified all the spots in the microarray images, this processing step is aimed to extract for each spot a set of features. Such analysis allows to describe the main characteristics of each spot by means of a reduced set of parameters, simplifying the problems of characterizing, storing and classifying data from microarray images.

The significant features to extract from spots are strictly dependent on the kind of analysis that is going to be performed, then it is not possible to define a general set of features. For this reason we just investigated for the features that are considered for almost all the researches. In particular, we considered the following spot features:

- spot (foreground) area: it is the number of pixels belonging the correspondent blob of the image.
- spot background area: it is the number of background pixels laying in the spot chess box.
- spot intensity: it is average intensity of the correspondent blob.
- spot background intensity: it is the average intensity of the background pixels in the spot chess box. Indeed, to reduce noise, just a proper subset of these pixels is considered (Yang et al., 2001).

- spot circularity: it is a measure of the circularity of the correspondent blob in the image.
- spot position error: it is the difference between the position of the correspondent blob in the image (its c.o.m.) and the position of the spot chess box centre.

All the described features and, if any, other specific once are stored in the 3D matrix illustarted above.

In this section we show the results obtained executing the presented algorithm on a real DNA microarray image acquired with the DNASER instrumentation. Figure 5.20 reports the grabbed image.

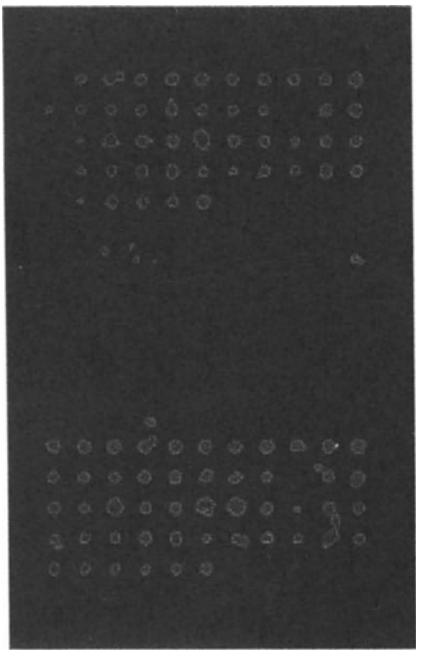

Figure5-21. Blob analysis extraction (Nicolini et al., 2002) (© 2002 IEEE).

As mentioned above, the image is very noisy and many spots are barely visible. We execute different segmentation processes on this image to compare their effectiveness. In particular, for both isodata and triangle algorithms, we considered the threshold search on the whole image (I_1), I_1 with rolling-ball pre-elaboration (RI_1), threshold search considering 4 sub-images (I_4) and I_4 with rolling-ball pre-elaboration (RI_4).

For both, isodata and triangle methods, cases I_4 and RI_4 performed the best and RI_1 was better then I_1. So the best results, also considering the

computational burden, was given by cases I_4. Furthermore, as shown in Figure 5.20 isodata I_4 outperformed triangle I_4 and then, in what follow, isodata I_4 is the segmentation algorithm used.

Figure 5.21 reports the blobs extracted using the presented blob analysis algorithm. Considering the real microarray structure, it easy to see that the image is corrupted by false and missing spots. Figure 5.22a shows the estimated grid lines and the effect of considering the estimated microarray structure to validate the spots consistency. In fact, the false spots in the central part of the image are erased, while the real spots on the first column are recovered. Finally, Figure 5.22b reports the spots that overcome the criteria of spot quality check.

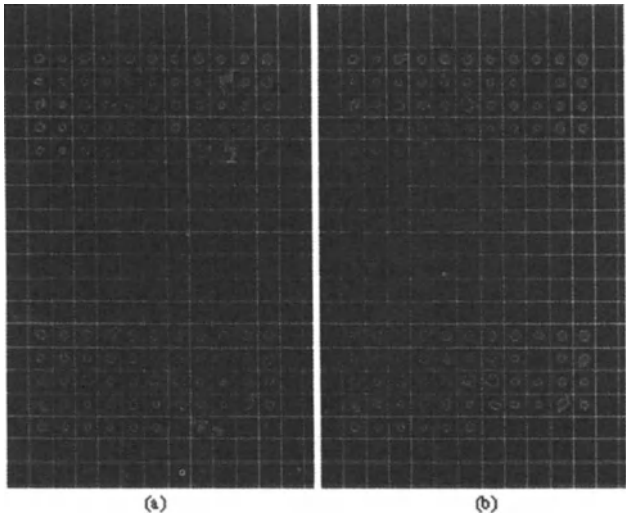

Figure5-22. (a) estimate grid lines and spots recovered; (b) spots that overcome the criteria of spot quality check (Nicolini et al., 2002) (© 2002 IEEE).

Blobs in Figure 5.22b are considered the spots present in the DNA microarray image and for them all the interesting features are extracted and stored in the 3D matrix.

We presented the DNASER, a new device for the DNA microarrays analysis based on CCD camera technology. The described prototype is a flexible analysis instrument. The special optomecanical instrumentation and the wide band ORCA II camera allow to acquire DNA microarray images at different frequencies simply changing two different interference filters. The spot analysis algorithm is fully automated and does not require any additional information about the DNA microarray geometry. According to

the relative position, the spot features are stored in a 3D structure that is appealing to build an efficient database, for classification and further processing purposes.

Preliminary experiments on a real DNA sample showed the different behaviors of the proposed spot analysis techniques and demonstrate the system effectiveness in recognizing and classifying samples.

DNA microarrays analysis devices can be used in the wide range of medical applications that require the DNA study and classification. In example, the DNASER can be used to characterize the cellular differences between different tissue type such us between normal cells and cancer cells at different stages of tumor progression, or between cancers with different responses to treatment, or between control cells and cells treated with a particular drug. To this purpose, our further work is aimed to furnish the system with a database of different microarrays features and to develop, using neural network, an automatic diagnostic tool for classifying samples on the basis of their gene expression pattern (Alon et al., 1999, Golub et al., 1999).

5.3 Unsolved protein structures of scientific and industrial interest

Among the numerous proteins of scientific and industrial interest (see Table 1.1 in Chapter 1), three protein of different classes were chosen until now to prove the principle of our new technology: chicken egg white lysozyme as model system, bovine cytochrome P450 Side Chain Cleavage (SCC) and human protein kinase CK2. All three gave positive results in both protein crystal growth and its structural characterization down to the atomic level At the beginning, chicken egg-white lysozyme has been utilized as a model system. Then this research has been focuses on the recombinant bovine cytochrome P450scc and, finally on human protein kinase CK2α catalytic subunit for their industrial relevance as shown in the earlier chapters.

The new protein thin-film template crystallization method then allows one to avoid random searching for the correct crystallization conditions and to obtain highly reproducible results.

Therefore, it has been shown that is possible to use the force of protein thin film nanotechnology to resolve the problems of the so far non crystallized proteins and to find a way to develop general systematic procedure for protein crystallization to be applied to a wide class of protein of significant industrial and health impact yet unsolved, such as important proteins in the control of cancer and infectious diseases (see Table 1.1 in Chapter 1).

Particularly P450 cytochromes represent a wide class of membrane proteins, extensively studied in the past for their potential use in medicine and pharmaceutics (Archakov et al., 2003; Bernhardt et al., 1998; Bernhardt, 1998, 2000; Shumyantseva et al., 2001; Usanov et al., 2002; Poulos et al., 1999; Eldarov et al., 1998). Unfortunately the difficulty gaining structural informations have hampered most of these potentials; only nanocrystallography appears capable to overcome these obstacles. In our laboratory, studies utilizing nanocrystallography are indeed underway and look very promising, extending with high probability of success to P4502b4 (Kiselyova et al., 1999) and others cytochromes (Poulos, 1991, Kiselyova et al., 1999) these nanotechnology-based procedures for crystallization and subsequent structural characterization at atomic resolution.

Chapter 6

FUTURE TRENDS

Some time ago an alternative route to the dominant top-down approach in lithography and microelectronics was postulated by few authors (see Nicolini, 1989). This bottom-up approach aimed to the fabrication of an hypothetical properly functionalized structure called "biochip" to be assembled at the nanoscale level from atoms and molecules by means of organic synthesis or by recombinant DNA technology.

However this messianic target remained a chimerical dream incapable to compete with the constant high development and miniaturization "top-down" of traditional silicon lithography, until very recently when organic synthesis, Langmuir - and self-assembly of polymers and biopolymers (Nicolini et al., 2001) brought new nanotechnological developments and large interest world-wide. The bottom-up approach now appears indeed achievable via nanotechnology and nanosurface chemistry (see the book by Rossof, 2001 for an updated overview).

One of the emerging future technological trends appears now the integration of structural and functional proteomics and advanced protein crystal technology with the broad interdisciplinary field of nanotechnology, for the promising development of new intelligent nanomaterials and new three-dimensional nanodevices of innovative physical and functional properties.

In addition to consolidate their application in life sciences and pharmaceutical industries as outlined in the previous chapter, proteomics and nanocrystallography appear capable in the future to address other demands in basic and applied sciences increasing their complementarities and their integration at the nanoscale level, particularly in those areas related to material sciences, including inorganic nanocrystals, and to information and communication technologies.

E. Pechkova et al., *Proteomics and Nanocrystallography*
© Springer Science+Business Media New York 2003

6.1 Novel composite biomaterials and nanodevices

The construction of usefull nano-structures via self-assembly of synthetic organic molecules has been successfully demonstrated for various applications time ago (see Lehn 1996 for overview), including molecular motors (Ward, 2000). The analogous use of biological molecules such as DNA or proteins, as building blocks' for the *in vitro* construction of nanostructures is less developed and its potential still far from being fully exploited.

Self-assembly of three dimensional nanostructured functional arrays is a major challenge in nanotechnology, mainly in the fields of photonic crystals, quantum dots arrays and metallic nanoparticles. Exploitation of the inherent potential in the use of biological macromolecules – DNA and proteins – as 'guiding template' for the construction of one and two dimensional nanoarrays of nanoparticles (Nimeyer et al., 2001) and quantum dots (Tessier et al., 2001) is just beginning to emerge.

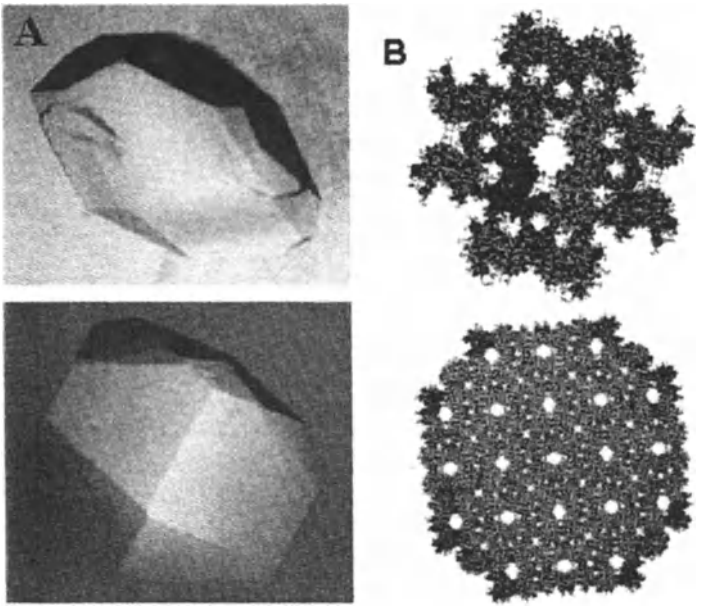

Figure 6-1. Two Lysozyme crystals (a) with their corresponding views of the crystal cavities (b) (courtesy of N. Dotan).

The array of inner spacings of protein crystals (Figure 6.1b) routinely prepared for X-ray crystallography attracted only little attention until now: it was noted that different crystallization conditions applied to same protein may result in different packing and attempts were made to analyse protein-protein interactions for better understanding of packing patterns (Padilla et al., 2001).

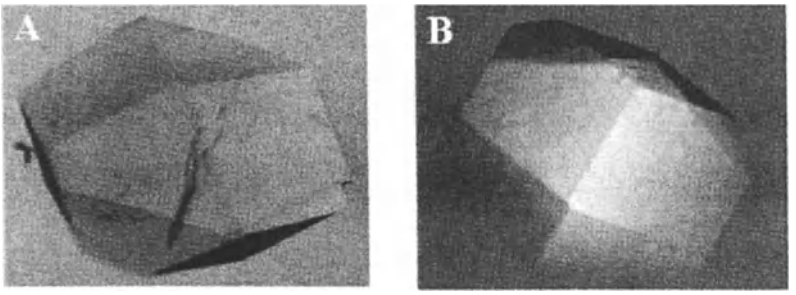

Figure 6-2. Lysozyme crystals stabilitation by crosslinking by glutaraldehyde: a) treated, b) untreated (courtesy of A. Freeman).

The use of protein crystal spacings as functional part for practical purposes was limited to the use of chemically crosslinked enzyme crystals as immobilized biocatalysts for a variety of synthetic applications with effective diffusion taking place via small channels. These studies has clearly demonstrated that protein crystals, routinely obtained either via common crystallization procedures or by the nanobiofilm templates here described, can be readily stabilized by chemical crosslinking e.g. with glutaraldehyde (Figure 6.2).

In this context it was also suggested (Vilenchik et al., 1998) that protein crystal spacing 'channels' could be used as 'natural zeolites' for chromatographic purposes.

Self-assembly of proteins into nano and microsized structures with subsequent spacing 'channels' may be affected via several mechanisms (see Dotan et al., 2001 for overview):

- in vitro reconstitution of purified natural structural protein e.g. reconstruction of bacterial S-layer on a supporting surface (see Figure 6.3; Sleytr et al., 2001 and 1999 for comprehensive review);
- protein crystallization from saturated solutions e.g. preparation of crystals for X-ray crystallography (see earlier part of this book);

- specific crosslinking of binding proteins by bi or multi ligands, e.g. crosslinking of lectins by di or oligosaccharides, in analogy to natural processes (Weber et al.,1998);

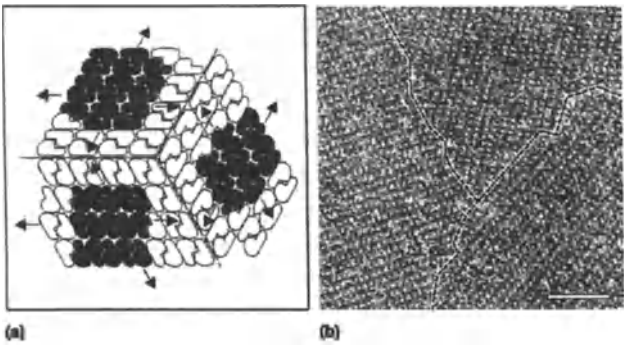

Figure 6-3. Schematic illustration of S-layer crystal growth at surfaces and interfaces which starts at several nucleation points an proceeds in in-plane until the boundary lines of growing crystalline domains meet (a). Transmission electron micrograph of a negatively stained preparation of a closed mosaic of crystalline S-layers domain with oblique lattice symmetry obtained by recrystallization on a lipid film. Bar, 100 nm (b) (courtesy of U. Sleytr).

- directed self-assembly of a binding protein into a pre-designed crystal by specific crosslinking affected by bi-ligand imposing predetermined relative orientation of the crosslinked binding protein, an approach recently introduced by our laboratory (Dotan et al., 1999);
- directed self-assembly of chimeric proteins into a pre-designed crystal by specific recognition of protein subunits into linear or circular structures, affected by synthetic chimeric protein 'building blocks' (Padilla et al., 2001).

Particularly promising appears the use of directed self-assembly of a binding protein via specific cross-linking into pre-designed diamond-like protein crystal (Dotan et al., 1999): the lower part of the Figure 6.4 displays the computer simulation of the array of the enzyme crystal cavities. In this case, the construction of electronic nanostructures has been successfully demonstrated, integrating in a novel '3D crystal engineering' approach protein 'building block' selection (a tetrahedral lectin) and molecular modeling (for bi-ligand crosslinker design), thereby potentially providing a versatile tool for the preparation of novel composite nanostructured materials with their internal cavities as 'guiding template' with potential applications in the area of photonic crystals and of semiconductors (Edrington et al., 2001; Norris and Vaslov 2001).

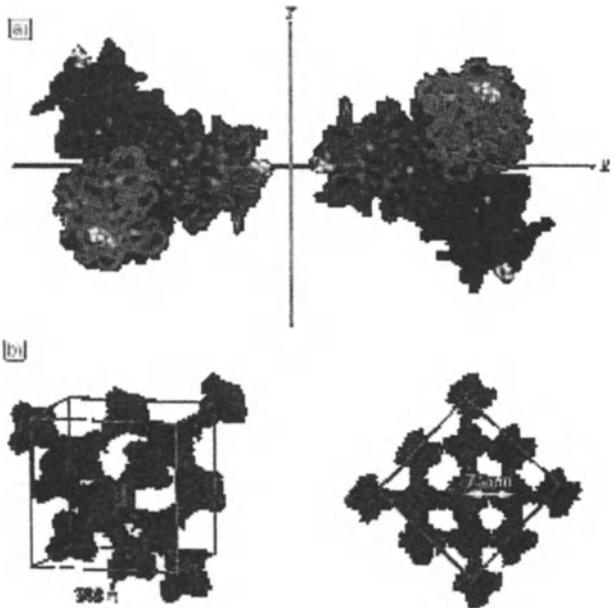

Figure 6-4. a) Model of two molecules of 1 approaching each other in a staggered orientation (dihedral angle -60°. The distance between anomeric oxygen atoms of the bound of mannoses is 10 Å. Two views of the unit cell predicated diamondlike supramolecular lattice formed by molecules of 1 cross-linked by 2 (courtesy of N. Dotan, Dotan et al, 1999).

The structural characterization of the above nanomaterials stabilized and chemically crosslinked (Dotan et al., 2001; Padilla et al., 2001) is carried out by X-ray crystallography, electron microscopy and chemical analysis. The stabilized protein crystals is typically equilibrated with solutions containing monomers, salts or metallic ions in order to yield uniform polymerization, crystallization or metallization within the cavities of the protein crystal.

This is shown in Figures 6.1 and 6.2 by the lysozyme enzyme, earlier described in this book to introduce nanocrystallography and here used as model for this study: the stabilized crystals equilibrated with a series of precursors does not appear to induce any distortion in the protein template. Lysozyme crystals were also readily stabilized by chemical crosslinking with full retention of crystal and protein three dimensional structures (Figure 6.2).

All crosslinked crystals retained their shape and size, when equilibrated with a series of monomers and their combinations, all dissolved in 25%

aqueous ethylene glycol, to allow for the mixing of water insoluble monomers following equilibration for 20 hrs at room temperature.

Similarly, apart from the monomer mixture containing hydroxyethylmethacrylate, all monomer mixtures tested were readily polymerized without distortion of crystal structure, as demonstrated in Figure 6.5 for the unique combination of acrylamide/styrene copolymerization (Dotan et al., 1999, 2001).

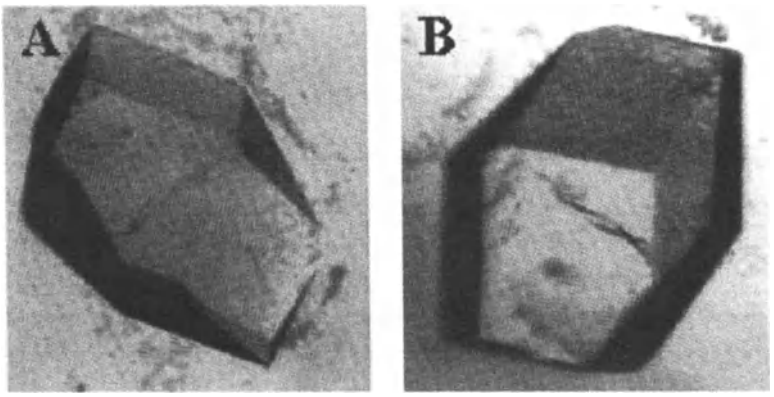

Figure 6-5. Retention of crystal structure following polimerization of acrylamide/styrene/EGD combination: a) equilibrated with monomers; b) polymerized (courtesy of A. Freeman).

Finally, the resulting complete mechanical, electrical and optical properties, which are still under experimental evaluation, could lead in the future to the concrete fabrication and use of a new family of crystal protein-based composite materials with exciting functional properties.

6.2 Nanocrystals

Self-assembled crystals of nanometer size can also be made of silver (Figure 6.6), cobalt, gold and/or nanoparticles and are fabricated by using reverse micelles or similar technologies (Pileni, 1997, 2002).

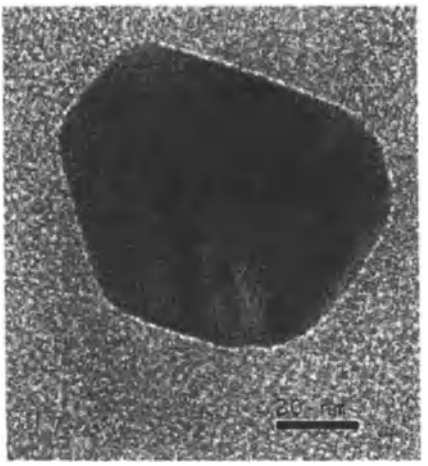

Figure 6-6. Silver crystal obtained by a recently developed procedure for electroless silver deposition (courtesy of A. Freeman).

Other examples of potentially interesting materials are calcium carbonate crystals (Figure 6.7) and nanohedra wich use symmetry to design self assembling protein cages, layers, crystals and filaments (Padilla et al., 2001).

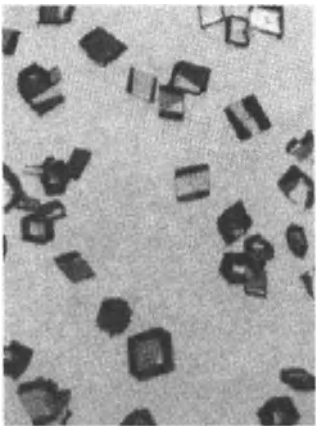

Figure 6-7. Calcium carbonate crystals (courtesy of A. Freeman).

All the above materials based on organic and inorganic technologies compete with the protein-based technologies earlier described in this

chapter, repeating the race to new electronic devices and systems which is under way world-wide between inorganic, organic and biological approaches. This book obviously points to the advantages of the latter protein (or nucleic acids) route described at length.

References

Addadi L., Weiner S., Geva M., On how proteins interact with crystals and their effect on crystal formation. Kardiol. 90, 92-98, 2001.

Aibara S., Shibata K., Morita Y., Protein crystallization in microgravity. Biol. Sci. Space 11, 339-345, 1997.

Akira S., Tsukiharab T., Spatiotemporal protein crystal growth studies using microfluidic silicon devices. J. Cryst. Growth, 196, 691-702, 1999.

Alderton G., Fevold H., J. Biol. Chem. 164, 19, 1946.

Allende J.E, Allende C.C., Protein kinases.4. Protein-kinase ck2 - an enzyme with multiple substrates and a puzzling regulation. FASEB J. 9, 313-323, 1995.

Alon U., Barkai N., Notterman D. A., Gish K., Ybarra S., Mack D., Levine A. J., Broad patterns of gene expression revealed by clustering analysis of tumor and normal colon tissues probed by oligonu-cleotide arrays. Proceedings of the National Academy of Sciences USA, 96, 6745–6750, 1999.

Amann E., Ochs B., Abel, K. J., Tightly regulated tac promoter vectors useful for the expression of unfused and fused proteins in Escherichia coli. Gene 69, 301-315, 1988.

Archakov A.I., Govorun V.M., Dubanov A.V., Ivanov Y.D., Veselovsky A.V., Lewi P., Janssen P. Protein-protein interactions as a target for drugs in proteomics. Proteomics 3, 380-391, 2003.

Bacon G., *X-ray and Neutron Diffraction*, Pergamon Press, Elmsford, N. Y. 1966.

Bartolucci S., Guagliardi A., Pedomne E., de Pascale D., Cannio R., Camardella L., Rossi M., NicAstro G., de Chiara C., Facci P., Mascetti G., Nicolini C., Thioredoxin from Bacillus acidocaldarius: characterization, high-level expression in Escherichia Coli and molecular modelling. Biochem. J. 328, 277-285, 1997.

Battistutta R., De Moliner E., Sarno S., Zanotti G., Pinna L.A. Structural features underlying selective inhibition of protein kinase CK2 by ATP site-directed tetrabromo-2-benzotriazole. Protein Science 10, 2200-2206, 2001.

Battistutta R., Sarno S., De Moliner E., Papinutto E., Zanotti G., Pinna L.A. The replacement of ATP by the competitive inhibitor emodin induces conformational modifications in the catalytic site of protein kinase CK2. J. Biol. Chem. 275, 29618-29622, 2000.

Beeston, B., Horne R., Markham, R., Electron Diffraction and Optical Diffraction Techniques, North-Holland Co., Amsterdam, 1973.

Berman H.M., Westbrook J., Feng Z., Gilliland G., Bhat T.N., Weissig H., Shindyalov I.N., Bourne P.E., The Protein Data Bank. Nucleic Acids Research, 28 235-242, 2000.

Bernhardt R., Electron transfer in mitochondrial steroid hydroxylating cytochrome P450 systems: role of adrenodoxin. in: *Biophysics of Electron Transfer and Molecular Bioelectronics* (Nicolini C., Ed.) Plenum Press, New York, pp. 51-66, 1998.

Bernhardt R., Pei-rang C., Grinberg A., Hannemann F., Weißgerber P., Müller J.J., Heinemann U., Protein recognition in mitochondrial steroid hydroxylation and electron transport. in: *Molecular Steroidogenesis* (Okamoto, M., Ishimura, Y., Nawata, H., Eds.) Universal Academy Press, Inc. Tokyo, Japan, pp. 53-56, 2000.

Bernhardt R., The role of adrenodoxin in adrenal steroidogenesis. Curr. Opinion Endocrinol. & Diabetes 7, 109-115, 2000.

Berzina T.S., L. Piras, V.I. Troitsky, Study of horseradish peroxidase activity in alternate-layer Langmuir–Blodgett films. Thin Solid Films 327-329, 621-629, 1998.

Bessho Y., Ataka M., Asai M., Katsura T., Analysis of the crystallization kinetics of lysozyme using a model with polynuclear growth mechanism. Biophys. J. 66, 310-313, 1994.

Bi R.C., Gui L.L., Han Q., Shen F.L., Shi K., Wang Y.P., Chen S.Z., Hu Y.L., Niu X.T., Dong J., Zhou Y.C., Lin N.Q., Protein crystallization in space Microgravity. Sci. Technol. 7, 203-206, 1994.

Bilderback D.H., Hoffman S.A., Thiel D.L., Nanometer spatial resolution achieved in hard X-ray imaging and laue diffraction applications. Science 263, 201-203, 1994.

Binning G., Quate C.F., Gerber C., Atomic Force Microscopy. Phys. Rev. Lett. 56, 930-933, 1986.

Blow D.M., Chayen N.E., Lloyd L.F., Saridakis E., Control of nucleation of protein crystals. Protein Science 3, 1638-1643, 1994.

Borgstahl G.E., Vahedi-Faridi A., Lovelace J., Bellamy H.D., Snell E.H., A test of macromolecular crystallization in microgravity: large well ordered insulin crystals. Acta Crystallogr D Biol Crystallogr 57, 1204-1207, 2001.

Bossemeyer D., Protein kinases--structure and function. FEBS Letters 369, 57-61, 1995.

Bradley D., Prater S., Steven C., Tuller S.C., Wilson L.J., Simplex optimization of protein crystallization conditions, Journal of Crystal Growth 196, 674-684, 1999.

Bragg W.L., X-ray crystallography. Scientic American 219, 58-70, 1968.

Bram A., Branden C.T., Craig C., Snigireva I., Riekel C., X-Ray diffraction from single spider silk fibre. J. Appl. Crystallogr. 30, 390-392, 1996.

Bras M., Cloareck J.P., Bessueille F., Souteryrand E., Martin J.R.; Chauvet J.R., Control of immobilization and hybridization on DNA chips by fluorescence spectroscopy. Journal of fluorescence 10, 247-253, 2000.

Brunger A.T., Adams P.D., Clore G.M., DeLano W.L., Gros P., Grosse Kunstleve R.W., Carter C.W. Methods Enzymol. 276, 74, 1997.

Brunger A.T., Adams P.D., Clore G.M., DeLano W.L., Gros P., Grosse-Kunstleve R.W., Jiang J.S., Kuszewski J., Nilges M., Pannu N.S., Read R.J., Rice L.M., Simonson T., Warren G.L., Crystallography & NMR system: A new software suite for macromolecular structure determination. Acta Crystallographica D 54, 905-921, 1998.

Bunick C., North A.C., Stubbs G., Evaporative microdialysis: an effective improvement in an established method of protein crystallization. Acta Crystallogr D Biol. Crystallogr. 56, 1430-1431, 2000.

Carrara E.A., Gavotti C., Catasti P., Nozza F., Berutti Bergotto L.L., Nicolini C.A., Improvement protein secondary structure prediction by combination of statistical algorithms and circular dichroism. Arch. Biochem. Bioph. 294, 107-114, 1992.

Carter C.W., Response Surface Methods for Optimizing and Improving Reproducibility of Crystal Growth Methods Enzymology 276, 74-99, 1997.

Caylor C.L., Dobrianov I., Lemay S.G., Kimmer C., Kriminski S., Finkelstein K.D., Zipfel W., Webb W.W., Thomas B.R., Chernov A.A., Thorne R.E., Proteins 36, 270-81, 1999.

CCP4. Collaborative Computational Project Number 4, Acta Crystallogr. D50, 760-763, 1994

Chantalat L., LeroY D., Filhol O., Nueda A., Benitez M.J., Chambaz E.M., Cochet C., Dideberg O., Crystal structure of the human protein kinase CK2 regulatory subunit reveals its zinc finger-mediated dimerization. EMBO J. 18, 2930-2940, 1999.

Chantalat L; Leroy D; Filhol O; Quitaine N; Chambaz EM; Cochet C; Dideberg O. Crystallization and preliminary X-ray diffraction analysis of the regulatory subunit of human protein kinase CK2. Acta Crystallographica. Section D, Biological Crystallography 55, 895-897, 1999.

Chayen N.E., A novel technique for containerless protein crystallization. Protein Eng 9, 927-929, 1996a.

Chayen N.E., Recent advances in methodology for the crystallization of biological macromolecules, J. Cryst. Growth 199, 649-655, 1999b.

Chayen N.E., Helliwell J.R., Space-grown crystals may prove their worth. Nature 398, 20, 1999.

Chayen N.E., Patrick D. Shaw S., Blow D.M., Microbatch crystallization under oil — a new technique allowing many small-volume crystallization trials. Journal Crystal Growth 122, 176-180, 1992.

Chayen N.E., Saridakis E., El-Bahar R., Nemirovsky Y., Porous silicon: an effective nucleation-inducing material for protein crystallization. J. Mol. Biol. 312, 591-595, 2001.

Chayen N.E., Saridakis E., Is lysozyme really the ideal model protein? Journal Cryst. Growth 232, 262-264, 2001.

Che D., Large-field fluorescence imaging apparatus. PATENT N° 049748 - March 27, 1998.

Choi J-Y., Pratap, J., Javed A., Zaidi K., Xing L., Balint E., Dalamandas S., boyce B., van Wijnen A.J., Lian J.B., Stein J.L., Jones S.N., Stein G.S., Subnuclear targeting of Runx/Cbfa/AML factors is essential for tissue- specific differentiation during embryonic development. PNAS 98,15, 8650-8655, 2001.

Chu S., DeRisi J., Eisen M., Mulholland J., Bottstein D., Brown P. O., Herskowitz I., The transcriptional program of sporulation in budding yeast. Science 282, 699–705, 1998

Chung S.K., Trinh E.H., Containerless protein crystal growth in rotating levitated drops. Journal of Crystal Growth 194, 384-397, 1998.

Croce C.M., How can we prevent cancer? Proc. Natl. Acad. Sci. USA 10986-10988, 2001.

Cusack S., Belrhali H., Bram A., Burghammer M., Perrakis A., Riekel, C., Small is beautiful: protein micro-crystallography. Nature Structural Biology 5, 634-637, 1998.

Darst S.A., Edwards A.M., Epitaxial growth of protein crystals from two-dimensional crystals on lipid layers. Curr. Opin. Struct. Biol. 5, 640-644, 1995.

Davies P.F., Polacek D.C., Compositions, kits, and methods for hydrodynamic stress-related regulation of gene expression. US PATENT N° 783836, February 14, 2001.

De Moliner E., Moro S., Sarno S., Zagotto G., Zanotti G., Pinna, L.A.. Battistutta, R. Inhibition of protein kinase CK2 by anthraquinone-related compounds - A structural insight. J. Biol. Chem. 278, 1831-1836, 2003.

Decher G., Fuzzy nanoassemblies: toward layered polymeric multicomposites. Science 277, 1232-1237, 1997.

Decher G., in Templating, Self-Assembly and Self-Organization, ed. J.P. Sauvage, and M.W. Hosseini (Pergamon, Oxford, 1996).

Decher G., Supramol. Chem. 9, 507, 1996.

Dobrianov I., Finkelstein K.D., Lemay S.G., Thorne R.E., X-ray topographic studies of protein crystal perfection and growth. Acta Crystallogr D Biol Crystallogr 54, 922-937, 1998.

Dotan N., Arad D., Frolow F., Freeman A., Self-assembly of a tetrahedral lectin into predesigned diamond like protein crystals. Angew. Chem. Int. Ed. 38, 2363-2366, 1999.

Dotan, N., Cohen, N., Kalid, O. Freeman, A. Supramolecular assemblies made of biological macromolecules. In: "Nano-surface chemistry" (Rossof, M. Ed) pp461-471, Marcel Dekker, NY, 2001.

Drenth J., Haas C., Nucleation in protein crystallization. Acta Crystallogr. D Biol. Crystallogr. 54, 867-72, 1998.

Du Bois R. N., Simpson E. R. , Tuckey J., Lambeth J. D., Waterman M. R., Evidence for a higher molecular weight precursor of cholesterol side-chain-cleavage cytochrome P450 and induction of mitochondrial and cytosolic proteins by corticotropin in adult bovine adrenal cells. Proceedings of the National Academy of Sciences USA 79, 1028-1032, 1981.

Dubrovsky T., Nicolini C., Preparation and immobilization of Langmuir Blodgett films of antibodies conjugated to enzyme for potentiometric sensor application. Sensors Actuators 22, 69-73, 1994.

Ducruix A., Giege R., in Crystallization of Nucleic Acids and Proteins. A Practical Approach, New York: Oxford University Press, pp 130–133, 1999.

Durbin S.D., Feher G., Protein crystallization. Annual Review Physical Chemistry 47, 171-204, 1996.

Durbin S.D., Feher G., Studies of crystal growth mechanisms of proteins by electron microscopy. Journal Molecular Biology 212, 763-764, 1990.

Edrington A.C., Urbans A.M., DeRege P., Chen C.X, Swager T.M., Hadjichristidis N., Xenidou M., Fetters L.J., Jonnopoulos J.D., Fink Y., Thomas E.L., Polymer based photonic crystals. Adv. Mater. 13, 421-425, 2001.

Edwards A.M., Darst S.A., Hemming S.A., Li Y., Kornberg R.D., Epitaxial growth of protein crystals on lipid layers. Nat. Struct. Biol. 1, 195-197, 1994.

Eisen M.B., Spellman P.T., Brown P.O., Botstein D., Cluster analysis and display of genome-wide expression patterns. Proceedings of the National Academy of Sciences USA, 95, 14863–14868, 1998.

Eldarov M.A., Sidorovich V.E., Pozmogova G.E., Skryabin K.G., Targeted expression of mammalian cytochromes P450scc and P4502b4 in yeast saccharomyces cerevisiae. in *Biophysics of electron transfer and Molecular Bioeletronics*, ed. C. Nicolini, Plenum Press New York, pp. 91-102, 1998.

Engstrdm P., Fiedler S., Riekel C., The microfocus beamline at the ESRF. Rev. Sci. Instrum. 66, 1348-1350, 1995.

Esposito L., Sica F., Sorrentino G., Berisio R., Carotenuto L., Giordano A., Raia C.A., Rossi M., Lamzin V.S., Wilson K.S., Zagari A., Protein crystal growth in the Advanced Protein Crystallization Facility on the LMS mission: a comparison of Sulfolobus solfataricus alcohol dehydrogenase crystals grown on the ground and in microgravity. Acta Crystallogr D Biol. Crystallogr. D54, 386-90, 1998.

Facci P., Erokhin V., Antolini F., Nicolini C., Chemically induced anisotropy in antibody Langmuir Blodgett films. Thin Solid Films 237, 19-21, 1994.

Facci P., Erokhin V., Nicolini C., Nanogravimetric gauge for surface density measurements and deposition analysis of LB films. Thin Solid Films 230, 86-89, 1993.

Facci P., Erokhin V., Nicolini C., Scanning tunneling microscopy of a monolayer of reaction centers. Thin Solid Films 243, 403-406, 1994.

Falini G., Fermani S., Conforti G., Ripamonti A., Protein crystallisation on chemically modified mica surfaces. Acta Crystallogr D Biol Crystallogr 58, 1649-1652, 2002.

Fermani S., Falini G., Minnucci M., Ripamonti A., Protein crystallization on polymeric film surfaces. J. Cryst. Growth 224, 327-334, 2001.

Fermın O., Novella M.L., Rondon D., Garcıa-Ruiz J-M., Growth of lysozyme crystals under microgravity conditions in the LMS (STS-78) mission, Journal of Crystal Growth 196 649-664, 1999.

Forsythe E.L., Pusey M.L., The effects of temperature and NaCl concentration on tetragonal lysozyme face growth rates. Journal of Crystal Growth 139, 89-94,1994.

Forsythe E.L., Snell E.H., Malone C.C., Pusey M.L., Crystallization of chicken egg white lysozyme from assorted sulfate salts. Journal of Crystal Growth 196, 332-343, 1999.

Galkin O., Vekilov P.G., Nucleation of protein crystals: critical nuclei, phase behavior, and control pathways. Journal of Crystal Growth 232, 63-76, 2001.

Garavito R.M., Picot D., Loll P.J., Strategies for crystallizing membrane proteins. J Bioenerg Biomembr 28, 13-27, 1996.

Garcia-Ruiz et al., Mater. Res. Bull. 28, 541-546, 1993.

Garcia-Ruiz J.M., Moreno A., Growth kinetics of protein single crystals in the gel acupuncture technique. J. Cryst. Growth 178, 393-401, 1997.

Garcia-Ruiz J.M., Moreno A., Investigations on protein crystal growth by the gel acupuncture method. Acta Cryst. D50, 484-490, 1994.

Giege R., Drenth, J. Ducruix, McPherson A., Saenger W. Crystallogenesis of biological macromolecules. Biological., microgravity and other physicochemical aspects. Progress in Crystal Growth and Characterization of Materials 30 237-281, 1995.

Golub T., Slonim D., Tamayo P., Huard C., Gaasenbeek M., Mesirov J., Coller H., Loh M., Dowing J., Caligiuri M., Bloomfield C., Lander E. Molecular classification of Cancer: class discovery and class prediction by gene expression monitoring. Science 286, 531-537, 1999.

Gonzalez A., Nave C., Radiation damage in protein crystals at low temperatures. Acta Crystallog. D50, 874-877, 1994.

Gouaux E., It's not just a phase: crystallization and X-ray structure determination of bacteriorhodopsin in lipidic cubic phases. Structure 6, 5-10, 1998.

Graves D.J., Su H.J., McKenzie S.E., Surrey S., Fortina. System for preparing microhybridization arrays on glass slides, Analytical Chemistry 70, 5085-5092, 1, 1998.

Grossowicz N., Ariel M., Weber T., Improved lysozyme assay in biological fluids, Clin. Chem. 25, 484-485, 1979.

Guerra B., Issinger O.G., Protein kinase CK2 and its role in cellular proliferation, development and pathology. Electrophoresis 20, 391-408, 1999.

Guerra B., Nienfind K., Pinna L.A., Schomburg D., Issinger O.G., Expression, purification and crystallization of the catalytic subunit of protein kinase CK2 from Zea mays. Acta Crystallogr D Biol Crystallogr 54, 143-145, 1998.

Guryev O., Dubrowsky T., Chernogolov A., Dubrovskaya S., Usnov S., Nicolini C., Orientation of cytochrome P450scc in Langmuir-Blodgett monolayers. Langmuir 13, 299-304, 1997.

Haire L.F., Ph.D. Thesis. University of London, 1996.

Han Q., Lin S.-X., The study of crystallization of estrogenic 17β-hydroxysteroid dehydrogenase with DHEA and DHT at elevated temperature. Biochemical Biophysical Research Communications 277, 100-106, 2000.

Hanks S.K., Quinn A.M., Hunter T., The protein kinase family: conserved features and deduced phylogeny of the catalytic domains. Science 241, 42-52, 1988.

Hanukoglu I., Hanukoglu Z., Stoichiometry of mitochondrial cytochromes P-450, adrenodoxin and adrenodoxin reductase in adrenal cortex and corpus luteum. Implications for membrane organization and gene regulation. Eur J Biochem 157, 27-31, 1986.

Harata K., X-Ray Structure of a monoclinic form of hen egg-white lysozyme crystallized at 313-k - comparison of 2 independent molecules. Acta Crystallogr D Biol Crystallogr 50 250, 1994.

Harpaz Y., Gerstain M., Chothia C., Volume changes on protein folding. Structure 2, 641-649, 1994.

Harris T. D., Hansen R.L.; Karsh W., Nicklaus; N.A., Trautman J.K., Method and apparatus for screening chemical compounds. US PATENT N° 724253, November 28, 2000.

Harrison J.F., Parker R.W., De Silva K.L., Lysozymuria and acute disorders of renal function. J. Clin. Pathol. 26, 278-284, 1973.

Hemming S.A., Bochkarev A., Darst S.A., Kornberg R.D., Ala P., Yang D.S., Edwards A.M., The mechanism of protein crystal growth from lipid layers. J. Mol. Biol. 246, 308-316, 1995.

Henderson R., The potential and limitations of neutrons, electrons and X-rays for atomic resolution microscopy of unstained biological molecules. Quart. Rev. Biophys. 28, 171-193, 1995.

Hiroshi O., Microscope, US PATENT N° 375385 - August 17, 1999.

Horn B.K.P., Robot Vision. MIT Press, chapter 4, 1986.

Huang Q.Q., Teng M.K., Niu L.W., Protein crystallization with a combination of hard and soft precipitants. Acta Crystallogr D Biol. Crystallogr. 55, 1444-1448, 1999.

Ivanov Yu D., Usanov S.A.,, Archakov A.I., Optical Biosensor Studies on the Productive Complex Formation between the Components of Cytochrome P450css Dependent Monooxygenase System. Biochem. Mol. Biol. Int. 47, 327-36, 1999.

Jacobs J.W., Fodor S.P.A., Tibtech. Applications of light-directed chemical synthesis, Combinatorial chemistry 12, 19-26 1994.

Jark W., Di Fonzo S., Lagomarsino S., Cedola A., di Fabrizio E., Bram A., Riekel C., Submicrometer beamsize observed at the exit of an X-ray waveguide.l. Appl. Phys. 80, 4831-4836, 1996.

Jianwei Q., Nobuko I.W., Solute convection during the whole process of protein crystal growth, Journal of Crystal Growth 219, 465-476, 2000.

Johnson L.N., Najdu J.,. Eur. J. Biochem. 29, 1669, 1990.

Judge R.A., Jacobs R.S., Frazier T., Snell E.H., Pusey M.L., The effect of temperature and solution pH on the nucleation of tetragonal lysozyme crystals. Biophys. J. 77, 1585-1893, 1999.

Judge R.A., Jacobs R.S., Frazier T., Snell E.H., Pusey M.L., The effect of temperature and solution pH on the nucleation of tetragonal lysozyme crystals. Biophys. J. 77, 1585-1593, 1999.

Karplus M., Petsko G.A., Molecular dynamics simulations in biology. Nature 347, 631-639, 1990.

Kastner M., Neubert D., High-performance metal chelate affinity chromatography of cytochromes P-450 using Chelating Superose. J. Chromatography 587, 43-54, 1991.

Kelliher M.A., Seldin D.C., Leder P., Tal-1 induces T cell acute lymphoblastic leukemia accelerated by casein kinase II alpha. Embo J. 15, 5160-5166 1996.

Kierzek A.M., Pokarowski P., Zielenkiewicz P., Lattice simulations of protein crystal formation. Biophysical Chemistry 77, 123-137, 1999.

Kierzek A.M., Pokarowski P., Zielenkiewicz P., Microscopic model of protein crystal growth. Biophys Chem 87, 43-61, 2000.

Kierzek A.M., Wolf W.M., Zielenkiewicz P., Simulations of nucleation and early growth stages of protein crystals. Biophys. J. 73, 571-580, 1997.

Kierzek A.M., Zielenkiewicz P., Models of protein crystal growth, Biophys. Chem. 91, 1-20, 2001.

Kiselyova O.I., Yaminsky I.V., Ivanov Y.D., Kanaeva I.P., Kuznetsov V.Y., Archakov A.I., AFM study of membrane proteins, cytochrome P450 2B4, and NADPH-cytochrome P450 reductase and their complex formation. Arch Biochem Biophys. 371, 1-7, 1999.

Kiselyova, O.L., Guriev, O.L., Krivosheev, A.V., Usanov, S.A., Yaminsky, I.V. Atomic force microscopy studies of Langmuir-Blodgett films of cytochrome P450scc (CYP11A1). Hemeprotein aggregation states and interaction with lipids. Langmuir 15, 1352-1359, 1999.

Koradi R., Billeter M., Wuthrich K., MOLMOL: a program for display and analysis of macromolecular structures. J. Mol. Graph. 14, 51-5, 29-32, 1996.

Kovalchuk M.V., Zheludeva S.I., Journal de Physique IV, Collogue C9, Suppl. au Journal de Physique III 4, C9-431, 1994.

Laemmli U.K., Cleavage of structural proteins during the assembly of the head of bacteriophage T4, Nature 227, 680-685, 1970.

Landau E.M., Rosenbusch J.P., Lipidic cubic phases: a novel concept for the crystallisation of membrane proteins. Proc. Natl. Acad.Sci. USA 93, 14532-14535, 1996.

Langmuir I., Schaefer V.I., J. Am. Chem. Soc. 60, 1351, 1938.

Laskowski R.A., MacArthur M.W., Moss D.S., Thornton J.M. Procheck - a program to check the stereochemical quality of protein structures. J. Appl. Crystallogr. 26, 283-291, 1993.

Lee S.W., Mao C., Flynn C.E., Belcher, a.M. Ordering of quantum dots using genetically engineered viruses. Science, 296, 892-895, 2002.

Lehn, J.M. Ed. Comprehensive supramolecular chemistry, Vol. 9, Oxford-Pergamon, 1996.

Lenhoff A.M., Pjura P.E., Dilmore J.G., Godlewski Jr. T.S., Ultracentrifugal crystallization of proteins: transport-kinetic modelling, and experimental behavior of catalase, Journal of Crystal Growth 180, 113-126, 1997.

Leslie A.G.W. Crystallographic Computing V (Moras, D., Podjarny, A.D. and Thierry, J.P. eds) , pp 27-38, Oxford University Press, Oxford. 1991

Li H., Yano J.K., Poulos T.L., Molecular replacement in P450 crystal structure determinations. Methods Enzymol. 357, 79-93, 2002.

Lin S.-X., Zhou M., Azzi A., Xu G.-J., Wakayama N.I., Ataka M., Magnet used for protein crystallization: novel attempts to improve the crystal quality, Biochemical and Biophysical Research Communications 275, 274-278, 2000.

Lvov Yu., Erokhin V., Zaitsev S., Biol. Mem. 4, 1477, 1991.

Malkin A.J., Kuznetsov Yu.G., Land T.A., DeYoreo J.J., McPherson A., Mechanisms of growth for protein and virus crystals.

Mascetti G., Vergani L., Diaspro A., Carrara S., Radicchi G., Nicolini C. Effect of fixatives on calf thymocyte chromatin: 3D hight resolution fluorescence microscopy. Cytometry 23, 110-119, 1996.

Matricardi V., Moretz R., Parson D., Electron diffraction of wet proteins:catalane. Science 177, 268-270, 1972.

McGee D.E., Practical protein crystallography, Academic press inc., New York, 1993.

McPherson A., Crystallization of proteins by variation of pH or temperature. Methods Enzymol. 114, 125-127, 1985.

McPherson A., in Preparation and Analysis of Protein Crystals, Malabar, FL: Krieger eds. pp 94–96, 1989.

McPherson A., Increasing the size of microcrystals by fine sampling of pH limits. J. Appl. Crystallogr. 28, 362-365, 1995.

McPherson A., Malkin A.J., Kuznetsov Yu.G., Atomic force microscopy in the study of macromolecular crystal growth. Annu. Rev. Biophys. Biomol. Struct. 29, 361-410, 2000.

McPherson A., Shlichta P., Heterogeneous and epitaxial nucleation of protein crystals on mineral surfaces. Science 239, 385-387, 1988.

McPherson A., Shlichta P., The use of heterogeneous and epitaxial nucleants to promote the growth of protein crystals. Journal of Crystal Growth 90, 47-50, 1988.

Michel H., Crystallization of Membrane Proteins, Boca Raton, FL: Chemical Rubber Company Press 1991.

Miller M. et al. Direct observatlon of micro arrangement in a single native celiulose fner by X-ray small-angle scattering. Macromolecules 31, 3953-3957, 1998.

Moreno A., Soriano-Garcia M., Crystal-growth kinetics of protein single crystals along capillary tubes in the gel-acupuncture technique. Acta Crystallogr D Biol Crystallogr 55, 577-580, 1999.

Morgan H., Pritchard DJ., Cooper J.M., Photo-patterning of sensor surfaces with biomolecular structures: characterisation using AFM and fluorescence microscopy. Biosensors and Bioelectronics 10, 841-846, 1995.

Müller M., Burghammer M., Flot D., Riekel C., Morawe C., Murphy B., Cedola A., Microcrystallography with an X-ray waveguide. J. Appl. Cryst. 33, 1246-1252, 2000.

Muller M., Burghammer M., Riekel C., Combined scanning microdiffraction and micro small-angle scattering at the microfocus beamline ID13 (ESRF).Nuclear Instruments and Methods in Physics Research A 467–468, 958–961, 2001.

Nadarajah A., Forsythe E.L., Pusey M.L., The averaged face growth-rates of lysozyme crystals - the effect of temperature. J. Crystal Growth 151, 163-172, 1995a.

Nadarajah A., Li M., Pusey M.L., Modeling the growth rates of tetragonal lysozyme crystals. Journal of Crystal Growth 156, 121-132, 1995b.

Nanev C., Penkova A., Nucleation of lysozyme crystals under external electric andultrasonic fields. Journal of Crystal Growth 232, 285–293, 2001.

Navaza J., AMORE - an automated package for molecular replacement. Acta Cristallogr. A50, 157-163, 1994.

Nguyen C., Rocha D., Granjeaud S., Baldit M., Bernard K., Naquet P., Jordan B. R. Differential gene expression in the murine thymus assayed by quantitative hybridization of arrayed cDNA clones, Genomics, 29, 207-216, 1995.

Nicolini C, Erokhin V, Ghisellini P, Paternolli C, Ram M K, Sivozhelezov V., P450scc engineering and nanostructuring for cholesterol sensing Langmuir 17, 3719-3726, 2001b.

Nicolini C., Biophysics and cancer, Plenum Press, 1986.

Nicolini C., De Chiara C., Nicastro G., Supersecondary solution structure of calf thymus histone H1 globular region. Quarterly of Magnetic Resonance in Biology and Medicine 2, 83-97, 1995.

Nicolini C., Erokhin V., Antolini F., Catasti P., Facci P., Thermal stability of protein secondary structure in Langmuir-Blodgett films. Biochim Biophys Acta 1158, 273-278, 1993.

Nicolini C., Erokhin V., Ram M.K., Supramolecular layer engineering for industrial nanotechnology, in Nano-surface chemistry, M. Rosoff (ed.), Marcel Dekker New York pp. 141-212, 2001a.

Nicolini C., Facci P., Alliata P., Scanning Probe Microscopy of Nucleosomes and Polynucleosomes. Nanobiology 4, 105-115, 1996c.

Nicolini C., Genome structure and Function: from chromosomes characterization to genes technology, ed. C. Nicolini, NATO ASI Series 3. High Technlogy Vol. 31, 1997a.

Nicolini C., Heat-Proof Enzymes By Langmuir-Blodgett Technique. Ann. N.Y. Acad. Sci. 799, 297-311, 1996a.

Nicolini C., Malvezzi M., Tomaselli A., Sposito D., Tropiano G., Borgogno E., DNASER I: layout and data analysis. IEEE Transaction on Nanobiosciences 1, 67-72, 2002.

Nicolini C., Metalloprotein engineerginfg for new materials, drugs and nanodevices in Biophysics of Electron Transfer and Molecular Bioelectronics, ed. C Nicolini (New York: Plenum) pp 1–31, 1998.

Nicolini C., Molecular Bioelectronics (New York: World Scientific) pp 1–266, 1996.

Nicolini C., Protein monolayer engineering: principles and application to biocatalysis. Trends in Biotechnology 15, 395-401, 1997b.

Nicolini C., Supramolecular architecture and molecular bioeletronics. Thin Solid Film, 284-285, 1-5, 1996b.

Nicolini C., Towards the Biochip, World Scientific Publishing Co. Singapore-NY 1-270, 1989.

Niefind K., Guerra B, Pinna L.A., Issinger O.-G., Schomburg, D., Crystal structure of the catalytic subunit of protein kinase CK2 from Zea mays at 2.1 angstrom resolution. EMBO J. 17, 2451-2462, 1998.

Niefind K., Guerra B., Ermakova I., Issinger O-G., Crystal structure of human protein kinase CK2: insights into basic properties of the CK2 holoenzyme. EMBO J. 20, 5320-5331, 2001.

Niefind K., Putter M., Guerra B., Issinger O.G., Schomburg D., CTP plus water mimic ATP in the active site of protein kinase CK2. Nat. Struct. Biol. 6, 1100-1103, 1999.

Nimeyer C.M., Nanoparticles, proteins and nucleic acids: biotechnology meets material science. Angew. Chem. Int. Ed. 40, 4128-4158, 2001.

Nollert P., Navarro J., Landau E.M., Crystallization of membrane proteins in cubo. Methods. Enzymol. 343, 183-99, 2002.

Norris, D.J., Vlasov, Y.A. Chemical approaches to three dimensional semiconductor photonic crystals. Adv. Mater. 13, 371-376, 2001.

Orlandini M., Semplici F., Ferruzzi R., Meggio F., Pinna L.A., Oliviero S., Protein kinase CK2 alpha ' is induced by serum as a delayed early gene and cooperates with Ha-ras in fibroblast transformation. J. Biol. Chem. 273, 21291-21297, 1998.

Othman Yu J.D., Farjo M.I., Zareparsi R., MacNee S., Yoshida S.P., Swaroop S., Evaluation and optimization of procedures for target labeling and hybridization of cDNA microarrays. Molecular Vision 8, 130-137, 2002.

Paddeu S., F. Antolini, T. Dubrovsky , C. Nicolini, Langmuir-Blodgett film of glutathione S-transferase immobilised on silanized surfaces. Thin Solid Films 268. 108-113, 1995.

Padilla J.E., Colovos C., Yeates T.O., Nanohedra: using symmetry to design self assembling protein cages, layers, crystals and filaments. PNAS 98, 2217-2221, 2001.

Pebay-Peyroula E., Rummel G., Rosenbus J.P., Landau E.M., X-ray Structure ot Bacteriorhodopsin at 2.5 Angstroms microcrystals grown in lipidic cubic phases. Science 277, 676-1681, 1997.

Pechkova E., Nicolini C. Accelerated protein crystal growth onto the protein thin film, Journal of Crystal Growth 231, 599-602, 2001.

Pechkova E., Nicolini C., From art to science in protein crystallization by means of thin film nanotechnology. Nanotechnology 13, 460-464, 2002a.

Pechkova E., Nicolini C., Protein nucleation and crystallization by homologous protein thin film template. J Cell Biochemistry 85, 243-251, 2002b.

Pechkova E., Nicolini C., The catalytic subunit of human kinase CK2: I Ultramicrocrystals grown by nanobiofilm template and their microfocus diffraction. Acta Crystallographica D, in press 2003a.

Pechkova E., Nicolini C., Nanocrystallography: a new approach to structural proteomics (a review). Trends in biotechnology, in press 2003b.

Pechkova E., Zanotti G., Nicolini C., The catalytic subunit of human kinase CK2: II Three dimensionl atomic structure. Acta Crystallographica D, in press 2003.

Pekarsky Y., Hallas C., Croce C.M., Molecular basis of mature T-cell leukemia. JAMA 286, 2308-2314, 2001.

Pekarsky Y., Hallas C., Croce C.M., Targeting mature T cell leukemia: new understanding of molecular pathways. Am. J. Pharmacogenomics 3, 31-36, 2003.

Pekarsky Y., Koval A., Hallas C., Bichi R., Tresini M., Malstrom S., Russo G., Tsichlis P. and Croce C.M. Tcl1enchances Akt kinase activity and mediates its nuclear translocation. PNAS 97, 3028-3033, 2000.

Pellegrini M, Wukovitz S.W., Yeates T.O., Simulation of protein crystal nucleation. Proteins 28, 515-521, 1997.

Pernecky S. J., Coon M. J. N-terminal modifications that alter P450 membrane targeting and function. Methods in Enzymology 272, 25-34 1996.

Perou C.M., Jeffrey S.S., van de Rijn M., Rees C.A., Eisen M.B., Ross D.T., Pergamenschikov A., Williams C.F., Zhu S. X., Lee J.C., Lashkari D., Shalon D., Brown P.O., Botstein D., Distinctive gene expression patterns in human mammary epithelial cells and breast cancers. Proceedings of the National Academy of Sciences 96, 9212–9217, 1999.

Pileni M.P., Nanosized particles made in colloidal assemblies. Langmuir 13, 3266-3276, 1997.

Pileni M.P., Two-dimensional and three-dimensional superlattices: syntheses and collective physical properties, in Nanosurface Chemistry, edited by M. Rosoff , Marcell Dekker N.Y. 315 2002.

Pinna L.A., Meggio F., Protein kinase CK2 ("casein kinase-2") and its implication in cell division and proliferation. Prog. Cell Cycle Res. 3, 77-97, 1997.

Pinna L.A., Ruzzene M., How do protein kinases recognize their substrates? Biochim. Biophys. Acta 1314, 191 1996.

Pitts J.E., Crystallization by centrifugation. Nature 355, 117, 1992.

Pjura P.E., Lenhoff A.M., Leonard S.A., Gittis A.G., Protein crystallization by design: chymotrypsinogen without precipitants. J. Mol. Biol. 300, 235-239, 2000.

Porter T.D., Larson J.R., Expression of mammalian P450s in Escherichia coli, Methods in Enzymology, 206, 108-116, 1991.

Poulos T.L., Li H., Raman C.S., Heme-mediated oxygen activation in biology: cytochrome c oxidase and nitric oxide synthase. Curr Opin Chem Biol. 3, 131-137, 1999.

Poulos T.L., Modeling of mammalian P450s on basis of P450cam X-ray structure. Meth. Enzymol 206, 11-30, 1991.

Poulos T.L., Raman C.S., Li H., NO news is good news. Structure 6, 255-258, 1998.

QUANTA. Version 98.1111, Molecular Simulation, Inc. 1986-191.

Rayment I., Reductive alkylation of lysine residues to alter crystallization properties of proteins methods, Enzymology 276, 171, 1997.

Rayment I., Small-scale batch crystallization of proteins revisited: an underutilized way to grow large protein crystals. Structure 10, 147-151, 2002.

Ridler T.W., Calvard S., Picture Thresholding using an iterative selection method, IEEE Trans. On System, Man, and cybernetics, SMC 8, pp.630-632. 1978.

Riekel C., Burghammer M., Müller M., Microbeam small-angle scattering experiments and their combination with microdiffraction. J. Appl. Cryst. 33, 421-423, 2000.

Riekel C., Cedola A., Heidelbach F., Wagner K. Micro-diffraction experiments on single polymeric fibres by synchrotron radiation. Macromolecules 30, 1033-1037, 1997.

Riekel C., New avenues in X-ray microbeam experiments. Rep. Prog. Phys. 63, 233-262 2000.

Riekel, C., Bösecke P., Diat O., Lorenzen M., Sanchez del Rio M., Snigireva I., A double focusing small-angle X-ray scattering camera at an ESRF-undulator. Rev. of Scientific Instruments 66, 987-994, 1995.

Roberts G.C.K., NMR of macromolecules, a practical approach, IRL Press 1993.

Rosenberger F., Howard S.B., Sowers J.W., Nyce T.A., Temperature dependence of protein solubility — determination and application to crystallization in X-ray capillaries. Journal of Crystal Growth 129, 1-12, 1993.

Rosenberger F.J., Protein crystallization. Journal of Crystal Growth 166, 40-54, 1996.

Rossof M., Ed. Nano-surface chemistry, Marcel Dekker, NY, 2001.

Salemme F.R., A free interface diffusion technique for the crystallization of protein for X-ray crystallography. Arch. Biochem. Biophys., 151-158, 1972.

Salerno M., Sartore M., Nicolini C., Towards a neural networks based on AFM. Probe Microscope 1, 333-334, 1999.

Sambrook J., Fritsch E., Maniatis T., Molecular Cloning, Cold Spring Harbor Laboratory Press, 1989.

Sammer J.B., Someers G.F., The Enzymes, Academic Press, New York 1943.

Sanjoh A., Tsukihara T., Spatiotemporal protein crystal growth studies using microfluidic silicon devices. J. Cryst. Growth, 196, 691-702, 1999.

Saridakis E., Chayen N.E., Improving protein crystal quality by decoupling nucleation and growth in vapor diffusion. Protein Sci. 9, 755-757, 2000.

Saridakis E., Shaw E.E.G., Stewart P.D., Lloyd L.F., Blow D.M., Acta Cryst. D50, 293-297, 1994.

Sartore M., Pace R., Ram M. K.,Nicolini C., Controlled-atmosphere chamber for atomic force microscopy investigations Review Scientific Instruments 71, 1–5, 2000.

Sartore M., Proceedings of the NI-Week98 Conference, National Instruments, Austin, TX 1998.

Sauerbrey G.Z., Z. Phys. 178, 457-462, 1964.

Sauter C., Lorber B., Giege R., Towards atomic resolution with crystals grown in gel: the case of thaumatin seen at room temperature. Proteins 48, 146-150, 2002.

Sazaki G., Nagatoshi Y., Suzuki Y., Durbin S.D., Miyashita S., Nakada T., Komatsu H., Solubility of tetragonal and orthorhombic lysozyme crystals under high pressure, Journal of Crystal Growth 196, 204-209, 1999.

Schena M., Heller R.A., Theriault T.P., Konrad K, Lachenmeir E., Davis R.W. Microarrays: Biotechnology's discovery platform for functional genomics. Trends in Biotechnology 16, 301-306, 1998.

Schena M., Shalon D., Davis R.W., Brown P.O. Quantitative monitoring of gene expression patterns with a complementary DNA microarray. Science 270, 467–470, 1995.

Schief W.R., Edwards T., Frey W., Koppenol S., Stayton P.S., Vogel V., Two-dimensional crystallization of streptavidin: in pursuit of the molecular origins of structure, morphology, and thermodynamics. Biomol. Eng. 16, 29-38, 1999.

Schwartz A.M., Berglund K.A., In situ monitoring and control of lysozyme concentration during crystallization in a hanging drop. Journal of Crystal Growth 210, 753-760, 2000.

Seldin D.C., Leder P. Casein kinase II alpha transgene-induced murine lymphoma: relation to theileriosis in cattle. Science 267, 894-897, 1995.

Shumyantseva V.V., Bulko T.V., Usanov S.A., Schmid R.D., Nicolini C., Archakov AI. Construction and characterization of bioelectrocatalytic sensors based on cytochromes P450. J. Inorg. Biochem. 87, 185-90, 2001.

Sleytr U.B., Messner P., Pum D., Sara, M. Crystalline bacterial surface layer (S-layer): from supramolecular cell structure to biomimetics and nanotechnology. Angew. Chem. Int. Ed. 38, 1034-1054, 1999.

Sleytr U.B., Sàra M., Pum D., Schuster B., Characterization and use of crystalline bacterial cell surface layers. Progress in Surface Science 68, 231-278, 2001.

Sreerama N., Woody R.W., Protein secondary structure from circular dichroism spectroscopy: combining variable selection principle and cluster analysis with neural network, ridge regression and self-consistent methods. Journal of Molecular Biology 242, 497-507, 1994.

Stein G.S., Lian J.B., Stein J.L., van Wijnen A.J., Montecino M., Pratap J., e Choi J., Zaidi K., Javed A., Gutierrez S., Intranuclear organization of RUNX transcriptional regulatory machinery in biological control of skeletogenesis and cancer, Blood Cells, Molecules, and Diseases 30, 170-176, 2003.

Stein G.S., Montecino M., van Wijnen A.J., Stein J.L., Lian J.B., Nuclear structure-gene expression interrelationships: implications for aberrant gene expression in cancer. Cancer Res. 60, 2067-2076. 2000b.

Stein G.S., van Wijnen A.J., Stein J.L., Lian J.B., Javed A., McNeil S., Shirwin M. Pockwinse Insight into Regulatory Factor Targeting to Transcriptionally Active Subnuclear Sites Experimental Cell Research 253, 110-116, 1999.

Stein G.S., van Wijnen A.J., Stein J.L., Lian J.B., Montecino M., Zaidi K., Javed A. Subnuclear organization and trafficking of regulatory proteins: implications for biological control and cancer. J. Cell. Biochem. Suppl. 35, 84-92 2000a.

Sternberg S., Biomedical Image Processing. IEEE Computer, 1983.

Stevens R.C., High throughput protein crystallization, Curr. Opin. Struct. Biology 10, 558-563, 2000.

Stewart D. H., Groelke J. W.; Thorp H. H., Eckhardt A. E., Detection of binding reactions using labels detected by mediated catalytic electrochemistry. US PATENT N° 722065 - November 24, 2000.

Stura E.A., Wilson I.A., Applications of the streak seeding technique in protein crystallization. J. Cryst. Growth. 110, 270-282, 1991.

Suzuki Y., Miyashita S., Sazaki G., Nakada T., Sawada T., Komatsu H., Effects of pressure on growth kinetics of tetragonal lysozyme crystals. Journal of Crystal Growth 208, 638-644, 2000.

Sygusch J., Coulombe R., Cassanto J.M., Sportiello M.G., Todd P., Protein crystallization in low gravity by step gradient diffusion method. J. Cryst. Growth 162, 167-72, 1996.

Taleb M., Didierjean C., Jelsch C., Mangeot J.P., Capelle B., Aubry A., Crystallization of proteins under an external electric field. J. Crystal Growth 200, 575-582, 1999.

Tang L., Guo B., van Wijnen A.J., Lian J.B., Stein J.L., Stein G.S., Wayne Zhou G., Preliminary Crystallographic Study of GlutathioneS-Transferase Fused with the Nuclear Matrix Targeting Signal of the Transcription Factor AML-1/CBF-α2. Journal of Structural Biology 123, 83-85, 1998.

Tessier P.M., Velev O.D., Kalambur A.T., Lenhoff A.M., Rabolt J.F., Kaler E.W., Structured metallic films for optical and spectroscopic applications via colloidal crystal templating. Adv. Mater. 13, 396-400, 2001.

Troitsky V.I., Berzina T.S., Petrigliano A., Nicolini C., Deposition of alternating LB monolayers with new technique. Thin Solid Films 284-285, 122-126, 1996b.

Troitsky V.I., Sartore M., Berzina S., Nardelli, D., Nicolini C., Instrument for depositino Langmuir-Blodgett films of alternatine monolayers using a protective layer. Review Scientific Instruments 67, 4216-4223, 1996a.

Troitsky, V.I., Ghisellini P., Pechkova E., Nicolini C., DNASER II. Novel surface patterning for biomolecular microarray. IEEE Transaction on Nanobiosciences 1, 73-77, 2002.

Tsekova D., Dimitrova S., Nanev C., Heterogeneous nucleation (and adhesion) of lysozyme crystals. J. Cryst. Growth 196 226-233, 1999.

Usanov S.A., Graham S.E., Lepesheva G.I., Azeva T.N., Strushkevich N.V., Gilep A.A., Estabrook R.W., Peterson J.A., Probing the interaction of bovine cytochrome P450scc (CYP11A1) with adrenodoxin: evaluating site-directed mutations by molecular modeling. Biochemistry 41, 8310-20, 2002.

Vekilov P.G., Protein crystal growth--microgravity aspects. Adv. Space Res. 24, 1231-1401, 1999.

Vekilov P.G., Rosenberger F., Protein crystal growth under forced solution flow: experimental setup and general response of lysozyme. Journal of Crystal Growth 186, 251-261, 1998.

Vergani L., Grasselli E., Ghisellini P., Pechkova E., Nicolini C., Cloning, Expresion, Crystallization, Strusctural., and Functional Studies of P450 and Kinase CK2, unpublished data 2002.

Vidal O., Roberta M.C., Arnouxb B., Capellea B., Crystalline quality of lysozyme crystals grown in agarose and silica gels studied by X-ray diffraction techniques. J. Cryst Growth 196, 559-571, 1999.

Vijayakumar S., Salerno J.C., Molecular modeling of the 3D structure of cytochrome P450scc. Biochim. Biophys. Acta 1160, 281, 1992.

Vilenchik L.Z., Griffith J.P., Clair St.N., Navia M.A., Margolin A.L., Protein crystals as novel microporous materials. JACS 120, 4290-4294, 1998.

Walling L.A., Peters N.R., Horn E.J., King R.W., New technologies for chemical genetics. Journal of Cellular Biochemistry. Supplement 37, 7-12, 2001.

Ward M.D., Motors in miniature. Chemistry Industry 7, 22-26, 2000.

Weber P.C., Overview of protein crystallization methods. Methods Enzymol. 276, 13-59, 1997.

Wiencek J.M., New strategies for protein crystal growth. Annu. Rev. Biomed. Eng. 1 505-534, 1999.

Williams P.A., Cosme J., Sridnar V., Johnson E. F., McRee D. F., Mammalian microsomal cytochrome P450 monooxygenase: structural adaptations for membrane binding and functional diversity, Molecular Cell 5, 121-131, 2000.

Wolde P.R., Frenkel D., Enhancement of protein crystal nucleation by critical density fluctuations. Science 277, 1975-1978, 1997.

Wutrich K., NMR of Proteins and Nucleic Acids, J. Wiley and Sons, New York ,1986.

Wyckoff R.W.G., Corey R.B., Science 84, 513, 1939.

Yanagiya S., Sazaki G., Durbin S.D., Miyashita S., Nakajima K., Komatsu H., Watanabe K., M.Motokawa, Effects of a magnetic field on the growth rate of tetragonal lysozyme crystals, Journal of Crystal Growth 208, 645-650. 2000.

Yang Y.H., Buckley M.J., Speed T.P., Analysis of cDNA microarray images. Brief Bioinform. 2, 341-349, 2001.

Ye J., Yan C., Di Francesco V., Beasley E.M., Nucleic acid molecules encoding human calcium/calmodulin (CaMK) dependent kinase proteins US PATENT N° 800960 - March 8, 2001.

Zack, G.W., Rogers W.E., Latt S.A., Automatic measurement of sister chromatid exchange frequency, Journal of Histochemistry and Cytochemistry, 25, 741-753, 1977.

Index

3D structure determination; 35, 38, 97, 128
Advanced method; 30
AFM
see Atomic force microscopy;
Arrayer; 141-144, 148, 151, 156
Atomic force microscopy; 20, 61, 67, 68, 69, 77, 118
Bacteriorhodopsin (BR); 28, 29
Biomolecular array; 7, 137, 141
Biosensors; 51
Brewster angle microscopy (BAM); 50, 55, 60, 61
Brilliance; 79, 80, 86, 87, 90, 91
Charge coupled device (CCD); 39, 90, 129, 141, 142, 150, 154-156, 163
Circular Dichroism (CD); 42-44, 61
Cholesterol; 2, 14, 111
Chromatography; 13, 14, 21, 121
Crystal growth; 10, 20, 22, 24, 26, 30-35, 50, 63, 67, 99-101, 104-106, 110, 111, 117, 136, 164, 170
Crystal nucleation; 20, 22, 24, 29, 31, 32, 34, 63, 102, 105, 110, 132
Crystallography; 35, 63, 79, 87, 97
Cy3; 142, 149, 150
Cytochrome P450scc; 2, 13-15, 43-44, 54, 56, 66, 77, 78, 91, 111-119, 164
DNA
chip; 7, 141
labeled; 142, 149, 150, 151
recombinant; 10, 11, 167
E. coli *see* Escherichia coli
Electron microscopy; 42, 50, 171
Electrophoresis; 3, 14, 15, 16, 22, 112, 121, 122, 123, 131, 149, 150
Escherichia coli; 12-14; 195; 205
European Synchrotron Radiation Facility (ESRF); 10, 29, 81-84, 87, 90-93, 110, 128
GST; 6
Hen egg white lysozyme (HEWL); 28
Immobilization; 3, 10, 50, 142-144, 151
Kinase
CK2; 13, 66, 119, 120, 123, 125, 127, 133, 136, 164
Ck2 catalytic subunit; 91, 119, 120, 126, 164
human; 12
Langmuir-Blodgett (LB); 51, 57, 58, 59, 63, 65, 99, 102
Langmuir-Schaefer film (LS); 57, 58, 65, 102, 116

LB *see* Langmuir-Blodgett film
LS *see* Langmuir-Schaefer film
Lysozyme; 5, 11, 23, 31-34, 42, 95, 99-105, 107-110, 114, 123, 136, 164, 168-169, 171
MALDI; 138, 140, 141
Microarray; 141-144, 150, 152-164,
Microcrystals; 4, 20, 28-29, 42, 68, 69, 80, 90-93, 95, 114, 116-119, 125-128
Microfocus; 4, 21, 29, 80, 85,87-93, 109, 110, 117, 127-130
Microgravity; 29, 30, 100
Molecular modeling; 15, 170
Nanocrystallography; 3, 51, 63, 136, 165
Nanocrystals; 3, 63, 167, 172
Nuclear magnetic resonance (NMR); 9, 23, 44, 48
P450scc *see* cytochrome P450scc
PCR; 149, 150
PDB *see* Protein Data Bank
Protein crystallization; 3, 6, 10, 20, 21-28, 30, 31, 35, 51, 64, 97, 99, 100, 113, 117, 124, 125, 136, 164, 169
Protein Data Bank (PDB); 78, 109, 110, 113, 119
Proteomics; 1, 4, 9, 16, 137, 167
Sauerbrey equation; 67
Scanning probe microscopy; 4, 42
Screening procedure; 26, 63, 101
SDS-PAGE; 13, 111, 121, 123
Site-specific mutagenesis; 11
Surface
  potential; 56-57, 61, 111, 136
  pressure; 52-57, 59, 63, 66, 103, 105-107, 110-112, 119, 123
Synchrotron radiation; 20, 61, 78, 81-82, 86, 90, 92-93, 95, 97, 109, 128
Synchrotron Radiation Facility; 10, 35, 80-81, *see also* ESRF
Thin film template method; 3, 42, 63, 90, 101, 109, 119, 125
Thin films; 50, 61, 63, 64, 113
Tocsy; 45, 46, 48
Transmission electron microscopy (TEM); 50
Trough; 4, 40, 64, 102, 112, 123
Vapour diffusion method; 10, 25, 64, 101, 109
Western blotting; 13
X-ray crystallography; 9, 20, 26, 29, 33, 35, 68, 169, 171